



Вол. 66, бр. 4
2018

ISSN 0042-8469

e-ISSN 2217-4753

УДК 623 + 355/359

ВОЈНО ТЕХНИЧКИ НАУЧНИ ЧАСОПИС МИНИСТАРСТВА ОДБРАНЕ РЕПУБЛИКЕ СРБИЈЕ

ЏЛасник





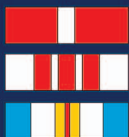
Том 66 № 4
2018

ISSN 0042-8469

e-ISSN 2217-4753

УДК 623 + 355/359

ВОЕННО-ТЕХНИЧЕСКИЙ НАУЧНЫЙ ЖУРНАЛ МИНИСТЕРСТВА ОБОРОНЫ РЕСПУБЛИКИ СЕРБИЯ



ВЕСТНИК





Vol. 66, Issue 4
2018

ISSN 0042-8469
e-ISSN 2217-4753
UDC 623 + 355/359

MILITARY TECHNICAL

SCIENTIFIC PERIODICAL OF THE MINISTRY OF DEFENCE OF THE REPUBLIC OF SERBIA

Courier



ISSN 0042-8469
e-ISSN 2417-4753
UDC 623 + 355/359



ВОЛУМЕН 66 • БРОЈ 4 • ОКТОБАР-ДЕЦЕМБАР 2018.



VOLUMEN 66 • BROJ 4 • OKTOBAR-DECEMBAR 2018.

ВТГ.МО.УПР.СРБ
www.vtg.mod.gov.rs
COBISS.SR-ID 4423938

ISSN 0042-8469
e-ISSN 2417-4753
UDC 623 + 355/359



ТОМ 66 • НОМЕР ВЫПУСКА 4 • ОКТЯБРЬ – ДЕКАБРЬ 2018.



VOLUME 66 • ISSUE 4 • OCTOBER – DECEMBER 2018

ВТГ.мо.упр.срб
www.vtg.mod.gov.rs
COBISS.SR-ID 4423938

Издавач:
МИНИСТАРСТВО ОДБРАНЕ РЕПУБЛИКЕ СРБИЈЕ
УНИВЕРЗИТЕТ ОДБРАНЕ У БЕОГРАДУ

Ректор
Доц. др Горан Радовановић, генерал-мајор

Институт за научне информације
Директор
Проф. др Силва Добрић

ГЛАВНИ И ОДГОВОРНИ УРЕДНИК ВОЈНОТЕХНИЧКОГ ГЛАСНИКА
мр Небојша Гаћеша, потпуковник
е-mail: nebojsa.gacesa@mod.gov.rs, tel.: 011/3603-260, 066/87-00-118, <http://orcid.org/0000-0003-3217-6513>

УРЕЂИВАЧКИ ОДБОР

- генерал-мајор проф. др Бојан Зрнић, Министарство одбране Републике Србије, Управа за одбрамбене технологије Сектора за материјалне ресурсе, председник Уређивачког одбора, <http://orcid.org/0000-0002-0961-993X>,
- генерал-мајор проф. др Младен Вуруна, Универзитет одбране у Београду, заменик председника Уређивачког одбора, <http://orcid.org/0000-0002-3558-4312>,
- пуковник проф. др Миленко Андрић, Универзитет одбране у Београду, Војна академија, <http://orcid.org/0000-0001-9038-0876>,
- мр Сергеј А. Аргунев, Хидрографско друштво, Санкт-Петербург, Руска Федерација, <http://orcid.org/0000-0002-5264-6634>,
- проф. др Исмаил Бег, Економски факултет у Лахорев, Лахорев, Пакистан, <http://orcid.org/0000-0002-4191-1498>,
- проф. др Стеван М. Бербер, Универзитет у Окланду, Одсек за електротехничко и рачунарско инжењерство, Окланд, Нови Зеланд, <http://orcid.org/0000-0002-2432-3088>,
- проф. др Сања Вранеш, Институт „Михајло Пупин“, Београд, <http://orcid.org/0000-0002-7054-6928>,
- проф. др Леонид И. Гречихин, Белоруска државна ваздухопловна академија, Минск, Република Белорусија, <http://orcid.org/0000-0002-5358-9037>,
- проф. др Александар В. Дорохов, Национални економски универзитет у Харкову, Харков, Украјина, <http://orcid.org/0000-0002-0737-8714>,
- проф. др Жељко Ђуровић, Универзитет у Београду, Електротехнички факултет, <http://orcid.org/0000-0002-6076-442X>,
- др Никола Жегарац, Српска академија изумитеља и научника, Београд, <http://orcid.org/0000-0002-1766-8184>,
- проф. др Алекса Ј. Зејак, Универзитет у Новом Саду, Факултет техничких наука, <http://orcid.org/0000-0001-5114-2867>,
- проф. др Вукица М. Јовановић, Old Dominion University Норфолк, САД, <http://orcid.org/0000-0002-8626-903X>,
- проф. др Бранко Ковачевић, Универзитет у Београду, Електротехнички факултет, <http://orcid.org/0000-0001-9334-9639>,
- др Сања Љ. Корица, Универзитет Унион - Никола Тесла, Београд, <http://orcid.org/0000-0002-7915-9430>,
- научни саветник др Ана И. Костов, Институт за рударство и металургију, Бор, <http://orcid.org/0000-0003-1893-7187>,
- ванр. проф. др Славољуб С. Лекић, Универзитет у Београду, Пољопривредни факултет, <http://orcid.org/0000-0002-4834-3550>,
- др Василије М. Мановић, Combustion and CCS Centre, Универзитет у Кранфилду, Кранфилд, Велика Британија, <http://orcid.org/0000-0002-8377-7717>,
- потпуковник ванр. проф. др Јаромир Марес, Универзитет одбране у Брну, Чешка Република, <http://orcid.org/0000-0002-1337-3821>,
- академик Гадимир В. Миловановић, Српска академија наука и уметности, Београд, <http://orcid.org/0000-0002-3255-8127>,
- ванр. проф. др Penumarthu Parvateesam Murthy, University Guru Ghasidas Vishwavidyalaya, Department of Pure and Applied Mathematics, Биласпур (Chhattisgarh), Индија, <http://orcid.org/0000-0003-3745-4607>,
- научни саветник др Предраг Петровић, Институт за телекомуникације и електронику ИРИТЕЛ АД, Београд, <http://orcid.org/0000-0002-0455-7506>,
- проф. др Славо Ј. Покорни, Висока школа за информационе технологије, рачунарски дизајн и савремено пословање, Београд, <http://orcid.org/0000-0002-3173-597X>,
- проф. др Стојан Раденовић, Универзитет у Београду, Машински факултет, <http://orcid.org/0000-0001-8254-6688>,
- проф. др Андреја Самчовић, Универзитет у Београду, Саобраћајни факултет, <http://orcid.org/0000-0001-6432-2816>,
- проф. др Николај И. Сидњаев, Московски државни технички универзитет „Н. Е. Бауман“, Москва, Руска Федерација, <https://orcid.org/0000-0002-5722-4553>,
- проф. др Јонел Старецу, Трансилванијски универзитет у Брашову, Румунија, <http://orcid.org/0000-0001-5947-7557>,
- научни саветник др Срећко С. Стопић, RWTH Aachen University, Faculty for Georesourcen and Materials Engineering, IME Process Metallurgy and Metal Recycling, Ахен, СР Немачка, <http://orcid.org/0000-0002-1752-5378>,
- проф. др Мирослав Д. Трајановић, Универзитет у Нишу, Машински факултет, <http://orcid.org/0000-0002-3325-0933>,
- доц. др Вадим Л. Хајков, Краснодар, Руска Федерација, <http://orcid.org/0000-0003-1433-3562>,
- проф. др Владимир Г. Чернов, Државни универзитет у Владимиру, Владимир, Руска Федерација, <http://orcid.org/0000-0003-1830-2261>,
- потпуковник мр Небојша Н. Гаћеша, уредник Војнотехничког гласника, секретар Уређивачког одбора, <http://orcid.org/0000-0003-3217-6513>.

Адреса редакције: ВОЈНОТЕХНИЧКИ ГЛАСНИК, Генерала Павла Јуришића Штурма 1, Београд

<http://www.vtg.mod.gov.rs>

<http://aseestant.ceon.rs/index.php/vtg/issue/current>

<http://scindeks.nb.rs/journaldetails.aspx?issn=0042-8469>

http://elibrary.ru/title_about.asp?id=53280

<https://doaj.org/toc/2217-4753>

е-mail: vojnotehnicki.glasnik@mod.gov.rs

Претплата на штампано издање: е-mail: vojnotehnicki.glasnik@mod.gov.rs; тел. 066/87-00-118

Рукописи се не враћају

Часопис излази тромесечно

Први штампани број *Војнотехничког гласника* објављен је 1. 1. 1953. године

Прво електронско издање *Војнотехничког гласника* на Интернету објављено је 1. 1. 2011. године

Војнотехнички гласник је лиценциран код EBSCO Publishing-а, највећег светског агрегатора часописа, периодике и осталих извора у пуном тексту. Комплетан текст *Војнотехничког гласника* доступан је у базама података EBSCO Publishing-а.

Штампа: Војна штампарија – Београд, Ресавска 40б, е-mail: vojna.stamparija@mod.gov.rs



Издательство:
МИНИСТЕРСТВО ОБОРОНЫ РЕСПУБЛИКИ СЕРБИЯ
УНИВЕРСИТЕТ ОБОРОНЫ В Г. БЕЛГРАД

РЕКТОР
Генерал-майор доц. д-р Горан Радованович

Институт научной информации
Директор
Профессор д-р Силва Добрич

ГЛАВНЫЙ И ОТВЕТСТВЕННЫЙ РЕДАКТОР ЖУРНАЛА «ВОЕННО-ТЕХНИЧЕСКИЙ ВЕСТНИК»
Кандидат технических наук Небойша Гачеша, подполковник
e-mail: nebojsa.gacesa@mod.gov.rs, тел.: +381 11 3603 260, +381 66 87 00 118, <http://orcid.org/0000-0003-3217-6513>
РЕДАКЦИОННАЯ КОЛЛЕГИЯ

- Генерал-майор профессор д-р Боян Зрнич, начальник Управления оборонительных технологий при Департаменте материальных ресурсов Министерства обороны Республики Сербия, председатель Редакционной коллегии, <http://orcid.org/0000-0002-0961-993X>.
- Генерал-майор профессор д-р Младен Вурвна, ректор Университета обороны в г. Белград, заместитель председателя Редакционной коллегии, <http://orcid.org/0000-0002-3558-4312>.
- Полковник профессор д-р Миленко Андрич, Университет обороны в г. Белград, Военная академия, <http://orcid.org/0000-0001-9038-0876>.
- Кандидат наук Сергей А. Аргунов, Гидрографическое общество, г. Санкт-Петербург, Российская Федерация, <http://orcid.org/0000-0002-5264-6634>.
- Профессор д-р Исмаат Бег, Экономический факультет в г. Лахор, шт. Пенджаб, Пакистан, <http://orcid.org/0000-0002-4191-1498>.
- Д-р Стеван М. Бербер, Оклендский университет, Департамент электроники и компьютерной инженерии, г. Окленд, Новая Зеландия, <http://orcid.org/0000-0002-2432-3088>.
- Профессор д-р Саня Вранеш, Институт «Михайло Пупин», г. Белград, <http://orcid.org/0000-0002-7054-6928>.
- Профессор д-р Леонид И. Гречишин, Белорусская государственная академия авиации, г. Минск, Республика Беларусь, <http://orcid.org/0000-0002-5358-9037>.
- Профессор д-р Александр В. Дорохов, Харьковский национальный экономический университет, г. Харьков, Украина, <http://orcid.org/0000-0002-0737-8714>.
- Профессор д-р Желько Джурович, Белградский университет, Электротехнический факультет, <http://orcid.org/0000-0002-6076-442X>.
- Д-р Никола П. Жегарац, Сербская академия изобретателей и ученых, г. Белград, <http://orcid.org/0000-0002-1766-8184>.
- Профессор д-р Алекса Зейяк, Университет в г. Нови Сад, Факультет технических наук, <http://orcid.org/0000-0001-5114-2867>.
- Д-р Вуица М. Иванович, Университет Олд Доминион, г. Норфолк, шт. Вирджиния, США, <http://orcid.org/0000-0002-8626-903X>.
- Профессор д-р Бранко Ковачевич, Белградский университет, Электротехнический факультет, <http://orcid.org/0000-0001-9334-9639>.
- Д-р Саня Л. Корица, Университет «Унион – Никола Тесла», г. Белград, <http://orcid.org/0000-0002-7915-9430>.
- Научный советник д-р Анна Костов, Институт горного дела и металлургии, г. Бор, <http://orcid.org/0000-0003-1893-7187>.
- Д-р Славолуб С. Лекич, Белградский университет, Сельскохозяйственный факультет, <http://orcid.org/0000-0002-4834-3550>.
- Д-р Василий М. Манович, Центр горения, сбора и хранения углерода, Университет Кранфилд, г. Кранфилд, Великобритания, <http://orcid.org/0000-0002-8377-7717>.
- Подполковник д-р Яромир Марес, Университет обороны в г. Брно, Чешская Республика, <http://orcid.org/0000-0002-1337-3821>.
- Профессор д-р Градимир В. Милованович, член Сербской академии наук, г. Белград, <http://orcid.org/0000-0002-3255-8127>.
- Д-р Пенумартхи Парватеесам Муртхи, Университет Гую Гхасидас Вишвавидялая, департамент фундаментальной и прикладной математики, г. Биласпур, шт. Чхаттисгарх, Индия, <http://orcid.org/0000-0003-3745-4607>.
- Научный советник д-р Предраг Петрович, Управляющий директор по вопросам исследовательских работ Института телекоммуникаций и электроники «IRITEL-AD» г. Белград, <http://orcid.org/0000-0002-0455-7506>.
- Профессор д-р Славко Покорни, Колледж информационных технологий, компьютерного дизайна и современного бизнеса, г. Белград, <http://orcid.org/0000-0002-3173-597X>.
- Профессор д-р Стоян Раденович, Белградский университет, Факультет машиностроения, <http://orcid.org/0000-0001-8254-6688>.
- Профессор д-р Андрея Самочич, Белградский университет, Факультет транспорта, <http://orcid.org/0000-0001-6432-2816>.
- Профессор д-р Николай И. Сидняев, Московский Государственный Технический Университет им. Н.Э. Баумана, Москва, Российская Федерация, <https://orcid.org/0000-0002-5722-4553>.
- Профессор д-р Йонел Старецу, Трансильванский университет в г. Брашов, Румыния, <http://orcid.org/0000-0001-5947-7557>.
- Научный советник д-р Сречко С. Стопич, Рейнско-Вестфальский технический университет г. Ахен, факультет георесурсов и технологий материалов, департамент металлургических технологий и обработки металлов, г. Ахен, ФРГ, <http://orcid.org/0000-0002-1752-5378>.
- Профессор д-р Мирослав Траянович, Университет в г. Ниш, Факультет машиностроения, <http://orcid.org/0000-0002-3325-0933>.
- Кандидат технических наук, доцент Вадим Л. Хайков, г. Краснодар, Российская Федерация, <http://orcid.org/0000-0003-1433-3562>.
- Профессор д-р Владимир Г. Чернов, Владимирский государственный университет, г. Владимир, Российская Федерация, <http://orcid.org/0000-0003-1830-2261>.
- Подполковник кандидат наук Небойша Гачеша, редактор журнала «Военно-технический вестник», секретарь Редакционной коллегии, <http://orcid.org/0000-0003-3217-6513>.

Адрес редакции: ВОЈНОТЕХНИЧКИ ГЛАСНИК, Генерала Павла Јуришића Штурма 1, Београд
<http://www.vtg.mod.gov.rs>
<http://aseestant.ceon.rs/index.php/vtg/issue/current>
<http://scindeks.nb.rs/journaldetails.aspx?issn=0042-8469>
http://elibrary.ru/title_about.asp?id=53280
<https://doaj.org/toc/2217-4753>
e-mail: vojnotehnicki.glasnik@mod.gov.rs

Подписка на печатную версию журнала: e-mail: vojnotehnicki.glasnik@mod.gov.rs; тел. +381 66 87 00 118
Присланные в редакцию журнала статьи не возвращаются.

Журнал выпускается ежеквартально

Первый номер журнала «Военно-технический вестник» выпущен 1.1.1953 года.

Первая электронная версия журнала размещена на интернет странице 1.1.2011 года.

«Военно-технический вестник» включен в систему EBSCO – всемирная академическая база данных и сервисов.

Типография: Војна штампарија – Београд, Ресавска 40б, e-mail: vojna.stamparija@mod.gov.rs



Publisher:
MINISTRY OF DEFENCE OF THE REPUBLIC OF SERBIA
UNIVERSITY OF DEFENCE IN BELGRADE

Rector
Major General Goran Radovanović, PhD, Assistant Professor

Institute for scientific information
Director
Professor Silva Dobrić, PhD

EDITOR IN CHIEF OF THE MILITARY TECHNICAL COURIER

Lt Col Nebojša Gaćeša MSc
e-mail: nebojsa.gacesa@mod.gov.rs, tel: +381 11 3603 260, +381 66 87 00 118, <http://orcid.org/0000-0003-3217-6513>

EDITORIAL BOARD

- Major General Bojan Znić, PhD, Professor, Ministry of Defence, Head of the Department for Defence Technologies, Material Resources Sector, Belgrade (Head of the Editorial Board), <http://orcid.org/0000-0002-0961-993X>
- Major General Mladen Vuruna, PhD, Professor, Rector of the University of Defence, Belgrade (Deputy Head of the Editorial Board), <http://orcid.org/0000-0002-3558-4312>
- Colonel Milenko Andrić, PhD, Professor, University of Defence in Belgrade, Military Academy, <http://orcid.org/0000-0001-9038-0876>
- Sergei A. Arzunov, MSc, Hydrographic society, St. Petersburg, Russian Federation, <http://orcid.org/0000-0002-5264-6634>
- Professor Ismat Beq, PhD, Lahore School of Economics, Lahore, Pakistan, <http://orcid.org/0000-0002-4191-1498>
- Stevan M. Berber, PhD, The University of Auckland, Department of Electrical and Computer Engineering, Auckland, New Zealand, <http://orcid.org/0000-0002-2432-3088>
- Professor Vladimir G. Chernov, DSc, Vladimir State University, Department of Management and Informatics in Technical and Economic Systems, Vladimir, Russian Federation, <http://orcid.org/0000-0003-1830-2261>
- Professor Aleksandr V. Dorohov, PhD, Kharkiv National University of Economics, Kharkiv, Ukraine, <http://orcid.org/0000-0002-0737-8714>
- Professor Željko Đurović, PhD, University in Belgrade, Faculty of Electrical Engineering, <http://orcid.org/0000-0002-6076-442X>
- Professor Leonid I. Gretchihin, PhD, Belarusian State Academy of Aviation, Minsk, Republic of Belarus, <http://orcid.org/0000-0002-5358-9037>
- Vukica M. Jovanović, PhD, Trine University, Allen School of Engineering and Technology, Department of Engineering Technology, Angola, Indiana, USA, <http://orcid.org/0000-0002-8626-903X>
- Associate professor Vadim L. Khaikov, PhD, Krasnodar, Russian Federation, <http://orcid.org/0000-0003-1433-3562>,
- Assistant Professor Sanja Li. Korica, PhD, University Union - Nikola Tesla, Belgrade, <http://orcid.org/0000-0002-7915-9430>
- Scientific Advisor Ana Kostov, PhD, Institute of Mining and Metallurgy, Bor, Serbia, <http://orcid.org/0000-0003-1893-7187>
- Professor Branko Kovačević, PhD, University of Belgrade, Faculty of Electrical Engineering, <http://orcid.org/0000-0001-9334-9639>
- Associate Professor Slavoljub S. Lekić, PhD, University of Belgrade, Faculty of Agriculture, <http://orcid.org/0000-0002-4834-3550>
- Vasilije M. Manović, PhD, Combustion and CCS Centre, Cranfield University, Cranfield, UK, <http://orcid.org/0000-0002-8377-7717>
- Lt Colonel Jaromir Mares, PhD, Associate Professor, University of Defence in Brno, Czech Republic, <http://orcid.org/0000-0002-1337-3821>
- Professor Gradimir V. Milovanović, PhD, Member of the Serbian Academy of Sciences and Arts, Mathematical Institute of the SASA, Belgrade, <http://orcid.org/0000-0002-3255-8127>
- Associate Professor Penumarthi Parvateesam Murthy, PhD, University Guru Ghasidas Vishwavidyalaya, Department of Pure and Applied Mathematics, Bilaspur (Chhattisgarh), India, <http://orcid.org/0000-0003-3745-4607>,
- Scientific Advisor Predrag Petrović, PhD, Executive Director for R&D and Radio Communications, Institute of telecommunications and electronics IRITEL AD, Belgrade, <http://orcid.org/0000-0002-0455-7506>
- Professor Slavko Pokorni, PhD, Information Technology School, Belgrade, <http://orcid.org/0000-0002-3173-597X>
- Professor Stojan N. Radenović, PhD, University of Belgrade, Faculty of Mechanical Engineering, <http://orcid.org/0000-0001-8254-6688>,
- Professor Andreja Samčović, PhD, University of Belgrade, Faculty of Transport, <http://orcid.org/0000-0001-6432-2816>,
- Professor Nikolay I. Sidnyaev, PhD, Bauman Moscow State Technical University, Moscow, Russian Federation, <https://orcid.org/0000-0002-5722-4553>
- Professor Ionel Staretu, PhD, Transilvania University of Brasov, Romania, <http://orcid.org/0000-0001-5947-7557>
- Scientific Advisor Srećko S. Stojić, PhD, RWTH Aachen University, Faculty for Georesources and Materials Engineering, IME Process Metallurgy and Metal Recycling, Aachen, Germany, <http://orcid.org/0000-0002-1752-5378>
- Professor Miroslav Trajanović, PhD, University of Niš, Faculty of Mechanical Engineering, <http://orcid.org/0000-0002-3325-0933>
- Professor Sanja Vraneš, PhD, Institute "Mihailo Pupin", Belgrade, <http://orcid.org/0000-0002-7054-6928>
- Professor Aleksa Zejak, PhD, University of Novi Sad, Faculty of Technical Sciences, <http://orcid.org/0000-0001-5114-2867>
- Nikola P. Žegarac, PhD, Serbian Academy of Inventors and Scientists, Belgrade, <http://orcid.org/0000-0002-1766-8184>
- Lt Colonel Nebojša Gaćeša, MSc, Editor of the Military Courier, (Secretary of the Editorial Board), <http://orcid.org/0000-0003-3217-6513>.

Address: VOJNOTEHNIČKI GLASNIK / MILITARY TECHNICAL COURIER, Generala Pavla Jurišića Šturma 1,
11000 Belgrade, Serbia

<http://www.vtg.mod.gov.rs/index-e.html>

<http://aseestant.ceon.rs/index.php/vtg/issue/current>

<http://scindeks.nb.rs/journaldetails.aspx?issn=0042-8469>

http://elibrary.ru/title_about.asp?id=53280

<https://doaj.org/toc/2217-4753>

e-mail: vojnotehnicki.glasnik@mod.gov.rs

Subscription to print edition: e-mail: vojnotehnicki.glasnik@mod.gov.rs; Tel. +381 66 87 00 118

Manuscripts are not returned

The journal is published quarterly

The first printed issue of the *Military Technical Courier* appeared on 1st January 1953.

The first electronic edition of the *Military Technical Courier* on the Internet appeared on 1st January 2011.

Military Technical Courier has entered into an electronic licensing relationship with EBSCO Publishing, the world's most prolific aggregator of full text journals, magazines and other sources. The full text of *Military Technical Courier* can be found on EBSCO Publishing's databases.

Printed by Vojna štamparija – Beograd, Resavska 40b, e-mail: vojna.stamparija@mod.gov.rs



САДРЖАЈ

ОРИГИНАЛНИ НАУЧНИ ЧЛАНЦИ

- Вадим Л. Хајков*
Процена вероватноће погађања циља једним хицем као резултат нумеричког решавања двоструких интеграла помоћу Mathcad-a739-756
- Срећко Р. Стопић, Бернд Г. Фридрих*
Растварање ретких земних метала сумпорном киселином из руда које садрже флуорокарбонатни минерал757-770
- Наташа Д. Кубуровић, Александар В. Голубовић,
Љиљана М. Бабинчев*
Развој нових паметних металних наноматеријала на бази титанијум-диоксида за фотокаталитичку и антимиљробну активност771-835
- Сања Љ. Корица, Аксел Рајнкостер, Уве Бекер*
Коинцидентна студија двоструке електронске емисије повезане са фотојонизацијом К-љуске C₆₀836-846
- Леонид И. Гречихин*
Негативни јони и њихова улога у развоју науке и технологије847-863

СТРУЧНИ ЧЛАНЦИ

- Михаило Р. Мрдак*
Анализа заосталих напона у биоинертним неорганским Керамичким плазма спреј превлакама864-879
- Иван А. Тот, Душан Љ. Богвићевић, Младен Б. Трикош,
Комлен Г. Паловић*
Fiware: Развојна платформа за веб ствари880-899
- Соња Р. Куљански Марић*
LDPC кодови за потребе заштите података на физичком нивоу900-919
- САВРЕМЕНО НАОРУЖАЊЕ И ВОЈНА ОПРЕМА920-939
Драган М. Вучковић, Милош М. Јевтић
- ПОЗИВ И УПУТСТВО АУТОРИМА940-956
- ОБАВЕШТЕЊА САРАДНИЦИМА И ЧИТАОЦИМА957-958

СОДЕРЖАНИЕ

ОРИГИНАЛЬНЫЕ НАУЧНЫЕ СТАТЬИ

- Вадим Л. Хайков*
Оценка вероятности попадания в мишень одиночным выстрелом как результат численного интегрирования математического выражения с двойным интегралом в программе Mathcad739-756
- Сречко Р. Стопич, Бернд Г. Фридрих*
Выщелачивание редкоземельных металлов серной кислотой из пород, содержащих фторкарбонаты757-770
- Наташа Д. Кубурович, Александр В. Голубович, Лиляна М. Бабинчев*
Разработка новых умных металлических наноматериалов на основе диоксида титана для фотокаталитической и антимикробной активностей771-835
- Саня Л. Корица, Аксел Райнкостер, Уве Бекер*
Исследование двойной электронной эмиссии, связанной с фотоионизацией к-оболочки C_{60} 836-846
- Леонид И. Гречихин*
Отрицательные ионы и их роль в развитии науки и технологии.....847-863

ПРОФЕССИОНАЛЬНЫЕ СТАТЬИ

- Михаило Р. Мрдак*
Анализ остаточных напряжений в биоинертных неорганических керамических покрытиях, нанесенных плазменным напылением864-879
- Иван А. Тот, Душан Л. Богичевич, Младен Б. Трикош, Комлен Г. Лалович*
Fiware: Развитие платформы для Интернета вещей880-899
- Соня Р. Кулянски Марич*
Низкоплотностные коды для защиты данных на физическом уровне....900-919

- СОВРЕМЕННОЕ ВООРУЖЕНИЕ И ВОЕННОЕ ОБОРУДОВАНИЕ920-939
Драган М. Вучкович, Милош М. Йевтич

- ПРИГЛАШЕНИЕ И ИНСТРУКЦИИ ДЛЯ АВТОРОВ РАБОТ940-956

- СООБЩЕНИЯ ДЛЯ АВТОРОВ И ЧИТАТЕЛЕЙ957-958

CONTENTS

ORIGINAL SCIENTIFIC PAPERS

- Vadim L. Khaikov*
Single shot hit probability estimation as a result of the numerical
solution of double integrals using Mathcad739-756
- Srećko R. Stopić, Bernd G. Friedrich*
Leaching of rare earth elements with sulfuric acid from bastnasite ores757-770
- Nataša D. Kuburović, Aleksandar V. Golubović, Ljiljana M. Babinčev*
Development of new smart metal nanomaterials based on
titanium-dioxide for photocatalytic and antimicrobial activities771-835
- Sanja Lj. Korica, Axel Reinköster, Uwe Becker*
Coincidence study of double electron emission associated with
K-shell photoionization of C₆₀836-846
- Leonid I. Gretchikhin*
Negative ions and their role in the development of science
and technology847-863

PROFESSIONAL PAPERS

- Mihailo R. Mrdak*
Analysis of residual stresses in bioinert inorganic plasma sprayed
ceramic coatings864-879
- Ivan A. Tot, Dušan Lj. Bogićević, Mladen B. Trikoš,
Komlen G. Lalović*
Fiware: A Web of things development platform880-899
- Sonja R. Kuljanski Marić*
LDPC codes for physical layer security900-919
- MODERN WEAPONS AND MILITARY EQUIPMENT920-939
Dragan M. Vučković, Miloš M. Jevtić

CALL FOR PAPERS AND INSTRUCTIONS FOR AUTHORS940-956

INFORMATION FOR CONTRIBUTORS AND READERS957-958

ОРИГИНАЛНИ НАУЧНИ ЧЛАНЦИ
ОРИГИНАЛЬНЫЕ НАУЧНЫЕ СТАТЬИ
ORIGINAL SCIENTIFIC PAPERS

SINGLE SHOT HIT PROBABILITY ESTIMATION AS A RESULT OF THE NUMERICAL SOLUTION OF DOUBLE INTEGRALS USING MATHCAD

Vadim L. Khaikov

independent researcher, Krasnodar, Russian Federation,
e-mail: wadimhaikow@inbox.ru,

ORCID iD:  <http://orcid.org/0000-0003-1433-3562>

DOI: 10.5937/vojtehg66-17433; <https://doi.org/10.5937/vojtehg66-17433>

FIELD: Applied Mathematics

ARTICLE TYPE: Original Scientific Paper

ARTICLE LANGUAGE: English

Abstract:

A geometric interpretation of single shot hit probability (P_{hit}) is a volume of the 3D space under the surface $f(y,z)$ described by the bivariate normal distribution and bounded from below by the YOZ plane with the target's contour (T-region). The P_{hit} is proposed to be estimated by a method based on the numerical integration of the double integral. The double integral integrand is the 2D normal distribution of the Y, Z system of random variables. The dispersion characteristics and the coordinates of the dispersion center are known in advance. The limits of the first and the second integral are described by the analytic functions which characterize the geometric shape of the T-region. The implementation of the offered method is as follows: the selected shooting target is partitioned into N geometric subregions and then analytic formula(s) for each subregion's boundaries is/are determined and each double integral is defined. The P_{hit} estimations are produced using a numerical integration in the computer software Mathcad. The results of the calculus of all P_{hit} values (for subregions) are added up (or subtracted) depending on the geometric relationships between the regions. The schema for solving P_{hit} numerically makes it possible to calculate the likelihood for targets with arbitrary geometric shapes and not just for rectangular-shaped silhouettes. For illustrating the operability of the proposed method, the P_{hit} for two kinds of head-type shooting targets has been evaluated. The developed method has been compared with the already existing works.

Key words: hit probability, numerical solution, shooting target, double integrals, shot dispersion, Mathcad.

Introduction

Computational methods for single shot hit probability estimation by shooting to targets were proposed in works (Rodney, 2012), (Svateev, 2014) and (Khaikov & Popovnin, 2018). The problem is solved by using a special tabular function or the mathematical function «*erf*», which is also known as the Gauss error integral (Zwillinger & Kokoska, 2000).

If the target contour is associated with a geometrical *T*-region and if it is replaced by a group of rectangles so that the area of the original *T*-region and the area of a new rectangle group are equal and the sides of all rectangles are parallel to the main dispersion axes, then, in this case, the hit probability of the *T*-region is equal to the sum of hit probabilities each of rectangles obtains after the «replacement» procedure (Abezgauz et al, 1970, pp.162-163), (Vodorezov, 2017, p.332).

The subjective side of the «replacement» method is an uncertainty in the methodology of its conduct, so it is often said that the breakdown of the *T*-region into rectangles is carried out «by eye». For example, in (Rodney, 2012, p.4), where the hit probability for RPG grenades fired at a helicopter is estimated, there is no explanation why the 2D representation of the Boeing CH-47 consists of six rectangles. Quite often in practice, there is a situation where it is necessary to assess hit probabilities for targets with complex contours.

The aim of the article¹ is in the first place to overcome the deficiency of the «replacement» method; and, in the second place, to develop a more accurate path for estimating the single shot hit probability in a target with an arbitrary contour. The main tool for solving this problem will be the double integral² and its geometric and physical interpretations.

The hit probability estimation process

Double integrals for hit probability determination. The calculation of the probability that a bullet (projectile) impacts a target is reduced to computing the hit probability into some region *T* of a complex geometric shape. Let the random point (*Z*, *Y*) in the plane be subject to the normal

¹ This article continues the cycle of works devoted to the use of the MATHCAD computer software for ballistic tasks of small arms and tubed artillery armament.

² It is known that, thanks to the use of the double integral, the area of a geometric figure and a mass of a flat plate with variable density can be calculated as well as the static moment and the center of gravity of a plate and its moment of inertia.

distribution. In this case, the axes of dispersion are parallel to the coordinate axes.

If the T region (letter « T » means a target) is a plane figure, and the probability of hit of the random variables Z and Y is determined by the normal (Laplace-Gauss) distribution $f(z, y)$, then the target hit probability is defined by the formula (1) (Venttsel', 2006, p.196)

$$P[(Z, Y) \in T] = \iint_T f(z, y) dz dy \quad (1)$$

where T – the region of integration in the zy -plane; z, y – the Cartesian coordinates; σ_z, σ_y – the standard deviation of the continuous random variables Z, Y ; m_z, m_y – coordinates of the center of dispersion (the mean of Z and Y); $f(z, y)$ – the integrand and the bivariate normal distribution law:

$$f(z, y) = \frac{1}{2\pi\sigma_z\sigma_y} \exp\left(-\left[\frac{(z - m_z)^2}{2\sigma_z^2} + \frac{(y - m_y)^2}{2\sigma_y^2}\right]\right) \quad (2)$$

The correlation coefficient (r) between Z and Y is 0 (Venttsel', 2006, p.191). In (1), the axes of dispersion are parallel to the coordinate axes.

If the contour of a planar T region is placed in the Cartesian coordinates and bound above and below by functions $y_2 = \varphi_2(z)$, $y_1 = \varphi_1(z)$, and to the left and right by lines $z = a, z = b$ (Fig. 1a), if each point inside T is described by equation $f(z, y)$ with parameters m_z, m_y and σ_z, σ_y (Fig. 1b), then the hit probability in T is determined by the double integral (Piskunov, 1985):

$$\iint_T f(z, y) dz dy = \int_a^b \int_{\varphi_1(z)}^{\varphi_2(z)} f(z, y) dz dy = \int_a^b dz \int_{\varphi_1(z)}^{\varphi_2(z)} f(z, y) dy.$$

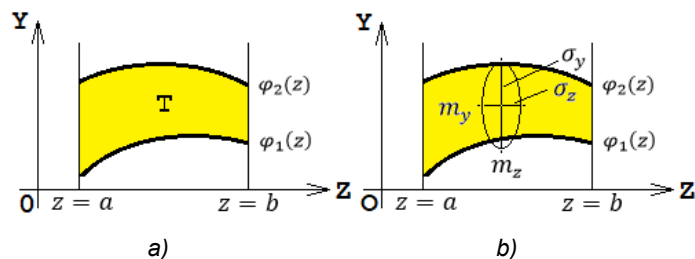


Figure 1 – 2D geometric interpretation of the double integrals (a) and a target hit probability (b)

Рис. 1 – Геометрическая интерпретация двойного интеграла (а) и вероятности попадания (б) в плоские мишени

Слика 1 – Дводимензионално представљање двоструких интеграла (а) и вероватноће поготка циља (б)

The limits of integration for $\varphi_1(z)$ and $\varphi_2(z)$ correspond with the dy . Similarly, the limits of integration a and b correspond with the dz . In this way

$$P[(Z, Y) \subset T] = \frac{1}{2\pi\sigma_z\sigma_y} \int_a^b \int_{\varphi_1(z)}^{\varphi_2(z)} \exp\left(-\left[\frac{(z - m_z)^2}{2\sigma_z^2} + \frac{(y - m_y)^2}{2\sigma_y^2}\right]\right) dz dy.$$

The geometric interpretation of target hit probability is the volume under a surface $f(y, z)$ ($A'B'C'D'E'F'$ region), which is a part of the bivariate normal distribution, limited from below the YOZ-plane the part of which the target contour borders ($ABCDEF$ is the T -region).

A three-dimensional geometric interpretation of hit probability is shown in Figure 2a. Figure 2b shows that the volume of the 3D-figure ($A'B'C'D'E'F'FABCDEF$) is equal to the hit probability in a target, the shape of which is equal to the base of the 3D-figure ($ABCDEF$ polygon = T region).

In the case that the calculation of the double integral is performed with respect to the OY axis, it is necessary to consider the following calculation scheme (Fig. 3). If the region T is correct in the direction of the OZ axis, then (Piskunov, 1985)

$$\iint_T f(z, y) dz dy = \int_c^d \left(\int_{f_1(y)}^{f_2(y)} f(z, y) dz \right) dy,$$

where $z = f_1(y)$, $z = f_2(y)$ are the equations of the curves that bound the region T to the left and to the right, respectively. The segment $[c; d]$ is the projection of the region T onto the axis OY .

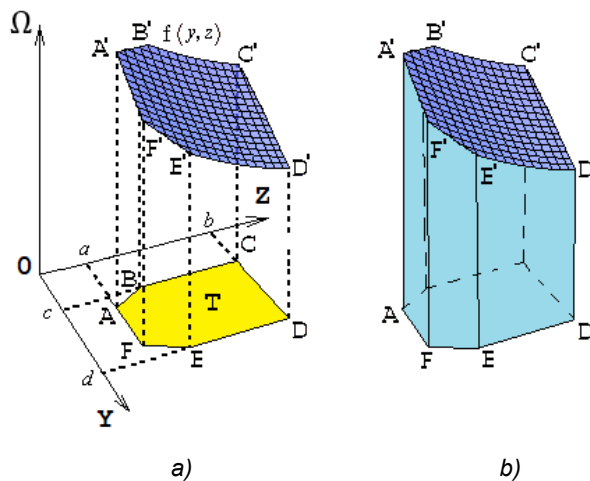


Figure 2 – 3D geometric interpretation of hit probability
 Рис. 2 – Пространственная геометрическая интерпретация вероятности попадания в цель
 Слика 2 – Тростандимензионално представљање вероватноће поготка

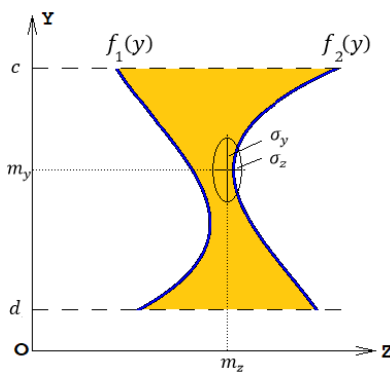


Figure 3 – The scheme for calculating a double integral with respect to the OY axis
 Рис. 3 – Схема вычисления двойного интеграла относительно оси OY
 Слика 3 – Шема за израчунавање двоструког интеграла у односу на OY осу

A general region T has the property of «correctness» in the direction of the axis OY (OZ) if any line passing through any interior point of this

region (T) is parallel to the axis OY (OZ) and intersects each of the two boundaries of the region at only one point, and each of the intersected boundaries is specified by one equation.

In addition, the following conditions must be fulfilled (see Fig. 1-3):

for OY axis (Fig. 3) $T = \{(z,y) | c \leq y \leq d, f_1(y) \leq z \leq f_2(y)\}$

for OZ axis (Fig. 1) $T = \{(z,y) | a \leq y \leq b, \varphi_1(z) \leq y \leq \varphi_2(z)\}$.

The triangle shows the point of the intersection of a line with the axis OY (OZ). The squares are the points of the intersection of a line with the functions $f_1(y)$, $f_2(y)$ or $\varphi_1(z)$, $\varphi_2(z)$.

A hit probability estimation algorithm. The basic algorithm of a hit probability numerical assessment consists of the following procedures:

- 1) the beginning;
- 2) to define the Cartesian coordinates (origin point, OZ axis, OY axis);
- 3) to construct the contour of the shooting target (T region);
- 4) to find the coordinates of the target contour;
- 5) to find an analytical expression of the boundaries of the target F_1, F_2 or ϕ_1, ϕ_2 ;
- 6) to describe the rectangle near the target (main rectangle);
- 7) to determine the location of the point of impact (POI) m_z, m_y ;
- 8) to determine the characteristics of the dispersion ellipse σ_z, σ_y ;
- 9) to calculate the hit probability in the basic rectangle ($P_{hit\ basic}$);
- 10) to determine the number of subregions N (for subtraction from the basic rectangle);
 - for each subregion j ($j \leq N$):
 - 11) to determine the limits for numerical integration;
 - 12) to solve numerically the inner integral;
 - 13) to solve numerically the outer integral and to get the hit probability of a subregion;
- 14) to sum the hit probabilities of all subregions to get the hit probability of subfigures ($P_{hit\ subreg} = P_{hit\ reg\ 1} + P_{hit\ reg\ i} + P_{hit\ reg\ N}$);
- 15) $P_{hit} = P_{hit\ basic} - P_{hit\ subreg}$;
- 16) the end.

If the shooting target is a figure symmetrical around the OY axis, then all of the above mentioned actions (of the basic algorithm) are performed with only one half of it. Only the left or the right part of the geometrical figure must be selected. To get the final hit probability, the number is multiplied by 2.

Hit probability of 2D head targets. Calculate the single shot hit probability if the sniper fires to the static head target, which is limited by 1, 2 types of military shooting targets. The distance between the target and the marksman is 400 m. The median deviations of the shot dispersion are expressed by the following dependence $B_h = B_d = 0.06$ m ($B_h=B_y$; $B_z=B_d$). The coordinates of the POI represent the midpoint of the target. Estimate the hit probability for the head target of the first and second types. The dimensions of the targets are shown in Fig. 4. The target dimensions are given in meters. Both targets simulate a human head in a protective military helmet. The OX axis is the horizontal distance from the OZ axis to the target direction (line OC).

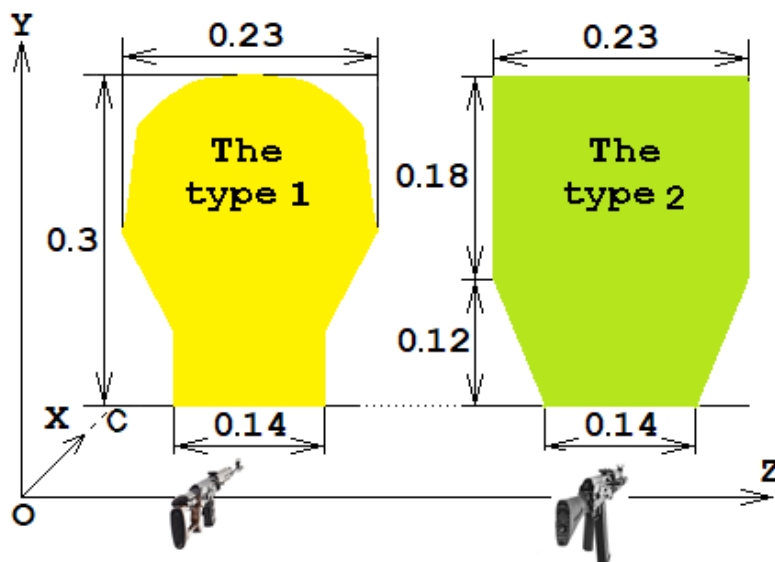


Figure 4 – Two types of 2D head shooting targets in the Cartesian coordinates YOZ
 Рис. 4 – Два типа плоских стрелковых головных мишеней в декартовых координатах YOZ
 Слика 4 – Два типа 2Д мета у облику главе у Декартовом координатном систему YOZ

The characteristics of the dispersion ellipse (semi-major and semi-minor axes) will be determined as a probable error (B) in meters. This dispersion characteristic, along with the standard deviation (σ), is used often in the theory of shooting. For normal distribution, the relationship between σ and B is

$$B = 0.6745 \sigma \quad \text{or} \quad \sigma = 1.4826 B .$$

The probable error height is characterized by B_h and the probable error deflection – B_d .

The contour of the targets is indicated using numbers. The points of the rectangle, inside which the target is located, are indicated using letters.

The contour of the head target of type 1 consists of 12 points: 1-2-3-4-5-6-7-8-9-10-11-12 (Fig. 5a). The dimensions of the targets (Fig. 5) are given in meters.

Points 6, 12 of the type 1 target belong to the axis of symmetry $O'Y'$ (1-2-3-4-5-6 + 6-7-8-9-10-11-12) (Fig. 5a). Therefore, the calculation will be conducted with the left half of this figure (points 12-1..6). The coordinates of the points for the contour line and the analytic functions of its elements for the head target of type 1 are collected in Table 1. The sign «cross» (Fig. 5a) means the position of the POI.

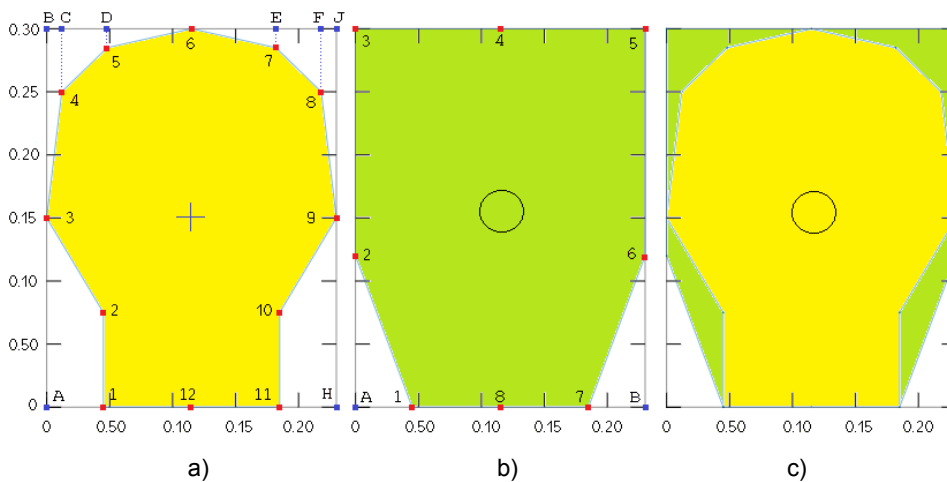


Figure 5 – The contour of the 2D head target type 1 (a), type 2 (b) and their comparison (c)

Рис. 5 – Контур плоской головной мишени типа 1 (а), типа 2 (б) и их сравнение (с)
Слика 5 – Контуре 2Д мета у облику главе типа 1 (а), типа 2 (б) и њихово поређење (ц)

The contour of the type 2 head target consists of 8 points (Fig. 5b). Points 4, 8 of the type 2 head target belong to the axis of symmetry $O'Y'$. So, the calculation will be conducted with the left half of this figure (points 1-6, 12). The coordinates of the points for the contour line and the analytic functions of its elements for the type 1 head target are collected in Table 3.

Table 1 – Coordinates of the points for the contour line for the head target of type 1
 Таблица 1 – Координаты точек контура мишени типа 1
 Табела 1 – Координате тачака контурне линије мете у облику главе типа 1

No. of points	Z, m	Y, m	Boundary points of line	Analytic function (Equation of a straight line)
1	0.045	0.000	1-2	$z(y) = 0.045$
2	0.045	0.075	2-3	$y(z) = -1.6667z + 0.15$
3	0.000	0.150	3-4	$y(z) = 8.3333z + 0.15$
4	0.012	0.250	4-5	$y(z) = 0.97222z + 0.23833$
5	0.048	0.285	5-6	$y(z) = 0.22388z + 0.27425$
6	0.115	0.300	6-7	$y(z) = -0.22388z + 0.32575$
7	0.182	0.285	7-8	$y(z) = -0.97222z + 0.46194$
8	0.218	0.250	8-9	$y(z) = -8.3333z + 2.06667$
9	0.230	0.150	9-10	$y(z) = 1.6667z - 0.23333$
10	0.185	0.075	10-11	$z(y) = 0.185$
11	0.185	0.000	11-12	$y(z) = 0$
12	0.115	0.000	12-1	$y(z) = 0$

Notes: the coordinates of the points are given according to Fig. 5a.
 The symmetry of the points is shown by the orange and green background.

Table 2 – Coordinates of the points for the contour line for the head target of type 2
 Таблица 2 – Координаты точек контура мишени типа 2
 Табела 2 – Координате тачака за контурну линију мете у облику главе типа 2

No. of points	Z, m	Y, m	Boundary points of line (of curves)	Analytic function (Equation of a straight line)
1	0.045	0.000	1-2	$y(z) = -0.26667z + 0.012$
2	0.000	0.012	2-3	$z(y) = 0$
3	0.000	0.300	3-4	$y(z) = 0.3$
4	0.115	0.300	4-5	$y(z) = 0.3$
5	0.230	0.300	5-6	$z(y) = 0.23$
6	0.230	0.012	6-7	$y(z) = 0.26667z - 0.04933$
7	0.185	0.000	7-8	$y(z) = 0$
8	0.115	0.000	8-1	$y(z) = 0$

Notes: the coordinates of the points are made according to Fig. 5b.
 The symmetry of the points is shown by the orange and green background.

A comparison of the forms of the type 1 target and the type 2 target is shown in Fig. 5c.

One sigma dispersion circle³ (zone) is shown in Figures 5b and 5c.

³ Dispersion area has the form of a circle because $\sigma_y = \sigma_z$ but in the case of $\sigma_y \neq \sigma_z$, it would be a dispersion ellipse.

The result of dividing the half of the type 1 target into four sections, the determination of five double integrals and the numerical computations of the double integrals are given in Table 3. The first double integral (region AB-6-12) describes the hit probability into a rectangle inside which there is 50% of the target contour.

The characteristics of the dispersion and the dispersion center are indicated in Table 3 after «Notes». The unit of measure is the meter.

*Table 3 – Characteristics of the base region and sub-regions for the type 1 target
Таблица 3 – Характеристики базовой области и подобластей мишени типа 1
Табела 3 – Карактеристике основне области и подобласти за metu типа 1*

No. of regions	Hit probabilities for regions	Hit probability as an expression with the double integral	Numerical estimation of hit probability
1. AB-6-12	$P_{hit_{basic}^{type1}}$	$\int_0^{0.115} \int_0^{0.3} f(z, y) dz dy$	0.266
2. A-3-2-1	$P_{hit_1^{type1}}$	$\int_0^{0.045} \int_0^{-1.6667 \cdot z + 0.15} f(z, y) dz dy$	0.027
3. 3-BC-4	$P_{hit_2^{type1}}$	$\int_0^{0.012} \int_{8.333 \cdot z + 0.15}^{0.3} f(z, y) dz dy$	2.3e-3
4. 4-CD-5	$P_{hit_3^{type1}}$	$\int_{0.012}^{0.048} \int_{0.97222 \cdot z + 0.23833}^{0.3} f(z, y) dz dy$	1.561e-3
5. 5-D-6	$P_{hit_4^{type1}}$	$\int_{0.048}^{0.115} \int_{0.22388 \cdot z + 0.27425}^{0.3} f(z, y) dz dy$	8.684e-4
Notes: $m_y = 0.115$ m; $m_z = 0.15$ m; $\sigma_y = \sigma_z = 1.4826 \cdot 0.06 = 0.089$ m. The numerical integration was performed due to computer algebra systems (CAS) Mathcad 15			

The probability of hitting the type 1 target is determined by the formula

$$P_{hit} = 2 \left[P_{hit_{basic}^{type1}} - \sum_{i=1}^4 P_{hit_i^{type1}} \right].$$

Substituting the data from Table 3 into the formula, we obtain the required hit probability.

$$P_{hit_{type1}} = 2 \cdot (0.266 - (0.027 + 2.3 \cdot 10^{-3} + 1.561 \cdot 10^{-3} + 8.684 \cdot 10^{-4})) = 0.468.$$

$$P_{hit_{type1}} = 46.8 \%$$

An estimate of the hit probability for a target of type 2 is carried out in a similar way. The result of dividing the half of the type 2 target into two sections, the determination of two double integrals and the numerical computations of the double integrals are given in Table 4.

*Table 4 – Characteristics of the base region and sub-regions for the type 2 target
Таблица 4 – Характеристики базовой области и подобластей мишени типа 2
Табела 4 – Карактеристике основне области и подобласти за мету типа 2*

No. of regions	Hit probabilities for regions	Hit probability as an expression with the double integral	Numerical estimation of hit probability
1. A-3-4-6	$P_{hit_{basic}^{type2}}$	$\int_0^{0.115} \int_0^{0.3} f(z, y) dz dy$	0.266
2. A-2-1	$P_{hit_1^{type2}}$	$\int_0^{0.045} \int_0^{-2.6667 \cdot z + 0.12} f(z, y) dz dy$	0.029
Notes: $m_y = 0.115$ m; $m_z = 0.15$ m; $\sigma_y = \sigma_z = 1.4826 \cdot 0.06 = 0.089$ m. The numerical integration was performed due to CAS Mathcad 15.			

The characteristics of the dispersion and the dispersion center by firing at targets of both type 1 and 2 are the same.

The hit probability for the type 2 target is determined by the formula:

$$P_{hit_{type2}} = 2 \left[P_{hit_{basic}^{type2}} - P_{hit_1^{type2}} \right] = 2 \cdot (0.266 - 0.029) = 0.474 \text{ or } 47.4\%.$$

The performed calculations have shown that with the identical dispersion characteristics and the identical location of the POI, the hit probability of the target 1 (46.8%) is less than the hit probability of the target 2 (47.4%). This fact is explained by the fact that the target area 2 is larger than the target area 1. This phenomenon is explained by the fact that the area of the target 2 is larger than the area of the target 1 (see Fig. 5c).

In this situation, the method of calculation gave an adequate result. The second test for the calculation method will relate to its solving despite a known result.

Verification by the comparison with the already existing, previously determined results. In order to verify the method developed in this article, we will perform 3 variants of hit probability estimates. As an example, we use the problem given in (Venttsel', 2006, p.197).

Shooting is carried out at a rectangular target of 9×12 (meters). The projectile dispersion characteristics are defined as probable errors: in the

longitudinal direction $B_y = 10$ m, in the lateral direction $B_z = 5$ m. The point of aiming (POA) is the center of the considered rectangular target. Thus the POA has the coordinates (0; 0). In view of the presence of shooting errors, the mean point of impact is displaced relative to the POA. The coordinates of the POI are (0; -4). Find the single shot hit probability.

The points (-4.5; -6), (-4.5; 6), (4.5; 6), (4.5; -6) are the four vertices of a rectangular target. The dispersion characteristics are expressed in the form of standard deviations (SD). The SD in the longitudinal direction is $\sigma_y = 1.4826 \cdot B_y = 14.826$ m. The SD in the lateral direction is $\sigma_z = 1.4826 \cdot B_z = 7.413$ m. Since the coordinates of the center of dispersion (namely the POI) are known, then $m_y = -4$, and $m_z = 0$.

Variant of calculation 1 uses a formula for the estimation of hit probability for the rectangle (Venttsel', 2006, p.197).

Let us write down the target hit probability formula into a rectangle (R -area), the dispersion axes of which are parallel to the sides of the rectangle (Germershausen, 1977, p.193):

$$P_{hit} [(Z, Y) \subset R] = \left[F\left(\frac{b - m_z}{\sigma_z}\right) - F\left(\frac{a - m_z}{\sigma_z}\right) \right] \cdot \left[F\left(\frac{d - m_y}{\sigma_y}\right) - F\left(\frac{c - m_y}{\sigma_y}\right) \right]. \quad (3)$$

$$P_{hit} [(Z, Y) \subset R] = \left[F\left(\frac{b - m_z}{\sigma_z}\right) - F\left(\frac{a - m_z}{\sigma_z}\right) \right] \cdot \left[F\left(\frac{d - m_y}{\sigma_y}\right) - F\left(\frac{c - m_y}{\sigma_y}\right) \right].$$

where $F(x)$ – the cumulative distribution function (CDF) of the standard normal distribution (Germershausen, 1977, p.193):

$$F(x) = \frac{1}{\sqrt{2\pi}} \int_{-\infty}^x \exp\left(-\frac{1}{2}t^2\right) dt.$$

In formula 3: m_y, m_z – the coordinates of the center of dispersion; σ_y, σ_z – the standard deviation; a, b, c, d – the borders of the target-rectangle sides, herewith $c \leq y \leq d, a \leq z \leq b$.

Taking into account the previously defined values, formula 3 is transformed into the form:

$$\begin{aligned}
 P_{hit} [(Z, Y) \subset R] &= \left[F\left(\frac{b}{\sigma_z}\right) - F\left(\frac{a}{\sigma_z}\right) \right] \cdot \left[F\left(\frac{d - m_y}{\sigma_y}\right) - F\left(\frac{c - m_y}{\sigma_y}\right) \right] = \\
 &= \left[F\left(\frac{4.5}{7.413}\right) - F\left(\frac{-4.5}{7.413}\right) \right] \cdot \left[F\left(\frac{6 - (-4)}{14.826}\right) - F\left(\frac{-6 - (-4)}{14.826}\right) \right] = \\
 &= \left[F\left(\frac{4.5}{7.413}\right) - F\left(\frac{-4.5}{7.413}\right) \right] \cdot \left[F\left(\frac{10}{14.826}\right) - F\left(\frac{-2}{14.826}\right) \right] = \\
 &= [F(0.60704) - F(-0.60704)] \cdot [F(0.67449) - F(-0.1349)] = \\
 &= [0.728088 - 0.271912] \cdot [0.75 - 0.446345] = 0.13852.
 \end{aligned}$$

So P_{hit} by shooting with the above mentioned projectile dispersion parameters is 13.85 %.

Variant of calculation 2 is based on the mathematical function «*erf*» (Khaikov & Popovnin, 2018). The error function is defined (Zwillinger & Kokoska, 2000, p.516) by

$$erf(x) = \frac{1}{\sqrt{\pi}} \int_0^x \exp(-t^2) dt.$$

There is a following relation between the cumulative distribution function $F(x)$ of the standard normal distribution and the function «*erf*» (Zwillinger & Kokoska, 2000, p.517):

$$F(x) = \frac{1}{2} \left[1 + erf\left(\frac{1}{\sqrt{2}}x\right) \right].$$

Therefore, formula 3 is transformed into the form (Khaikov & Popovnin, 2018)

$$P_{hit} = \frac{1}{4} \left[erf\left(\frac{b - m_z}{\sqrt{2}\sigma_z}\right) - erf\left(\frac{a - m_z}{\sqrt{2}\sigma_z}\right) \right] \cdot \left[erf\left(\frac{d - m_y}{\sqrt{2}\sigma_y}\right) - erf\left(\frac{c - m_y}{\sqrt{2}\sigma_y}\right) \right].$$

Taking into account the data given in the task, we obtain

$$P_{hit} = \frac{1}{4} \left[erf\left(\frac{b}{\sqrt{2}\sigma_z}\right) - erf\left(\frac{a}{\sqrt{2}\sigma_z}\right) \right] \cdot \left[erf\left(\frac{d - m_y}{\sqrt{2}\sigma_y}\right) - erf\left(\frac{c - m_y}{\sqrt{2}\sigma_y}\right) \right].$$

Substitute the initial data in the formula and perform the estimation

$$P_{hit} = \frac{1}{4} \left[\operatorname{erf} \left(\frac{4.5}{\sqrt{2} \cdot 7.413} \right) - \operatorname{erf} \left(\frac{-4.5}{\sqrt{2} \cdot 7.413} \right) \right] \cdot \left[\operatorname{erf} \left(\frac{6 - (-4)}{\sqrt{2} \cdot 14.826} \right) - \operatorname{erf} \left(\frac{-6 - (-4)}{\sqrt{2} \cdot 14.826} \right) \right] = 0.13852.$$

The results of the calculations for versions 1 and 2 are the same.

Variant of calculation 3 uses a numerical integration of the double integral.

The purpose of this comparison is to show the universality of the developed method for calculating the hit probability for targets of rectangular shapes as well as for targets with arbitrary contours.

For a shooting target with a rectangular shape, we write the double integral

$$P_{hit} = \frac{1}{2\pi\sigma_z\sigma_y} \int_a^b \int_{\varphi_1(z)}^{\varphi_2(z)} f^*(z, y) dz dy = \frac{1}{2\pi\sigma_z\sigma_y} \int_{-4.5}^{4.5} dz \int_{-6}^6 f^*(z, y) dy,$$

$$f^*(z, y) = \exp \left(- \left[\frac{(z-0)^2}{2\sigma_z^2} + \frac{(y-(-4))^2}{2\sigma_y^2} \right] \right).$$

For numerical integration, we use the possibilities of the computer software Mathcad 15. The Mathcad code is below. All variables have been described previously.

$$\begin{array}{lllll} a := -4.5 & b := 4.5 & c := -6 & d := 6 & TOL := 0.0001^4 \\ m_y := -4 & m_z := 0 & \sigma_y := 14.826 & \sigma_z := 7.413 & \end{array}$$

$$\frac{1}{2\pi} \frac{1}{\sigma_z} \frac{1}{\sigma_y} \int_a^b \int_c^d \exp \left[- \left[\frac{(z-m_z)^2}{2\sigma_z^2} + \frac{(y-m_y)^2}{2\sigma_y^2} \right] \right] dy dz = 0.139.$$

As in the first two cases, we obtained a single shot hit probability, which is 0.139 or 13.9%.

⁴ The accuracy of the calculation in the Mathcad software is determined by the value of the system variable TOL, which is equal to 0.001 by default.

The coordinates m_y , m_z of the POI for rifles and pistols can be obtained by calculating the «average trajectory» (Khaikov, 2018). For example, for a sniper rifle SVD-63 (7.62mm Dragunov sniper rifle) the results of the work (Khaikov, 2017) can be used.

Conclusion

A geometric interpretation of single shot hit probability of a target is the volume under a surface $f(y,z)$, which is described by a bivariate normal distribution and limited from below the YOZ plane with a target contour (T -region).

The hit probability (P_{hit}) is preferably to be estimated by the numerical integration of the double integral. The integrand of the double integral is the two-dimensional normal distribution of a system of random variables Y and Z . The dispersion characteristics and the coordinates of the dispersion center are known in advance. The limits of two integrals are described by the analytic functions characterizing the geometric shape of the target boundaries.

The developed schema for the numerical solution of the P_{hit} makes it possible to calculate the probability for targets with arbitrary geometric shapes.

The estimation of the hit probability for the type 1 and type 2 head targets, if the coordinates of the POI represent the target midpoint and $B_y = B_z = 0.06$ m, is as follows: it is 46.8% for the type 1 target and 47.4% for the type 2 target. The P_{hit} estimations are produced using numerical integration in the computer application *Mathcad*.

The developed method was compared with the already existing works and was verified by hit probability calculations for two types of head shooting targets. The result of the comparison is a difference in the third digit after the decimal point.

References

- Abezgauz, G.G., Tron', A.P., Kopenkin, Yu.N. & Korovina, I.A. 1970. Spravochnik po veroyatnostnym raschetam. Moscow: Voennoye izdatel'stvo ministerstva oborony SSSR (in Russian). (In the original: Абезгауз, Г.Г., Тронь А.П., Копенкин Ю.Н., Коровина И.А. 1970. Справочник по вероятностным расчётам. Москва: Военное издательство министерства обороны СССР).
- Germershausen, R. (ed.) 1977. *Rheinmetall Waffentechnisches Taschenbuch*. Düsseldorf: Rheinmetall GmbH (in German).

Khaikov, V.L. 2017. Ballistical mathematical model of the Dragunov sniper rifle based on a ballistic coefficients estimation using tabular firing table data. *Military Enginery, Counter-terrorism technical devices*, 16(11-12/113-114), pp.16-23 (in Russian).

Khaikov, V.L. 2018. Improvement of longitudinal motion description for axisymmetric body due to the functional ballistical matrix. *Electronic Information Systems*, 2(17), pp.101-115 (in Russian).

Khaikov, V.L., & Popovnin, Y.M. 2018. Using mathematical software Microsoft Excel, Matlab/Octave for hit-probability assessment in standard shooting-targets. *Military Enginery, Counter-terrorism technical devices*, 16(3-4/117-118), pp.96-103 (in Russian).

Piskunov, N.S. 1985. *Differentsial'noye i integral'noye ischisleniya*. Tom 2. Moscow: Nauka (in Russian). (In the original: Пискунов Н.С. 1985. *Дифференциальное и интегральное исчисления*. Том 2. Москва: Наука).

Rodney, S. 2012. RPG encounter modeling. *SURVIAC Bulletin*, 27(1), pp.1-5.

Svateev, V.A. 2014. Tochnyy sposob raschota veroyatnosti popadaniya v figurnyuyu tsel'. *Bulletin of the Academy of Military Sciences*, 49(4), pp.61-66 (in Russian). (In the original: Сватеев В.А. 2014. Точный способ расчёта вероятности попадания в фигурную цель. Вестник Академии военных наук. 2014. Т. 49, № 4. С. 61-66.)

Venttsel', Ye.S. 2006. *Teoriya veroyatnostey*. Moscow: Vysshaya shkola (in Russian). (In the original: Вентцель Е.С. 2006. *Теория вероятностей*. Москва: Высшая школа).

Vodorezov, Yu.G. 2017. *Teoriya i praktika strel'by iz narezного dlinnostvol'nogo strelkovogo oruzhiya*. Chast' 1. Moscow: Moskovskiy Gosudarstvennyy Tekhnicheskiy Universitet (in Russian). (In the original: Водорезов, Ю.Г. 2017. *Теория и практика стрельбы из нарезного длинноствольного стрелкового оружия*. Часть 1. Москва: Московский Государственный Технический Университет).

Zwillinger, D., & Kokoska, S. 2000. *Standard Probability and Statistics tables and formulae*. London - New York: Chapman & Hall CRC.

ОЦЕНКА ВЕРОЯТНОСТИ ПОПАДАНИЯ В МИШЕНЬ
ОДИНОЧНЫМ ВЫСТРЕЛОМ КАК РЕЗУЛЬТАТ ЧИСЛЕННОГО
ИНТЕГРИРОВАНИЯ МАТЕМАТИЧЕСКОГО ВЫРАЖЕНИЯ С
ДВОЙНЫМ ИНТЕГРАЛОМ В ПРОГРАММЕ MATHCAD

Вадим Л. Хайков,
независимый исследователь, г. Краснодар, Российская Федерация

ОБЛАСТЬ: прикладная математика
ВИД СТАТЬИ: оригинальная научная статья
ЯЗЫК СТАТЬИ: английский

Резюме:

Вероятность попадания одиночным выстрелом в цель предложено оценивать формулой, основу которой составляет двойной интеграл. Подынтегральная функция описывает двумерное рассеивание системы случайных величин Y, Z с заранее заданными параметрами координат рассеивания и среднеквадратических отклонений по направлениям Y, Z . Пределы интегрирования описывают геометрическую форму стрелковой мишени и являются аналитическими функциями границ мишени. В статье предложен алгоритм решения задачи оценки вероятности попадания, который позволяет вычислять вероятности попадания в мишени произвольной геометрической формы. На первом шаге алгоритма производится разбиение цели на N геометрических подобластей. Далее для каждой из подобластей записывается двойной интеграл и с помощью численного интегрирования получают его количественную оценку. Далее результаты вычислений (вероятности попаданий в подобласти) складываются (вычитаются). С целью численного интегрирования двойного интеграла использована среда математических вычислений *Mathcad*. Для иллюстрации работоспособности предложенного метода приведены расчёты определения вероятности попадания в головную цель двух видов.

Ключевые слова: вероятность попадания, численное решение, стрелковая мишень, двойной интеграл, рассеивание пуль, *Mathcad*.

**ПРОЦЕНА ВЕРОВАТНОЋЕ ПОГАЂАЊА ЦИЉА ЈЕДНИМ ХИЦЕМ
КАО РЕЗУЛТАТ НУМЕРИЧКОГ РЕШАВАЊА ДВОСТРУКИХ
ИНТЕГРАЛА ПОМОЋУ МАТНСАD-а**

Вадим Л. Хајков
независни истраживач, Краснодар, Руска Федерација

ОБЛАСТ: примењена математика
ВРСТА ЧЛАНКА: оригинални научни чланак
ЈЕЗИК ЧЛАНКА: енглески

Сажетак:

Вероватноћа поготка циља једним хицем представља се геометријски запремином испод површине $f(y,z)$ која је описана биваријантном нормалном расподелом ограниченом контуром циља (област T) испод равни YOZ . Предлаже се да се вероватноћа поготка (P_{hit}) процењује методом заснованим на нумеричкој интеграцији двоструког интеграла. Интегранд двоструког интеграла је дводимензионална нормална расподела система случајних варијабли Y и Z . Карактеристике растурања и

координате центра растурања познате су унапред. Границе два интеграла описане су аналитичким функцијама које карактеришу геометријски облик контура циља. Изабрани циљ се прво дели на N геометријских подобласти, а затим се за границе сваке од њих одређују аналитичке формуле и пише двоструки интеграл. Вероватноћа поготка процењује се нумеричком интеграцијом у *Mathcad*-у. Резултати израчунавања свих вероватноћа поготка (свих подобласти) сабирају се или одузимају, зависно од геометријских односа између подобласти. Шема нумеричког израчунавања вероватноће поготка омогућава израчунавање вероватноће за мете произвољног геометријског облика, а не само за правоугаоне мете. Да би се илустровала операбилност предложеног метода, процењена је вероватноћа поготка за две врсте мета у облику главе. Предложени метод упоређен је с резултатима већ постојећих радова.

Кључне речи: вероватноћа поготка, нумеричко решавање, мета, двоструки интеграл, растурање погодака, *Mathcad*.

Paper received on / Дата получения работы / Датум пријема чланка: 14.05.2018.
 Manuscript corrections submitted on / Дата получения исправленной версии работы / Датум достављања исправки рукописа: 22.06.2018.
 Paper accepted for publishing on / Дата окончательного согласования работы / Датум коначног прихватања чланка за објављивање: 24.06.2018.

© 2018 The Author. Published by Vojnotehnički glasnik / Military Technical Courier (www.vtg.mod.gov.rs, втг.мо.упр.срб). This article is an open access article distributed under the terms and conditions of the Creative Commons Attribution license (<http://creativecommons.org/licenses/by/3.0/rs/>).

© 2018 Автор. Опубликовано в «Военно-технический вестник / Vojnotehnički glasnik / Military Technical Courier» (www.vtg.mod.gov.rs, втг.мо.упр.срб). Данная статья в открытом доступе и распространяется в соответствии с лицензией «Creative Commons» (<http://creativecommons.org/licenses/by/3.0/rs/>).

© 2018 Аутор. Објавио Војнотехнички гласник / Vojnotehnički glasnik / Military Technical Courier (www.vtg.mod.gov.rs, втг.мо.упр.срб). Ово је чланак отвореног приступа и дистрибуира се у складу са Creative Commons лиценцом (<http://creativecommons.org/licenses/by/3.0/rs/>).



LEACHING OF RARE EARTH ELEMENTS WITH SULFURIC ACID FROM BASTNASITE ORES

Srećko R. Stopić^a, Bernd G. Friedrich^b

RWTH Aachen University, IME Process Metallurgy and Metal Recycling, Aachen, Federal Republic of Germany

^a e-mail: sstopic@ime-aachen.de,

ORCID iD: <http://orcid.org/0000-0002-1752-5378>

^b e-mail: bfriedrich@ime-aachen.de,

ORCID iD: <http://orcid.org/0000-0002-2934-2034>

DOI: 10.5937/vojtehg66-17177; <https://doi.org/10.5937/vojtehg66-17177>

FIELD: Chemical Technology

ARTICLE TYPE: Original Scientific Article

ARTICLE LANGUAGE: English

Summary:

Dissolution of rare earth elements from bastnasite ores was studied using sulfuric acid at the atmospheric pressure. The one step strategy with sulfuric acid was studied further and the results showed that filtering difficulties do not happen for the chosen parameter combinations. Furthermore, the best parameter combinations were those with low temperatures and low acid concentrations. All in all, direct leaching is a simple process that uses the cheapest acid on the market and offers good leaching recoveries. Attention should be given to the formation of gel, especially when taking the process to the large scale, and the subsequent elimination of Ca from the leachate.

Key words: rare earth elements, hydrometallurgy, bastnasite, sulfuric acid.

Introduction

Rare earth elements are a group of metallic elements of the periodic table, often overlooked, but very significant in today's industrial landscape and modern lifestyle. Like other metals, rare earths are silvery-gray, malleable, ductile, and conduct electricity.

ACKNOWLEDGMENTS: The research leading to these results has received funding from the European Community's Seventh Framework Programme (Call identifier FP7-NMP-2012-LARGE-6) under grant agreement n°309373. This publication reflects only the author's view, exempting the Community from any liability. Project website: www.eurare.eu. We would like to thank FEN Minerals, Norway, for sending their Rodberg sample and for their discussion in our experimental work.

They appear in nature in the form of oxides and other compounds, but with one particularity – the chemical similarity between all of them is so astounding that they all occur together in their bearing minerals, substituting one another at the molecular level (Gupta& Krishnamurthy, 2005), (Castor et al, 2006, pp.769-792).

Europe has never been known for having rich and substantial rare earth deposits; they do, however, exist in the continent's northern area, especially in the Scandinavian countries. As lower grade ores and different mineral formations are coming into the focus of industrial interest, many research projects have been set up. The European Commission has been willing to participate in these efforts through the EURARE project, aimed at setting "the basis for the development of a European Rare Earth Element industry" and to "safeguard the interrupted supply of rare earth raw materials and products crucial to sectors of the EU economy". (Chen, 2011, pp.1-6)

Bastnasite ((La,Ce)CO₃F is a fluorocarbonate of the cerium group found in ore deposits, metamorphic zones and pegmatites. In average, it contains 70% rare earth oxides (most of them belonging to the light fraction), particularly lanthanum, cerium and neodymium (Rare Earth Elements, British Geological Survey). The amount of thorium present in the mineral is negligible. This mineral is the primary source of rare earth oxides in Bayan Obo, China and Mountain Pass, California, the two most world-relevant rare earth mining complexes (Hoshino et al, 2016, pp.129-291). At the Mountain Pass Mine in California and the Bayan Ono mine in China, bastnasite concentrate containing between 60 -70% REO is commercially processed via a calcination/HCl leach route to recover the rare earth elements.

The sulfuric acid leaching process was studied for processing roasted ore of Dechang bastnasite in Sichuan, China, in order to obtain rare earth elements (Feng et al, 2013, pp.849-854). Using particle size (0.074-0.100mm), 1.5 mol/L sulfuric acid concentration, mass ratio of liquid to solid 8 and stirring speed of 500 rpm, the reaction rate of the leaching process can be controlled by diffusion through the product/ash layer, as described by the shrinking-core model, and the calculated activation energy of 9.97, which is typical for a diffusion controlled process.

Geological surveys carried out in Norway have revealed the existence of a rare earth deposit south west of Oslo, and one of its ores, named Rodberg, is thought to be an especially promising source of rare earth elements. The chemical nature and the grain size of Rodberg's bastnasite minerals are however quite different from those of other ores

being currently exploited, which is why Rodberg requires a custom-made process for rare earth recovery. Traditional rare earth ore processing methods are due to Rodberg’s mineralogical characteristics not easily applicable and have been discarded. The reason for this is the low grain size of Rodberg’s rare earth bearing minerals within the rock formation (Balomenos et al, 2017, pp.142-153). The grain size of rare earth bearing minerals determines whether it is easy or not to obtain a rare earth concentrate through physical separation from other minerals of low value. The first step in separating the minerals is known as mineral liberation: ores are ground in order for rare earth minerals to become detached from the rest of the ore material. The rare earth minerals such as eudialyte and steenstrupine can be then separated from the ore and the result is a rare earth physical concentrate. Working with a concentrate in further processing steps increases the efficiency of leaching and chemical treatment, and is the way extraction methods have been traditionally designed. Two alternative processing possibilities have been proposed for the treatment of bastnasite ore, both of them related to the high presence of iron oxides in the ore.

1) The first of these processing possibilities consists of conducting direct leaching. Since Rodberg is formed by a matrix of iron oxides in which the rare earth elements – carbonates – are embedded, acids are expected to attack the rare earth minerals more readily than the more stable iron oxide matrix. This means that it would be possible to reduce acid consumption as well as the excess dissolution of unwanted species in the leaching operation without the need of a concentrate.

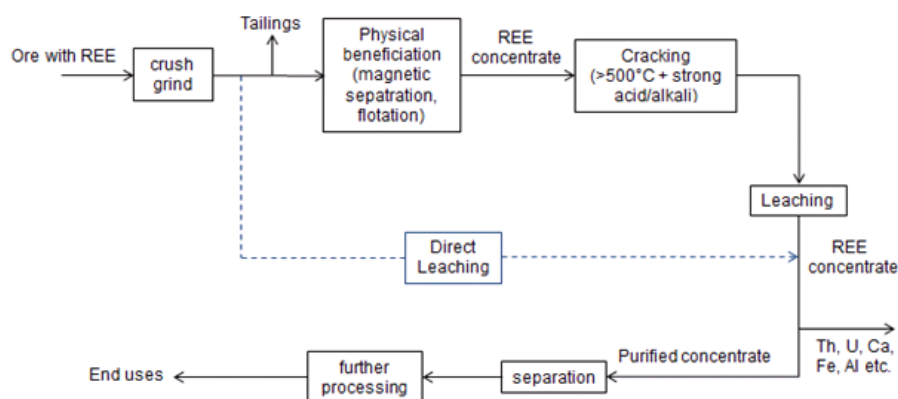
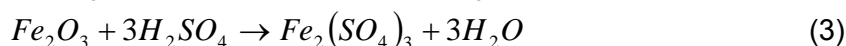


Figure 1 – Traditional and Direct leaching route for processing of bastnasite
 Рис. 1 – Традиционный и прямой метод обработки фторкарбонатов
 Слика 1 – Традиционални и директни метод обраде флуорокарбонатног
 минерала

The main equations ruling dissolution in sulfuric acid are described as:



2) The second processing route is related to the carbothermic reductive smelting of the bastnaesite ore for steel manufacture, producing metallic iron and a slag. Once smelted, the slag should contain a high fraction of rare earth elements together with other compounds that normally appear in slags. Therefore, the slag can be considered a rare earth concentrate suitable for leaching operations in acid and for subsequent recovery of REEs.

Experimental work

Material

The experiments were performed using the bastnasite ore with a higher content of iron in the form of iron-oxides (73,1 %), as shown in Table 1.

Table 1 – Composition of the sample of the bastnasite ore
Таблица 1 – Состав образцов руды с содержанием фторкарбонатов
Табела 1 – Состав узорка руде која садржи флуорокарбонатни минерал

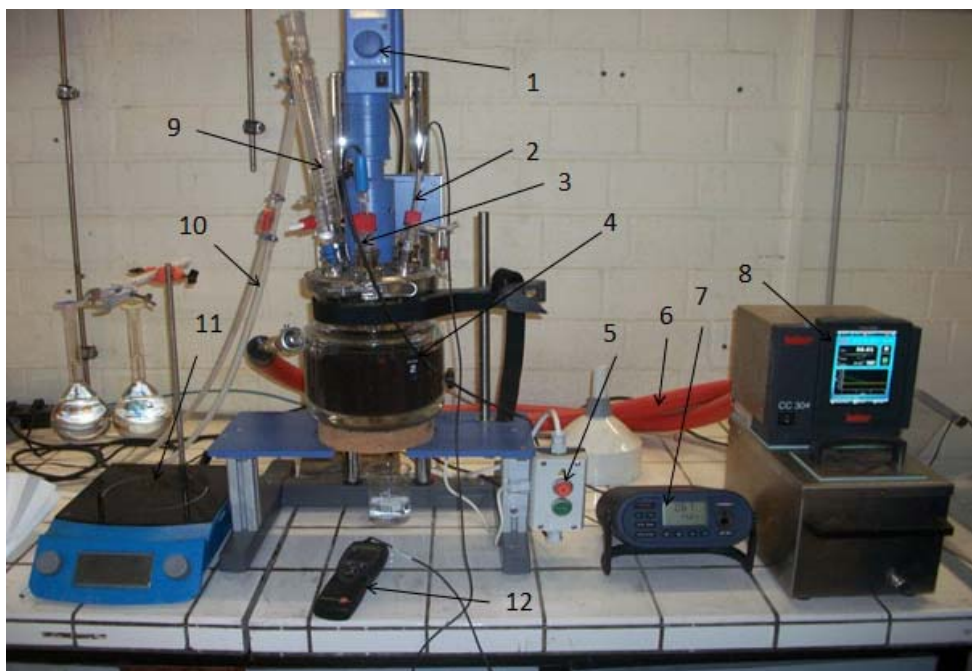
Element	Fe (%)	Ca (%)	Mg (%)	Mn (%)	Si (%)	La (%)	Ce (%)	Nd (%)	Pr (ppm)	Sm (ppm)	Gd (ppm)	Tb (ppm)	Y (ppm)
Amount	73,1	6,75	0,5	0,45	1,39	0,16	0,61	0,45	831	512	93	< 10	< 10

The total REE (La+Ce+Pr+Nd+Sm+Gd) content is 1.36%. Although the content of thorium was about 1000 ppm, the behavior and precipitation of this metal during the sulfuric acid leaching will not be considered in this work.

Experimental procedure

The direct leaching process of bastnasite was performed using the hydrometallurgical equipment shown in Figure 2.

The 2l-capacity reactor is based on a double-walled glass container, where the desired temperature for the experiment is programmed in device number 8, and heated water is pumped between the reactor's walls to keep uniform temperature in the tank. A coiled condenser prevents vapor fumes from leaving the reactor, while a series of openings can be used to introduce a thermocouple and a pH meter. The reactor is also equipped with a broad stainless steel stirrer.



- | | | |
|--------------------------------|-------------------------------------|-----------------------------|
| 1. stirring speed control | 6. pipes for temperature regulation | 9. condensator |
| 2. thermocouple | 7. pH reader | 10. pipes for condensator |
| 3. pH meter | 8. water pumping and heating | 11. heating induction plate |
| 4. double-walled glass reactor | | 12. temperature reader |
| 5. security stop | | |

Figure 2 – Hydrometallurgical equipment for direct leaching process

Рис. 2 – Гидрометаллургическое оборудование для прямого выщелачивания

Слика 2 – Хидрометалушка опрема за процес директног растварања

The experiments were carried out as outlined below. First, the diluted sulfuric acid solutions were prepared and poured into the reactor. When the experiment temperature was 65°C and higher, the acid was

preheated in an induction plate to save time. The reactor was then covered, the condensation circuit turned on, and the pipes were connected to the temperature control device, already programmed at the desired temperature. The stirring speed was then selected, and the previously weighed bastnasite ore was poured with a funnel through one of the openings. The stopwatch was activated. The pH readings were noted during the duration of the experiment. Once the reaction time was over, the necessary devices were stopped and disconnected to allow opening the lid. The container's content was filtered using a vacuum filtering machine and the leachate was collected. Afterwards, the solid remains in the reactor container were washed out with distilled water onto the same filter paper and both were soaked with distilled water for neutralization. These filter papers were carried to a drying oven set at 105°C for 4h. The dried residue was weighed. Some samples precipitated white crystals a few hours after the leaching operation. Filtration was carried out and the precipitate was once again weighed.

Experimental design

The five chosen parameters for the leaching process were: sulfuric acid concentration, temperature, dissolution time, solid-liquid ratio and stirring speed. Each parameter was made to have 5 levels. For example, temperature can be varied between the levels 20, 35, 50, 65, and 80 °C. Table 2 summarizes these parameters and their levels.

Table 2 – Factors and levels for the experimental design
 Таблица 2 – Факторы и этапы планирования эксперимента
 Табела 2 – Фактори и нивои планирања експеримента

	level 1	level 2	level 3	level 4	level 5
acid concentration (mol/l)	1	1,5	2	2,5	3
temperature (°C)	20	35	50	65	80
time (min)	20	50	80	110	140
solid-liquid ratio (g/l)	50	100	150	200	250
stirring speed (rpm)	40	70	100	130	160

Determining the levels of a variable requires an in-depth understanding of the process, including the limits within which it makes sense to range these values, and the likelihood that these values will contribute to an optimal performance characteristic. The number of levels chosen is an important matter, since more levels mean more accuracy but also an increase in the number of experiments to be conducted. Experimental design for the determination of an optimal parameter

combination was used according to the Taguchi method (Khaw et al, 1995, pp.225-245). One of the advantages of the Taguchi method in relation to the traditional methods for experimental design (such as full factorial design) is that it allows for the analysis of a large number of parameters ranging along a large number of levels, with the minimum of experiments.

Table 3 – Experimental design
Таблица 3 – Планирование эксперимента
Табела 3 – Планирање експеримента

experiment number	conc. (mol/l)	temp.(°C)	time (min)	s-l ratio (g/l)	str. Speed (rpm)
1	1	20	20	50	40
2	1	35	50	100	70
3	1	50	80	150	100
4	1	65	110	200	130
5	1	80	140	250	160
6	1,5	20	50	200	100
7	1,5	35	80	250	130
8	1,5	50	110	50	160
9	1,5	65	140	100	40
10	1,5	80	20	150	70
11	2	20	80	100	160
12	2	35	110	150	40
13	2	50	140	200	70
14	2	65	20	250	100
15	2	80	50	50	130
16	2,5	20	110	250	70
17	2,5	35	140	50	100
18	2,5	50	20	100	130
19	2,5	65	50	150	160
20	2,5	80	80	200	40
21	3	20	140	150	130
22	3	35	20	200	160
23	3	50	50	250	40
24	3	65	80	50	70
25	3	80	110	100	100

Results and discussion

The liquors collected where in a range of colors going from very clear yellow to dark brown. In a few cases, the solution was completely colorless.



Figure 3 – The obtained solutions in experiments 11, 13 and 25

Рис. 3 – Полученные в ходе эксперимента растворы

Слика 3 – Добијени раствори у експериментима 11, 13 и 25

As expected, after two or three hours, a white precipitate appeared at the bottom of many liquor bottles. This precipitate kept on appearing for two or three days after leaching had been carried out. The texture of this precipitate varied significantly. Crystals were thick in some cases, while in other cases they were extremely small, forming gels. The existence of gels could be easily seen while filtering the precipitate because filtering became extremely difficult and even lasted an hour or two. The appearance of gel during filtering operations and the texture of other filtered precipitates is given in Figure 4.

The formation of gel is a serious problem, because filtering operations become unviable, and rare earth elements are lost. In the collected data, the amount of the formed gel was categorized as high, medium or low. High levels of gel meant that the filtering operation of 1l liquor took between 1 and 2h.



Figure 4 – Typical gel formation in Experiment. 13
Рис. 4 – Типичное образование геля в эксперименте 13
Слика 4 – Карактеристично формирање гела у експерименту 13

The following observations can be made from the obtained results presented in the graphs in Figure 5 to describe the effects of the reaction parameters on the REE behavior during dissolution from the bastnasite ore.

- Sulfuric Acid concentration: Concentration only affects the recovery of REEs slightly. Middle and middle-low concentrations give the best results.
- Temperature: High temperatures hinder the dissolution of REEs. This is consistent with literature (the solubility of rare earth sulfates increases as temperatures decrease). Middle ranged temperatures are the best option.
- Time: Dissolution increases with time during the first hour of leaching and remains high for longer times.
- Solid to liquid ratio: Higher solid to liquid ratios are more favorable than low ones. This is not a common behavior for mineral dissolution.
- Stirring speed: A minimum of stirring is needed for dissolution to be effective.

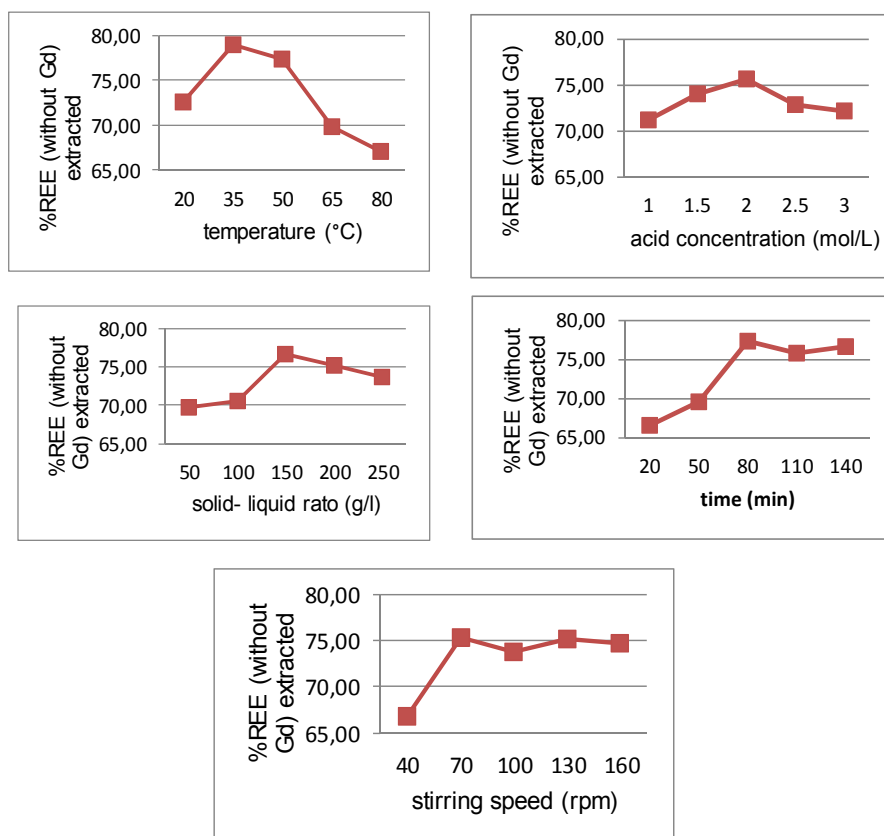


Figure 5 – Main effects graphs for rare earth extraction from bastnasite ore by direct leaching with sulfuric acid

Рис. 5 – Графики основных эффектов экстракции редкоземельных элементов из фторкарбоната, путем прямого выщелачивания, с помощью серной кислоты
Слика 5 – Приказ утицаја главних параметара екстракције ретких земаља директним растварањем руда које садрже флуорокарбонатни минерал

The optimum of each factor is the level with a maximum mean; in other words, the highest value in the main effects graphs: 2M, 35°C, 80min, 150g/l and 70rpm. No experiment has been done for this parameter combination. However, there is a very similar experiment, experiment number 12 (2M, 35°C, 110min, 150g/l and 70 rpm), where the only difference is 20min longer leaching time, with high gel formation. This means that there is danger that the optimal parameter combination would be affected by gel, and it is, therefore, not a suitable option.

We can also conclude that the levels chosen for each factor were convenient, since the maximum dissolution of REEs happens in the middle values of levels.

From all the experiments, the one with the highest average of REEs dissolved is experiment number 3 (1M, 50°C, 80min, 150g/l and 100rpm). For this combination, all rare earth elements except Nd and Sm dissolve to their highest value (96.7% of cerium, 95% for praseodymium, 79.58% for lanthanum). The average of REEs extracted is also at its highest point with 85.12%. Neodymium is most difficult to extract: the maximum dissolution occurs for experiment 13 (2M, 50°C, 140min, 200g/l and 70rpm). Unfortunately, this experiment produces gel. The second best value for Nd is also experiment 3 that produces no gel. Other advantages of experiment number 3 are that it requires a minimum amount of acid, and that the dissolution of Fe is especially low with only 2.19%.

A high amount of gel was formed in experiments 7, 12 13, 17 and 23. What these experiments have in common is that they were all carried out at temperatures of 35 and 50°C. Concentration does not seem to be a decisive factor. There is gel for concentrations of 1.5, 2 and 3M. None of the 1M experiments produced gel. The 2,5M experiments did not have gel either, although lower and higher concentrations did cause gel formation. However, the experiments with a concentration of 2,5M and in the range of temperatures mentioned were performed with lower solid per liquid ratios. Most other experiments with gel were performed with 200 to 250g/l of bastnasite ore. The formation of gel is connected to the dissolution of silicium and silica undergo hydrolysis. Unfortunately, experiments with gel are between those with higher rare earth recovery ratios. Experiments 7, 12 and 13 give the three best dissolution values for REEs after experiment 3. Although this is not studied here, dry digestion process can be applied in order to prevent gel formation (Davris et al, 2017, pp.115-122), (Ma et al, 2018, p.267).

The leaching process of bastnasite ore is a very complicated process where many chemical components and mechanisms are taking place at the same time and are guided by different driving forces. Many dissolution studies have been carried out so far, in which the object was to understand the dissolution behavior of individual minerals or more simple mixtures with similar dissolution characteristics. The recovery of rare earths from Rodberg bastnasite ore with sulfuric acid is however surrounded by many phenomena, including the precipitation of calcium sulfate, calcite passivation, re-dissolution and re-precipitation of gypsum and anhydrate, adsorption of rare earths by calcium sulfate crystals and gel formation. These phenomena are influenced by factors such as concentration and temperature to different extents. The result is an extremely complicated system.

Although the detailed analysis of means was in some cases not able to provide clear trends in the dissolution of bastnasite ore, it did help identify some of the main factors involved in the dissolution of components and the amount of formed precipitates or solid residues.

Conclusion

Sulfuric acid leaching of Rodberg bastnasite ore from Norway containing an average of 1.36 % REEs was studied in the direct leaching process. The one step strategy with sulfuric acid was studied further and the results showed that filtering difficulties do not happen for all parameter combinations. The optimum of each factor is the level with a maximum mean; in other words, the highest value in the main effects graphs: 2M, 35°C, 80min, 150g/l and 70rpm.

Furthermore, the best parameter combinations were those with low temperatures and low acid concentrations. All in all, it is a simple process that uses the cheapest acid on the market and offers good leaching recoveries. Attention should be given to the formation of gel, especially when taking the process to the large scale, and the subsequent elimination of Ca from the leachate. If these issues are solved, sulfuric acid leaching represents the best option for processing the bastnaesite ore. In order to solve it, dry digestion process with sulfuric acid and subsequent leaching with water were proposed.

References

- Balomenos, E., Davris, P., Deady, E., Yang, J., Panias, D., Friedrich, B., Binnemans, K., Seisenbaeva, G., Dittrich, C., Kalvig, P., & Paspaliaris, I. 2017. The EURARE Project: Development of a Sustainable Exploitation Scheme for Europe's Rare Earth Ore Deposits. *Johnson Matthey Technology Review*, 61(2), pp.142-153. Available at: <https://doi.org/10.1595/205651317x695172>.
- Castor, B., James, B., & Hedrick, B. 2006. Rare Earth Elements. In J.E. Kogel, N.C. Trivedi, & J.M. Barker Eds., *Industrial Minerals and Rocks*, pp.769-792.
- Chen, Z. 2011. Global rare earth resources and scenarios of future rare earth industry. *Journal of Rare Earths*, 29(1), pp.1-6. Available at: [https://doi.org/10.1016/s1002-0721\(10\)60401-2](https://doi.org/10.1016/s1002-0721(10)60401-2).
- Davris, P., Stopic, S., Balomenos, E., Panias, D., Paspaliaris, I., & Friedrich, B. 2017. Leaching of rare earth elements from eudialyte concentrate by suppressing silica gel formation. *Minerals Engineering*, 108, pp.115-122. Available at: <https://doi.org/10.1016/j.mineng.2016.12.011>.
- Feng, X., Long, Z., Cui, D., Wang, L., Huang, X., & Zhang, G. 2013. Kinetics of rare earth leaching from roasted ore of bastnaesite with sulfuric acid. *Transactions of Nonferrous Metals Society of China*, 23(3), pp.849-854. Available at: [https://doi.org/10.1016/s1003-6326\(13\)62538-8](https://doi.org/10.1016/s1003-6326(13)62538-8).

Gupta, C.K., & Krishnamurthy, N. 2005. *Extractive Metallurgy of Rare Earths*. Boca Raton, FL: CRC Press. chapter 1. 2; ISBN 0415333407 9780415333405.

Hoshino, M., Sanematsu, K., & Watanabe, Y. 2016. REE Mineralogy and Resources. In *Handbook on the physics and chemistry of rare earths*. Elsevier BV, pp.129-291. Available at: <https://doi.org/10.1016/bs.hpcr.2016.03.006>.

Khaw, J.F.C., Lim, B.S., & Lim, L.E.N. 1995. Optimal design of neural networks using the Taguchi method. *Neurocomputing*, 7(3), pp.225-245. Available at: [https://doi.org/10.1016/0925-2312\(94\)00013-i](https://doi.org/10.1016/0925-2312(94)00013-i).

Ma, Y., Stopić, S., Gronen, L., Milivojevic, M., Obradovic, S., & Friedrich, B. 2018. Neural Network Modeling for the Extraction of Rare Earth Elements from Eudialyte Concentrate by Dry Digestion and Leaching. *Metals*, 8(4), p.267. Available at: <https://doi.org/10.3390/met8040267>.

Rare Earth Elements, British Geological Survey, Natural environment research council, center for sustainable mineral development, 2011. November, downloaded on November 24th 2013 from: <https://www.bgs.ac.uk/downloads/start.cfm?id=1638>.

ВЫЩЕЛАЧИВАНИЕ РЕДКОЗЕМЕЛЬНЫХ ЭЛЕМЕНТОВ СЕРНОЙ КИСЛОТОЙ ИЗ ПОРОД, СОДЕРЖАЩИХ ФТОРКАРБОНАТЫ

Сречко Р. Стопич, Бернд Г. Фридрих
Технический университет города Ахен,
Институт металлургических процессов и рециклирования металлов,
Федеративная Республика Германия

ОБЛАСТЬ: химические технологии
ВИД СТАТЬИ: оригинальная научная статья
ЯЗЫК СТАТЬИ: английский

Резюме:

В данной работе представлены результаты исследований по растворению редкоземельных элементов из руд, содержащих фторкарбонаты, с помощью серной кислоты, при атмосферном давлении. Результаты выщелачивания с помощью серной кислоты показали, что фильтрование в процессе выбора различных параметров не влечет за собой негативных последствий. Наилучшие показатели были при комбинировании параметров с наиболее низкими температурами и наименьшей концентрацией кислоты. Прямое выщелачивание представляет собой весьма простой процесс, в осуществлении которого используется самая дешевая кислота на рынке сбыта. Особое внимание следует уделять образованию геля, особенно если в течение процесса использовался большой объем раствора, а также на последующее удаление кальция из раствора.

Ключевые слова: редкоземельные элементы, гидрометаллургия, фторкарбонаты, серная кислота.

РАСТВОРАЊЕ ЕЛЕМЕНАТА РЕТКИХ ЗЕМАЉА СУМПОРНОМ КИСЕЛИНОМ ИЗ РУДА КОЈЕ САДРЖЕ ФЛУОРОКАРБОНАТНИ МИНЕРАЛ

Срећко Р. Стопић, Бернд Г. Фридрих
Технички универзитет у Ахену, Институт за процесну металургију и рециклирање метала, Савезна Република Немачка

ОБЛАСТ: хемијске технологије
ВРСТАЧЛАНКА: оригинални научни чланак
ЈЕЗИК ЧЛАНКА: енглески

Сажетак:

Испитивано је растварање елемената ретких земаља из руда које садрже флуорокарбонатни минерал помоћу сумпорне киселине при атмосферском притиску. Резултати растварања у једном кораку помоћу сумпорне киселине показују да не долази до проблема приликом филтрирања при избору разних параметара. Најбоље су се показале комбинације параметара с ниским температурама и малим концентрацијама киселине. Директно растварање је једноставан процес у којем се користи најјефтинија киселина на тржишту. Посебну пажњу треба обратити на формирање гела, нарочито током процеса с већим запреминама раствора, као и на накнадно уклањање калцијума из раствора.

Кључне речи: елементи ретких земаља, хидрометалургија, флуорокарбонатни минерал, сумпорна киселина.

Paper received on / Дата получения работы / Датум пријема чланка: 15.04.2018.
Manuscript corrections submitted on / Дата получения исправленной версии работы / Датум достављања исправки рукописа: 01.07.2018.
Paper accepted for publishing on / Дата окончательного согласования работы / Датум коначног прихватања чланка за објављивање: 03.07.2018.

© 2018 The Authors. Published by Vojnotehnički glasnik / Military Technical Courier (www.vtg.mod.gov.rs, втг.мо.упр.срб). This article is an open access article distributed under the terms and conditions of the Creative Commons Attribution license (<http://creativecommons.org/licenses/by/3.0/rs/>).

© 2018 Авторы. Опубликовано в «Военно-технический вестник / Vojnotehnički glasnik / Military Technical Courier» (www.vtg.mod.gov.rs, втг.мо.упр.срб). Данная статья в открытом доступе и распространяется в соответствии с лицензией «Creative Commons» (<http://creativecommons.org/licenses/by/3.0/rs/>).

© 2018 Аутори. Објавио Војнотехнички гласник / Vojnotehnički glasnik / Military Technical Courier (www.vtg.mod.gov.rs, втг.мо.упр.срб). Ово је чланак отвореног приступа и дистрибуира се у складу са Creative Commons licencom (<http://creativecommons.org/licenses/by/3.0/rs/>).



DEVELOPMENT OF NEW SMART METAL NANOMATERIALS BASED ON TITANIUM-DIOXIDE FOR PHOTOCATALYTIC AND ANTIMICROBIAL ACTIVITIES

*Nataša D. Kuburović^a, Aleksandar V. Golubović^b,
Ljiljana M. Babinčev^c*

^a Eco Energy Engineering & Consulting, Belgrade, Republic of Serbia,
e-mail: natasa.kuburovic@eeec.rs,
ORCID iD: <http://orcid.org/0000-0003-2565-6607>

^b University of Belgrade, Institute of Physics, Center for Solid State
Physics and New Materials, Belgrade, Republic of Serbia,
e-mail: golubovic@ipb.ac.rs,
ORCID iD: <http://orcid.org/0000-0003-4618-424X>

^c University of Priština, Faculty of Technical Sciences,
Kosovska Mitrovica, Republic of Serbia
e-mail: ljiljana.babincev@pr.ac.rs
ORCID iD: <http://orcid.org/0000-0001-6290-1902>

DOI: 10.5937/vojtehg66-17261; <https://doi.org/10.5937/vojtehg66-17261>

FIELD: Chemical & Materials Engineering, Catalytic processes and
Composite Materials

ARTICLE TYPE: Original Scientific Paper

ARTICLE LANGUAGE: English

ACKNOWLEDGMENT: The first author would like to express her gratitude to Dr Suzana Dimitrijević – Branković, full professor at the Faculty of Technology and Metallurgy, University of Belgrade, for her kind help in the preparation of microorganisms and their measurements during the experimental research, as well as for her useful suggestions. Also, the first author is especially grateful to colleague Dr Antonije Onjia, Ph. D. Sci Ch. Eng., Associate Professor at the Faculty of Technology and Metallurgy, University of Belgrade, owner and long lasting director of the Anahem Laboratory d.o.o., for his generous help and the opportunities to support necessary analyses during the first author's scientific research work done in his lab. The photocatalytic and coupled photocatalytic-microbiological experiments were carried out in the Laboratory of the Department for Organic Chemistry at the Faculty of Technology and Metallurgy, University of Belgrade, which the first author used for scientific research work during her PhD study in Inorganic Chemical Technology and Chemical Engineering. The microbiological activity experiments were carried out in the Laboratory of Biochemical Engineering and Biotechnology at the FTM BU. The synthesis and part of characterization of TiO₂ nanoparticles were carried out in the Center for Solid State Physics and New Materials at the Institute of Physics, University of Belgrade. The GC-MS determinations were carried out in the Laboratory of the "Occupational Safety and Environmental Protection, Beograd doo".

Abstract:

The subject of this study was the synthesis, characterization and testing of titanium (IV) oxide nanoparticles (TiO_2 -NPs) and their lanthanum (La^{3+}), iron (Fe^{3+}) and vanadium (V^{3+}) dopants for the photocatalytic and microbiological activity, as well as their comparison with the catalytic activity of the tested commercial TiO_2 (Degussa P-25[®] and anatase nanoparticles, 99.9 %, Alfa Aesar Lancaster). The TiO_2 -NPs photocatalysts were synthesized and doped with different metal dopants concentrations for different calcination durations, such as: TiO_2 -NPs (anatase-NPs, calcination duration of 5 and 7 h), La^{3+} (0.65, 1, 2, 3, 4, 5 and 6 wt. %, calcination duration of 7 h), Fe^{3+} (1, 2.5, 3.0 and 5 wt. %, calcination duration of 7 and 24 h), and V^{3+} (10 wt. %, calcination duration of 7 and 24 h). The *Pseudomonas aeruginosa* strains DV 2739 and ATCC 9023 were used as model microorganisms in the microbiological experiments performed in a microbiological cabinet. The photocatalytic and coupled photocatalytic-microbiological processes were performed in a slurry-catalyst bath circulation photoreactor in the presence of direct UV radiation simulated with a sodium lamp SONT UV400 in lab conditions. The study has demonstrated that the catalyst sample S28, an La-dopant with a concentration of 1wt. %, displays the best photocatalytic properties among all La-dopants, while the best photocatalytic activity among all catalysts was achieved in S111 sample, an Fe-dopant of titania (5 wt. %, calcination duration of 7 h). Our results also show different degradation rates for TiO_2 doped with V^{3+} of 10.0 wt. %, samples S93 and S96, synthesized with different duration times (7h and 24h, respectively) and calcination heating rates (66.7 and 135 °C/h, respectively), which can be explained by anomalies in their behavior. Finally, the best antimicrobial activity is obtained in S24 sample, an Fe-dopant for which it was shown that 0.25 mg/L could be toxic for microorganisms. In accordance with our results of superior Fe-dopant characteristics and theoretical knowledge for TiO_2 nanoparticles doped with Ag, Au and Fe, we get directions for further studies of their photocatalytic and antimicrobial activities, as well as for the development of TiO_2 -nanoparticles and nanotubes for enhancing antibiotics and their use in cancer treatment.

Key words: titanium-dioxide, TiO_2 -nanoparticles, TiO_2 doped with La^{3+} , Fe^{3+} and V^{3+} , calcination duration, *Pseudomonas aeruginosa* strains DV 2739 and ATCC 9023, photocatalytic activity, antimicrobial activity.

Introduction

Titanium, the ninth most abundant element in the Earth's crust, can be found in the form of minerals: ilmenite, rutile and titanium. In its most stable form as titanium (IV) oxide (TiO_2), it can be found in three possible crystalline forms: brookite (orthorhombic), rutile (tetragonal) and anatase

(tetragonal). From a photocatalytic point of view, only rutile and anatase are relevant, the latter having the highest photocatalytic activity, as reported by Fernandez-Ibanez et al (Fernández-Ibáñez et al, 2004). Among different options available in the market, Degussa P-25[®] is one of the most efficient and tested nanomaterials, in the form of powder with a particle size of around 25 nm, forming aggregates of several hundred nanometers to several micrometers in the aqueous solution with a surface of 50m²/g, consisting of 70% anatase and 30% rutile. It is well known that TiO₂ with the anatase molecular structure was found to be a superior photocatalytic material for purification and disinfection of water and the air, as well as for the remediation of hazardous waste (Hoffmann et al, 1995), (Fujishima et al, 2000). Nanomaterials like TiO₂ nanoparticles (TiO₂-NPs), smaller than approximately 100 nm in diameter, have become a new generation of advanced materials due to their novel and interesting optical, dielectric, and photocatalytic properties from size quantization (Alivisatos, 1996). The challenge for the so-called nanotechnologies is to achieve perfect control of nanoscale-related properties, which obviously requires correlating the parameters of the synthesis process, such as: self-assembly, microlithography, sol-gel, polymer curing, electrochemical deposition, laser ablation, etc. with the resulting nanostructure (Gouadec et al, 2007). Many efforts have been devoted to research, development and production of advanced TiO₂-NPs with controlled size, shape, and porosity for use in thin films, nanowires and electrodes, catalysts, ceramics and composite materials. The effects of nanometer sizes are caused by the large surface-to-volume ratio, resulting in more atoms along the grain boundaries than in the bulk material, which can be explained by the fact that if many particles reduce their size, more attractive interactions between the particles become dominant so attractive forces lead them to aggregate or agglomerate, which results in nanoparticle aggregates (NPAs). The control of the particle size distribution and the aggregate structure is the key criterion for product quality considering that the desired product properties can vary with the particle size, as well as the degree of aggregation or aggregate structure. It has been accepted that NPs can exist in two states within a liquid: stable, i.e. particles separate, non-adhering and dispersed, and aggregated or flocculated, i.e. adherent and randomly clumped (Schwarzer & Peukert, 2005). This clumping can occur due to van der Waals attractive forces or may be caused by magnetic or other attractions imposed by externally imposed fields. For the calculation of the particle-particle interaction, the DLVO theory can be employed (Hunter, 2000). Hence, it is very important to realize that the NPs being

used in experiments, especially in a suspension or colloid form, have the properties (e.g., size distribution) which are different from those specified by manufactures; in experimental processes such as sonication, autoclave, pH value, etc., the state or properties of the particles may be changed, so it is essential that the experiments are carried out with care (Sungkaworn et al, 2008). With the increasing use of NPs in commerce, to date few studies have investigated the toxicological and environmental effects of NPs. Exposure to nanoparticle substances can be an important risk factor for human health. The sub-micron size of NPs offers a number of distinct advantages over micro particles (MPs). NPs have in general relatively higher intracellular uptake rate compared to MPs, which was demonstrated in studies in which 100 nm size NPs showed 2.5 fold greater uptakes compared to 1 μm and 6 fold higher uptakes compared to 10 μm NPs in Caco-2 cell line, as reported by Waliszewski (Waliszewski, 1997). Similar results were obtained when these formulations of NPs and MPs were tested in a rat in situ intestinal loop model. The efficiency of uptake of 100 nm sized particles was 15–250 fold greater than larger sized (1 and 10 μm) MPs (Zhang & Sun, 2004). In this rat study, it was found that NPs were able to penetrate throughout the sub mucosal layers while the larger size MPs were predominantly localized in the epithelial lining. Also, TiO_2 or titanium could be used as an alternative complement to conventional technology for biocides activity via photocatalysis. It is well known that photocatalytic events occur when the UVA/UVB with wavelengths of lower than 385nm ($365 < \text{wavelength} < 385$) illumination of TiO_2 (band-gap energy of anatase, 3.2 eV; for rutile, 3.0 eV) and subsequent formation of electron/hole pairs are numerous and very complex; the following electron/hole separation, the two charge carriers migrate to the surface through diffusion and drift, in competition with a multitude of trapping and recombination events in the lattice bulk. The carriers are poised, at the surface, to initiate redox chemistry with suitable pre-adsorbed acceptor and donor molecules in competition with recombination events to yield radioactive and nonradioactive emissions, and/or trapping of the charge carriers into shallow traps at lattice sites (e.g., anion vacancies, Ti^{4+} , and others). Thus, on absorption of UV light, titanium particles yield superoxide radical anions and hydroxyl radicals that can initiate oxidations (Hoffmann et al, 1995).

It is also well known that thinner nanowires (NWs) may further enhance the sensitivity of the devices owing to an increased surface-to-volume ratio, as Chueh et al. reported (Chueh et al, 2007). This study has shown the investigation of the $\text{RuO}_2/\text{TiO}_2$ core/shell structure

photoconductivity under the UV illumination of 256 nm (4.9 eV), which is strong enough to excite the electron-hole pair near the band edge, and their results suggest the potential application of NWs as interconnects and optoelectronic devices

Photocatalytic-biological inactivation is explained by the attack of oxygen-derived molecular species or reactive oxygen species (ROS), especially radicals photo generated at the surface of the TiO₂ catalysts like O₂⁻, HO₂⁻ and OH, although the mechanism of cell death or damage has not been understood yet (Maness et al, 1999). Also, oxygen-derived molecular species or reactive oxygen species (ROS) such as superoxide (O₂⁻) and hydrogen peroxide (H₂O₂) are produced in cells as a result of aerobic metabolism. Excess generation of these species can result in damage to macromolecules such as the DNA and lipids (Maness et al, 1999). Photocatalytic TiO₂ nanoparticles, as showed by Xu et al. (Xu et al, 1998) in their experimental research, have features to kill malignant cells through a series of oxidized chain reactions and induce the malignant cells to be stressed by ROS. Then, the cells were stressed to death either through apoptosis or necrosis depending on the used dosage. Finally, photocatalytic TiO₂ nanoparticles can severely destruct the cellular membrane system and cause the cellular genetic macromolecules damage through the reactive oxygen species accumulation within the cells, and even induce cell death. The result of this research (Xu et al, 1998) also partly reveals the mechanism of cell death by photocatalytic TiO₂ nanoparticles, which is very important for the direction of the research and development of photocatalytic TiO₂ nanoparticles in biomedical application.

Anpo (Anpo, M. 2004) reported that the nanosized anatase TiO₂, due to a large surface area and band-gap energy, showed better photo activity than their bulk phase. However, the nanosized anatase-TiO₂ transforms to the rutile structure at temperatures about 600°C and this phase transformation of TiO₂ greatly reduces surface areas of the particles (Zhang & Sun, 2004), which may result in the decrease in photocatalytic ability of TiO₂. It was found that the stability temperature of the anatase-TiO₂ can be increased by doping TiO₂ with lanthanide ions; so it is believed that the development of high-temperature stabilized photocatalysts is important for immobilizing the photocatalyst on the working objects by chemically bonding, the process of which commonly requires relatively high temperatures. Zhang & Sun (Zhang & Sun, 2004) studied the microstructure and the photocatalytic properties of lanthanide doped TiO₂ prepared by a sol-gel method and they reported that La, Eu, Gd or Yb dopants significantly inhibited the nanosized TiO₂ phase

transformation of anatase-to-rutile. It was also found that transition metal oxides are extensively employed as catalysts, because they possess featured active centers to adsorb reaction molecules. Titania doped with iron ions shows superior activity due to its unique half-filled electronic configuration and shallow trapping compared to other metal dopants with closed shell electronic configuration, which can be more effective to influence the photo activity (Yan et al, 2015), (Liu & Zhang, 2013), (Ramli et al, 2015), (Su et al, 2015), (Dinesh et al, 2015), (Flak et al, 2015), (Su et al, 2012), (Wang et al, 2012). Theoretical and experimental studies show that Fe doping can effectively reduce the trapping density and charge recombination, resulting in drastically improved adsorption, reported Huang et al (Huang et al, 2016).

Many studies by the authors: Heller (Heller, 1995), Ollis et al (Ollis et al, 1991), Sitkiewitz & Heller (Sitkiewitz & Heller, 1996), Takeuchi et al (Takeuchi et al, 2003) and Uchida et al (Uchida et al, 1993); using TiO₂ photodecomposition of pollutants with the aim of developing methods to purify water and the air have been carried out. For the bactericidal activity, several results have been reported using TiO₂ powder (Cai et al, 1991), (Ireland et al, 1993), (Matsunaga & Okochi, 1995), (Watts et al, 1995) and (Wei et al, 1994), and TiO₂-coated materials for this purpose (Kikuchi et al, 1997). However, few studies have investigated the impacts of TiO₂ in cancer science or in the field of oncology, as reported by Minhua et al. (Minhua, X. et al. 1998). However, the actual factors that control the photo catalytic activity of specific TiO₂ particles are still unknown, and the detailed studies of the effects of TiO₂ on biological systems in dark condition have been very rare. Cancer has been a leading cause of human death in the world, but it is not too much known about the biological mechanisms leading to the establishment or the growth of malignant tumors. Many attempts have been made in recent decades to describe the basic biological mechanisms of tumor growth. Benign masses generally have smooth, circumscribed, and well-defined contours, whereas malignant tumors commonly have rough, speculated, and ill-defined contours (Sungkaworn et al, 2008). Also, Fe-doped TiO₂ nanotubes (NTs) can be a potential photosensitizer for the near-visible light driven photodynamic therapy (PDT) against cervical cancer cells (HeLa). Fe-doped TiO₂ nanoparticles exhibited none or lower dark cytotoxicity than un-doped TiO₂ nanotubes, which confirms their superior biocompatibility. Under the near-visible light irradiation (~405 nm), Fe-doped TiO₂ nanoparticles showed higher photo-cytotoxic efficacy than un-doped TiO₂ nanoparticles, which was found to be dependent on the nanoparticles concentration, but not on the incubation time of the cells

after the near-visible light irradiation. The highest activity was observed in 0.70 and 1.40 wt. % Fe-TiO₂ nanoparticles (Flak et al, 2015).

The aim of this study is finding the optimum synergetic effects of the synthesized type of smart TiO₂-nanoparticles and their different metal dopant concentration on photocatalytic, microbiological and antimicrobial activities in aerobic conditions, which will give us further directions of the development of TiO₂ nanoparticles for environmental and biomedical applications.

Background of the TiO₂-Particle Synthesis

Many studies have been conducted on the synthesis of TiO₂-nanoparticle catalysts that will have adequate nanometres-sized effects, as well as other relevant catalyst and electrochemical characteristics, which can give best performances for photocatalytic, photo-electrochemical and antimicrobial activities.

Nedeljkovic et al. (Nedeljković et al, 1997) performed a TiO₂ nanoparticles ultrasonic spray pyrolysis using a colloidal solution of 10⁻² M TiO₂ at 800°C. The experimentally determined value of the mean diameter of TiO₂ was 286 nm. It differed significantly from the expected theoretical values between 132 nm and 195 nm. Jokanovic et al. (Jokanović et al, 2004) explained the design of nanostructured hollow sized particles during the ultrasonic spray pyrolysis method, which was in comparison between theoretically estimated and experimentally obtained ring thickness about 7-15 %. The mean sub particle size estimated by the theoretical model was 4.7 nm. Depending on the type of packing, the mean diameter of the hollow sphere was different: for hexagonal packing - 87 nm, for cubic packing - 95 nm, which is in accordance with the theoretical model developed by Jokanović.

Backman et al. (Backman et al, 2004) produced nanosized TiO₂ particles using flame reactors and aerosol pyrolysis. The measured median sizes of TiO₂ prepared from titanium (IV) tetraisopropoxide Ti(OC₃H₇)₄ were 13 nm at 600-1100°C reactor's temperature and 22 nm at 1100°C, respectively. The fundamental problem was the presence of carbon in the product that is produced at 1100°C since the processes of coalescence agglomeration and sintering are dominant at higher reaction temperatures (1100°C), as opposed to 600°C. The desired crystalline anatase phase of TiO₂ was formed at high temperature. The TEM and BET analyses of TiO₂-nanoparticles confirmed that by changing the temperature values the surface area and phase content can be controlled.

Aruna et al reported a nanosized rutile TiO_2 particle synthesis via a hydrothermal method without mineralizers, which contaminate the samples and induce undesirable characteristics (Aruna et al, 2000). It is also used for preparing two sets of titania colloids (with and without stirring) the similar procedure by hydrothermal synthesis of titanium (IV) isopropoxide and nitric acid with pH value of 0.5. Stirring that maintains homogeneity in the solution during the hydrothermal process was highly important when a homogeneous product was required. The rutile nanocrystals of titania prepared by the hydrothermal method with a particle size of about 20 nm have a large surface area and are relatively stable at high temperatures.

Ahonen et al (Ahonen et al, 1999) synthesized TiO_2 -powders in the aerosol pyrolysis process of the freshly-prepared and well-mixed 0.2 M solution of titanium (IV) n-butoxide in n-butanol at a temperature range between 200 and 580°C in the air and the nitrogen atmosphere. Anatase powder was formed at 500°C in nitrogen, and at 580°C in the air, while the anatase to rutile transformation appeared in thermal annealing in the air. Physico-chemical phenomena occurring during the formation of particles were described in this paper (Ahonen et al, 1999).

The methodology for the preparation of TiO_2 films, based on the process of ultrasonic spray pyrolysis using TiO_2 nanoparticles as a precursor was reported by Blesic et al (Blešić et al, 2002). Blesic et al have shown an advantage of the usage of TiO_2 colloids in the process of ultrasonic spray pyrolysis. In the methodology, the growth mechanism of the TiO_2 films formation is explained layer-by-layer. The compact smooth film or a porous structure might be obtained by adjusting the substrate temperature, and the mean diameter of particles can be adjusted changing the concentration of the precursor and a frequency of aerosol.

Panić et al (Panić et al, 2003) synthesized titanium anodes with an active RuO_2 coating of two different thicknesses from the oxide suspended in ethanol, as an "ink" method, while the oxide itself was synthesized by the hydrolysis of ruthenium ethoxide in an ethanolic solution (alkoxide route). The authors showed that the anodes prepared *via* the alkoxide route are more active in the chlorine evolution reaction than the anode prepared from the inorganic oxide sol, due to their larger real surface area; it was also shown that the coating mass on the anode does not influence significantly the anode activity in the chlorine and oxygen evolution reaction at low over potentials. It can be explained that more compact thick coating appears to be more active for the chlorine evolution at higher overpotentials, due to forced micro-convections in the pores (Panić et al, 2003).

The sol-gel chemistry has recently been involved in a general and powerful approach to preparing inorganic materials, as reported by Lakshmi et al (Lakshmi et al, 1996). The sol-gel method has been proven to be a very flexible and promising means in view of the controlled synthesis of Au, Ag and other metal nanoparticle embedded metal oxides, as well as relevant for photocatalytic applications, which includes the synthesis of anatase titanium dioxide, anatase titanium dioxide doped with La, Fe, V, Au, Ag and other photocatalytic systems. Metal nanoparticles dopants as Ag, Cu and Au demonstrate a strong absorption band in the visible or near IR spectrum due to plasmin resonance. The position of the plasmin resonance band depends on the size and shape of metallic NP, so the NP plasma resonance control can be adjusted for a useful spectral region, e.g. for the region of the biological tissue transparency (between ~ 650 nm – 1200 nm). In this region, tissues (blood, bones, skin) are transparent. The metal NP is inert in the biological media, so it can be excited by light ~ 650 nm – 1200 nm if it were injected in the body. It allows, as reported by Huang et al (Huang et al, 2006), carrying out the photo thermal therapy in the near-Infrared Region by using gold-nanorods.

The great interests for antimicrobial effect research of new materials based on the nanosized particles toward pathogens is explained by the increase of new microbiological strains resistant to antibiotics, as well as by the motivation to further study disinfection possibilities of new systems based on nanosized particles. Microbes resistant to silver occur pretty rarely in the nature, which is very important for the application of process of TiO₂ photocatalysis using silver ions or silver colloids for disinfection of microbes; therefore, the application of metallic plasmin nanoparticles represents a promising approach to the photothermolysis of bacterial cell or cancer cells. New materials with hybrid nanoparticles made from metallic and wide band semiconductors TiO₂ and ZrO₂ are suggested for medical and their environmental applications. Further research and studies are aimed at the development of the preparation of hybrid nanoparticles (hNPs) comprised by metal-nanoparticles (La, Fe, V, Ag, Au, etc.) on the wide band gap semiconductors (TiO₂) and the study of antimicrobial effects against gram-negative and gram-positive bacteria in dark, under excitation by the visible light and UV-A light. We expected different mechanisms of hNP's action on bacteria under light activation. Effect of hNP's disinfection in dark towards the bacterial films formation will be studied in detail. The hNP's surface modification will be developed in vivo for biomedical applications. The administrated nanoparticles are eliminated from the circulation within seconds to minutes through the

reticula-endothelial system without surface modifications. Oxide nanoparticles will be obtained by processes such as mechanic-chemical synthesis, hydrothermal method, pyrolysis, plasma-chemical method, sol-gel technology and precipitation methods. By using zirconium or titanium salt of different nature and different agent-precipitated and various dopants, one can control the structure and the surface state of oxide nanoparticles.

It is well known that the traditional disinfection methods such as chlorine-based technologies lead to the formation of chloroorganic disinfection by-products (DBPs) with carcinogenic and mutagenic effects on mammals (Richardson, 2003); so, it is important to develop advanced disinfection processes and applications for sustainable supply of drinking water. Marugán et al (Marugán et al, 2010) in their study are focused on the evaluation of analogies and differences found when comparing the TiO₂ photocatalytic treatment for chemical oxidation and microorganism's inactivation, using methylene blue and *Escherichia coli* as references, respectively. The activation of both processes is based on the same physicochemical phenomena and consequently a good correlation between them is observed when analyzing the effect of operational variables such as the catalyst concentration or the incident radiation flux. Both factors influence common stages such radiation absorption and generation of reactive oxygen species. However, different microbiological aspects, such as osmotic stress, repairing mechanism, regrowth, bacterial adhesion to the titania surface, etc. make disinfection kinetics significantly more complex than the first-order profiles usually observed for the oxidation of chemical pollutants (Marugán et al, 2010). This study has shown that bacterial inactivation reactions are found to be extremely sensitive to the composition of water and modifications of the catalysts in comparison with the decolorization of the dye solutions, showing opposite behaviors in the presence of chlorides, incorporation of silver to the catalysts or the use of different types of immobilized TiO₂ systems. The complex structure of living cells, the existence of several mechanisms for cell regeneration, and the possibility of post-irradiation regrowth could be considered as drawbacks when microorganism inactivation is compared to the oxidation of chemical pollutants; it is, therefore, particularly difficult to model the microbiological aspects involved in the disinfection treatment process (Marugán et al, 2010).

In recent years, researchers in the field of photocatalysis have paid more attention to the study of hybrid nanoparticle systems such as Ag nanoparticles on the TiO₂ surface, which use UV-A light for the excitation of photocatalysts. Photo induced bactericidal activity of nanostructured

TiO₂, and the deposition effect of silver and bimetallic Ag/Ni nanoparticles on the pathophysiological properties of titanium films were investigated. The model of microorganisms for antimicrobial activity of films was evaluated against *Pseudomonas fluorescens B-22* (gram-negative bacteria) and *Lactococcus lactis ssp. lactate 411* (gram-positive bacteria). The silver-modified TiO₂ film demonstrates the highest photo biocide efficiency, enhancing the bactericidal activity of UV light cca. 71 times, which results from the radical improvement of microorganism adsorption and suppression of recombination of photo produced charge carriers (Skorb, E.V. et al, 2008). Recently gold-doped TiO₂ (Au/TiO₂) nanocomposites have been investigated to enhance the photocatalytic efficiency of TiO₂ in decomposing organic compounds and photo killing bacteria.

Photocatalytic systems based on hybrid nanoparticles with UV excitation are suggested for the production of new medical products. Ag/titanium dioxide (TiO₂)-coated silicon catheters were easily fabricated with Ag nanoparticles deposition on both the inside wall and the outside wall of TiO₂-coated catheters by the TiO₂ photocatalysis. This is an application of the silicon catheters coated with TiO₂ which possess a self-sterilizing and self-cleaning property combined with UV light illumination (Ohko et al, 2001). Yao et al (Yao et al, 2008) reported that similarly to 15 nmol cm⁻² of Ag, 99% effective sterilization occurred in a very short time: 20 min for *E. coli*, 60 min for *Pseudomonas aeruginosa*, and 90 min for *Staphylococcus aureus*; the Ag/TiO₂-coated catheters possessed a strong self-cleaning property. The photocatalytic decomposition rate of methylene blue dye using UV illumination representing the self-cleaning capability, on an Ag/TiO₂ catheter which was loaded with 2 nmolcm⁻² of Ag, was similarly 1.2 times higher (at maximum) than that on the TiO₂ coating alone. Furthermore, Ag nanoparticles can be pre-eminently and uniformly deposited onto the TiO₂ coating, and the amount of Ag was easily controllable from a few nanomoles per square centimeter to 70 nmolcm⁻² by changing the UV illumination time for the TiO₂ photocatalysis. This catheter type shows a great promise in lowering the incidence of catheter-related bacterial infections (Yao et al, 2008).

Experimental

Material

Methyl-tertiary-butyl-ether (MTBE, purity ≥ 99.5 %), hydrogen peroxide (35%), methanol (99.8%), sodium carbonate (NaCO₃), ammonium hydroxide (NH₄OH) and ethanol (all three purity grades were

99.9%), barium hydroxide octahydrate ($[\text{Ba}(\text{OH})_2 + 8\text{H}_2\text{O}]$, 98%), phenolphthalein, Tryptic Soy Broth (TSB) and Caseinhydrolysate Glucose Yeast extract Broth (Base) were obtained from Merck Millipore, hydrogen chloride (35%) from Lachema, and sodium hydroxide from Euro Hemija. Titanium dioxides were purchased from Alfa Aesar Lancaster (anatase nanopowder, 99.9%) and Degussa AG Frankfurt (TiO_2 powder, P-25[®]), and used as such. The *Pseudomonas aeruginosa* strains ATCC 9023 and DV 2739 were used in the experiments researching microbial activity and inactivity. All other chemicals used in the synthesis of catalyst, such as $\text{LaCl}_3 \cdot 7\text{H}_2\text{O}$, $\text{FeCl}_3 \cdot 6\text{H}_2\text{O}$, VCl_3 , and TiCl_4 were obtained from Merck Millipore as the analytical grade.

Method

The experimental research in this study consists of the following components:

1. Preparation of catalysts;
2. Characterization of catalysts;
3. Research of photocatalytic activities:
 - I Experiments of photocatalytic activities; and
 - II Coupled photocatalytic–microbiological experiments;
4. Research of microbial activity and inactivity:
 - I Microbial activity and inactivity of coupled photocatalytic–microbiological experiments; and
 - II Experiments of antimicrobial activities.

The commercial TiO_2 catalysts, as anatase nanopowder and Degussa P-25[®], synthesized TiO_2 -nanoparticles catalysts (calcination duration of 5 and 7h), and synthesized TiO_2 nanoparticles based catalysts doped with different concentrations of following metals: La^{3+} (0.65, 1, 2, 3, 4, 5 and 6 wt. %), Fe^{3+} (1, 2.5, 3.0 and 5 wt. %, with calcination duration of 7 and 24 h), and V^{3+} (10 wt. %, with calcination duration of 7 and 24 h); were tested in the photocatalytic, coupled photocatalytic–microbiological and antimicrobial activities for different concentrations of the MTBE water solution. These experiments were performed in a slurry-catalyst bath circulation photoreactor in the presence of direct ultraviolet (UV) radiation simulated with a sodium lamp SONT UV400 in lab conditions. Also, both commercial titania (Degussa P-25[®] and anatase powder, purity: 99.9 %), synthesized TiO_2 nanoparticles (synthesized at 550 °C with a calcination duration of 5 h), TiO_2 nanoparticles doped La^{3+} (5 wt. %, with a calcination duration of 7 h) and Fe^{3+} ions (2.5 wt. %, with a calcination duration of 7 h) were tested in the antimicrobial activity

experiments. TiO₂-nanoparticles and their dopants catalysts were synthesized and characterized before our experiments. *Pseudomonas aeruginosa* strain ATCC 9023 was used as a model microorganism in the coupled photocatalytic–microbiological and first antimicrobial activity experiments, and *Pseudomonas aeruginosa* strain DV 2739 was used as a model microorganism in the second antimicrobial activity experiments. The antimicrobial activity experiments were performed in a microbiological cabinet. The experiments are very important for the determination of the microorganism toxicity point with TiO₂ nanoparticle catalysts, i.e. the concentration at which the release of microorganisms occurs.

Photoreactor

The photocatalytic and coupled photocatalytic-microbiological experiments in the MTBE water solution were tested in a bath slurry-catalyst circular photoreactor (Fig.1). The photoreactor consisted of a 92 cm long quartz tube (inner diameter 19 cm and outer diameter 21 cm), and slurry circulated through the system by the pump, from the storage tank through the control valve and the reactor, and back to the storage tank that is thermo stated at 30 °C. This set-up of the system provided uniform distribution of the photo catalyst. The storage tank has a volume of 2 liters, which is operational in full capacity for all experiments.

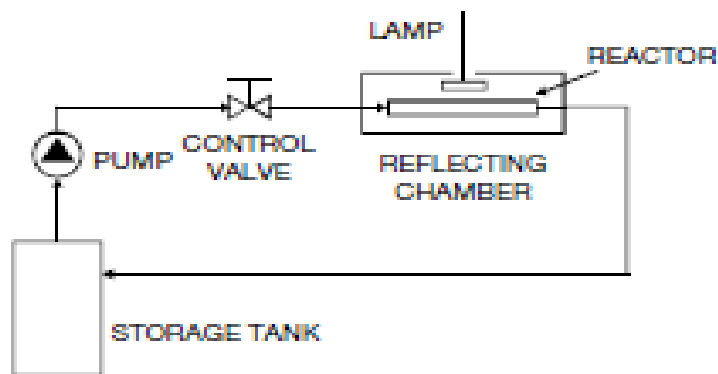


Figure 1 – Experimental apparatus for the photocatalytic and coupled photocatalytic-microbiological experiments

Рис. 1 – Экспериментальная аппаратура для фотокаталитического и комбинационного фотокаталитично-микробиологического эксперимента
Слика 1 – Експериментална апаратура за фотокаталитички и комбинавани фотокаталитичко-микробиолошки експеримент

The ultraviolet radiation needed for the photoreaction in the experiments was provided by a sodium lamp, SON-T UV400. The lamp produced a photon flux of $960 \mu\text{molm}^{-1}\text{s}^{-2}$ in two different wavelength intervals: 380-518 nm and 540-800 nm, as well as at the local maximum at 333 nm. The distance between the reactor and the sodium lamp was 17 cm. The reactor was in a chamber with the reflecting aluminum foil inner walls in order to provide a uniform UV radiation pattern and intensity for the experiments.

MTBE as a model compound

Methyl-tertiary-butyl-ether (MTBE) has been used as a high constituent and as a replacement for the anti-knocking agent (tetra ethyl lead) of gasoline since the late 1970s. MTBE is a colorless, transparent and flammable liquid whose harmful effects on the environment and the ecosystem have been confirmed over time. It is one of the most dangerous pollutants for human health in the environment; it is frequently detected in wastewater, groundwater, watercourses, drinking water and the soil. The purification and bioremediation of MTBE polluted groundwater is very slow; it is particularly difficult to treat, due to high MTBE solubility in the water ($48.000 \mu\text{g/L}$) and its low volatility (The Merck index, 1996), (Shaffer & Uchrin, 1997). Also, The EPA characterized MTBE as a potential cancerogenic compound in the environment and suggested the concentration limit of 20-40 $\mu\text{g/L}$ for the compound in drinking water (Squillace et al, 1996), (Pontius, 1998). Also, the California Department of Health Services has adopted 5 $\mu\text{g/L}$ as the maximum MTBE concentration levels (California Code of Regulations, 1999).

Catalyst preparation

The sol-gel method was used for the synthesis of pure and doped anatase nanopowders with iron (Fe^{3+}), lanthanum (La^{3+}) and vanadium ion (V^{3+}). Titanium (IV) chloride (TiCl_4 , 99.0% pure, Merck) was used as the precursor in the synthesis process. Hydrogel, titanium (IV) hydroxide $\text{Ti}(\text{OH})_4$, was obtained by the hydrolysis of TiCl_4 at 0°C with a controlled addition of 2.5 wt. % aqueous ammonia into the aqueous solution of TiCl_4 (0.3 mol/l) and a careful control of the solution's pH value of 9.3 for pure TiO_2 nanoparticles, as well as La, Fe and V-dopants of TiO_2 -nanoparticles (Golubović et al, 2009a), (Grujić-Brojčin et al, 2014). TiCl_4 is soluble in water but it experiences rigorous reaction at 20°C which can be very important when performing this reaction at a lower temperature. After aging in the mother liquor for 5h, the as-prepared hydrogel was

filtered and washed out with distilled water until complete removal of chlorine ions. The obtained $\text{Ti}(\text{OH})_4$ hydrogel was converted to its ethanol gel by repeated exchanges with anhydrous ethanol for several times (by repeated introduction of anhydrous ethanol). The obtained Alco gel represents the starting point for the production of TiO_2 nanoparticles. Alco gel was placed in a vessel, dried at 280°C and calcined at a temperature of 550°C for 5, 7 and 24 h (depending of the sample types); after that, it was converted to nanoparticles. Dopants were in the form of chloride ($\text{LaCl}_3 \cdot 7\text{H}_2\text{O}$ and $\text{FeCl}_3 \cdot 6\text{H}_2\text{O}$ and VCl_3) and mixed with TiCl_4 in the adequate ratio before hydrolysis.

The heating rate, duration of calcination for pure (S05, S06, S07, S08, S10, S11, S99 and S102), La-doped (S16, S18, S28, S38, S40a, S48, S52a and S64), Fe-doped (S24, S111-S112, S117-S120), V-doped (S93 and S96) and their different wt. % of TiO_2 dopants samples are specified in Table 1 at the Result and Discussion Section: Synthesis conditions. All samples except S05, S06, S10, S99 and S102 samples were used to test photocatalytic, microbiological and antimicrobial activities, while these pure titania nanoparticles were used for a comparative analysis in accordance with their temperature profile.

Characterization of the catalysts

X-Ray Power Diffraction (XRPD) was used for the identification of the crystalline phases, the quantitative phase analysis and the estimation of the crystallite size and strains, as explained earlier (Golubović et al, 2009a), (Grujić-Brojčin et al, 2014). The XRPD patterns for TiO_2 -nanoparticles for pure samples (S07, S08 and S10) and La-dopants with 0.65 and 1 mol % of lanthanum ions (S18 and S28 samples) have been collected on a Philips diffract meter (PW1710) employing $\text{Cu K}_{\alpha 1,2}$, in the scanning range of 2θ between 20 and 80° with the step size of 0.06° and the counting time of 41 s/step. Higher La-dopants concentrations of titanium (IV) dioxide nanoparticle patterns, such as in S52a (4 wt. %) and S64 (6 wt. %) samples, have been collected in the same range by using a Stoe Stadi MP diffract meter ($\text{Cu K}_{\alpha 1}$ radiation, primary beam germanium monochromatic linear PSD detector, Bragg-Brentano geometry), at every 0.01° , with a counting time of 80 s/step. A full-prof computer program was used for the structure refinements, the quantitative phase analysis and the estimation of the average crystallite size and strains (Rodriguez-Carvajal, 2008). The instrumental resolution function for the size-strain analysis was obtained by parameterizing the

profiles of the diffraction pattern of an LaB₆ (NIST SRM660a) standard specimen.

The composition/quality of TiO₂ nanoparticles patterns of the samples such as S06 and S11, as well as their following La-dopants patterns of S18, S28, S40a and S64 samples was analysed on a SEM (JOEL JSM-6460LV, with the operating voltage of 20 keV) equipped with the EDS (INCAx-sight) detector and the "INAX-stream" pulse processor (Oxford instruments).

An Atomic Force Microscope – AFM (Omicron B002645 SPM PROBE VT AFM 25) in the contact mode was used to create an image of the surface topology of the TiO₂ nanoparticles doped: La-dopant as S18 pattern and Fe-dopant S111 patterns of the samples.

The porous structure of the catalysts has been evaluated from the adsorption/desorption isotherms of N₂ measured on the TiO₂ samples such as S05, S06, S11, S18, S28 and S40a at 136°C using the gravimetric McBain method. The main parameters of porosity such as the specific surface area and the pore volume have been estimated by the BET method and the α_s -plot, as reported by Kaneko et al (Kaneko et al, 1998) and the references therein. The pore size distributions have been estimated from the experimental nitrogen sorption data by the BJH and CPSM methods (Golubović et al, 2013), (Barrett et al, 1951).

The Raman scattering measurements of the chosen TiO₂-nanoparticles patterns of samples such as S11, S99 and S102 and their doped patterns of samples such as S48, S93 and S96 were performed in the backscattering geometry at room temperature in the air using a Jobin-Yvon T64000 triple spectrometer, equipped with a confocal microscope and a nitrogen-cooled charge coupled device detector. To avoid local heating due to laser irradiation, the spectra have been excited by a 514.5 nm line of Ar⁺/Kr⁺ ion laser with an output power of less than 5 mW.

Measurement of photocatalytic activities

The photocatalytic activities of TiO₂ (commercial and synthesized nanoparticles) and their La³⁺, Fe³⁺ and V³⁺ dopants were evaluated by the degradation of the MTBE water solution. The photocatalytic degradation of the water polluted by MTBE in lab conditions was carried out as described in our previous research, as reported by Kuburovic et al (Kuburovic et al, 2005, 2007, 2009) and presented at a conference (Kuburovic & Orlovic, 2010) as a part of the Preliminary study of photocatalytic wastewater treatments conducted in lab conditions using water samples from the Belgrade sewage system.

The photocatalytic activity measurement was performed in two types of experiments: the photocatalytic experiments and the coupled photocatalytic-microbiological experiments. The photocatalytic experiments were carried out in the presence of TiO₂ (commercial and synthesized nanoparticles) and their dopant catalysts.

The stock solution for the first experiment type (photocatalytic experiment) was prepared by stirring 2 ml of MTBE with 8 ml of ethanol (both Merck Millipore). The prepared stock solution was mixed with distilled water (2L volume) from which 10 ml of water was extracted for all photocatalytic experiments.

The stock solution for the second experiment type (coupled photocatalytic-microbiological experiments) was prepared by stirring 1 ml of MTBE with 9 ml of ethanol (both Merck Millipore). The prepared stock solution was mixed with distilled water (2L volume) from which 30 ml of water was extracted in two steps: in the first step, 10 ml of water was extracted, added to the stock solution and mixed; in the second step, 20 ml of water solution was extracted followed by the addition of 20 ml of the microorganism (MO) *Pseudomonas aeruginosa strain ATCC 9023* in a concentration of 10⁷ CFU mL⁻¹.

The resulting water solution (in both experiments, with the MO and without it) of MTBE was poured into the photoreactor and thus prepared for each experiment. Each experiment began with a circulation in the photoreactor and the burning of the UV lamp. When the photoreactor started to work in the uniform mode, 10 minutes after the beginning, the experiment was started with zero time. After the completion of the experiment, the reactor was thoroughly washed and sterilized, and after that prepared for the next experiment. The method of preparing the MO for the coupled photo catalytic-microbiological experiments was explained in the part entitled Measurements of the Microbiological Growth.

The GC-MS determinations in the photocatalytic activity experiments were carried out on an Agilent Technologies gas chromatographer equipped with a mass detector using the headspace (GC/MSD/Headspace – 7890A/5975C/G1888). Nitrogen was used as a carrier gas.

The total oxygen carbon (TOC) analysis was carried out by the Astro-Zellwenger LabToc-2100 as in the previous research the results of which are compared in the study.

The kinetics of CO₂ evolution during the photocatalytic activity experiment for titania nanopowders Fe-dopants consisted of flushing the CO₂ produced by oxygen into a flask containing a 10⁻² M of Ba(OH)₂

solution followed by titration with a 0.001 N HCl solution. Phenolphthalein was used as an indicator.

The quantification of the bacterial cultures from all tested solutions in microbiological activity and inactivity during the coupled photocatalytic-microbiological experiments was carried out on the Shimadzu Cary "UV 1700" UV-VIS spectrophotometer, and for the antimicrobial activity, the experiments were carried out on a calorimeter analog photo calorimeter, Labtronics, India.

Measurement of the microbiological growth

The research of microbial activity and inactivity can be conducted with the measurements of the microbiological growth using optical density. The methodology of both experiments is presented in the text below.

Microbial activity and inactivity of the coupled photocatalytic-microbiological experiments

Our research of the microorganism activity from the coupled photocatalytic-microbiological experiments was performed on the model microorganism (MO) *Pseudomonas aeruginosa strain ATCC 9023* in the presence and without TiO₂-nanoparticles and their La, Fe and V-dopants at the batch slurry-catalyst circular photoreactor.

The MO model was a fresh bacterial culture of around 10⁹ CFU mL⁻¹ of a stationary concentration prepared by the inoculation of 100 mL Tryptic Soy Broth (TSB) enriched with 0.6 % of Caseinhydrolysate Glucose Yeast extract Broth (Base) (both Merck Millipore) and aerobic incubation at 37°C under rotary shaking for 24 h. We thus obtained an TSB enriched substrate for the experiment and the zero control samples (k₀). After that, the TSB enriched base substrate in a volume of 20 mL was additionally enriched with a 0.5 µl/ml of the MTBE stock solution (as the first control sample – k₁) and centrifuged for each experiments and rinsed twice with sterile ultrapure water (Milli-Q, 18.2 MΩ cm) before diluting 20 mL of the resultant bacterial suspension to 2 L to prepare the reacting suspensions, with an initial concentration of viable bacteria around 10⁷ CFU mL⁻¹.

The experiment started 10 minutes (contact time) after mixing the water solution of MTBE with the 20 mL prepared MO, *Pseudomonas strain ATCC 9023* (10⁷ CFU mL⁻¹), testing catalysts, at the batch slurry-catalyst circular photoreactor and switching the recirculation pump. The photocatalytic experiments were followed during 150 minutes, depending

on the experiment. The contact time was necessary for the habituation of the MO on the MTBE solution and the catalyst, as well as for preparing the uniform sodium lamp to work.

The quantification of *Pseudomonas aeruginosa* strain ATCC 9023 from all tested solutions has been determined on the Shimadzu Cary "UV 1700" UV-VIS spectrophotometer at 550 nm. Optical density was also measured when each component (MTBE water solution, MO, catalyst) was added to the MTBE water solution after mixing in the photoreactor. In this experiment, an increase in the absorption of the solution to 648 nm was observed, as a measure of increase of the MO growth and its microbiological activity.

Experiments of the antimicrobial activities

Pseudomonas aeruginosa strains ATCC 9023 and DV 2739 were used as model microorganisms for the experiments on antimicrobial activities, performed in a microbiological cabinet. Namely, *Pseudomonas aeruginosa* strain ATCC 9023 was used earlier for our preliminary research, the results of which were presented as an oral presentation by Kuburovic (Kuburovic & Dimitrijevic-Brankovic, 2006) at the EMEC7 Conference, but they have not been published yet. After our preliminary study, *Pseudomonas aeruginosa* strain DV 2739 was used in all other experiments on antimicrobial activities.

A fresh bacterial culture of around 10^9 CFU mL⁻¹ of a stationary concentration was prepared for both experiments, by the inoculation of 50 mL Tryptic Soy Broth (TSB) enriched with 0.6 % Casein hydro lysate Glucose Yeast extract Broth (Base) (both Merck Millipore) and aerobic incubation at 37°C under rotary shaking for 24 h. We thus obtained an TSB enriched base substrate for the experiments and the zero control samples (k_0), which was seeded individually on the following samples:

- I Preliminary research: The volume of 2.0 ml of the TSB enriched base substrate for each of five samples was seeded with different concentrations of the MTBE stock solution of 0.15; 0.25; 0.5; 1.0 and 2.0 µl/ml, respectively. Also, the volume of 2.0 ml of the TSB enriched base substrate was seeded for three new samples with the 0.5 µl/ml of MTBE stock solution with 0.1 g/L TiO₂ (anatase TiO₂ nanoparticles, 99.9 %, Alfa Aesar Lancaster), FeCl₃ in a concentration of 5 µl/ml and the catalyst-reagent system TiO₂ and FeCl₃ in the ratio of 1:1 in the concentration of 5 µl/ml, respectively. All such prepared samples were centrifuged for each experiment and rinsed twice with sterile ultrapure water (Milli-Q,

18.2 MΩ cm) before diluting 2 mL of the resultant bacterial suspension to prepare the initial concentration of viable bacteria of around 10^7 CFU mL⁻¹. We also prepared two following control samples for each experiment: the TSB enriched base substrate (without anything else) and the TSB enriched base substrate that was seeded with an initial concentration of 0.50 μl/ml of the MTBE stock solution;

- II Antimicrobial activity research: The volume of 2.0 ml of the TSB enriched base substrate was seeded for twenty-four samples (6 samples in 4 different concentrations) with 0.5 μl/ml of the MTBE stock solution with different concentrations of TiO₂ nanoparticle catalysts such as: commercial TiO₂ (anatase, 99.9 %, Alfa Aesar Lancaster) and P-25 (Degussa P-25®), synthesized as pure S11 sample and doped TiO₂ nanoparticles sample, S16 (La-dopant) and S24 (Fe-dopant), as well as the catalyst-reagent system of TiO₂ and FeCl₃ in the ratio of 1:1 in the concentration of 5 μl/ml, respectively; each in several concentrations: 0.05, 0.10, 0.20 and 0.25 mg/L. All such prepared samples were centrifuged for each experiment and rinsed twice with sterile ultrapure water (Milli-Q, 18.2 MΩ cm) before diluting 2 mL of the resultant bacterial suspension to prepare the initial concentration of viable bacteria of around 10^7 CFU mL⁻¹. We also prepared two following control samples for each experiment: the TSB enriched base substrate (without anything else) and the TSB enriched base substrate that was seeded with the initial concentration of 0.50 μl/ml of the MTBE stock solution;

The MTBE stock solution for both experiment types was prepared by stirring 1 ml of MTBE (Merck Millipore) with 9 ml of ultrapure water (Milli-Q, 18.2 MΩ cm) without ethanol, which gave the MTBE concentration of 0.50 μl/ml. The photo activity of the catalysts on *Pseudomonas aeruginosa strains ATCC 9023 and DV 2739* in both experiments was investigated in a microbiological chamber illuminated sample with an UV-A lamp at 366 nm.

The quantification of *Pseudomonas aeruginosa strains ATCC 9023 and DV 2739* from all tested solutions has been performed on an analog photocolormeter (Labtronics, India) at 550 nm. In this experiment, a reduction in the absorption of the solution to 648 nm was observed, as a measure of decrease of the MO growth and their antimicrobial activity.

Results and Discussion

Synthesis conditions

The properties of the synthesized pure and doped titanium (IV) oxide nanoparticles by the sol-gel method synthesis determined the main of the following parameters: the pH value in the hydrolysis process, the precursor type, the temperature and the duration of hydrolysis (aging) and drying, and Alco gel. The most important are the ones of the calcination process parameters: heating rate, temperature, calcination cooling and duration rate. Titanium (IV) chloride (TiCl₄), as a cheap compound, is the primary starting material for the commercial production of titanium powders. The sol-gel method synthesis entails the hydrolysis of a precursor molecule solution aiming to obtain first a suspension of colloidal particles - the sol and then a gel composed of aggregated sol particles, which is in the further processing thermally treated yielding to the desired nanoparticles material. The process takes the following direction:



This reaction can be written in a chemical way as



The pH value of the precursor solution is a decisive factor in controlling the final particle size and shape, the crystal phase and the agglomeration (Zhang & Sun, 2004) due to its crucial influence on the relative rates of hydrolysis and polycondensation. Aruna et al (Aruna, et al, 2000) have found that the main hydrolysate in this reaction is $[\text{Ti(OH)}_n(\text{H}_2\text{O})_{6-n}]^{(4-n)+}$, where the amount of water varies with the relative rates of hydrolysis and polycondensation.

The titanium monomers formed during the reaction in the precursor solution play a significant role in the condensation process (Sun, J., et al. 2002) and in the formation of the final gel structure containing precursor molecules (Díaz-Díez, M.Á., et al, 2003). Since the intention was to obtain TiO₂ nanoparticles in the anatase form, the pH value of the solution during the hydrolysis process was chosen to be 9.3 which is in accordance with the pH value of 9.4 used by Venz et al (Venz, P.A. et al. 2000) for the same sol state and tetra isopropyl titanate used as a precursor. The pH value is several pH-units above the pH value where

the zeta-potential is zero (isoelectric point), as shown by Venz et al (Venz, P.A. et al. 2000). This is suitable for obtaining the stable sol with the maximum reduction of particle aggregation.

Aging is a process during which the gel properties can be changed as a result of polymerization, coarsening and phase transformation as reported by Wang et al (Wang et al, 2012). The nano crystallite growth presents the coalescence of small neighboring crystallites that become oriented due to the atomic diffusion or discrete orientation attachment. The aging conditions were the same in all experiments, with the temperature of 0°C and the process duration of 5 h. This is in accordance with the literature data (He, D. et al. 2007; Hari-Bala, G.Y., et al. 2006). The influence of aging on the properties of synthesized anatase nanoparticles was thus eliminated.

Titanium hydroxide was dried and calcined at high temperature, in order to obtain crystalline TiO₂-nanoparticles by the sol-gel method synthesis. In our experiment, as shown by Golubovic et al (Golubović et al, 2009a), the drying temperature was always 280°C, while the process duration was 4 h. The influence of the calcination parameters on the physical-chemical properties of anatase nanopowders and their dopants was examined by changing the heating rates (55, 67.5 and 135°C/h) and their influence of three different calcination durations (5, 7 and 24) with the constant of the calcination temperature (550°C) and their cooling rate (37.42°C/h). Only S07 sample was synthesized with a little different value of the calcination temperature and the cooling rate from all other samples, at 500°C and 37.42°C/h respectively, which can be seen in Table 2.

Some of the sol-gel synthesis parameters for the chosen TiO₂ samples (pure and doped), which are the subject of this paper are listed in Table 1.

The temperature profiles for pure TiO₂-nanoparticles of S05, S06, S07, S08, S10, S11, S99 and S102 samples (Table 2) were obtained, investigated and reported earlier (S07, S08 and S10, as A2, A3 and A6 profile samples; S05 and S06, S99 and S102 with a calcination duration of 5, 7 and 24 h, respectively): Golubovic et al (Golubović et al, 2009a), (Golubovic et al, 2013) and Scepanovic et al (Šćepanović et al, 2010) without S11 sample that is here for the comparison purposes.

During the sol-gel synthesis, we prepared pure and doped TiO₂-nanoparticles. Based on the presented synthesis data in Tables 1 and 2, the models of the sample temperature profiles for pure TiO₂-NPs, S05, S06, S07, S08, S10 and S99 and their dopants are shown in the text below.

Table 1 – Selected parameters for pure TiO₂-NPs and their La³⁺, Fe³⁺ and V³⁺ dopants
 Таблица 1 – Выбранные параметры чистых TiO₂-НЧ и их La³⁺, Fe³⁺ и V³⁺ допантов
 Табела 1 – Одабрани параметри за чисте TiO₂-НЧ-е и њихове La³⁺, Fe³⁺ и V³⁺ допанте

Pure TiO ₂ -NPs	La-doped TiO ₂ -NPs	Fe-doped TiO ₂ -NPs	V-doped TiO ₂ -NPs	wt. % dopant	Calcination		
					Heating rate [°C/h]	T [°C]	t [h]
S05					55	550	5
S06					55	550	7
S07					55	500	7
S08					55	550	7
S10					135	550	7
S11					55	550	5
	S16			5.0	67.5	550	7
	S18			0.65	67.5	550	7
		S24		2.5	135	550	7
	S28			1.0	135	550	7
	S38			5.0	135	550	7
	S40a			2.0	135	550	7
	S48			3.0	135	550	7
	S52a			4.0	135	550	7
	S64			6.0	135	550	7
			S93	10	67.5	550	7
			S96	10	135	550	24
S99					67.5	550	7
S102					135	550	24
		S111		5.0	135	550	7
		S112		5.0	135	550	24
		S117		1.0	135	550	7
		S118		1.0	135	550	24
		S119		3.0	135	550	7
		S120		3.0	135	550	24

Pure and dopants of the model of the S07 sample temperature profile:

These samples were not doped, they were synthesized as S05, S06, S07 and S11 samples, all four with this temperature profile; the only differences between the samples are that S11 sample has a shorter calcination duration of 5 hours (than the calcination duration of 7 h for the other three samples), and that only S07 sample has a lower cooling temperature (500°C, and for the other three is 550°C)

Table 2 – The parameters of the sol-gel process for the same TiO₂-NPs samples (Golubović et al, 2009a), (Golubović et al, 2013) and (Šćepanović et al, 2010). Only S11 sample has not been reported earlier

Таблица 2 – Параметри золь-гель процеса по тем же образцам TiO₂-НЧ (Golubović et al, 2009a), (Golubović et al, 2013) и (Šćepanović et al, 2010). Не был опубликован только образец С11

Табела 2 – Параметри сол-гел процеса за исте узорке TiO₂-НЧ-а (Golubović et al, 2009a), (Golubović et al, 2013) и (Šćepanović et al, 2010). Само узорак С11 није објављен раније

Sample	Aging		Drying			Calcination			
	t [h]	T [°C]	Duration [h]	T [°C]	t [h]	Heat. rate [°C/h]	T [°C]	t [h]	Cooling rate [°C/h]
S05	5	0	2	280	4	55	550	5	37.42
S06	5	0	2	280	4	55	550	7	37.42
S07	5	0	2	280	4	55	500	7	36.46
S08	5	0	2	280	4	55	550	7	37.42
S10	5	0	2	280	4	135	550	7	37.42
S11	5	0	2	280	4	55	550	5	37.42
S99	5	0	2	280	4	67.5	550	7	37.42
S102	5	0	2	280	4	135	550	24	37.42

Pure and dopants of the model of the S08 sample temperature profile:

- Dopants of lanthanum: S16 (wt. 5.0 %) and S18 (wt. 0.65 %) samples;
- Dopants vanadium: S93 (wt. 10 %) sample.

Pure and dopants of the model of the S10 sample temperature profile:

- Dopants of lanthanum: S28 (wt. 1.0 %), S38 (wt. 5.0 %), S40a (wt. 2.0 %), S48 (wt. 3.0 %), S52a (wt. 4.0 %) and S64 (wt. 6.0 %) samples;
- Dopant of iron: S24 (wt. 2,5 %), S111-S112 (wt. 5.0 %), S117-S118 (wt. 1.0 %) and S119-S120 (wt. 3.0 %) samples. The samples of S112, S118 and S120 had a longer calcination duration of 24 h (calcination duration of 7 h, for S111, S117 and S119 samples);

Pure and dopants of the model of the S99 sample temperature profile:

- Dopants vanadium: S93 (wt. 10 %) sample;

Pure and dopants of the model of the S102 sample temperature profile:

- Dopant of vanadium: S96 (wt. 10%) sample.

The results of XRD and XRPD diffractions

The XRPD and XRD patterns of pure and some La-doped TiO₂ nanopowders are shown from Figure 2 to Figure 4. The most intensive diffraction picks can be ascribed to the anatase crystal structure (JCPDS card 78-2486). Structure refinements have been performed by the Rietveld method: the lattice parameters, the unit cell volume, the average crystallite size and the average strain in the anatase and brookite phase, and the results of the quantitative phase analysis for brookite (brookite content) are summarized in Table 3, as partially reported earlier by (Golubović et al, 2009a), (Golubović et al, 2013), (Grujić-Brojčin et al, 2014) and (Šćepanović et al, 2010). The value of the anatase a parameter for the chosen tested samples considered and compared in Table 3 varies around its reference value ($a_0 = 0.378479(3)$ nm), whereas the value of the c parameter is slightly lower than the reference one ($c_0 = 0.951237(1)$ nm), as reported by Grujić-Brojčin (Grujić-Brojčin et al, 2014) earlier; except for the sample labeled as S96. The unit cell volume of all samples of La-doped TiO₂ is also lower in comparison with the reference value, except for the pure TiO₂. The structural refinement has revealed that the anatase crystallite size of the doped samples is decreased from 15.0 to 17.5 nm in the pure TiO₂ (S06, S05 and S11, respectively) to 12 nm in the La-doped samples. The pure TiO₂-nanoparticles strain is slightly increased with doping (Table 3). The brookite phase is highly disordered in all samples, which is indicated with a large value of the average strain in brookite crystallite.

The chosen XRD diffractograms of the chosen pure TiO₂-nanoparticles patterns labeled as S07, S08 and S10 are presented in Figure 2, which has been reported earlier by Golubović et al (Golubović et al, 2009a).

The XRPD patterns labeled as S28, S52a and S64 of anatase TiO₂-NPs doped with different wt. concentration of lanthanum (1 wt. %, 4 wt. % and 6 wt. %, respectively) are presented from Figure 3 to Figure 5, respectively. Figure 4 has been reported earlier by Golubović et al (Golubović et al, 2009b) as a conference poster.

Table 3 – The results of the Rietveld analyses of the samples (the unit cell parameters and the unit volume of anatase, the average crystallite size and the average strain in the anatase and brookite mineral forms and the content of brookite form) for pure and La and Fe-doped TiO₂-NPs (the values in the parentheses represent the estimated standard deviations) (Golubović et al, 2009a), (Golubović et al, 2013), (Šćepanović et al, 2010), (Grujić-Brojčin et al, 2014)

Таблица 3 – Резултати проведенног по методу Ритвелда анализа образцов (параметри елементарной ячейки анатаза, в том числе ее объема, средний размер кристаллитов и средняя твердость анатаза и брукита и состав форм брукита) чистых и La и Fe легированных TiO₂-НЧ-е (значения в скобках представляют допустимые отклонения) (Golubović et al, 2009a), (Golubović et al, 2013), (Šćepanović et al, 2010), (Grujić-Brojčin et al, 2014)

Табела 3 – Резултати Ритвалдоеве анализе узорака (параметри јединичне ћелије и јединичне запремине анатаса, просечна величина кристалита и просечна сила у минералној форми анатаса и брукита и садржај брукитне форме) за чисте и La и Fe допирание TiO₂-НЧ-е (вредности у заградама представљају процњена стандардна одступања) (Golubović et al, 2009a), (Golubović et al, 2013), (Šćepanović et al, 2010), (Grujić-Brojčin et al, 2014)

Sample	Dopant wt. %	Anatase					Brookite			
		a (nm)	c (nm)	V (10 ⁻³ nm ³)	Cryst. size (nm)	Strain (x10 ⁻³)	Content (%)	Cryst. size (nm)	Strain (x 10 ⁻³)	
S05	0.0	0.37873(0)	0.9496(4)	136.21(4)	15.4					
S06	0.0	0.37852(0)	0.9484(1)		17.5					
S07	0.0	0.37844(1)	0.94838(4)		12	4.5	17	12	16.9	
S08	0.0	0.37856(1)	0.94860(4)		12	4.2	16	35	19.6	
S10	0.0	0.37884(1)	0.94980(3)		10	3.4	10	58	16.8	
S11	0.0	0.37884(1)	0.94980(5)	136.31(1)	15	3	10(2)	58	17	
S18	0.65	0.37895(2)	0.9485(1)	136.21(2)	12	4	42(5)	2	29	
S28	1.0	0.37880(2)	0.94780(1)	136.01(2)	10	5	24(3)	26	22	
S40a	2.0	0.37853(2)	0.94908(9)	135.99(2)	12	8	21(1)	12	8	
S48	3.0	0.37823(6)	0.9471(3)	135.49(5)	12	8	21(4)	12	8	
S16	5.0	0.37874(3)	0.9485(1)	136.06(2)	12	8	22(2)	12	8	
S96	10.0	0.37719	0.95266							
Reference value: a ₀ = 0.378479(3) nm, c ₀ = 0.951237(1) nm, and V ₀ = 136.26(1) (10 ⁻³ nm ³)										

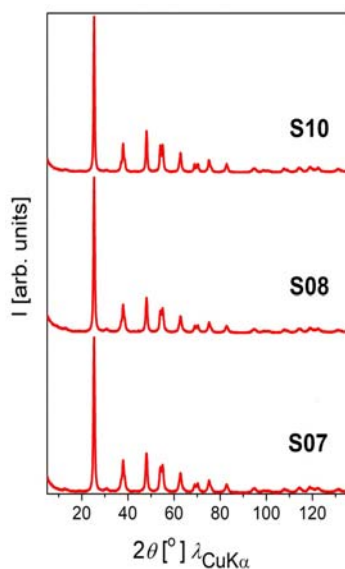


Figure 2 – XRD diffract grams of the chosen temperature profiles of TiO_2 samples (Golubović et al, 2009a)

Рис. 2 – XRD-дифрактограммы, выбранных температурных профилей образцов TiO_2 (Golubović et al, 2009a)

Слика 2 – XRD дифрактограми одабраних температурних профила TiO_2 узорака (Golubović et al, 2009a)

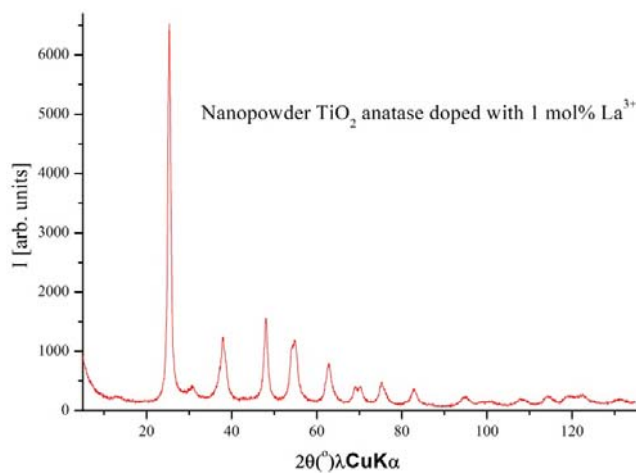


Figure 3 – XPRD diffract gram for S28 sample

Рис. 3 – XPRD-дифрактограмма образца C28

Слика 3 – XPRD дифрактограм за узорак C28

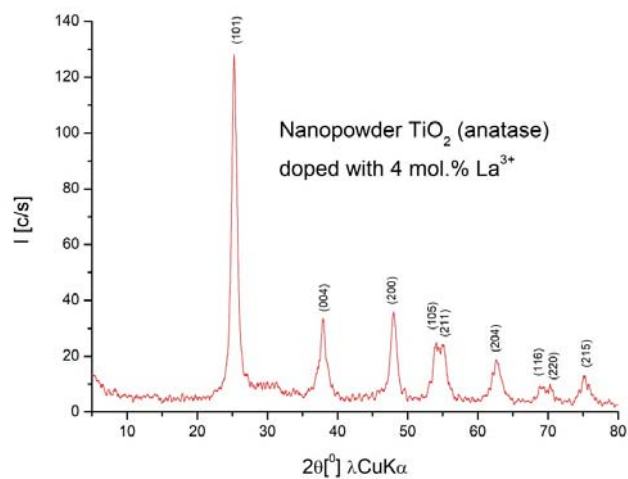


Figure 4 – XPRD diffract gram for S52a sample (Golubović et al, 2009b)
 Рис. 4 – XPRD-дифрактограмма образца C52a (Golubović et al, 2009b)
 Слика 4 – XPRD дифрактограм за узорак C52a (Golubović et al, 2009b)

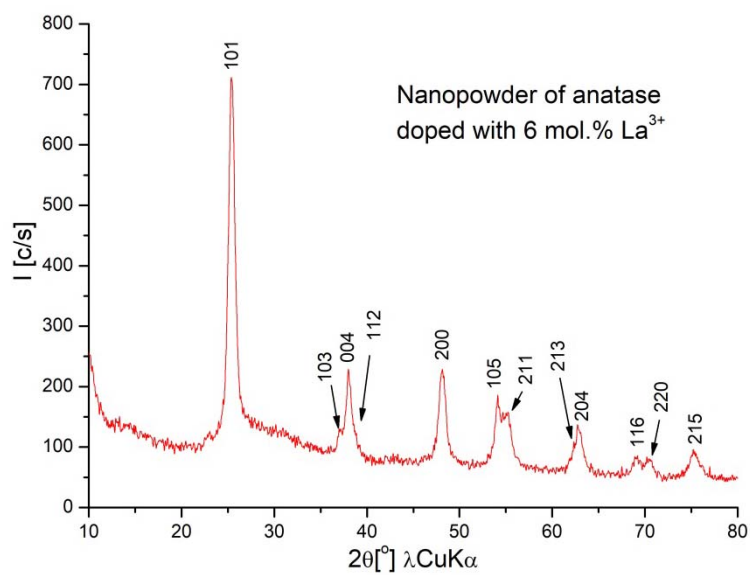


Figure 5 – XPRD diffract gram for S64 sample
 Рис. 5 – XPRD-дифрактограмма образца C64
 Слика 5 – XPRD дифрактограм за узорак C64

The results of the Raman spectroscopy

In the Raman mode of synthesized pure La and V-doped TiO₂-NPs, which are the subject of this paper, the anatase Raman mode dominates (Ohsaka et al, 1978), (Šćepanović et al, 2007): E_{g(1)} (~143 cm⁻¹), E_{g(2)} (~198 cm⁻¹), B_{1g} (~398 cm⁻¹), A_{1g}+B_{1g} (~518 cm⁻¹), and E_{g(3)} (~639 cm⁻¹), as reported by Golubovic et al (Golubović et al, 2009a), (Golubović et al, 2013), Grujic-Brojcin et al (Grujić-Brojčinet al, 2014) and Scepnanovic et al (Šćepanović et al, 2010). The Raman spectra of the chosen pure and some La³⁺ and V³⁺ doped TiO₂ nanoparticles were measured at room temperature. Some of these spectra are shown in Figure 6 and Figure 7, as the samples labeled as S11 (pure TiO₂-NP) and S48 (3 wt. %):

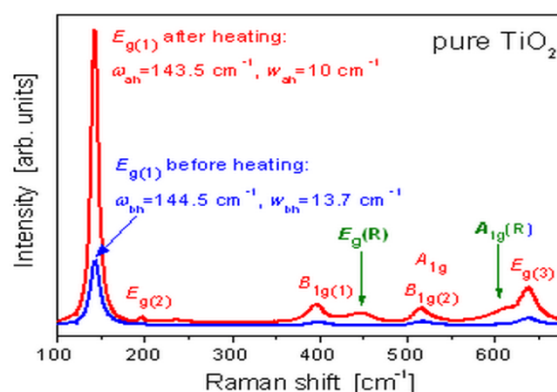


Figure 6 – Raman scattering spectra for S11 sample (Golubović et al, 2009b)
 Рис. 6 – Рамановская спектроскопия образца С11 (Golubović et al, 2009b)
 Слика 6 – Раманов расејани спектри за узорак С11 (Golubović et al, 2009b)

On the poster at the conference presented earlier in Figures 6 and 7, Golubovic et al (Golubovic, A. et al. 2009b) reported that the heating of pure TiO₂-nanoparticles (S11 sample) to 800°C causes redshift and narrowing of anatase E_{g(1)}. The Raman mode as well as the appearance of new Raman modes were assigned to the rutile phase. After the same heating treatment, there are neither a drastic change of E_{g(1)} Raman mode in the spectra of La-doped sample labeled as S48 nor the appearance of additional modes. Therefore, it can be concluded that doping with La³⁺ ions stabilizes the TiO₂ nanostructure in the anatase phase at high temperature. The frequencies of the anatase modes in V-doped TiO₂-nanoparticles shift more with different synthesis conditions, in comparison to their counterparts, as it can be seen from the data listed in Table 4, reported earlier (Šćepanović et al, 2010).

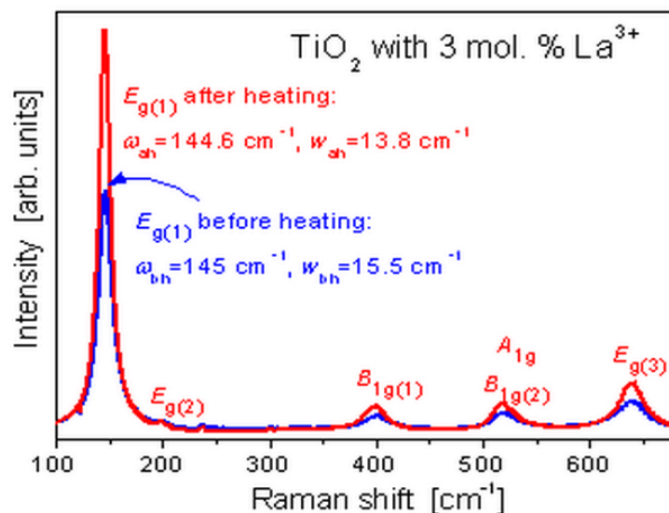


Figure 7 – Raman scattering spectra for S48 sample (Golubović et al, 2009b)
 Рис. 7 – Рамановская спектроскопия образца С48 (Golubović et al, 2009b)
 Слика 7 – Раманови расејани спектри за узорак С48 (Golubović et al, 2009b)

Table 4 – Frequencies of the anatase Raman modes in the pure and V-doped TiO₂ nanoparticle samples
 Таблица 4 – Частота Рамановского режима для атанаса чистых и V-легированных образцов наночастиц TiO₂
 Табела 4 – Фреквенције Раманових режима за атанас у чистим и V-допираним TiO₂ наночестицама

Sample	Raman frequencies of anatase modes (cm ⁻¹)				
	E _g (1)	E _g (2)	B _{1g} (1)	A _{1g} (1)+B _{1g} (2)	E _g (3)
S93	145.3	198.4	397.0	516.5	637.7
S96	148.9	201.9	394.6	514.2	633.4
S99	143.7	197.7	396.8	518.7	639.6
S102	143.8	197.8	397.0	518.8	639.7

The Raman mode of TiO₂-nanoparticles for the chosen pure and V-doped samples, labeled as S99, S93 and S96, respectively, feature twelve well-resolved bands at about 101, 143, 284, 305, 406, 478, 531, 699, 810, 926, 996 and 1020 cm⁻¹, as reported by Scepanovic et al (Šćepanović et al, 2010). The frequencies of these additional Raman modes, which can be related to the presence of vanadium, are listed in Table 5.

Table 5 – Frequencies of the V-related Raman modes in the V-doped anatase TiO₂-NPs
Таблица 5 – Частоты V-связанных в Рамановском режиме в V-легированных фазах анатаза TiO₂-НЧ

Табела 5 – Фреквенције за V-повезане Раманове режиме у V-допираној фази анатас TiO₂-НЧ-а

Sample	Raman frequencies (cm ⁻¹)											
	1	2	3	4	5	6	7	8	9	10	11	12
V ₂ O ₅	100	143	283	303	407	477	526	696	-	-	995	-
S93	101	143	284	305	406	479	532	700	808	924	996	1017
S96	-	143	284	308	-	-	-	699	810	934	996	1027

The measured values of the data from Table 4 and Table 5 have been reported earlier by Scepanovic et al (Šćepanović et al, 2010); it has been reported earlier that the presence of the additional Raman mode in the spectra of doped samples unambiguously shows that vanadium ions formed vanadium oxides (mostly V₂O₅) and some other vanadate structures in V-doped nanopowders. This confirms that a higher concentration of V in TiO₂ tends to stabilize V in the 5+ state predominantly, as reported by Bhattacharyya et al (Bhattacharyya et al, 2010). However, the change in pure TiO₂-nanoparticles of the Raman modes in those samples reveals that a certain amount of vanadium ions is introduced into the TiO₂ crystal lattice, which strongly depends on the conditions of the synthesis, such as the calcination heating rate and its duration.

The Results of the ESM

For TiO₂, La and Fe dopants nanoparticles, the particle size distributions were obtained by the elastic sphere model (ESM) and presented in Figures 8 and 11, respectively. In Figure 8, we can see that the mean particle size was around 12 nm for the La-dopant TiO₂-nanoparticles samples up to 4 wt. % of lanthanum ions, compared to pure anatase. The value of the mean particle size is increased for a higher lanthanum ion concentration.

The mean particle size was around 15.5 nm for S111 sample of Fe-dopant of TiO₂ nanoparticles in a concentration of 5 wt. %, synthesized at the calcination duration of 7 h, as shown in Figure 11, compared to the same concentration of the La-dopant (Figure 8).

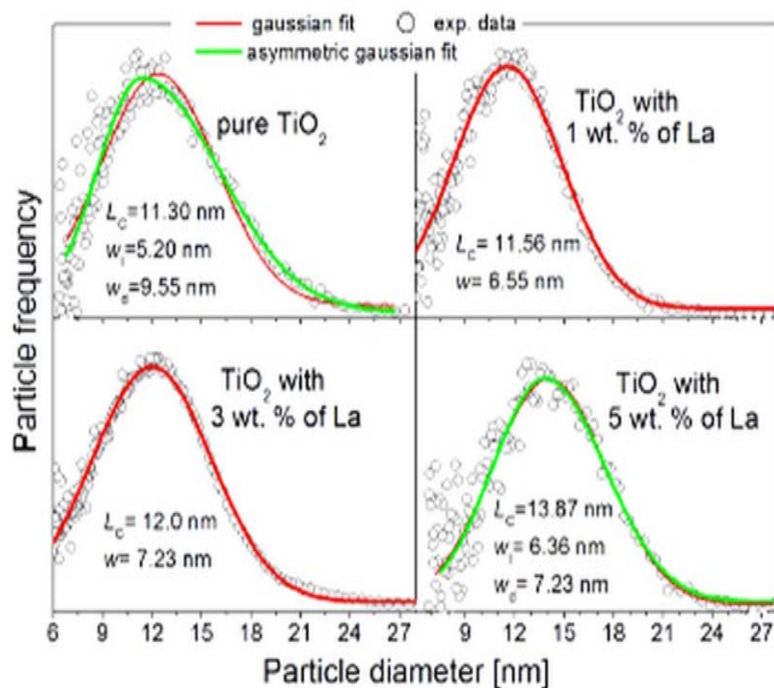


Figure 8 – Particle size distributions in the pure and La-doped TiO_2 samples such as S11, S28, S48 and S16 (Golubović et al, 2009b)

Рис. 8 – Распределение частиц по размерам в чистых и легированных La образцах TiO_2 , таких как C11, C28, C48 и C16 (Golubović et al, 2009b)

Слика 8 – Дистрибуција величине честица у чистим и La-допираним TiO_2 узорцима, као C11, C28, C48 и C16 (Golubović et al, 2009b)

The results of the Atomic Force Microscopy Measurements

The surface of the lanthanum and iron doped TiO_2 nanoparticles sample labeled as S18 (0.65 wt. %) and S111 (5.0 wt. %) recorded by the AFM in the non-contact mode is shown in Figures 9 (Golubović et al, 2009b), 10 and 12, respectively. These images are recorded on doped La and Fe-doped TiO_2 -nanoparticles, previously dispersed in ethanol, deposited on freshly cleaved highly oriented prolific graphite (HOPG). From these images, we can observe that sample S18 consists of very small nanocrystals of 12 nm and greater agglomerated particles. Also, sample S111 consists of several larger nanocrystals, with a large number of agglomerates arranged as it can be seen on its particle histogram in Figure 11.

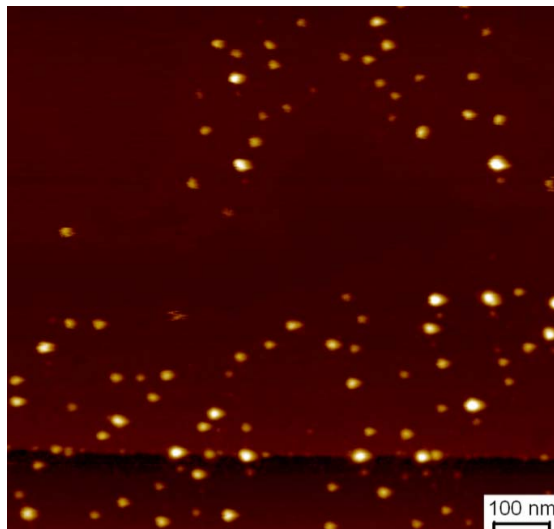


Figure 9 – AFM image of S18 sample (anatase doped with 0.65 wt. % La^{3+})
(1000 x 1000 nm)

Рис. 9 – AFM изображение C18 образца (анатаз легированный с 0.65 вес. % La^{3+})
(1000 x 1000 nm)

Слика 9 – AFM слика C18 узорка (анатаз допиран са 0.65 теж. % La^{3+})
(1000 x 1000 nm)

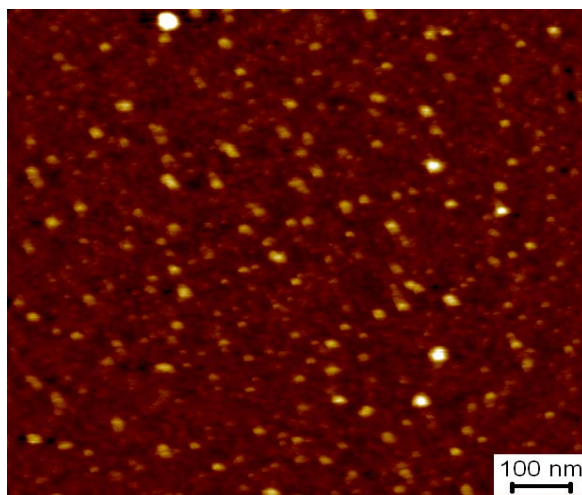


Figure 10 – AFM image of an S111 anatase nanoparticle sample doped with
5 wt. % Fe^{3+} and a calcination duration of 7 h (1000 x 1000 nm)

Рис. 10 – AFM изображение C111 образца наночастиц анатаза легированных с 5
вес. % Fe^{3+} и временем прокаливания - 7 ч. (1000 x 1000 nm)

Слика 10 – AFM слика C111 узорка анатас наночестице допиране са
5 теж. % Fe^{3+} и време трајања калцинације од 7 ч (1000 x 1000 nm)

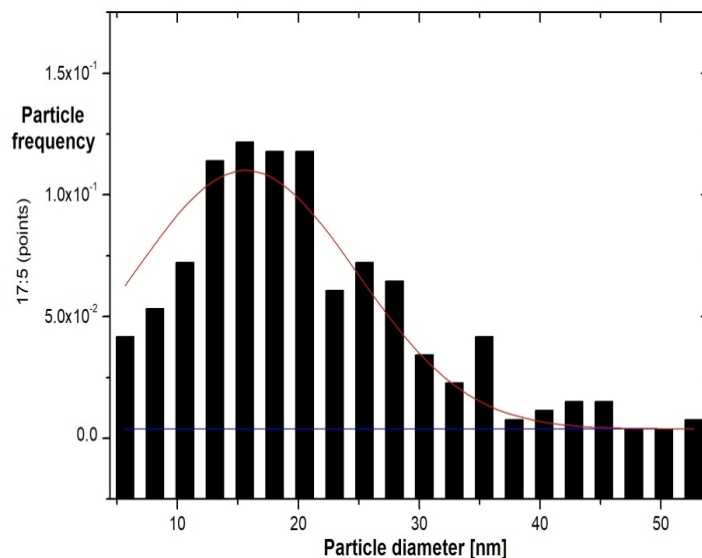


Figure 11 – Particle histogram for the Fe-doped TiO_2 -NP of S111 sample
 Рис. 11 – Гистограмма частиц образца С111 (Fe-допант TiO_2 -НЧ)
 Слика 11 – Хистограм честица за узорак С111 (Fe-допант TiO_2 -НЧ-а)

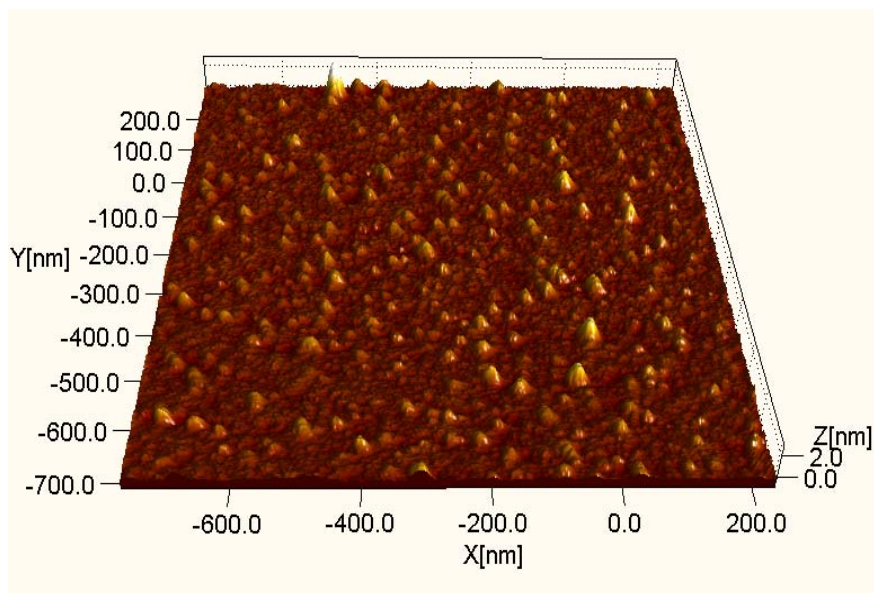


Figure 12 – AFM image of S111 sample - display at an angle
 Рис. 12 – AFM изображение образца С111 – вид под наклоном
 Слика 12 – AFM слика узорка С111 – приказ под углом

Results of the EDS

The chemical compositions of pure and some chosen La-doped TiO₂-nanoparticles have been estimated by the EDS method, and summarized in Table 6, which was partially reported earlier (Golubović et al, 2013), (Grujić-Brojčin et al, 2014).

Table 6 – EDS results for pure and some chosen La-doped TiO₂-NPs
Таблица 6 – EDS результаты по чистым и некоторым La легированным TiO₂-НЧ
Табела 6 – EDS резултати за чисте и неке изабране La допирание TiO₂-НЧ-а

	La (wt. %)	EDS data					
		O (wt. %)	Ti (wt. %)	Na (wt. %)	Cl (wt. %)	La (wt. %)	Total (wt. %)
S06	0.0	32.72	64.54	1.84	0.90	0.0	100
S11	0.0	39.46	60.54	-	-	0.0	100
S18	0.65	42.91	57.09	-	-	0.0	100
S28	1.0	49.71	49.44	-	-	0.85	100
S40a	2.0	44.59	53.45	-	-	1.96	100
S64	6.0	41.71	52.39	-	-	5.91	100

The EDS data (shown in Table 6) and the spectra of pure and La-doped of TiO₂-nanoparticles patterns of samples have been reported earlier by Golubovic et al. (Golubović et al, 2013), for S06 sample and Grujić-Brojcin et al (Grujić-Brojčin et al, 2014), for S11, S18, S28, S40a and S64 samples). These analyzes have shown that only S06 sample synthesized with a calcination duration of 7 h consists of sodium (Na⁺) and chlorine (Cl⁻) ions, which has not been detected in the other observed samples, as we can see in Table 6. Golubovic et al (Golubović et al, 2013) have reported earlier that short duration of calcination may also be the reason for a relatively high concentration of sodium (Na⁺) and chlorine (Cl⁻) ions in the sample with a calcination duration of 1 h. We can see, in Table 6, that the oxygen weight percent in the pure TiO₂-nanoparticle sample is close to stoichiometric TiO₂ (40.0 wt. %), and that the percent of oxygen is higher in the La-doped samples. Based on the data obtained from the EDS measurement method, the final molar La/Ti ratio is lower than at the beginning of the synthesis process; which is estimated at around 63 % of the starting value, except in the case of the sample doped with 0.65 wt. % of La. Finally, the results also show that a low content of La (0.65 wt. %) could not be detected in S18 sample by the EDS method.

Results of the BET

The porous properties of the TiO₂-nanoparticles samples such as P-25, S05, S06, S11, S18, S28 and S40a have been estimated by the BET, BJH and CPMS methods and summarized in Table 7 which has been partially reported earlier (Golubović et al, 2013), (Grujić-Brojčin et al, 2014).

Table 7 – Porous properties of the chosen TiO₂ samples (P-25, S05, S06, S11, S18, S28 & S40a): specific surface area (S_{BET} , S_{meso} , S_{mic} & S_{BJH}), pore volume (V_p & V_{mic}), mean pore diameters obtained from different methods (\bar{D}_{BET} , \bar{D}_{BJH} & \bar{D}_{CPMS}), CPMS fitting parameter (N_s) and the predicted tortuosity factor (τ)

Таблица 7 – Характеристики пористой структуры, выбранных образцов TiO₂ (P-25, S05, S06, S11, S18, S28 и S40a): удельная поверхность (S_{BET} , S_{meso} , S_{mic} & S_{BJH}), объем пор (V_p и V_{mic}) различными методами (\bar{D}_{BET} , \bar{D}_{BJH} & \bar{D}_{CPMS}), CPMS параметры настройки (N_s) и коэффициент извилистости (τ)

Табела 7 – Порозна својства одабраних узорака TiO₂ (P-25, S05, S06, S11, S18, S28 и S40a): специфична површина (S_{BET} , S_{meso} , S_{mic} & S_{BJH}), запремина пора (V_p и V_{mic}) Средњи пречници пора добијени различитим методама (\bar{D}_{BET} , \bar{D}_{BJH} & \bar{D}_{CPMS}), CPMS параметар за подешавање (N_s) и процењени фактор тортуозности (τ)

Parameters	Sample						
	P-25	S05 (0.0)	S06 (0.0)	S11 (0.0)	S18 (0.65)	S28 (1.0)	S40a (2.0)
S_{BET} (m ² g ⁻¹)	13	17	51	58	79	84	78
S_{meso} (m ² g ⁻¹)	13	17	51	-			
S_{mic} (m ² g ⁻¹)	-	-	-	-			
S_{BJH} (m ² g ⁻¹)	-		-	58.2	79.4	83.8	78.1
V_p (cm ³ g ⁻¹)	0.024	0.030	0.088	0.160	0.185	0.258	0.215
V_{mic} (cm ³ g ⁻¹)	-	-	-	-			
\bar{D}_{BET} (nm)	7.5	7.1	6.9	7.1	6.0	7.9	7.1
\bar{D}_{BJH} (nm)	7.4	6.7	6.8	7.1	6.3	7.7	7.5
\bar{D}_{CPMS} (nm)	7.7	7.4	7.1	8.1	6.9	7.7	7.5
N_s	5.5	8	4	8	13	12	11
τ	3.0	4.0	2.7	4.1	5.3	4.4	4.6

In order to investigate the effect of the chosen TiO₂ nanoparticles and their lanthanum doped catalysts on the pore structure and the adsorption ability, the nitrogen sorption isotherm measurements have been carried out. The specific surface area (S_{BET}) and the pore volume (V_p) obtained by the BET method, and the mesopore diameter calculated from both the BET and the BJH (\bar{D}_{BET} , \bar{D}_{BJH} , respectively) for the chosen samples can be seen in Table 7, the data of which have been shown earlier by Golubovic et al (Golubović et al, 2013) for P-25, S05 and S06

patterns of samples and by Grujić-Brojčin et al (Grujić-Brojčin et al, 2014), for S11, S18, S28 and S40a patterns of samples, respectively.

Based on the porosity parameters obtained from the standard nitrogen adsorption isotherms determined from the α_c plot (Kaneko et al, 1998), we can also establish that the chosen TiO₂ samples are completely mesoporous nanoparticles. The value of S_{BET} in the La-doped samples, S18 and S28: 79 and 84 m²g⁻¹, respectively, are higher than those in the pure TiO₂ nanoparticles samples, S05, S06 and S11: 17, 51 and 58 m²g⁻¹ respectively. Also, the values of S_{BET} for the synthesis of TiO₂ nanoparticles, in the range of 17-58 m²g⁻¹ are greater than S_{BET} of Degussa P-25[®] in the value of 13 m²g⁻¹. The mean pore diameters, obtained from the BET results ($\frac{1}{4}D_{BET} \bullet 4V_p = S_{BET}$) were in good agreement with the diameters obtained by the BJH method. The most commonly used method entitled as the BJH method for the determination of the pore size distribution (PSD) listed in Table 7, as reported by Barrett (Barrett et al, 1951), is estimated from the desorption branch of the hysteresis isotherm loops. Also, the CPSM method (Salmas & Androustopoulos, 2001), (Androustopoulos & Salmas, 2000) for the PSD evaluation has been applied. In this method, the pore structure is considered as a statistically large number of independent, non-intersected corrugated pores, made of a series of N_s cylindrical segments of equal length, with randomly distributed diameters of mesopores nanoparticles (Golubović et al, 2013), (Salmas & Androustopoulos, 2001), (Androustopoulos & Salmas, 2000). The CPSM fitting parameter N_s , mentioned above, is also listed in Table 7: higher values of N_s have been obtained for the doped samples, which can be associated with a more complex pore structure in the doped samples (Salmas & Androustopoulos, 2001). As a result of the CPSM, the pore tortuosity factor τ is also estimated and listed in Table 7, as a measure of diffusion through porous media based on the nitrogen sorption hysteresis data (Golubović et al, 2013), (Salmas & Androustopoulos, 2001). The dependence of the tortuosity factor on the La-content in the doped samples shows the same tendency as N_s (Grujić-Brojčin et al, 2014); higher values of τ are obtained for the doped samples, with the maximum in S18 sample with $\tau = 5.3$. This points to the most complex pore structure consisting of interconnected pore segments with different diameters in this sample.

Finally, we expect that the best catalytic properties of the chosen TiO₂-NPs samples are found in S11 as pure and in S28 dopant sample that doped TiO₂ nanoparticles in a concentration of 1.0 mole % of La³⁺ ions, based on the value of the S_{BET} in Table 7. If we compare the

properties of S05 samples synthesized with the calcination duration of 5 h and S06 and S11 samples, whose calcination duration was 7 h, we can determine that the catalysts calcined for 7 h have better properties. The best properties found in S11 sample for pure TiO₂ nanoparticles, as seen in Table 7, led us to choose this pure TiO₂ sample for photocatalytic research and testing in our study.

Result of the photocatalytic activities

The photocatalytic activity was measured in four experiments: three experiments of photocatalytic activities and one coupled photocatalytic–microbiological experiment. All experiments were carried out in a bath slurry-catalyst circular photoreactor, in dark and under direct ultraviolet radiation simulated with a sodium SONT UV400 lamp, with the initial concentrations of 1.00 ml/L and 0.50 ml/L MTBE in the water solution, respectively, depending on the types of experiments.

Results of the experiments of the photocatalytic activities

The experimental investigation of the photocatalytic degradation of MTBE was performed in three different experiments. The initial concentration in all these experiments was 1.00 ml/L and the solutions were thermo-stated at 30°C. All solutions were tested for 60 minutes in the bath slurry-catalyst circular photoreactor in aerobic conditions and their degradation rate was measured in 15-minute intervals.

The first experiment was carried out under direct UV radiation simulated with the sodium SONT UV400 lamp in the photoreactor with the initial concentration of 0.50 ml/L of the MTBE water solution and different types of synthesized TiO₂ nanoparticles, using the following samples of TiO₂ nanoparticles: S07 (pure TiO₂ nanoparticles), S18, S28, S38, S40a, S48, S52a and S64 (TiO₂ nanoparticles doped with La³⁺ in the following concentration: 0.65; 1.0; 2.0; 3.0; 4.0; 5.0 and 6.0 wt. %, respectively) and one commercial TiO₂ nanoparticles catalyst (Degussa P-25®). The concentration of all catalysts used in the experiment was 0.1 g/L. The results of the measurements of the detected reduction of the MTBE concentration during all experiments at the GC/MSD/Headspace are shown in Table 8.

Our results in the experiment show that the best photocatalytic efficiency was obtained in TiO₂ doped with La³⁺ of 1 wt. %, but the fastest drop in the polluted MTBE concentration in the water solution was achieved in TiO₂ doped with La³⁺ of 3 wt. %.

Table 8 – Photocatalytic degradation of the MTBE initial concentration of 1.00 ml/L with different concentrations of La-doping of TiO₂-NPs and pure TiO₂-NPs (synthesized and commercial Degussa P-25[®]) in a concentration of 0.1 g/L

Таблица 8 – Фотокаталитическая деградация МТБЭ начальной концентрации 1,00 ml/L с различной концентрацией La - легированных TiO₂-НЧ и чистых TiO₂-НЧ (синтезировано в коммерческих целях Degussa P-25[®]) с концентрацией 0,1 g/L
Табела 8 – Фотокаталитичка деградација МТБЕ почетне концентрације од 1,00 ml/L са различитом концентрацијом La -допинта TiO₂-НЧ-а и чистих TiO₂-НЧ-а (синтезираног и комерцијалног Degussa P-25[®]) у концентрацији од 0,1 g/L

Time UV (min)	S07	P-25	Samples TiO ₂ doped with different wt. % La ³⁺						
			S18 (0.65)	S28 (1.0)	S40a (2.0)	S48 (3.0)	S52a (4.0)	S38 (5.0)	S64 (6.0)
0	1.000	1.000	1.000	1.000	1.000	1.000	1.000	1.000	1.000
15	-	-	0.797	-	-	0.184	0.678		0.671
30	0.659	-	0.188	0.180	0.198	-	0.132		0.410
45			0.095	0.062	-	-		0.225	0.239
60	0.093	0.488	-	-	0.122	0.178	0.052	-	-

The second experiment was carried out under direct ultraviolet radiation simulated with the SONT UV400 lamp in the photoreactor with the initial concentration of 1.00 ml/L of the MTBE water solution in presence of the catalyst synthesized TiO₂-nanoparticles doped with different concentrations of Fe³⁺ ions and their two calcination durations of 7 and 24 h. We tested the photocatalytic activities catalysts and their dependence on the calcination duration of the following samples: S111 - S112 (5 wt. %, calcination duration of 7 and 24h, respectively), S117 - S118 (1 wt. %, calcination duration of 7 and 24h, respectively), and S119 - S120 (3 wt. %, calcination duration of 7 and 24h, respectively), as a photocatalytic degradation degree of MTBE in the water solution. The carbon-dioxide evolution during the experiment is shown in Table 9 in comparison with pure TiO₂-nanoparticles: synthesized S07 catalyst sample and commercial catalyst – Degussa P-25[®], determined at the GC/MSD/Headspace (as shown In Table 8). The concentration of all catalysts used in the experiment was 0.1 g/L.

Our results in the second experiment show that the best photocatalytic efficiency was found in TiO₂ doped with the highest concentration of Fe³⁺ ions dopant, 5 wt. % and the calcination duration time of 7 h. The greatest difference in the degradation degree versus the calcination duration is the highest concentration catalyst, and the smallest concentration is 3 wt. % of the Fe-doped TiO₂ nanoparticle catalyst.

Table 9 – Photocatalytic degradation of MTBE as the percentage of the total CO₂ yield, the initial concentration of 1.00 ml/L MTBE in the water solution with different concentrations of Fe-doping of TiO₂-NPs and pure TiO₂-NPs (synthesized and commercial Degussa P-25[®]) in a concentration of 0.1 g/L

Таблица 9 – Фотокаталитическая деградация МТБЭ как процент общего выброса CO₂, с начальной концентрацией 1,00 ml/L МТБЭ в водном растворе с различной концентрацией Fe- легированных TiO₂-НЧ и чистых TiO₂-НЧ (синтезировано в коммерческих целях Degussa P-25[®]) с концентрацией 0,1 g/L

Табела 9 – Фотокаталитичка деградација МТБЕ-а као проценат укупног приноса CO₂, почетне концентрације од 1,00 ml/L МТБЕ у воденом раствору са различитом концентрацијом Fe-допинга од TiO₂-НЧ-а и чистих TiO₂-НЧ-а (синтетизованог и комерцијалног Degussa P-25[®]) у концентрацији од 0,1 g/L

Time UV (min)	S07	P-25	Samples TiO ₂ doped with different wt. % Fe ³⁺					
			S111 (5.0)	S112 (5.0)	S117 (1.0)	S118 (1.0)	S119 (3.0)	S120 (3.0)
0	0.000	0.000	0.000	0.000	0.000	0.000	0.000	0.000
15	-	-	0.273	0.258	-	0.180	0.323	-
30	0.341		0.550	0.486	0.442	0.402	-	0.494
45			0.845	-	0.765	0.702	0.827	0.664
60	0.907	0.512	0.976	0.931	0.905	0.899	0.928	0.922

The third experiment was carried out under direct UV light exposure simulated with the SONT UV400 lamp in the photoreactor with the initial concentration of 1.00 ml/L of the MTBE water solution in the presence of different catalyst types of synthesized TiO₂ nanoparticles, using the following samples of TiO₂ nanoparticles: S07 (pure TiO₂-NP), S93 and S96 (TiO₂-NPs doped with 10 wt. % V³⁺), S28 (TiO₂-NPs doped with 1.0 wt. % La³⁺), and commercial TiO₂ nanoparticles (Degussa P-25[®]). The results of the measurement of the detected reduction of the MTBE concentration during the experiments were determined at the GC/MSD/Headspace. The results of the photocatalytic degradation of MTBE (Table 9) for the samples such as S117, S119 and S111 (TiO₂-NPs doped with 1.0, 3.0 and 5.0 wt. % Fe³⁺, respectively, with the duration time of 7 h for all samples) are shown for comparison in Table 10. The concentration of all catalysts used in the experiment was 0.1 g/L.

Table 10 – Photocatalytic degradation of the MTBE initial concentration of 1.00 ml/L with La, Fe and V-doping of TiO₂-NPs and pure TiO₂-NPs (synthesized and commercial Degussa P-25[®]) in a concentration of 0.1 g/L

Таблица 10 – Фотокаталитическая деградация МТБЭ начальной концентрации 1,00 ml/L с La Fe и V - легированных TiO₂-НЧ и чистых TiO₂-НЧ (синтезировано в коммерческих целях Degussa P-25[®]) с концентрацией 0,1 g/L

Табела 10 – Фотокаталитичка деградација МТБЕ-а почетне концентрације од 1,00 ml/L са La, Fe и V-допингом TiO₂-НЧ-а и чисто TiO₂-НЧ-а (синтезираног и комерцијалног Degussa P-25[®]) у концентрацији од 0,1 g/L

Time UV (min)	S07	P-25	Samples TiO ₂ doped with different wt. % V ³⁺		La ³⁺ , wt %	Fe ³⁺ , wt. %		
			S93 (10.0)	S96 (10.0)	S28 (1.0)	S117 (1.0)	S119 (3.0)	S111 (5.0)
0	1.000	1.000	1.000	1.000	1.000	1.000	1.000	1.000
15	-	-	0.345	-	-	-	0.777	0.727
30	0.659	-	-	0.650	0.180	0.558	-	0.450
45	-	-	0.152	-	0.062	0.235	0.173	0.155
60	0.093	0.488	-	-	-	0.095	0.072	0.024

Our results in the experiment show that the best photocatalytic efficiency was found in TiO₂ doped with La³⁺ of 1.0 wt. % (S28 sample) for 45 minutes, but the fastest drop in the polluted MTBE concentration in the water solution was in TiO₂ doped with V³⁺ of 10.0 wt. % (sample S93). Also, our results show different degradation rates for TiO₂ doped with V³⁺ of 10.0 wt. %, S93 and S96 samples, synthesized with different duration times (7 and 24 h, respectively). This can be explained by a different nanomaterial structure. If we compare the results in Table 10, we can see that the best degree of the total MTBE degradation in 60 minutes is achieved in S111 and S119 catalysts, which were doped with 3.0 and 5.0 wt. % of Fe, respectively, but their total MTBE degradation is smaller for 45 minutes compared to the case when we used the La-dopant of TiO₂-NPs as a catalyst (S28 sample).

Results of the coupled photocatalytic–microbiological experiment

The experimental investigation of the coupled photocatalytic-microbiological degradation of MTBE was performed in one experiment. The initial concentration in the experiment was 0.50 ml/L, and the solutions were thermo-stated at 30°C.

The experiment was carried out under direct ultraviolet light exposure simulated with the UV lamp in the batch slurry-catalyst circular photoreactor in the presence of the microorganism (MO) *Pseudomonas aeruginosa strain ATCC 9023* with the initial concentration of 10⁷ CFU

mL⁻¹ (as explained in the following experimental part: *Microbial activity and inactivity of the coupled photocatalytic-microbiological experiment*) and with different concentrations (0.25, 0.50, 0.75 and 1.0 g/L) of commercial TiO₂ nanoparticles – Degussa P-25 (Degussa P-25[®], AG Frankfurt), and without a catalyst. The results of this research are shown in Table 11. All solutions were tested for 150 minutes in the photoreactor and gas chromatography with a mass detector using the headspace (GC/MSD/Headspace) has been applied in 15-minute intervals, and we presented only three time intervals (0, 60 and 150 minutes).

Table 11 – Photocatalytic activity of the coupled photocatalytic-microbiological processes in the first experiment

Таблица 11 – Фотокаталитическая активность комбинационного фотокаталитично-микробиологического процесса первого эксперимента
Табела 11 – Фотокаталитичка активност комбинационих фотокаталитичко-микробиолошких процеса у првом експерименту

Serial No.	Time (min)	I sol. (%)	II sol. (%)	III sol. (%)	IV sol. (%)	V sol. (%)	VI sol. (%)
1	0.00	1.000	1.000	1.000	1.000	1.000	1.000
2	60.0	0.371	0.308	0.512	0.664	0.325	0.172
3	150.0	0.144	0.144	0.199	0.344	0.119	0.030
Legend (MTBE w. sol. (c=500 ml/L) + MO (c=10 ⁷ CFU mL ⁻¹)):							
I sol: UV lamp without TiO ₂ ; II sol: UV lamp + TiO ₂ (1.0 g/L); III sol: Dark experiment (without UV lamp);				IV sol: UV lamp + TiO ₂ (0.50 g/L); V sol: UV lamp + TiO ₂ (0.25 g/L); VI sol: UV lamp + TiO ₂ (0.75 g/L).			

The results in Table 11 show that the best degradation degree of MTBE was obtained in the VI solution, when we used direct UV radiation simulated with the sodium lamp - SONT UV400 and 0.75 g/L of TiO₂ powder Degussa P-25[®] for 60 and 150 minutes. The results of the I and II solutions show that the TiO₂ catalyst in a concentration of 1.0 g/L achieved the detoxification effect on the MO after 60 minutes of the coupled process of the MTBE degradation; a better result was also achieved when we used the lamp and TiO₂ powder Degussa P-25[®] in the concentration of 0.25 g/L. Also, the IV solution presented that the dark experiment (without the UV lamp and the catalyst) resulted in a higher MTBE degradation degree than in the I, II and IV solutions, especially in the highest concentration as well as in the effect of aeration condition in all experiments. These results show that TiO₂ and direct ultraviolet radiation simulated with the sodium lamp - SONT UV400 inactivate and kill microorganisms. The optical density results have proven this assertion by measuring the microbial activity and inactivity in the coupled

photocatalytic-microbiological experiment, which is shown in the text below.

Results of the microbiological growth

The measurements of the microbiological growth for the selected *Pseudomonas aeruginosa* strains (ATCC 9023 and DV 2739) were studied in three experiments, one as the microbial activity and inactivity in the coupled photocatalytic-microbiological experiment and two in the experiments on antimicrobial activities. The coupled photocatalytic-microbiological experiment was performed in the batch slurry-catalyst circular photoreactor, in dark and under direct ultraviolet radiation simulated with the SONT UV400 lamp. The experiments on antimicrobial activities were carried out in the microbiological cabinet. The text below gives the optical density values, measured during these experiments.

Results of the microbial activity and inactivity of the coupled photocatalytic-microbiological experiment

The microbial activity and inactivity of the coupled photocatalytic-microbiological experiment are determined by the optical density measurement for the MTBE solutions in the colorimeter, at 550 nm. The results are shown in Table 12.

Our results show the following characteristics of the coupled photocatalytic-microbiological experiment:

- I solution: This experimental result shows that there has been a linear increase in the growth of microorganisms, with the reduction of concentration of MTBE in the water solution at 90 and 150 minutes. The reduction of the concentration of MTBE is actually achieved owing to the combined influence of UV radiation simulated by the sodium lamp and the MO in aerobic conditions, which is shown in the coupled photocatalytic-microbiological degradation of MTBE (Tab. 11) and the MO activity (Tab. 12);
- II solution: The experiment with direct ultraviolet radiation simulated with the sodium lamp and the TiO₂ catalyst at a concentration of 1.0 g / L in the presence of MO showed an increase in the MO growth (30.0 min.); constant values (30.0 to 45.0) and low (45.0 to 75.0), after which a low drop in the MO growth occurred. Also, a somewhat greater decrease in the MTBE concentration was achieved than in the I solution at the end of the experiment (t = 150 min); the MTBE degradation

degree was identical in both experiments (Tab. 11); also, a slightly lower MTBE concentration was achieved, as in accordance with the I solution, but at the end of the experiment ($t = 150$ min), the identical MTBE degradation rates in both experiments are achieved, as shown in Table 11;

- III solution: Our result in the dark condition experiment showed that there has been a decrease in the MO growth to 135.0 minute, after which the MO growth increased. The effect in the last 15-20 minutes is possible to be explained by the aerobic conditions which caused the degradation degree of MTBE in the water solution at the end of the experiment.
- IV and V solution: The results of both experiments showed a very similar profile of the catalyst influence (inactivity of activity) with direct artificial irradiation of the lamp on the MO in the aerobic conditions, and a reduced MO growth at the end of both experiments. A high degradation degree of MTBE in the water solution was obtained in the V solution compared to the IV solution due to a greater MO number and the catalyst concentration, as shown in Tables 11 and 12, respectively.
- VI solution: Our experiment results showed that there was an increase in the MO growth at the 30th minute, followed by the MO growth reduction until the end of the experiment. This phenomenon can be explained in the following way: in the first 15 minutes, a high concentration of the catalyst inactivated the MO; after that, the MO accommodated to this condition and grew in the next 15 minutes due to the feeding with MTBE in aeration conditions. At the moment of a large decomposition of MTBE, which is formed in the coupled process, the detoxification of the microorganisms occurs.

By comparing the results of the I to VI solution experiments, we have found out that the best results are achieved in the VI solution experiment due to the excessive concentration of the catalyst, which has a large inactivating effect on the MO. It has negatively affected the coupled photocatalytic-microbiological processes. Therefore, the best property of the coupled photocatalytic-microbiological experiment is achieved with the initial concentration of 0.75 g/L Degussa P-25[®] TiO₂ nanopowder as the maximally effective photo catalyst for our experimental conditions.

Table 12 – Microbial growth for *Pseudomonas aeruginosa* strain ATCC 9023, with the initial concentration of 10^7 CFU mL⁻¹ at 0.50 ml/L of the MTBE water solution
 Таблица 12 – Рост микроорганизмов штамма бактерий *Pseudomonas aeruginosa* ATCC 9023 с начальной концентрацией 10^7 CFU mL⁻¹ на 0,50 ml/L водного раствора МТБЭ
 Табела 12 – Микробни раст за сој бактерије *Pseudomonas aeruginosa* ATCC 9023 почетне концентрације од 10^7 CFU mL⁻¹ у воденом раствору МТБЕ-а концентрације од 0,50 ml/L

Serial No.	Time (min)	I sol.	II sol.	III sol.	IV sol.	V sol.	VI sol.
1	0.00	0.039	2.395	0.043	1.380	1.428	1.852
2	15.0	0.050	2.436	0.040	1.256	1.461	1.642
3	30.0	0.052	2.659	0.042	1.173	1.403	2.051
4	45.0	0.041	2.659	0.036	1.438	1.364	1.623
5	60.0	0.080	2.334	0.032	1.452	1.432	1.577
6	75.0	0.098	2.683	0.046	1.350	1.375	1.595
7	90.0	0.089	2.290	0.035	1.286	1.395	1.621
8	105.0	0.099	2.232	0.026	1.387	1.360	1.502
9	120.0	0.103	2.280	0.029	1.314	1.323	1.670
10	135.0	0.129	2.232	0.074	1.256	1.265	1.565
11	150.0	0.104	-	0.076	1.199	1.297	1.481
Legend (MTBE w. sol. (c=0.50 ml/L) + MO (c= 10^7 CFU mL ⁻¹):							
I sol: UV lamp without TiO ₂ ; II sol: UV lamp + TiO ₂ (1.0 g/L); III sol: Dark experiment (without UV lamp);				IV sol: UV lamp + TiO ₂ (0.50 g/L); V sol: UV lamp + TiO ₂ (0.25 g/L); VI sol: UV lamp + TiO ₂ (0.75 g/L).			

Results of the experiments of antimicrobial activities

The antimicrobial activities are examined by the measurement of the optical density for the MTBE solutions of *Pseudomonas aeruginosa* strains ATCC 9023 as the model microorganism (MO) for the first experiment. We investigated the effect of different concentrations of MTBE (0.15, 0.25, 0.50 and 1.5 ml/L), as well as a commercial titania catalyst (anatase, purity 99.9 %, Alfa Aesar Lancaster, c=0.1 g/L) and the catalyst-reagent system TiO₂ and FeCl₃ (TiO₂:FeCl₃ = 1:1, c=0.1 g/L) on the growing of the MO. The results were obtained by measuring the optical density in the colorimeter, at 550 nm, and presented in Figure 13.

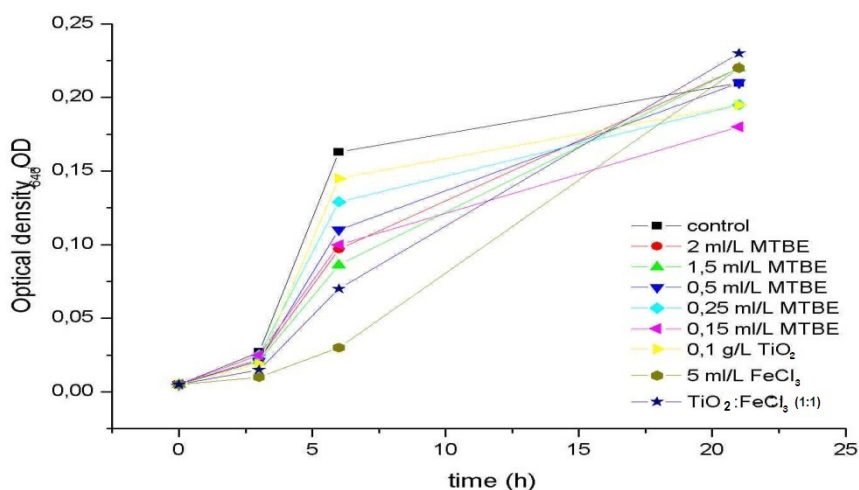


Figure 13 – The effect of different concentrations of MTBE, catalysts and reagents on the growth of *Pseudomonas aeruginosa* strain ATCC 9023

Рис. 13 – Влияние различных концентраций МТБЭ, катализатора и реагента на рост штамма бактерий *Pseudomonas aeruginosa* ATCC 9023

Слика 13 – Утицај различите концентрације МТБЕ-а, катализатора и реагенса на раст соја бактерије *Pseudomonas aeruginosa* ATCC 9023

Our results showed that the highest *Pseudomonas aeruginosa* strain ATCC 9023 growth was obtained with a high MTBE concentration of 1.5 ml/L. The Fenton reagent and the catalyst-reagent system of TiO₂ and FeCl₃ in the ratio of 1:1 have a stimulation effect on the growth of microorganisms. Finally, the best microbiological growth was achieved with the catalyst-reagent system TiO₂ and FeCl₃ in the ratio of 1:1, which can be explained with a coupled stimulation influence of the Fenton reagent in a combination with anatase titania nanopowder in equal portions. It is the best nutrition for bacteria and their growth in our experiment.

In the second experiment, we measured the effect of different types and concentrations of catalysts on antimicrobial activities of *Pseudomonas aeruginosa* strain DV 2739, as a model microorganism. We studied six different catalysts, such as titania nanopowder catalysts: commercial titania anatase nanopowder (A), titania power Degussa P-25[®], the catalyst-reagent system of anatase TiO₂ and FeCl₃ in the ratio of 1:1 (A-Fe), synthesised nanopowder TiO₂ (S11 sample), synthesised nanopowder TiO₂ doped with 2.5 wt. % of Fe³⁺ (S24 sample, duration time

of 7h) and synthesised nanopowder TiO_2 doped with 5.0 wt. % of La^{3+} (S16 sample, duration time of 7 h), all in four concentrations of 0.05, 0.1, 0.2 and 0.25 mg/L. The quantified results of the measurements on the colorimeter are shown in the following Tables (Tab. 13 to Tab. 16).

Table 13 – The effect of $c=0.05$ mg/L of different catalyst types on the microbial growth for *Pseudomonas aeruginosa* strain DV 2739, with the initial concentration of 10^7 CFU mL^{-1} at 1.00 ml/L of the MTBE water solution

Таблица 13 – Влияние $c=0.05$ mg/L различных типов катализаторов на рост штамма бактерий *Pseudomonas Aeruginosa* DV 2739, с начальной концентрацией 10^7 CFU mL^{-1} на 1.00 ml/L водного раствора МТБЭ

Табела 13 – Утицај различитих типова катализатора концентрације од 0.05 mg/L на микробни раст за сој бактерије *Pseudomonas aeruginosa* DV 2739, почетне концентрације од 10^7 CFU mL^{-1} у воденом раствору МТБЕ-а концентрације од 1,00 ml/L

Time (h)	0.05 mg/L catalysts							
	A	P-25	S11	S24	S16	A-Fe	K (only TSB base)	K ₁ (TSB base + MTBE)
0	0.025	0.110	0.000	-	-	0.040	0.000	0.005
1	0.060	0.115	0.010	0.010	0.045	0.060	0.000	0.020
2	0.045	0.115	0.015	0.015	0.055	0.065	0.000	0.005
3	0.045	0.125	0.018	0.015	0.050	0.072	0.000	0.010
After 20 h, we added <i>Pseudomonas aeruginosa</i> strain DV 2739 (MO)								
Time (h)	0.05 mg/L titania powder and titania based catalysts							
	A	P-25	S11	S24	S16	A-Fe	K (only TSB base)	K ₁ (TSB base + MTBE)
20	0.062	0.125	0.020	0.027	0.045	0.065	0.010	0.020
24	0.290	0.360	0.275	0.280	0.310	0.335	0.270	0.280
25	0.315	0.380	0.270	0.280	0.310	0.320	0.270	0.280
26	0.310	0.370	0.270	0.280	0.320	0.330	0.280	0.290
27	0.310	0.360	0.270	0.280	0.310	0.330	0.290	0.295
44	0.300	0.360	0.250	0.275	0.300	0.330	0.260	0.270
47	0.280	0.360	0.260	0.265	0.310	0.325	0.250	0.265
49	0.280	0.360	0.240	0.270	0.290	0.320	0.250	0.260
51	0.280	0.360	0.255	0.255	0.300	0.320	0.255	0.260
grow	0.255	0.250	0.255	0.255	0.255	0.280	0.255	0.255

Table 14 – The effect of $c=0.10$ mg/L of different catalyst types on the microbial growth for *Pseudomonas aeruginosa* strain DV 2739, with the initial concentration of 10^7 CFU mL^{-1} at 1.00 ml/L of the MTBE water solution

Таблица 14 – Влияние $c=0.10$ mg/L различных типов катализаторов на рост штамма бактерий *Pseudomonas Aeruginosa* DV 2739, с начальной концентрацией 10^7 CFU mL^{-1} на 1.00 ml/L водного раствора МТБЭ

Табела 14 – Утицај различитих типова катализатора концентрације од 0.10 mg/L на микробни раст за сој бактерије *Pseudomonas aeruginosa* DV 2739, почетне концентрације од 10^7 CFU mL^{-1} у воденом раствору МТБЕ-а концентрације од 1,00 ml/L

Time (h)	0.10 mg/L catalysts							
	A	P-25	S11	S24	S16	A-Fe	K (only TSB base)	K ₁ (TSB base + MTBE)
0	0.155	0.190	0.032	0.015	0.030	0.175	0.000	0.005
1	0.175	0.200	0.040	0.030	0.055	0.207	0.000	0.020
2	0.200	0.195	0.055	0.040	0.055	0.210	0.000	0.005
3	0.210	0.200	0.055	0.035	0.060	0.220	0.000	0.010
After 20 h, we added <i>Pseudomonas aeruginosa</i> strain DV 2739 (MO)								
Time (h)	0.10 mg/L titania powder and titania based catalysts							
	A	P-25	S11	S24	S16	A-Fe	K (only TSB base)	K ₁ (TSB base + MTBE)
20	0.200	0.200	0.055	0.033	0.040	0.195	0.010	0.020
24	0.430	0.430	0.320	0.300	0.315	0.440	0.270	0.280
25	0.440	0.420	0.310	0.280	0.310	0.430	0.270	0.280
26	0.440	0.420	0.320	0.290	0.310	0.460	0.280	0.290
27	0.440	0.420	0.310	0.310	0.310	0.450	0.290	0.295
44	0.420	0.420	0.310	0.280	0.310	0.470	0.260	0.270
47	0.410	0.410	0.300	0.275	0.300	0.430	0.250	0.265
49	0.410	0.410	0.290	0.285	0.300	0.440	0.250	0.260
51	0.410	0.420	0.310	0.290	0.305	0.440	0.255	0.260
grow	0.255	0.230	0.278	0.275	0.275	0.265	0.255	0.255

Table 15 – The effect of $c=0.20$ mg/L of different catalyst types on the microbial growth for *Pseudomonas aeruginosa* strain DV 2739, with the initial concentration of 10^7 CFU mL⁻¹ at 1.00 ml/L of the MTBE water solution

Таблица 15 – Влияние $c=0.20$ мг/л различных типов катализаторов на рост штамма бактерий *Pseudomonas Aeruginosa* DV 2739, с начальной концентрацией 10^7 CFU mL⁻¹ на 1.00 мл/л водного раствора МТБЭ

Табела 15 – Утицај различитих типова катализатора концентрације од 0.20 мг/л на микробни раст за сој бактерије *Pseudomonas aeruginosa* DV 2739, почетне концентрације од 10^7 CFU mL⁻¹ у воденом раствору МТБЕ-а концентрације од 1,00 мл/л

Time (h)	0.20 mg/L catalysts							
	Anat	P-25	S11	S24	S16	A-Fe	K (only TSB base)	K ₁ (TSB base + MTBE)
0	0.190	0.275	0.053	0.046	0.085	0.160	0.000	0.005
1	0.210	0.300	0.072	0.080	0.125	0.207	0.000	0.020
2	0.250	0.300	0.080	0.080	0.125	0.210	0.000	0.005
3	0.240	0.300	0.083	0.080	0.116	0.260	0.000	0.010
After 20 h, we added <i>Pseudomonas aeruginosa</i> strain DV 2739 (MO)								
Time (h)	0.20 mg/L titania powder and titania based catalysts							
	A	P-25	S11	S24	S16	A-Fe	K (only TSB base)	K ₁ (TSB base + MTBE)
20	0.240	0.310	0.080	0.086	0.105	0.220	0.010	0.020
24	0.460	0.480	0.330	0.340	0.345	0.450	0.270	0.280
25	0.470	0.500	0.320	0.350	0.355	0.460	0.270	0.280
26	0.470	0.490	0.320	0.350	0.350	0.460	0.280	0.290
27	0.465	0.490	0.330	0.350	0.350	0.440	0.290	0.295
44	0.440	0.490	0.320	0.360	0.350	0.460	0.260	0.270
47	0.430	0.480	0.320	0.340	0.350	0.460	0.250	0.265
49	0.435	0.475	0.310	0.340	0.340	0.450	0.250	0.260
51	0.430	0.490	0.325	0.350	0.350	0.470	0.255	0.260
grow.	0.240	0.215	0.272	0.304	0.265	0.310	0.255	0.255

Table 16 – The effect of $c=0.25$ mg/L of different catalyst types on the microbial growth for *Pseudomonas aeruginosa* strain DV 2739, with the initial concentration of 10^7 CFU mL^{-1} at 1.00 ml/L of the MTBE water solution

Таблица 16 – Влияние $c=0.25$ mg/L различных типов катализаторов на рост штамма бактерий *Pseudomonas Aeruginosa* DV 2739, с начальной концентрацией 10^7 CFU mL^{-1} на 1.00 ml/L водного раствора МТБЭ

Табела 16 – Утицај различитих типова катализатора концентрације од 0.25 mg/L на микробни раст за сој бактерије *Pseudomonas aeruginosa* DV 2739, почетне концентрације од 10^7 CFU mL^{-1} у воденом раствору МТБЕ-а концентрације од 1,00 ml/L

Time (h)	0.25 mg/L catalysts							
	A	P-25	S11	S24	S16	A-Fe	K (only TSB base)	K ₁ (TSB base + MTBE)
0	0.380	0.620	0.060	0.110	0.175	0.540	0.000	0.005
1	0.410	0.640	0.090	0.130	0.210	0.560	0.000	0.020
2	0.420	0.640	0.100	0.130	0.210	0.570	0.000	0.005
3	0.440	0.640	0.095	0.125	0.202	0.560	0.000	0.010
After 20 h, we added <i>Pseudomonas aeruginosa</i> strain DV 2739 (MO)								
Time (h)	0.25 mg/L titania powder and titania based catalysts							
	A	P-25	S11	S24	S16	A-Fe	K (only TSB base)	K ₁ (TSB base + MTBE)
20	0.430	0.650	0.100	0.127	0.185	0.520	0.010	0.020
24	0.630	0.750	0.290	0.380	0.445	0.690	0.270	0.280
25	0.640	0.740	0.330	0.380	0.455	0.675	0.270	0.280
26	0.640	0.740	0.350	0.370	0.460	0.680	0.280	0.290
27	0.630	0.740	0.330	0.380	0.450	0.690	0.290	0.295
44	0.620	0.775	0.340	0.400	0.460	0.700	0.260	0.270
47	0.620	0.750	0.340	0.380	0.460	0.710	0.250	0.265
49	0.620	0.760	0.340	0.390	0.450	0.700	0.250	0.260
51	0.620	0.760	0.330	0.380	0.460	0.720	0.255	0.260
grow.	0.240	0.140	0.270	0.270	0.285	0.180	0.255	0.255

The results of our experimental research of the influence of the types and different concentrations of catalysts on the increase of the MO growth showed the following:

1. Catalyst concentration of 0.05: The best MO growth at the lowest catalyst concentration is obtained for the samples in this order: S24 & S11 (identical values), then A (titania powder anatase), P-25 (Degussa P-25[®]) and A-Fe (catalyst system titania powder anatase - FeCl₃);

2. Catalyst concentration of 0.10: The best MO growth at the catalyst concentration of 0.10 g/L is obtained for the samples in this order: S24 (titania doped Fe^{3+}), then S11 (titania nanopowder), S16 (titania doped La^{3+}), A, A-Fe and P-25;
3. Catalyst concentration of 0.20: The best MO growth at the catalyst concentration of 0.20 g/L is obtained for the samples in this order: S24, then S16, S11, A-Fe, A, and P-25;
4. Catalyst concentration of 0.25: The best MO growth at the catalyst concentration of 0.25 g/L is obtained for the samples in this order: S11, then S24, S16, A, A-Fe, and P-25.

Based on these results from Table 13 to Table 16, it can be concluded that the optical density drops between 26 and 27 hours after the start of the experiment, i.e. between 6 and 7 after adding the MO for all concentrations, there was a decrease in optical density in all samples. Nevertheless, S11, S16 and S24 samples showed tendencies for growth after this fall, which suggests that these samples represent suitable catalysts for the coupled photocatalytic-microbiological experiment. The catalyst-reagent system of $\text{TiO}_2\text{-FeCl}_3$ in the ratio of 1:1 achieved very similar results for the 0.20 mg/L catalyst concentration. The best MO growth was obtained in S16 for the 0.25 mg/L catalyst concentration.

Also, S11, S16 and S24 samples showed the same tendency in contrast to the other catalysts used in which optical density increased during the entire experiment of 0.25 mg /L. Therefore, the best antimicrobial activity is obtained in S24 sample; it has also been shown that 0.25 mg/L could be toxic for microorganisms, and our subsequent research using more sophisticated instrumental techniques can confirm it.

Correlation between the results

Correlating the parameters of the sol-gel synthesis process with the resulting properties of nanostructure systems is necessary for the understanding and systematic control of the nanomaterial properties and their quality. Namely, the control of particle size distribution and aggregate structure is the key criterion for product quality. This section describes the influence of the variation of some synthesis parameters on the change in the structural properties of the obtained anatase nanoparticles, examined by XRD, Raman spectroscopy and the BET analysis of their photocatalytic and microbiological activity. Both XRD and Raman spectroscopy could enable more precise determination of the average particle size, compared to AFM measurements (Golubović et al,

2009a). In the obtained AFM images, it was not possible to detect subtle variations in the particle size, of the order of few nanometers.

The presented results and the results reported earlier by Golubovic et al (Golubović et al, 2009a) have shown that the properties of TiO₂ nanoparticles depend on a few parameters of the sol-gel synthesis process. The nanoparticles size and content of brookite in the produced nanoparticles are the result of a subtle interplay between many synthesis parameters such as the type of the precursor, the temperature and the heating rate of the calcination process and the pH value of the hydrothermal solution. It is important to be able to investigate partial influence of the parameters on the efficiency of catalysts.

The influence of the calcination temperature on the anatase nanoparticles size, as reported by Gouadec et al (Gouadec et al, 2007), Bersani et al (Bersani et al, 1998) and Golubovic et al (Golubović et al, 2009a), shows a tendency of the particle size to increase with an increase in calcination temperature. When all other synthesis parameters are fixed, a higher calcination temperature leads to the formation of larger nanoparticles, as shown by Golubovic et al. (Golubović et al, 2009a). This is confirmed by our results shown in Table 3 and Table 7.

The pH value shown can influence significantly the polymorphous structure of TiO₂ nanopowders: low and neutral pH values result in the production of TiO₂ nanopowders containing brookite and sometimes rutile, while the alkali solution with a high pH value leads to the formation of anatase nanoparticles with high stability during calcination (Ovenstone & Yanagisawa, 1999). The pH value was set to 9.3 for the synthesis of titania nanoparticles, pure and dopants. Based on the data shown in Table 3, It seems that the alkali pH value is not high enough to avoid the formation of brookite from the TiCl₄ precursor although the literature suggested (Pottier, a. et al. 2001) that brookite phase was observed only in acidic solutions.

Therefore, we fixed the parameters, such as the pH value at 9.3, in order to obtain a single-digit result of the influence of the key parameters on the catalytic efficiency and the microbial activity and inactivity, i.e. its dependence on the dopant concentration, calcination duration, calcination temperature and their free surface of the mesoporous catalyst (S_{BET}). Our results showed that the values of S_{BET} in the La-doped samples (S18 and S28), 79 and 84 m²g⁻¹, respectively, are higher than those in pure TiO₂ nanoparticle samples (S05, S06 and S11), 17, 51 and 58 m²g⁻¹, respectively. It explains the best photocatalytic activity of S28 sample in Table 8. It explains that the particle size and its free surface are the key factor for photocatalytic and antimicrobial activities. The best

performance of S111 sample in all experiments is shown from Figure 9 to Figure 12, as a comparison between S18 and S111 samples. When we compare S93 and S96 samples (Table 10) synthesized using different duration times (7 and 24 h, respectively), our results show different degradation rate for the TiO_2 doped with V^{3+} of 10.0 wt. %, which can be explained by the anomalies in the behavior of the photocatalyst synthesized at higher calcination temperature. We expected that S96 sample would have higher activity than S93 sample due to its heating rates during the calcination process (135 and 67.5°C/h, respectively). If we compare our results from the preliminary study reported earlier (Kuburovic et al, 2009) with the results from Table 8 to Table 10, a higher degradation rate with a lower catalyst concentration loading can be explained with a synergetic influence of the aerobic condition effect and a slightly higher temperature ($\Delta T = 5^\circ\text{C}$) in the photocatalytic activity experiments. In addition, the photocatalytic and photothermolytic effects on the degradation of MTBE in water should be considered at elevated temperatures in aerobic conditions. The further detailed research will explain the impact of values of the parameters of different processes in order to obtain the optimum values for the parameters for photocatalytic, microbiological and their antimicrobial activities.

Conclusion

Mesoporous pure as well as La, Fe and V-doped titanium (IV) oxide nanoparticle photo catalysts prepared by the sol-gel method have been extensively characterized by various sophisticated techniques and their photocatalytic and antimicrobial activities tested. The photocatalytic activity, microbiological activity and inactivity in the bath slurry-catalyst circular photoreactor were researched in detail and gave us the directions for a further study of titania-based catalysts.

We investigated the photocatalytic activity of titania doped with different concentrations of lanthanum. It was shown that the best photocatalytic efficiency was obtained with TiO_2 doped with La^{3+} of 1 wt. % for 45 minutes, but the fastest drop in the polluted MTBE concentration in the water solution was achieved by TiO_2 doped with La^{3+} of 3 wt. %. These results also showed the fastest drop during the photocatalytic degradation of MTBE in the water solution in S93 sample (TiO_2 doped with V^{3+} of 10.0 wt. %), and then in 28 sample (TiO_2 doped with La^{3+} of 1.0 wt. %) for 45 minutes. Our results also show different degradation rates for TiO_2 doped with V^{3+} of 10.0 wt. %, S93 and S96 samples synthesized with different duration times (7 and 24 h, respectively) and

calcination heating rates (66.7 and 135°C/h, respectively), which can explain their anomalous behavior. The best photocatalytic efficiency is achieved with S111 sample, which can be explained by its drastically improved adsorption and superior activity of the Fe-dopant of titania nanoparticles owing to its unique half-filled electronic configuration and shallow trapping compared to other metal dopants tested in our study.

Our results showed that the best coupled photocatalytic-microbiological properties are achieved when we use direct ultraviolet radiation simulated with the sodium lamp SONT UV400 with the initial concentration of 0.75 g/L Degussa P-25[®]TiO₂ nanopowder for 60 and 150 minutes. These results show that TiO₂ and direct ultraviolet radiation simulated with the sodium lamp SONT UV400 in lab conditions and titania in the concentration of 1.0 g/L have the effect of inactivating and killing microorganisms. The optical density results have proven this assertion by measuring the microbial activity and inactivity in the coupled photocatalytic-microbiological experiment. We also studied the antimicrobial activity of *Pseudomonas aeruginosa strain DV 2739* which was seeded with different concentrations of MTBE and catalysts. The biggest *Pseudomonas aeruginosa strain DV 2739* growth was obtained with a high MTBE concentration of 1.5 ml/L. The Fenton reagent and the catalyst-reagent system of TiO₂ and FeCl₃ in the ratio of 1:1 have a stimulation effect on the growth of microorganisms. Finally, the best microbiological growth was achieved with the catalyst-reagent system of TiO₂ and FeCl₃ in the ratio of 1:1, which can be explained by the coupled stimulation influence of the Fenton reagent and anatase titania nanopowder in equal portions. It is the best nutrition for bacteria and their growth in our experiment. In accordance with the results in the previous experiment, we expected that the TiO₂ nanoparticles doped with Fe³⁺ can give the best growth of microorganisms. It was the reason for the research and testing different concentrations of TiO₂ nanoparticle catalysts carried out in another experiment in order to obtain the optimum concentration and type of catalyst for antimicrobial activity, as well as the limits which microorganisms can reach to give them the best performance for the coupled photocatalytic-microbiological experiments. Based on these results, it can be determined that the optical density drops between 26 and 27 hours after the start of the experiment, i.e. between 6 and 7 after adding the MO. For all concentrations, there was a decrease in optical density in all samples. Nevertheless, S11, S16 and S24 samples showed tendencies for growth after this fall, which suggests that these samples represent suitable catalysts for coupled photocatalytic-microbiological experiments. The catalyst-reagent system

of TiO₂-FeCl₃ in the ratio of 1:1 achieved very similar results for the catalyst concentration of 0.20 mg/L. The best MO growth was obtained in S16 for 0.25 mg/L catalyst concentration. So, the best antimicrobial activity was obtained in S24 sample; it was also shown that 0.25 mg/L could be toxic for microorganisms, and our subsequent research using more sophisticated instrumental techniques can confirm it. The results showed that the effect of the optical density concentration and the MO growth is in a direct correlation with the structure of TiO₂ nanoparticle catalyst and the doper metal type.

Our results of the superior Fe-dopant characteristics together with the theoretical knowledge on TiO₂ nanoparticles doped with Ag (van Grieken et al, 2009), (Ménesi et al, 2009), Au (Huang et al, 2006) and Fe (Flak et al, 2015) give us directions for further studies of their photocatalytic and antimicrobial activities, as well as for the development of TiO₂-nanoparticles and nanotubes for enhancing antibiotics and their use in the cancer treatment. Finally, in our further studies, we will research in detail the impact of different values of the parameters of different processes such as irradiance wavelength, light penetration and irradiance intensity, Influence of temperature, substrate concentration and chemical characteristics, retention time, flow, temperature and pH value, initial concentration of the compound and the catalyst, dissolved oxygen, optimal areas of wavelength radiation for individual phases decomposition process, absorption and selective absorption, etc. in order to obtain the optimum values for the parameters for photocatalytic, microbiological and antimicrobial activities, as well as their synergetic effects for their environmental and biomedical applications in real conditions. All this will ultimately explain the mechanisms of these processes.

References

Ahonen, P.P., Kauppinen, E.I., Joubert, J.C., Deschanvres, J.L., & Tendeloo, G.V. 1999. Preparation of nanocrystalline titania powder via aerosol pyrolysis of titanium tetrabutoxide. *Journal of Materials Research*, 14(10), pp.3938-3948. Available at: <https://doi.org/10.1557/jmr.1999.0533>.

Alivisatos, A.P. 1996. Semiconductor Clusters, Nanocrystals, and Quantum Dots of the Total Environment. *Science*, 271(5251), pp.933-937. Available at: <https://doi.org/10.1126/science.271.5251.933>.

Androutsopoulos, G.P., & Salmas, C.E. 2000. A New Model for Capillary Condensation–Evaporation Hysteresis Based on a Random Corrugated Pore Structure Concept: Prediction of Intrinsic Pore Size Distributions. 1. Model Formulation. *Industrial & Engineering Chemistry Research*, 39(10), pp.3747-3763. Available at: <https://doi.org/10.1021/ie0001624>.

Aruna, S.T., Tirosh, S., & Zaban, A. 2000. Nanosize rutile titania particle synthesis via a hydrothermal method without mineralizers. *Journal of Materials Chemistry*, 10(10), pp.2388-2391. Available at: <https://doi.org/10.1039/b001718n>.

Backman, U., Tapper, U., & Jokiniemi, J.K. 2004. An aerosol method to synthesize supported metal catalyst nanoparticles. *Synthetic Metals*, 142(1-3), pp.169-176. Available at: <https://doi.org/10.1016/j.synthmet.2003.08.007>.

Barrett, E.P., Joyner, L.G., & Halenda, P.P. 1951. The Determination of Pore Volume and Area Distributions in Porous Substances. I. Computations from Nitrogen Isotherms. *Journal of the American Chemical Society*, 73(1), pp.373-380. Available at: <https://doi.org/10.1021/ja01145a126>.

Bersani, D., Lottici, P.P., Lopez, T., & Ding, X. 1998. A Raman Scattering Study of PbTiO₃ and TiO₂ Obtained by Sol-Gel. *Journal of Sol-Gel Science and Technology*, 13(1/3), pp.849-853. Available at: <https://doi.org/10.1023/a:1008602718987>.

Bhattacharyya, K., Varma, S., Tripathi, A.K., Bharadwaj, S.R., & Tyagi, A.K. 2008. Effect of Vanadia Doping and Its Oxidation State on the Photocatalytic Activity of TiO₂ for Gas-Phase Oxidation of Ethene. *The Journal of Physical Chemistry C*, 112(48), pp.19102-19112. Available at: <https://doi.org/10.1021/jp807860y>.

Blešić, M., Šaponjić, Z., Nedeljković, J., & Uskoković, D. 2002. TiO₂ films prepared by ultrasonic spray pyrolysis of nanosize precursor. *Materials Letters*, 54(4), pp.298-302. Available at: [https://doi.org/10.1016/s0167-577x\(01\)00581-x](https://doi.org/10.1016/s0167-577x(01)00581-x).

Cai, R., Hashimoto, K., Itoh, K., Kubota, Y., & Fujishima, A. 1991. Photokilling of Malignant Cells with Ultrafine TiO₂ Powder. *Bulletin of the Chemical Society of Japan*, 64(4), pp.1268-1273. Available at: <https://doi.org/10.1246/bcsj.64.1268>.

California Code of Regulations. 1999. Title 22, Section 64449, January 07th.

Chueh, Y.L., Hsieh, C.H., Chang, M.T., Chou, L.J., Lao, C.S., Song, J.H., Gan, J.-Y., Wang, Z.L. 2007. RuO₂ Nanowires and RuO₂/TiO₂ Core/Shell Nanowires: From Synthesis to Mechanical, Optical, Electrical, and Photoconductive Properties. *Advanced Materials*, 19(1), pp.143-149. Available at: <https://doi.org/10.1002/adma.200601830>.

Dinesh, G.K., Anandan, S., & Sivasankar, T. 2015. Sonophotocatalytic treatment of Bismarck Brown G dye and real textile effluent using synthesized novel Fe(0)-doped TiO₂ catalyst. *RSC Advances*, 5(14), pp.10440-10451. Available at: <https://doi.org/10.1039/c4ra07685k>.

Fernández-Ibáñez, F., Malato, S., & de Nieves, L.F.J. 2004. *Propiedades coloidales de partículas de TiO₂: Aplicación al tratamiento foto catalítico solar de aguas*. Madrid, Spain: CIEMAT.

Flak, D., Coy, E., Nowaczyk, G., Yate, L., & Jurga, S. 2015. Tuning the photodynamic efficiency of TiO₂ nanotubes against HeLa cancer cells by Fe-doping. *RSC Advances*, 5(103), pp.85139-85152. Available at: <https://doi.org/10.1039/c5ra17430a>.

Golubović, A., Šćepanović, M., Kremenović, A., Aškračić, S., Berec, V., Dohčević-Mitrović, Z., & Popović, Z.V. 2009a. Raman study of the variation in anatase structure of TiO₂ nanopowders due to the changes of sol-gel synthesis conditions. *Journal of Sol-Gel Science and Technology*, 49(3), pp.311-319. Available at: <https://doi.org/10.1007/s10971-008-1872-3>.

Golubović, A., Šćepanović, M., Aškračić, S., Grujić-Brojčin, M., Dohčević-Mitrović, Z., Kremenović, A., & Popović, Z.V. 2009b. Influence of La³⁺-dopant on anatase nanopowders synthesized by sol-gel method. In *238th American Chemical Society National Meeting & Exposition, Washington DC, Abstract of Scientific Papers*. Washington DC. pp.INOR 1262642.

Golubović, A., Abramović, B., Šćepanović, M., Grujić-Brojčin, M., Armaković, S., Veljković, I., Babić, B., Dohčević-Mitrović, Z., Popović, Z.V. 2013. Improved efficiency of sol-gel synthesized mesoporous anatase nanopowders in photocatalytic degradation of metoprolol. *Materials Research Bulletin*, 48(4), pp.1363-1371. Available at: <https://doi.org/10.1016/j.materresbull.2012.11.098>.

Gouadec, G., & Colombar, P. 2007. Raman Spectroscopy of nanomaterials: How spectra relate to disorder, particle size and mechanical properties. *Progress in Crystal Growth and Characterization of Materials*, 53(1), pp.1-56. Available at: <https://doi.org/10.1016/j.pcrysgrow.2007.01.001>.

van Grieken, R., Marugán, J., Sordo, C., Martínez, P., & Pablos, C. 2009. Photocatalytic inactivation of bacteria in water using suspended and immobilized silver-TiO₂. *Applied Catalysis B: Environmental*, 93(1-2), pp.112-118. Available at: <https://doi.org/10.1016/j.apcatb.2009.09.019>.

Grujić-Brojčin, M., Armaković, S., Tomić, N., Abramović, B., Golubović, A., Stojadinović, B., Šćepanović, M. 2014. Surface modification of sol-gel synthesized TiO₂ nanoparticles induced by La-doping. *Materials Characterization*, 88, pp.30-41. Available at: <https://doi.org/10.1016/j.matchar.2013.12.002>.

Heller, A. 1995. Chemistry and Applications of Photocatalytic Oxidation of Thin Organic Films. *Accounts of Chemical Research*, 28(12), pp.503-508. Available at: <https://pubs.acs.org/doi/abs/10.1021/ar00060a006>. Accessed: 15 May 2018.

Hoffmann, M.R., Martin, S.T., Choi, W., & Bahnemann, D.W. 1995. Environmental Applications of Semiconductor Photocatalysis. *Chemical Reviews*, 95(1), pp.69-96. Available at: <https://doi.org/10.1021/cr00033a004>.

Huang, F., Yan, A., & Zhao, H. 2016. Influences of Doping on Photocatalytic Properties of TiO₂ Photocatalyst. In W. Cao Ed., *Semiconductor Photocatalysis - Materials, Mechanisms and Applications*. IntechOpen. Available at: <https://doi.org/10.5772/63234>.

Huang, X., El-Sayed, I.H., Qian, W., & El-Sayed, M.A. 2006. Cancer Cell Imaging and Photothermal Therapy in the Near-Infrared Region by Using Gold Nanorods. *Journal of the American Chemical Society*, 128(6), pp.2115-2120. Available at: <https://doi.org/10.1021/ja057254a>.

Hunter, R. 2000. *Foundations of colloid Science*. Oxford, Great Britain: University Press. ISBN: 9780198505020, Second Edition.

Ireland, J., Klostermann, P., Rice, E., & Clark, R. 1993. Inactivation of *Escherichia coli* by titanium dioxide photocatalytic oxidation. *Applied and Environmental Microbiology*, 59(5), pp.1668-1670. Available at: <http://aem.asm.org/content/59/5/1668.full.pdf+html>. Accessed: 15 May 2018.

Jokanović, V., Spasić, A.M., & Uskoković, D. 2004. Designing of nanostructured hollow TiO₂ spheres obtained by ultrasonic spray pyrolysis. *Journal of Colloid and Interface Science*, 278(2), pp.342-352. Available at: <https://doi.org/10.1016/j.jcis.2004.06.008>.

Kaneko, K., Ishii, C., Kanoh, H., Hanzawa, Y., Setoyama, N., & Suzuki, T. 1998. Characterization of porous carbons with high resolution α -analysis and low temperature magnetic susceptibility. *Advances in Colloid and Interface Science*, 76-77, pp.295-320. Available at: [https://doi.org/10.1016/s0001-8686\(98\)00050-5](https://doi.org/10.1016/s0001-8686(98)00050-5).

Kikuchi, Y., Sunada, K., Iyoda, T., Hashimoto, K., & Fujishima, A. 1997. Photocatalytic bactericidal effect of TiO₂ thin films: dynamic view of the active oxygen species responsible for the effect. *Journal of Photochemistry and Photobiology A: Chemistry*, 106(1-3), pp.51-56. Available at: [https://doi.org/10.1016/s1010-6030\(97\)00038-5](https://doi.org/10.1016/s1010-6030(97)00038-5).

Kuburovic, N., & Dimitrijevic-Brankovic, S. 2006. Coupling of the photocatalytic and microbiological degradation processes for the organic pollutants destruction. In *Seventh European Meeting on Environmental Chemistry (EMEC7)*, December 9th, Brno, Czech Republic, oral presentation - OP45, pp.66.

Kuburovic, N.D., Golubovic, A., Todorovic, Z., Gasic, S., & Solevic, T. 2009. Photocatalytic degradation of wastewater polluted by methyl-tertiary-butyl-ether using titanium-dioxide and doped titanium-dioxide. In *Proceedings of the 4th IASME/WSEAS International Conference on Water Resources, Hydraulics & Hydrology (WHH')*, ISBN: 978-960-474-057-4. Cambridge, UK, pp.19-24, February 24-26.

Kuburovic, N., & Orlovic, A. 2010. Photocatalytic wastewater treatment from sewage Belgrade. In *International Conference: Wastewater, municipal solid waste and hazardous waste*, 29th March – 01st April, Subotica, Serbia.

Kuburovic, N., Todorovic, M., Drmanic, S. Raichevic, V. And Jovanovic, Lj. 2005. Aerobic bioremediation of water polluted by methyl tertiary butyl ethers. In *Proceeding of the 2nd World Conference on Biomass for Energy, Industry and Climate protection*, Italy, pp.1608-1611.

Kuburovic, N., Todorovic, M., Raicevic, V., Orlovic, A., Jovanovic, Lj., Nikolic, J.,..., Solevic, T. 2007. Removal of methyl tertiary butyl ether from wastewaters using photolytic, photocatalytic and microbiological degradation processes. *Desalination*, 213(1-3), pp.123-128. Available at: <https://doi.org/10.1016/j.desal.2006.03.605>.

Lakshmi, B.B., Dorhout, P.K., & Martin, C.R. 1997. Sol-Gel Template Synthesis of Semiconductor Nanostructures. *Chemistry of Materials*, 9(3), pp.857-862. Available at: <https://doi.org/10.1021/cm9605577>.

Liu, T., & Zhang, H. 2013. Novel Fe-doped anatase TiO₂ nanosheet hierarchical spheres with 94% {001} facets for efficient visible light photodegradation of organic dye. *RSC Advances*, 3(37), p.16255. Available at: <https://doi.org/10.1039/c3ra40875b>.

Maness, P., Snolinski, S., Blake, D., Wolfrum, Z., & Jacoby, W. 1999. Solar Treatment as an Alternative for Water Disinfections. *Applied and Environmental Microbiology*, 65(9), pp.4094-4098.

Marugán, J., van Grieken, R., Pablos, C., & Sordo, C. 2010. Analogies and differences between photocatalytic oxidation of chemicals and photocatalytic inactivation of microorganisms. *Water Research*, 44(3), pp.789-796. Available at: <https://doi.org/10.1016/j.watres.2009.10.022>.

Matsunaga, T., & Okochi, M. 1995. TiO₂-Mediated Photochemical Disinfection of *Escherichia coli* Using Optical Fibers. *Environmental Science & Technology*, 29(2), pp.501-505. Available at: <https://doi.org/10.1021/es00002a028>.

Ménesi, J., Kékesi, R., Oszkó, A., Zöllmer, V., Seemann, T., Richardt, A., & Dékány, I. 2009. Photocatalysis on silver-layer silicate/titanium dioxide composite thin films at solid/vapour interface. *Catalysis Today*, 144(1-2), pp.160-165. Available at: <https://doi.org/10.1016/j.cattod.2009.02.030>.

Nedeljković, J.M., Šaponjić, Z.V., Rakočević, Z., Jokanović, V., & Uskoković, D.P. 1997. Ultrasonic spray pyrolysis of TiO₂ nanoparticles. *Nanostructured Materials*, 9(1-8), pp.125-128. Available at: [https://doi.org/10.1016/s0965-9773\(97\)00034-2](https://doi.org/10.1016/s0965-9773(97)00034-2).

Ollis, D.F., Pelizzetti, E., & Serpone, N. 1991. Environmental Applications of Semiconductor Photocatalysis. *Environmental Science & Technology*, 25(9), pp.1522-1529. Available at: <https://doi.org/10.1021/es00021a001>.

Ohko, Y., Utsumi, Y., Niwa, C., Tatsuma, T., Kobayakawa, K., Satoh, Y., Kubota, Y., Fujishima, A. 2001. Self-sterilizing and self-cleaning of silicone catheters coated with TiO₂ photocatalyst thin films: A preclinical work. *Journal of Biomedical Materials Research*, 58(1), pp.97-101. Available at: [https://doi.org/10.1002/1097-4636\(2001\)58:1<97::aid-jbm140>3.0.co;2-8](https://doi.org/10.1002/1097-4636(2001)58:1<97::aid-jbm140>3.0.co;2-8).

Ohsaka, T., Izumi, F., & Fujiki, Y. 2005. Raman spectrum of anatase, TiO₂. *Journal of Raman Spectroscopy*, 7(6), pp.321-324. Available at: <https://doi.org/10.1002/jrs.1250070606>.

Ovenstone, J., & Yanagisawa, K. 1999. Effect of Hydrothermal Treatment of Amorphous Titania on the Phase Change from Anatase to Rutile during Calcination. *Chemistry of Materials*, 11(10), pp.2770-2774. Available at: <https://doi.org/10.1021/cm990172z>.

Panic, V., Dekanski, A., Miskovic-Stankovic, V., Milonjic, S., & Nikolic, B. 2003. The role of the concentration profile of titanium oxide on the electrochemical behavior of RuO₂-TiO₂ coatings obtained by the sol-gel procedure. *Journal of the Serbian Chemical Society*, 68(12), pp.979-988. Available at: <https://doi.org/10.2298/0352-51390312979p>.

Pontius, F.W. 1998. New horizons in federal regulation. *Journal - American Water Works Association*, 90(3), pp.38-50. Available at: <https://doi.org/10.1002/j.1551-8833.1998.tb08394.x>

Pottier, A., Chanéac, C., Tronc, E., Mazerolles, L., & Jolivet, J. 2001. Synthesis of brookite TiO₂ nanoparticles by thermolysis of TiCl₄ in strongly acidic aqueous media. *Journal of Materials Chemistry*, 11(4), pp.1116-1121. Available at: <https://doi.org/10.1039/b100435m>.

Ramli, R.M., Chong, F.K., Omar, A.A., & Murugesan, T. 2014. Performance of Surfactant Assisted Synthesis of Fe/TiO₂ on the Photodegradation of Diisopropanolamine. *CLEAN - Soil, Air, Water*, 43(5), pp.690-697. Available at: <https://doi.org/10.1002/clen.201300186>.

Richardson, S.D. 2003. Disinfection by-products and other emerging contaminants in drinking water. *TrAC – Trends in Analytical Chemistry*, 22(10), pp.666–684.

Rodriguez-Carvajal, J. 2008. *FullProf computer program*. Available at: <http://www.ill.eu/sites/fullprof/index.html>. Accessed: 17 May 2018.

Salmas, C.E., & Androustopoulos, G.P. 2001. A Novel Pore Structure Tortuosity Concept Based on Nitrogen Sorption Hysteresis Data. *Industrial & Engineering Chemistry Research*, 40(2), pp.721-730. Available at: <https://doi.org/10.1021/ie000626y>.

Schwarzer, H., & Peukert, W. 2005. Prediction of aggregation kinetics based on surface properties of nanoparticles. *Chemical Engineering Science*, 60(1), pp.11-25. Available at: <https://doi.org/10.1016/j.ces.2004.06.050>.

Shaffer, K.L., & Uchrin, C.G. 1997. Uptake of Methyl Tertiary Butyl Ether (MTBE) by Groundwater Solids. *Bulletin of Environmental Contamination and Toxicology*, 59(5), pp.744-749. Available at: <https://doi.org/10.1007/s001289900543>.

Sitkiewitz, S., & Heller, A. 1996. Photocatalytic oxidation of benzene and steatic on sol-gel derived TiO₂ thin films attached to glass. *New Journal of Chemistry*, 20, pp.233-241.

Squillace, P.J., Zogorski, J.S., Wilber, W.G., & Price, C.V. 1996. Preliminary Assessment of the Occurrence and Possible Sources of MTBE in Groundwater in the United States, 1993–1994. *Environmental Science & Technology*, 30(5), pp.1721-1730. Available at: <https://doi.org/10.1021/es9507170>.

Su, R., Bechstein, R., Kibsgaard, J., Vang, R.T., & Besenbacher, F. 2012. High-quality Fe-doped TiO₂ films with superior visible-light performance. *Journal of Materials Chemistry*, 22(45), p.23755. Available at: <https://doi.org/10.1039/c2jm34298g>.

Su, Y., Wu, Z., Wu, Y., Yu, J., Sun, L., & Lin, C. 2015. Acid Orange II degradation through a heterogeneous Fenton-like reaction using Fe–TiO₂ nanotube arrays as a photocatalyst. *Journal of Materials Chemistry A*, 3(16), pp.8537-8544. Available at: <https://doi.org/10.1039/c5ta00839e>.

Sungkaworn, T., Triampo, W., Nalakarn, P., Triampo, D., Tang, I.M., Lenbury, Y., & Picha, P. 2008. The Effects of TiO₂ Nanoparticles on Tumor Cell Colonies: Fractal Dimension and Morphological Properties. *International Journal of Medical and Health Sciences, World Academy of Science, Engineering and Technology*, 2(1), pp.20-27.

Šćepanović, M.J., Grujić-Brojčin, M., Dohčević-Mitrović, Z.D., & Popović, Z.V. 2007. Temperature dependence of the lowest frequency E_g Raman mode in laser-synthesized anatase TiO₂ nanopowder. *Applied Physics A*, 86(3), pp.365-371. Available at: <https://doi.org/10.1007/s00339-006-3775-x>.

Šćepanović, M., Aškračić, S., Grujić-Brojčin, M., Golubović, A., Dohčević-Mitrović, Z., Matović, B., & Popović, Z.V. 2010. Raman Study of Vanadium-Doped Titania Nanopowders Synthesized by Sol-Gel Method. *International Journal of Modern Physics B*, 24(06n07), pp.667-675. Available at: <https://doi.org/10.1142/s0217979210064289>.

Takeuchi, M., Dohshi, S., Eura, T., & Anpo, M. 2003. Preparation of Titanium-Silicon Binary Oxide Thin Film Photocatalysts by an Ionized Cluster Beam Deposition Method. Their Photocatalytic Activity and Photoinduced Super-Hydrophilicity. *J. Phys. Chem. B*, 107 (51), pp.14278–14282. Available at: <https://pubs.acs.org/doi/pdf/10.1021/jp0308514>.

The Merck index: an encyclopedia of chemicals, drugs, and biologicals. 1996. Ed. Susan Budavari, Maryadele J. O'Neil, Ann Smith, Patricia E. Heckelman, Joanne F. Kinneary. Whitehouse Station, NJ: Merck & co Inc. - 12th Edition. Available at: <https://www.ncbi.nlm.nih.gov/nlmcatalog/9609686>.

Uchida, H., Itoh, S., & Yoneyama, H. 1993. Photocatalytic Decomposition of Propylamide Using TiO₂ Supported on Activated Carbon. *Chemistry Letters*, 22(12), pp.1995-1998. Available at: <https://doi.org/10.1246/cl.1993.1995>.

Waliszewski, P. 1997. Complexity, dynamic cellular network and tumourgenesis. *Polish Journal of Pathology*, 46, pp.235-241.

Wang, S., Lian, J.S., Zheng, W.T., & Jiang, Q. 2012. Photocatalytic property of Fe doped anatase and rutile TiO₂ nanocrystal particles prepared by sol-gel technique. *Applied Surface Science*, 263, pp.260-265. Available at: <https://doi.org/10.1016/j.apsusc.2012.09.040>.

Watts, R.J., Kong, S., Orr, M.P., Miller, G.C., & Henry, B.E. 1995. Photocatalytic Degradation of Toxins Secreted to Water by Cyanobacteria and Unicellular Algae and Photocatalytic Degradation of The Cells of Selected Microorganisms. *Water Research*, 29(1), pp.95-100. Available at: [https://doi.org/10.1016/0043-1354\(94\)e0122-m](https://doi.org/10.1016/0043-1354(94)e0122-m).

Wei, C., Lin, W.Y., Zainal, Z., Williams, N.E., Zhu, K., Kruzic, A.P., Smith R.L., Rajeshwar, K. 1994. Bactericidal Activity of TiO₂ Photocatalyst in Aqueous Media: Toward a Solar-Assisted Water Disinfection System. *Environmental Science & Technology*, 28(5), pp.934-938. Available at: <https://doi.org/10.1021/es00054a027>.

Xu, M., Ma, J., Gu, J., & Lu, Z. 1998. Photocatalytic TiO₂ nanoparticles damage to cellular membranes and genetic supramolecules. *Supramolecular Science*, 5(5-6), pp.511-513. Available at: [https://doi.org/10.1016/s0968-5677\(98\)00063-7](https://doi.org/10.1016/s0968-5677(98)00063-7).

Yan, J., Zhang, Y., Liu, S., Wu, G., Li, L., & Guan, N. 2015. Facile synthesis of an iron doped rutile TiO₂ photocatalyst for enhanced visible-light-driven water oxidation. *Journal of Materials Chemistry A*, 3(43), pp.21434-21438. Available at: <https://doi.org/10.1039/c5ta07003a>.

Yao, B., Wang, L., Wang, C., Wang, Y., & Zhao, G. 2007. Preparation and Performances of RuO₂/TiO₂ Films Photocatalyst Supported on Float Pearls. *Chinese Journal of Chemical Physics*, 20(6), pp.789-795. Available at: <https://doi.org/10.1088/1674-0068/20/06/789-795>.

Zhang, A., & Sun, Y. 2004. Photocatalytic killing effect of TiO₂ nanoparticles on Ls-174-t human colon carcinoma cells. *World Journal of Gastroenterology*, 10(21), pp.3191-3193. Available at: <https://doi.org/10.3748/wjg.v10.i21.3191>.

РАЗРАБОТКА НОВЫХ УМНЫХ МЕТАЛЛИЧЕСКИХ НАНОМАТЕРИАЛОВ НА ОСНОВЕ ДИОКСИДА ТИТАНА ДЛЯ ФОТОКАТАЛИТИЧЕСКОЙ И АНТИМИКРОБНОЙ АКТИВНОСТЕЙ

Наташа Д. Кубурович^а, Александр В. Голубович^б,
Лиляна М. Бабинчев^в

^а Eco Energy Engineering & Consulting, г. Белград, Республика Сербия

^б Белградский университет, Институт физических исследований,
Отделение физики твердого тела и новых материалов,
г. Белград, Республика Сербия

^в Университет в г. Приштина, Факультет технических наук,
г. Косовска Митровица, Республика Сербия

ОБЛАСТЬ: химическая инженерия и материаловедение,
каталитические процессы и композиционные материалы

ВИД СТАТЬИ: оригинальная научная статья

ЯЗЫК СТАТЬИ: английский

Резюме:

Предметом данного исследования являются синтез, классификация и испытания наночастиц титана (IV) оксида (TiO₂-НЧ-а) и легирования лантана (La³⁺), железа (Fe³⁺) и ванадия (V³⁺) для фотокаталитической и микробиологической активностей, а также сравнение с каталитическим активностями испытанными в коммерческих целях TiO₂ (P25, Degussa®) и наночастиц анатаза, чистоты 99,9%, компанией Alfa Aesar из Ланкастера). Наночастицы диоксида титана были синтезированы и легированы с различной концентрацией металлических допантов, при различной продолжительности процесса прокаливания: TiO₂-НЧ

(анатаз-НЧ, время процесса прокаливания 5 и 7 часов), La³⁺ (0.65, 1, 2, 3, 4, 5 и 6 вес. %, продолжительность прокаливания 7 часов), Fe³⁺ (1, 2, 5, 3,0 и 5 вес. %, продолжительность прокаливания 7 и 24 часа) и V³⁺ (10 вес. %, продолжительность прокаливания 7 и 24 часа). Штамм „Pseudomonas aeruginosa DV 2739“ использован в качестве модели микроорганизмов в микробиологических экспериментах, проведенных в микробиологической лаборатории. Совместный процесс фотокаталитических и микробиологических испытаний эксперимента проводился в каталитической ванне при прямом концентрированном ультрафиолетовом излучении от натриевой лампы SONT UV 400, симулирующей солнечное излучение. Исследование показало, что образец катализатора C28, La-легирующей примеси с концентрацией 1 вес. %, обладает лучшими фотокаталитическими свойствами по сравнению с другими La-допантами, в то время, как лучшая фотокаталитическая активность была достигнута в образце S111, Fe-легирующей примеси диоксида титана (5 вес.%, продолжительность прокаливания составляет 7 часов). Результаты нашего исследования также показали различную степень деградации при применении V-допанта TiO₂ с концентрацией 10 вес.% образцы C93 и C96 были синтезированы при различной продолжительности прокаливания (67.5 и 135 °С/ч, поочередно), что можно считать аномалией в их поведении. И наконец лучшая антимикробная активность получена в образце CS24, Fe-легирующей примеси, которая показала, что 0,25 мг/л является токсичным для микроорганизмов. Результаты нашего исследования о преимущественных характеристиках Fe-легирующей примеси и теоретические знания о наночастицах TiO₂, легированных Ag, Au и Fe, безусловно облегчат исследователям дальнейшую работу в изучении фотокаталитической и антимикробной активностей, а также развития наночастиц TiO₂ и нанотрубок, с целью усиления действия антибиотиков и их применения при лечении онкологических заболеваний.

Ключевые слова: диоксид титана, TiO₂-наночастицы, TiO₂ легированные La³⁺, Fe³⁺ и V³⁺, продолжительность прокаливания, штаммы Pseudomonas aeruginosa DV 2739 и ATCC 9023, фотокаталитическая активность, антимикробная активность.

РАЗВОЈ НОВИХ ПАМЕТНИХ МЕТАЛНИХ НАНОМАТЕРИЈАЛА НА БАЗИ ТИТАНИЈУМ-ДИОКСИДА ЗА ФОТОКАТАЛИТИЧКУ И АНТИМИКРОБНУ АКТИВНОСТ

Наташа Д. Кубуровић^а, Александар В. Голубовић^б,
Љиљана М. Бабинчев^в

^а Eco Energy Engineering & Consulting, Београд, Република Србија

^б Универзитет у Београду, Институт за физику, Центар за физику чврстог стања и нове материјале, Београд, Република Србија

^в Универзитет у Приштини, Факултет техничких наука, Косовска Митровица, Република Србија

ОБЛАСТ: хемијско инжењерство и инжењерство материјала,
каталитички процеси и композитни материјали

ВРСТА ЧЛАНКА: оригинални научни чланак

ЈЕЗИК ЧЛАНКА: енглески

Сажетак:

Предмет ове студије била је синтеза, карактеризација и тестирање наночестица титанијум (IV) оксида (TiO₂-НЧ-а) и њихових допаната лантана (La³⁺), гвожђа (Fe³⁺) и ванадијума (V³⁺) за фотокаталитичку и микробиолошку активност, као и њихово поређење са каталитичким активностима тестираних комерцијалних TiO₂ (Дегуса П-25[®] и наночестица анатаса, чистоће 99,9%, Алфа Аесар из Ланкестера). Титанијум-диоксид наночестице су синтетизоване и допиране различитим концентрацијама металних допаната, током различитог трајања калцинације, као што су: TiO₂-НПс (анатас-НПс, време трајања калцинације од 5 и 7 h), La³⁺ (0.65, 1, 2, 3, 4, 5 и 6 тежинских %, са трајањем калцинације од 7 h), Fe³⁺ (1, 2, 5, 3,0 и 5 тежинских %, са трајањем калцинације од 7 и 24 h) и V³⁺ (10 тежинских %, са трајањем калцинације од 7 и 24 h). Сојеви „Pseudomonas aeruginosa DV 2739 и ATCC 9023” коришћени су као модел микроорганизама у микробиолошком делу експеримената који су изведени у микробиолошком кабинету. Заједнички фотокаталитички и микробиолошки процеси изведени су у циркуларном фотореактору са емулгованим катализатором у присуству директног УВ зрачења симулираног натријумовом лампом „SONT UV400”. Студија је показала да узорак катализатора С28, Ла-допанта са концентрацијом од једног тежинског %, показује најбоље фотокаталитичке особине од свих Ла-допаната, али најбољу фотокаталитичку активност од свих катализатора постигнут је код С111 узорка, Fe-допанта (5 тежинских %, трајање калцинације од 7 h). Наши резултати такође показују различити степен деградације када је коришћен V-допант TiO₂, у концентрацији од 10 тежинских %, узорци С93 и С96, синтетисани са различитим трајањем калцинације (7 и 24 h) и брзином загревања током

калцинације (67,5 i 135 °C/h, редом), што се може објаснити аномалијом у њиховом понашању. Коначно, најбоља антимикуробна активност добијена је коришћењем узорка S24, Fe-допанта, који је показао да концентрација од 0,25 mg/L може бити токсична за микроорганизме. У складу са нашим резултатима супериорних карактеристика Fe-допанта и теоријских знања за наночестице TiO₂ допираних Ag, Au и Fe, дошло се до смерница за даља истраживања њихове фотокаталитичке и антимикуробне активности, као и за развој титанијум-диоксид наночестица и нанотуба за унапређење антибиотика и њихову употребу у лечењу рака.

Кључне речи: титанијум-диоксид, TiO₂-наночестице, TiO₂ допирани са La³⁺, Fe³⁺ и V³⁺, трајање калцинације, Сојеви *Pseudomonas aeruginosa* DV 2739 и ATCC 9023, фотокаталитичка активност, антимикуробна активност.

Paper received on / Дата получения работы / Датум пријема чланка: 24.04.2018.
Manuscript corrections submitted on / Дата получения исправленной версии работы / Датум достављања исправки рукописа: 04.07.2018.
Paper accepted for publishing on / Дата окончательного согласования работы / Датум коначног прихватања чланка за објављивање: 06.07.2018.

© 2018 The Authors. Published by Vojnotehnički glasnik / Military Technical Courier (www.vtg.mod.gov.rs, втг.мо.упр.срб). This article is an open access article distributed under the terms and conditions of the Creative Commons Attribution license (<http://creativecommons.org/licenses/by/3.0/rs/>).

© 2018 Авторы. Опубликовано в «Военно-технический вестник / Vojnotehnički glasnik / Military Technical Courier» (www.vtg.mod.gov.rs, втг.мо.упр.срб). Данная статья в открытом доступе и распространяется в соответствии с лицензией «Creative Commons» (<http://creativecommons.org/licenses/by/3.0/rs/>).

© 2018 Аутори. Објавио Војнотехнички гласник / Vojnotehnički glasnik / Military Technical Courier (www.vtg.mod.gov.rs, втг.мо.упр.срб). Ово је чланак отвореног приступа и дистрибуира се у складу са Creative Commons licencom (<http://creativecommons.org/licenses/by/3.0/rs/>).



COINCIDENCE STUDY OF DOUBLE ELECTRON EMISSION ASSOCIATED WITH K-SHELL PHOTOIONIZATION OF C₆₀

Sanja Lj. Korica^a, Axel Reinköster^b, Uwe Becker^c

^a University Union – Nikola Tesla, Faculty for Ecology and Environmental Protection, Belgrade, Republic of Serbia + Fritz-Haber-Institut, Department of Molecular Physics, Berlin, Federal Republic of Germany, e-mail: koricasanja@gmail.com, ORCID iD: <http://orcid.org/0000-0002-7915-9430>

^b Fritz-Haber-Institut, Department of Molecular Physics, Berlin, Federal Republic of Germany

^c Fritz-Haber-Institut, Department of Molecular Physics, Berlin, Federal Republic of Germany

DOI: 10.5937/vojtehg66-16527; <https://doi.org/10.5937/vojtehg66-16527>

FIELD: Molecular Physics, Photoelectron-Photoion Spectroscopy

ARTICLE TYPE: Original Scientific Paper

ARTICLE LANGUAGE: English

Abstract:

The (multiple) photoionization and subsequent fragmentation of the C₆₀ molecule was studied with the synchrotron radiation after removing electrons from the inner K-shell. Our intention was especially focused on the dynamics of the subsequent fragmentation. In addition to 'normal' (non-coincident) electron and ion time-of-flight spectroscopy, we investigated this topic with the help of an electron–electron-coincidence measurement. Our experiment shows that in these processes C^{q+}₆₀ ions with charge states up to 3+ and several smaller C^{q+}_{60-2m} fragments are formed. In addition, the broad peak besides the C(1s) line, usually referred to as the 'plasmon' peak, has been observed.

Key words: molecular physics, photoelectron-photoion spectroscopy, plasmon excitation.

Introduction

Since the discovery of C₆₀ molecule (Kroto et al, 1985, pp.162-163), (Krätschmer et al, 1990, pp.354-358) many studies were performed to investigate its fundamental properties. Due to its high symmetry, C₆₀

ACKNOWLEDGMENT: The authors are indebted to the *Deutsche Forschungsgemeinschaft* (DFG) and to the *Bundesministerium für Bildung und Forschung* (BMBF) for the financial support.

represents an ideal cluster with many possible applications. Its properties are mainly driven by its unique molecular structure like a spherical shell (Kusmany et al, 1993), (Korica et al, 2005, pp.132031-132035). So far, only a little is known about the C_{60} fragmentation after K-shell ionization (Aksela et al, 1995, pp.2112-2115), (Karvonen et al, 1997, pp.3466-3472), (Leiro et al, 2003, pp.205-213). For the main fragmentation channel, the (successive) emission of neutral C_2 has been proposed for a low charge state (Scheier et al, 1994, pp.77–93), although the emission of other neutral carbon atoms/small clusters is also present (Lykke, 1995, pp.1354–1357). Even triply charged fullerene ions appear to be rather stable (Bernard et al, 2003, pp.196–200). Highly charged C_{60} ions often decay through *fission* processes leading to a multiply charged fullerene and at least one other charged carbon atom or cluster, or they undergo *multi-fragmentation* processes leading exclusively to small, charged and neutral carbon clusters (Reinköster et al, 2003, pp.263–267).

Experiment

The measurements were performed at the HASYLAB undulator beam line BW3 in Hamburg and at the BESSYII dipole beamline TGM4 in Berlin using monochromatized synchrotron radiation whose wavelength can be scanned with a resolution set to an appropriate value. Measurements of Ne/Ar-resonances were carried out to check the accuracy of the monochromator settings. The photon beam crosses an effusive beam of C_{60} molecules, provided by an oven heated to 500 °C. Outgoing electrons are detected in time-of-flight (TOF) electron spectrometers at two different angles with respect to the electric vector of the ionizing radiation (Fig1.(a)). Appropriate voltages can be applied to the TOF-analysers to keep a constant resolution of the electron spectra for different photon energies. Some measurements were recorded in the coincidence mode. Additional fullerene ion data were accumulated using a multi-hit capable ion spectrometer with a pulsed electrical separation field (Fig.1(b)). The positively charged C_{60} ions or fragments are separated according to their mass-per-charge ratio by a pulsed field (pulse amplitude = 820 V, duration = 10 μ s, repetition rate = 12 kHz, rise time < 15 ns, field length = 5 mm). The ions are accelerated into a potential of -2800 V (field length = 4 mm) followed by a 200 mm long field-free drift tube. After passing the drift tube, the ions hit the detector surface which is held at a constant voltage of -3300 V. The distance from the drift tube to the detector is 5 mm. The detector consists of a Z-stack of MCPs with an active diameter of 40 mm.

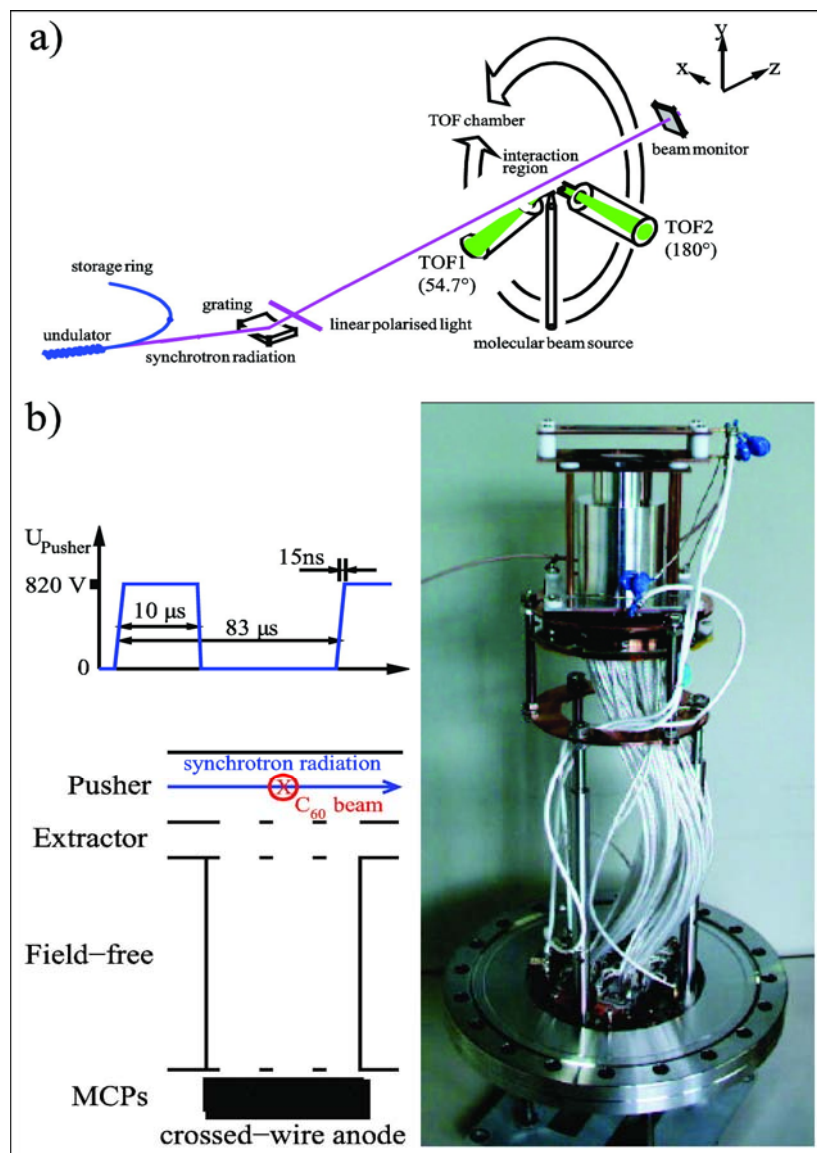


Figure 1 – Sketch of the experimental set-up. (a) beam source with the electron time-of-flight (TOF) spectrometer. (b) schematic view and picture of the ion spectrometer
 Рис. 1 – Изображение экспериментального устройства (а) источник света с TOF спектрометром. (б) ионный спектрометр
 Слика 1 – Приказ експерименталног уређаја: (а) извор снопа са TOF спектрометром, (б) јонски спектрометар

Results and discussion

Inner shell ionization and fragmentation of C₆₀ molecule

Figure 2 shows an example of the ion spectrum recorded at the photon energy of 390 eV. The inset shows the low-mass region of the spectrum. A rough classification of different processes is indicated by different coloured areas. In these processes, C^{q+}₆₀ ions with charge states up to 3+ and several smaller C^{q+}_{60-2m} fragments have been observed. This is in accordance with the previous claim that the main fragmentation channel is the emission of neutral C₂. Large singly charged carbon clusters (such as C⁺₃₀, C⁺₂₉, or C⁺₂₀) have no particular stability and one ought to expect additional species with similar sizes (such as C⁺₃₁ or C⁺₂₁), which have not been observed. For all photon energies used, no small charged carbon fragments resulting from fission or multi-fragmentation processes are observed.

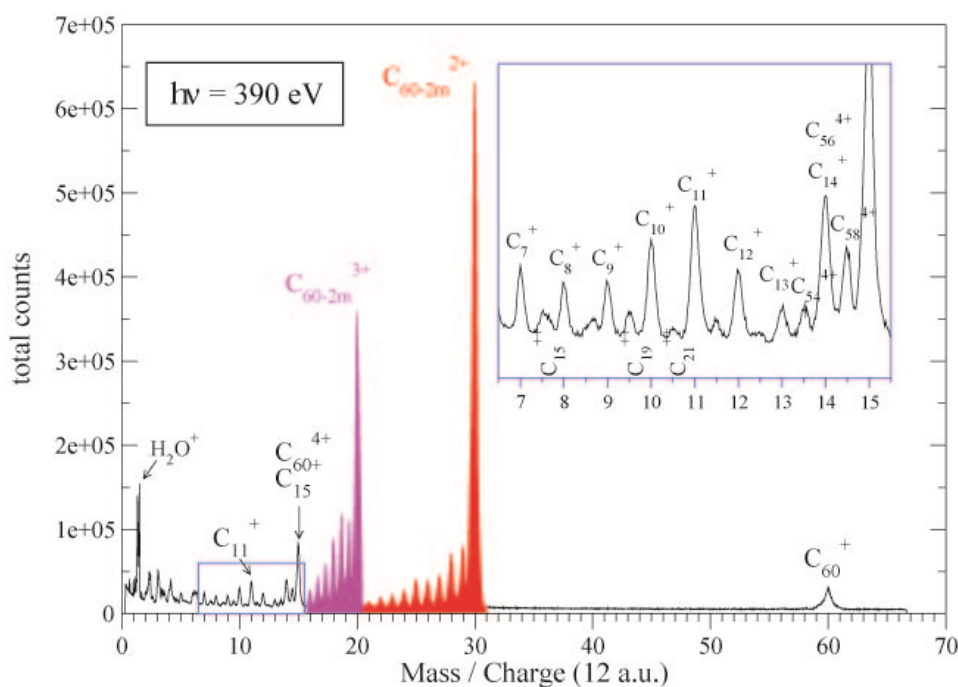


Figure 2 – Ion spectrum recorded with a photon energy of 390 eV
Рис. 2 – Ионный спектр, записанный на энергии фотона 390 eV
Слика 2 – Ионски спектар снимљен на енергији фотона од 390 eV

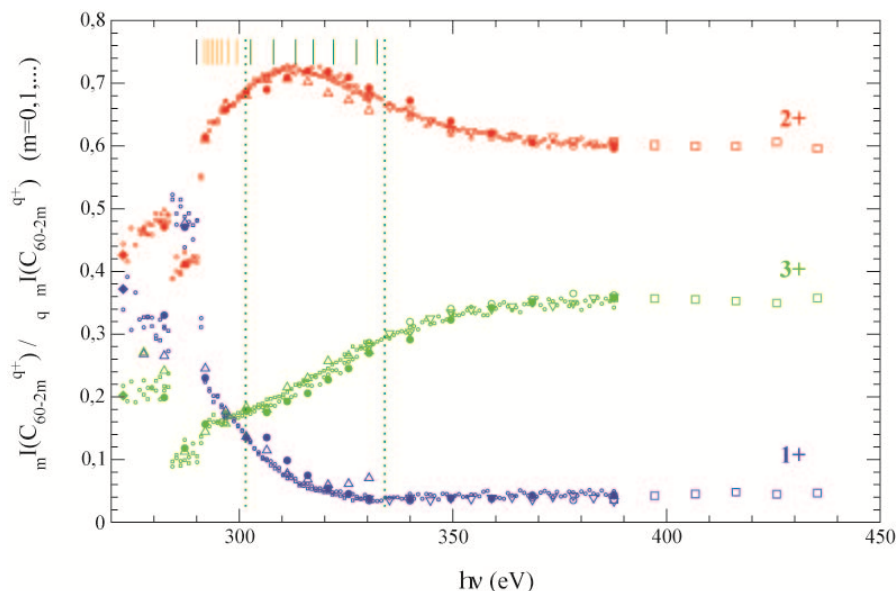


Figure 3 – Contributions of singly, doubly, and triply charged fullerene ions for several photon energies. Different scans are marked by different symbols. The results of the coincident electron spectrum are marked by 'e'. The vertical lines indicate the C(1s) threshold (Δ), electron shake-up levels (Δ), and plasmon excitation energies (Δ) (Leiro et al, 2003, pp.205-213). The high amount of triply charged fullerene can be explained by double Auger and electron shake-off processes, observed in the electron-electron-coincidence map (Fig.4).

Рис. 3 – Вклад однозарядных, двухзарядных и трехзарядных ионов фуллерена по нескольким значениям энергии фотонов. Разные сканы отмечены различными символами. Результаты совпадающего электронного спектра обозначены «e». Вертикальные линии обозначают C(1s) порог (Δ), электронные уровни shake-up (Δ) и энергию возбуждения плазмы (Δ) (Leiro et al, 2003, pp. 205-213). Высокий процент трехзарядных фуллеренов можно объяснить двойными Оже- процессом и электронным shake-up процессом, которые видны на карте совпадений электронов (рис.4).

Слика 3 – Доприноси једноструко, двоструко и троструко наелектрисаних јона фулерена за неколико вредности енергије фотона. Различити скенови су означени различитим симболима. Резултати коинцидентног електронског спектра означени су са 'e'. Вертикалне линије означавају C(1s) границу (Δ), електронске шејк-ап нивое (Δ) и енергије плазмонских ексцитација (Δ) (Leiro et al, 2003, pp.205-213). Висок проценат троструко наелектрисаних фулерена може се објаснити двоструким Ожеовим и електронским шејк-оф процесима, који се могу видети на електрон-електрон коинцидентној мапи (слика 4).

Figure 3 shows contributions of singly, doubly and triply charged fullerene ions for several photon energies. These results indicate that, above the carbon K-shell of C₆₀, the main products are doubly and triply charged fullerenes. C₆₀⁺ is the most abundant ion in the low energy region. The relative C₆₀²⁺ yield compared to the C₆₀⁺ yield first increases with increasing photon energy and stagnates above ≈350 eV at a nearly constant level. The yield of triply charged C₆₀³⁺ is similar to the yield of C₅₈²⁺. Different doubly charged C_{60-2m}²⁺ fragments appear step by step with increasing photon energy. The yields of singly charged fragments exhibit an enhancement in certain photon energy regions; at high photon energies, these yields decrease and are only slightly visible.

So the obtained ion yield spectroscopy of gas phase C₆₀ is corroborated by the corresponding photoelectron measurements (Korica et al, 2018). The continuous intensity distribution in the photoelectron spectra can be either the result of direct double photoionization or double-Auger decay. The quality of the former K-shell photoelectron measurements was insufficient to disentangle these two contributions experimentally (Aksela et al, 1995, pp.2112-2115), (LeBrun et al, 1994, pp.3965-3968), (Brühwiler et al, 1993, pp.3721-3724), (Krummacher et al, 1993, pp.8424-8429). In general, the disentanglement of the two processes on the basis of normal ion or electron spectroscopy is not unambiguously possible.

Electron-electron coincidence spectroscopy of excited C₆₀

Electron–electron-coincidence measurements were carried out to get a deeper understanding about the fundamental processes causing the many-electron emission in C₆₀. Here, a separation of different underlying processes can be better achieved. (Fig. 4).

Shake-off electrons are abundant at low-kinetic energies. Therefore, even at such high photon energies, shake-off processes are important to understand the yields of the multiply charged C₆₀ ions besides the Auger and double Auger processes. In the case that two shake-off electrons leave the C₆₀ molecule, the energy sharing is very asymmetric. The faster of the two shake-off electrons contributes significantly to the broad peak besides the C(1s) main line, usually referred to as the 'plasmon' peak (Hertel et al, 1992, pp.784-787), (Leiro et al, 2003, pp.205-213); this possibility has been unrevealed so far.

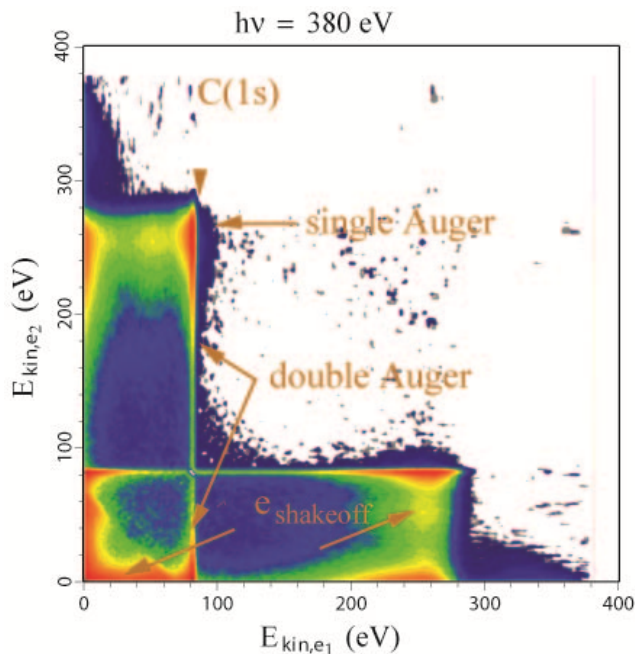


Figure 4 – Electron-electron coincidences as a function of the kinetic energy of the two detected electrons. The coincidence map was recorded with a photon energy of 380 eV.
 Рус. 4 – Карта совпадений электронов как функция кинетической энергии двух обнаруженных электронов. Карта совпадений записана на энергии фотона 380 eV.
 Слика 4 – Електрон-електрон коинциденце као функција кинетичке енергије два детектована електрона. Коинцидентна мапа снимљена је на енергији фотона од 380 eV.

Conclusion

We have studied the photoionization of the C_{60} molecule above the C(1s) threshold, in the photon energy range $h\nu=(330-390)$ eV. A careful analysis of the spectra yielded a surprising and unexpected result.

Clear hints have been found that the major contribution to the triply charged ion yield is the direct double photoionization of C_{60} . However, in contrast to most atoms and molecules, it is driven by the plasmon excitation associated with the K-shell photoionization of the fullerenes. Whereas the K-shell satellites are still bound core excited ionic states of the C_{60} molecule, plasmon excitations at higher binding energies are already in the double electron emission continuum. This causes a specific intensity distribution and explains the origin of the broad resonance features in the continuum part of the spectrum and an unusual high amount of triply charged fullerenes of 40%.

References

- Aksela, S., Nömmiste, E., Jauhiainen, J., Kukk, E., Karvonen, J., Berry, H.G., Sorensen, S.L. & Aksela, H. 1995. Photofragmentation of C₆₀ Molecules following Resonance Excitation and Ionization near the C 1s Edge. *Physical Review Letters*, 75(11), pp.2112-2115. Available at: <https://doi.org/10.1103/physrevlett.75.2112>.
- Bernard, J., Martin, S., Chen, L., Cederquist, H., Salmoun, A., & Brédy, R. 2003. A single ion (Ar q+ q =1,3 or C 60 3+) in a conic electrode electrostatic trap. *Nuclear Instruments and Methods in Physics Research Section B: Beam Interactions with Materials and Atoms*, 205, pp.196-200. Available at: [https://doi.org/10.1016/s0168-583x\(03\)00553-6](https://doi.org/10.1016/s0168-583x(03)00553-6).
- Brühwiler, P.A., Maxwell, A.J., Rudolf, P., Gutleben, C.D., Wästberg, B., & Mårtensson, N. 1993. C1s autoionization study of electron hopping rates in solid C₆₀. *Physical Review Letters*, 71(22), pp.3721-3724. Available at: <https://doi.org/10.1103/physrevlett.71.3721>.
- Hertel, I.V., Steger, H., de Vries, J., Weisser, B., Menzel, C., Kamke, B., & Kamke, W. 1992. Giant plasmon excitation in free C₆₀ and C70 molecules studied by photoionization. *Physical Review Letters*, 68(6), pp.784-787. Available at: <https://doi.org/10.1103/physrevlett.68.784>.
- Karvonen, J., Nömmiste, E., Aksela, H., & Aksela, S. 1997. Photoion spectra of C₆₀ molecules at resonance excitation and ionization energies near the C 1s edge. *Journal of Chemical Physics*, 106(9), pp.3466-3472. Available at: <https://doi.org/10.1063/1.473442>.
- Korica, S., Reinköster, A., & Becker, U. 2018. Strong enhancement of double Auger decay following Plasmon excitation in C₆₀. *Vojnotehnički glasnik/Military Technical Courier*, 66(3), pp.483-494. Available at: <https://doi.org/10.5937/vojtehg66-16269>.
- Korica, S., Rolles, D., Reinköster, A., Langer, B., Viefhaus, J., Cvejanović, S., & Becker, U. 2005. Partial cross sections and angular distributions of resonant and nonresonant valence photoemission of C₆₀. *Physical Review A*, 71(1), pp.132031-132035. Available at: <https://doi.org/10.1103/physreva.71.013203>.
- Krätschmer, W., Lamb, L.D., Fostiropoulos, K., & Huffman, D.R. 1990. Solid C₆₀: a new form of carbon. *Nature*, 347(6291), pp.354-358. Available at: <https://doi.org/10.1038/347354a0>.
- Kroto, H.W., Heath, J.R., O'Brien, S.C., Curl, R.F., & Smalley, R.E. 1985. C₆₀: Buckminsterfullerene. *Nature*, 318(6042), pp.162-163. Available at: <https://doi.org/10.1038/318162a0>.
- Krummacker, S., Biermann, M., Neeb, M., Liebsch, A., & Eberhardt, W. 1993. Close similarity of the electronic structure and electron correlation in gas-phase and solid C₆₀. *Physical Review B*, 48(11), pp.8424-8429. Available at: <https://doi.org/10.1103/physrevb.48.8424>.

Kusmany, H., Fink, J., Mehring, M., & Roth, S. 1993. Electronic Properties of Fullerenes. In *Springer Series in Solid-State Sciences*. Berlin: Springer. Vol. 177.

LeBrun, T., Berry, H.G., Cheng, S., Dunford, R.W., Esbensen, H., Gemmell, D.S., Kanter, E.P., & Bauer, W. 1994. Ionization and Multifragmentation of C_{60} by High-Energy, Highly Charged Xe Ions. *Physical Review Letters*, 72(25), pp.3965-3968. Available at: <https://doi.org/10.1103/physrevlett.72.3965>.

Leiro, J.A., Heinonen, M.H., Laiho, T., & Batirev, I.G. 2003. Core-level XPS spectra of fullerene, highly oriented pyrolytic graphite, and glassy carbon. *Journal of Electron Spectroscopy and Related Phenomena*, 128(2-3), pp.205-213. Available at: [https://doi.org/10.1016/s0368-2048\(02\)00284-0](https://doi.org/10.1016/s0368-2048(02)00284-0).

Lykke, K.R. 1995. Fragmentation of C_{60} : Experimental detection of C, C_2 , C_3 , and C_4 by xuv postionization. *Physical Review A*, 52(2), pp.1354-1357. Available at: <https://doi.org/10.1103/physreva.52.1354>.

Reinköster, A., Siegmann, B., Werner, U., & Lutz, H.O. 2003. Ion-impact induced excitation and fragmentation of C_{60} . *Radiation Physics and Chemistry*, 68(1-2), pp.263-267. Available at: [https://doi.org/10.1016/s0969-806x\(03\)00295-0](https://doi.org/10.1016/s0969-806x(03)00295-0).

Scheier, P., Dünser, B., Wörgötter, R., Lezius, M., Robl, R., & Märk, T.D. 1994. Appearance and ionization energies of singly, doubly and triply charged C_{60} and its fragment ions produced by electron impact ionization. *International Journal of Mass Spectrometry and Ion Processes*, 138, pp.77-93. Available at: [https://doi.org/10.1016/0168-1176\(94\)04034-6](https://doi.org/10.1016/0168-1176(94)04034-6).

ИССЛЕДОВАНИЕ ДВОЙНОЙ ЭЛЕКТРОННОЙ ЭМИССИИ, СВЯЗАННОЙ С ФОТОИОНИЗАЦИЕЙ К-ОБОЛОЧКИ C_{60}

Саня Л. Корица^а, Аксел Райнкостер^б, Уве Бекер^в

^а Университет «Унион – Никола Тесла», Факультет экологии и охраны окружающей среды, г. Белград, Республика Сербия + Институт им. Фрица Габера, Отделение молекулярной физики, г. Берлин, Федеративная Республика Германия

^б Институт им. Фрица Габера, Отделение молекулярной физики, г. Берлин, Федеративная Республика Германия

^в Институт им. Фрица Габера, Отделение молекулярной физики, г. Берлин, Федеративная Республика Германия

ОБЛАСТЬ: молекулярная физика, фотоэлектрон-фотоионная спектроскопия

ВИД СТАТЬИ: оригинальная научная статья

ЯЗЫК СТАТЬИ: английский

Резюме:

(Многогранная) фотоионизация и проводительная фрагментация молекулы C_{60} исследовалась с помощью синхротронного излучения после выброса электрона из

внутренней K-оболочки. Наше исследование было сосредоточено на динамике проводимой фрагментации. Кроме «нормальной» (несовпадающей) электронной и ионной спектроскопии, применялись и другие методы измерений, так например, было проведено измерение электронного совпадения. Наш эксперимент показал, что в течение этих процессов формируются C^{q+}_{60} ионы с зарядом до трех + и несколько небольших C^{q+}_{60-2m} фрагментов. Кроме того, был выявлен широкий пик рядом с основной линией C (1s), так называемым «плазмон».

Ключевые слова: молекулярная физика, фотоэлектрон-фотоионная спектроскопия, возбуждение плазмона.

КОИНЦИДЕНТНА СТУДИЈА ДВОСТРУКЕ ЕЛЕКТРОНСКЕ ЕМИСИЈЕ ПОВЕЗАНЕ СА ФОТОЈОНИЗАЦИЈОМ К-ЉУСКЕ C_{60}

Сања Љ. Корица^а, Аксел Рајнкостер^б, Уве Бекер^в

^а Универзитет Унион – Никола Тесла, Факултет за екологију и заштиту животне средине, Београд, Република Србија + Институт Фриц Хабер, Одсек за молекуларну физику, Берлин, Савезна Република Немачка

^б Институт Фриц Хабер, Одсек за молекуларну физику, Берлин, Савезна Република Немачка

^в Институт Фриц Хабер, Одсек за молекуларну физику, Берлин, Савезна Република Немачка

ОБЛАСТ молекуларна физика, фотоелектронско-фотојонска спектроскопија

ВРСТА ЧЛАНКА: оригинални научни чланак

ЈЕЗИК ЧЛАНКА: енглески

Сажетак:

Фотојонизација (вишеструка) и пратећа фрагментација молекула C_{60} проучавана је уз помоћ синхротронског зрачења након избацивања електрона из унутрашње К-љуске. Наше истраживање било је посебно фокусирано на динамику пратеће фрагментације. Поред „нормалне“ (некоинцидентне) електронске и јонске ТОФ спектроскопије, ову тему изучавали смо и уз помоћ електрон-електрон коинцидентног мерења. Наш експеримент показује да се у овим процесима формирају C^{q+}_{60} јони са наелектрисањем до 3+ и неколико мањих C^{q+}_{60-2m} фрагмената. Поред тога, поред главне C(1s) линије уочен је широки пик, тзв. плазмон.

Кључне речи: физика молекула, фотоелектронска-фотојонска спектроскопија, плазмонска екситација.

Paper received on / Дата получения работы / Датум пријема чланка: 11.02.2018.
Manuscript corrections submitted on / Дата получения исправленной версии работы /
Датум достављања исправки рукописа: 12.04.2018.
Paper accepted for publishing on / Дата окончательного согласования работы / Датум
коначног прихватања чланка за објављивање: 14.04.2018.

© 2018 The Authors. Published by Vojnotehnički glasnik / Military Technical Courier
(www.vtg.mod.gov.rs, втг.мо.упр.срб). This article is an open access article distributed under the
terms and conditions of the Creative Commons Attribution license
(<http://creativecommons.org/licenses/by/3.0/rs/>).

© 2018 Авторы. Опубликовано в «Военно-технический вестник / Vojnotehnički glasnik / Military
Technical Courier» (www.vtg.mod.gov.rs, втг.мо.упр.срб). Данная статья в открытом доступе и
распространяется в соответствии с лицензией «Creative Commons»
(<http://creativecommons.org/licenses/by/3.0/rs/>).

© 2018 Аутори. Објавио Војнотехнички гласник / Vojnotehnički glasnik / Military Technical Courier
(www.vtg.mod.gov.rs, втг.мо.упр.срб). Ово је чланак отвореног приступа и дистрибуира се у
складу са Creative Commons licencom (<http://creativecommons.org/licenses/by/3.0/rs/>).



NEGATIVE IONS AND THEIR ROLE IN THE DEVELOPMENT OF SCIENCE AND TECHNOLOGY

Leonid I. Gretchikhin

Belarusian State Academy of Communications,

Minsk, Republic of Belarus,

e-mail: gretchihin@yandex.ru,

ORCID iD:  <http://orcid.org/0000-0002-5358-9037>

DOI: 10.5937/vojtehg66-17262; <https://doi.org/10.5937/vojtehg66-17262>

FIELD: Nanotechnology

ARTICLE TYPE: Original Scientific Paper

ARTICLE LANGUAGE: English

Abstract:

Negative ions are formed in the process of the interaction between the electron with the integrated electric dipole moment and the induced electric dipole moment due to polarization. In the continual regime, at orbital velocity, the emission of negative ions from the surface of the heat-shielding coating leads to the formation of a double electric layer with a very dense plasma while at the escape velocity the same emission of negative ions creates an explosive character of burning of the heat-shielding coating. In the free molecular flow regime, the emission of negative ions results in intense violet-blue glow while high positive potentials are induced on the surface of an aircraft. In nanotechnologies, the ionization of negative ions determines the parameters of vacuum arc discharge. Negative ions participate in the formation of an electrostatic machine in the human body.

Key words: negative ions, electric dipole moment, double electric layer, polarization, electrostatic machine.

Introduction

When studying the formation and destruction of negative ions, researchers have encountered a peculiar structure of negative ions. Different atoms and, especially, molecules respond to the bond with extra electrons each in its own way. This was confirmed when quantum mechanics was applied to describe the structure of the electron affinities of neutral atoms and molecules and to determine the electron affinity energies. It was found out that some atoms and molecules have greater electron affinities while the others, on the contrary, do not respond at all to the presence of free electrons in their nearest environment. For lack of

any adequate theoretical model of the formation of negative ions, the effective use of negative ions as catalysts to achieve optimal conditions for all parameters of processes in various fields of technology is essentially limited. Therefore, it is vital to set the following goal: to consider in great detail what kinds of chemical bonds arise in the process of negative ions formation, and further, based on this knowledge, to find out the influence of negative ions on the technological processes used in the production of various machines, mechanisms, and equipment. To reach the goal, it is essential to solve the following problems:

1. To provide an explanation of the process of negative ions formation for various atomic and molecular systems.
2. To determine the role of negative ions in space exploration.
3. To consider the influence of negative ions in nanotechnologies.
4. To find out the positive role of negative ions in the human body.

Let us consider, one after another, these problems.

Formation of Negative Ions of Atoms and Molecules

Theoretical calculations of electron affinity energies performed using quantum-mechanical methods did not make it possible to obtain convincing agreement with the experimental data (Massey, 1976). An especially inadequate situation relates to complex atoms and molecules. Table 1 shows particular values of electron affinities for certain atoms.

*Table 1 – Parameters of Atoms of the First Group of the Periodic Table
Таблица 1 – Параметры атомов первой группы таблицы Менделеева
Табела 1 – Параметри атома прве групе периодног система елемената*

Atoms	Parameters of atoms				
	$r_a, \text{Å}$	Z^*	$\rho_a \cdot 10^{30}$ ($\text{Å} \cdot \text{m}$)	EA (eV)	$\Delta r / r_1$
H	0.529	0.500	0	0.754	0.0555
Li	2.049	0.766	0	0.609	0.1130
Na	2.227	0.794	4.34	0.548	0.1066
Rb	2.979	0.864	11.88	0.486	0.1163
Cu	1.762	0.945	42.45	1.228	0.1590
Ag	1.934	1.017	38.00	1.302	0.1718

Negative ions possessing a relatively high electron affinity are formed for atoms which feature a closed shell in the S-state formed

during electron capture. As this takes place, the change in potential energy presents the electron affinity energy:

$$EA \cong -\frac{Z^* e^2}{4\pi\epsilon_0} \left(\frac{1}{r_2} - \frac{1}{r_1} \right) \approx \frac{Z^* e^2}{4\pi\epsilon_0 r_1} \frac{\Delta r}{r_1}, \quad (1)$$

where Z^* is the effective nuclear charge of the neutral atom, e is the electron charge, r_1 and r_2 are the distances between the atom's center and the electron of the neutral atom and between the atom's center and the electron of the negative ion, correspondingly, and ϵ_0 is the dielectric permittivity of vacuum.

It follows from (1) that, when the negative ion of hydrogen is formed, the relative increase in the radius of rotation of the captured electron amounts to a noticeable value: $\frac{\Delta r}{r_1} \approx 0.05546$ while for lithium the

increase is: $\frac{\Delta r}{r_1} \approx 0.1130$. Table 1 presents the values of the increase for

other atoms. Table 1 shows the values of the radii of neutral atoms, the effective nuclear charges of neutral atoms, and the values of the electric built-in dipole moments. It follows from the data presented in Table 1 that the deformation of the initial electron shells of neutral atoms upon capture of an electron is quite substantial. The presence of the built-in electric dipole moment of large magnitude leads to an increase in the electron affinity energy of an atom. Theoretical calculations of electron affinity energies performed using quantum-mechanical methods did not reflect in full measure the dynamics of the formation of negative ions in atomic structures. It is necessary to take into account the presence of the built-in electric dipole moment in atoms and, along with the covalent chemical bond using the Heitler-London method, other possible types of chemical bonds will be also taken into consideration. Below we show how to take into account the above conditions, following (Gretchikhin & Kamarouskaya, 2016, pp.447-464).

Formation of Negative Ions in Atoms

The paper (Gretchikhin, 2008) showed that in complex atomic systems, the deformation of spherically symmetric s -states occurs due to the interaction of p - s , d - s or f - s electron shells; as a result, a built-in electric dipole moment, relative to the center of a complex atom, arises. Calculations of the built-in electric moment, taking into account Hund's

rule, were performed for the majority of atoms in the periodic table. During the capture of a free electron by a neutral atom, there is no interaction with the positive nucleus of the atom, since the nucleus of the atom is completely screened by the electrons around the atom. However, as the free electron approaches the atom, its electric field polarizes the atomic system. In this case, the interaction with the displaced cloud of all electrons of the neutral atom arising due to polarization takes place, but not with the effective charge of the nucleus.

In the presence of the built-in electric dipole moment in the atom, the interaction between an external free electron and the electric dipole is activated. In this situation, the atom is able to gain an electron and to become a negative ion. Under the action of the electric field of this electron, the displacement of the electron cloud of the neutral atom relative to its center occurs in all energy states. If the external field is created by an external electron, then the condition of equilibrium of forces for the electron inside the atom in k -th state is as follows:

$$\frac{e^2}{4\pi\epsilon_0 r_0^2} = \frac{Z_k^* e^2}{4\pi\epsilon_0 r_k^2} - \frac{Z_k^* e^2}{4\pi\epsilon_0 (r_k + \Delta r_k)^2}. \quad (2)$$

where r_k is the radius of electron rotation of the atom in the k -state, Z_k^* is the effective nuclear charge of the atom in the k -th state for the electron under consideration, and r_0 is the radial distance of the negative ion from the atom center.

Hence, the displacement of the outer electron cloud of the k -th energy state relative to the atom's center is as follows:

$$\Delta r_k \approx \frac{r_k^3}{2Z_k^* r_0^2}. \quad (3)$$

The energy of the interaction of the outer electron with the built-in electric dipole of the atom with taking into account the energy for polarization represents the electron affinity and is expressed as follows:

$$EA \cong -\frac{2ep_d}{4\pi\epsilon_0 r_0^2} + \sum_k \frac{Z_k^* e^2}{4\pi\epsilon_0} \left[\frac{1}{r_0} - \frac{1}{r_0 + \Delta r_k} \right]. \quad (4)$$

Here, p_d is the built-in electric dipole moment of the neutral atom. It is obvious that the potential of the interaction between the electron and the neutral atom will be minimal. Otherwise, the system will not be stable. That is the reason why the electron affinity and the negative ion radius are determined by the minimum value of the interaction potential (4). The results of the interaction potential calculations for the atoms of carbon,

oxygen, copper and titanium have been performed in (Gretchikhin & Kamarouskaya, 2016, pp.447-464).

Electron affinity energy can be measured with high accuracy, i.e. with an accuracy within 3%. Therefore, using the values of electron affinity of an atom makes it possible to obtain real values of built-in electric dipole moments of complex atomic systems and, at the same time, the negative ion radius.

The electron affinity of the carbon atom for the atom's radius $r_a = 1,091 \text{ \AA}$, the distance of the valence electron of the negative ion from the atom's center $r_0 = 1,095 \text{ \AA}$ and $p_d = 3,935 \cdot 10^{-30} \text{ C}\cdot\text{m}$, equals to the experimental value of 1.263 eV. The radius of the carbon atom is slightly bigger than the value obtained using the quantum-mechanical method: 0.905 \AA (Brattsev, 1966) and 0.922 (Radzig & Smirnov, 1985). For atom's radius of 0.905 \AA the experimental value of the electron affinity is realized in the negative ion at the distance from the atom's center of 1.02 \AA and for the built-in electric dipole moment $p_d = 3,089 \cdot 10^{-30} \text{ C}\cdot\text{m}$.

For the oxygen atom with the value of the built-in electric dipole moment $p_{d,O} = 2,891 \cdot 10^{-30} \text{ C}\cdot\text{m}$, the atom's radius of 0.7073 \AA and the negative ion's radius $r_0 = 1,04 \text{ \AA}$ the electron affinity energy equals 1.4611 eV, the value which corresponds to the measured one.

Therefore, electron affinity of atoms is determined by the interaction of the outer electron with the built-in electrical moment of the complex atomic system as well as by coulombic interactions of the electrons of negative ions with the electrons of the neutral atom of all energy states and atom nuclei.

Negative Ions of Diatomic Molecules

Electric dipole moments in diatomic molecules are oriented opposite to each other. It follows from the composition of diatomic molecules that they can gain two electrons and become a doubly charged negative ion. Electron affinity energy for a singly charged negative ion is as follows:

$$EA_m \cong -\frac{2ep_{d,1}}{4\pi\epsilon_0 r_1^2} + \frac{2ep_{d,2}}{4\pi\epsilon_0 r_2^2} + \frac{e\Delta Q}{4\pi\epsilon_0 r_m} + \sum_k \frac{Z_k^* e^2}{4\pi\epsilon_0} \left[\frac{1}{r_1 + r_n} - \frac{1}{r_1 + r_n + \Delta r_k} \right]. \quad (5)$$

Here, $\Delta r_k = \frac{r_{eff}^3}{2Z_k^* r_1^2}$ and it determines the displacement of the

valence electron cloud in the molecule; Z_k^* is the effective molecular

charge in the k -state; r_{eff} is the effective molecular radius; r_1 is the distance to the center of the nearest atom determined by the position of the interaction potential minimum; r_m is the distance to the molecule center, r_n is the additional distance to the next atom, equal to r_e , $p_{d,1}$ and $p_{d,2}$ are the built-in electric dipole moments of the ions of the interacting atoms, correspondingly; and ΔQ is the induced charge occurring as a result of the valence electrons exchange at the covalent bond in the diatomic molecule.

The sum in the potential (5) considers the energy input for the polarization of the valence electron cloud of the diatomic molecule and for the polarization of the electron cloud of the positive core atoms. In particular, the theoretical calculation of the electron affinity value using (5) for the carbon molecule for the effective radius of the interacting atoms of 0.905 Å (Radzig & Smirnov, 1985) and for the electric dipole moment of a singly charged negative ion of the atom of the molecule positive core $p_{d,i} = 1,976 \cdot 10^{-30}$ C·m amounts to the experimentally obtained value of 3,39 eV for the distance from the nearest atom of 0.7643 Å, i.e. the distance to which the electron approaches the atom center in the diatomic molecule.

Electron Affinity of Triatomic Molecules

A triatomic molecule is formed as a result of the atom interaction with a diatomic molecule. During this process, the common electron shell is formed by all three valence electrons of complex atoms. That is the reason why the positive core of the triatomic molecule contains singly charged positive ions of the initial atoms. The built-in electric dipole moments of the single ions are arranged so as to maximally increase the bond energy between the atom and the diatomic molecule.

At the same time, the distance between the atoms corresponds to a bit bigger interval than the equilibrium distance between the atoms in the diatomic molecule. The nearest atom in the diatomic molecule is considered as the central one.

The distances of the atoms from the central atom are approximately equal; it is designated as r_e . Other distances expressed in terms of r_e are as follows:

$$r_1 = 2r_e \sin(\alpha/2); \quad r_2 = r_e \sqrt{1,25 - \cos \alpha}; \quad r_3 = r_e \sin(\alpha/2),$$

where α is the central angle in the triatomic molecule.

The triatomic molecule captures the electron to its outer orbit. The electron affinity of a triatomic molecule is determined by the interaction with the integrated dipole moments of all three ions of the positive core and by its polarization. The distance of the captured electron from the molecule's center does not exceed the molecule's effective radius. The electron affinity energy of the positive core of the triatomic molecule is mainly determined by the interaction between the valence electron and the built-in electric dipole moment of the nearest ion. The distance to which the electron approaches the nearest ion of the atomic core does not exceed the radius of the triply charged ion of the molecule. The resultant binding energy of the valence electron of the negative ion of the triatomic molecule equals to:

$$EA_1 = -E_1 + E_2 + E_3 + E_4 - E_5 + E_6, \quad (6)$$

$$\text{where } E_1 = \frac{2ep_d}{4\pi\epsilon_0 r^2}; E_2 = \frac{e\Delta Q}{4\pi\epsilon_0 (r+r_e/2)}; E_3 = \frac{e\Delta q}{4\pi\epsilon_0 (r+r_2)};$$

$$E_4 = \frac{2\cos(\pi-\alpha)ep_d}{4\pi\epsilon_0 (r+r_e)^2}; E_5 = \frac{2ep_d \cos\left(\frac{\pi-\alpha}{2}\right)}{4\pi\epsilon_0 (r+r_1)^2};$$

$$E_6 = \sum_k \frac{Z_k^* e^2}{4\pi\epsilon_0} \left(\frac{1}{r+r_2/2} - \frac{1}{r+r_2/2+\Delta r_k} \right)$$

$$\text{and } \Delta r_k = \frac{r_{\text{eff}}^3}{2Z_k^* (r+r_2/2)^2}.$$

Here, ΔQ and Δq are the charges induced inside the diatomic molecule and between the outer atoms and the diatomic molecule, correspondingly, determined using the Heitler-London method.

When the triatomic molecule becomes a doubly charged negative ion, the bound energy of the second electron weakens and can be determined using the following formula

$$EA_2 = EA_1 + \frac{e^2}{4\pi\epsilon_0 3r_a}. \quad (7)$$

The following results have been obtained:

1. When considering the electron affinity of an atom, the interaction of an electron with the built-in electric dipole moment of a neutral atom and the repulsive forces between the valence electrons of neutral atoms and a negative ion in accordance with Coulomb's law will be considered.

2. The electron affinity of a diatomic molecule is determined by the electron interaction with two built-in electric dipole moments of the atomic ion, the induced negative cloud at the boundary of the atoms within the molecule, as well as by the Coulomb's interactions of the valence electrons of the negative ion and those of the neutral molecule.

3. In the process of electron capture by a triatomic molecule, the electron affinity energy is determined by the interaction of an electron with the built-in electric dipole moments of all three ions forming the positive core of the molecule as well as by the Coulomb's interactions of the outer electron of the triatomic molecule and the induced charges.

Negative ions play a special role in various fields of engineering and human activity. During the exploration of outer space, the researchers encountered the formation and ionization of negative ions. In nanotechnologies, negative ions make it possible to improve both the technologies of nanomaterials manufacture and the physical properties of materials. As for the influence of negative ions on the functions of the human body, their impact is invaluable.

Negative Ions in Space Exploration

As rocket technologies were developed, it became necessary to find out what processes of interaction with the environment accompany the rocket flights into space. The first studies in this domain were performed during the flights of a geophysical rocket along a ballistic trajectory in the 50s of the last century (Johnson & Heppner, 2012, pp.575-575). The results showed that only negative ions with masses of 46, 32, 29, 22, 16 or, expressed in percentage, 96.5; 1.6; 0.2; 1.0; 0.7 were present at the surface of the rocket at the altitude of 131 km. Positive ions N_2^+ were present in the illuminated zone. Ions with mass numbers of 46, 32 and 16 are identified as NO_2^- , O_2^- , and O^- . Mass numbers 29 and 22 correspond to the products of gasification of the rocket surface. These can be molecules COH^- and Na^- . The presence of negative ions at the rocket surface indicates an intense surface catalysis with the formation of negative ions. These results served as an impetus for intensive studies of negative ions formation during flights of rockets and spacecraft.

The first problem researchers faced was interrupted radio communication occurring at flight altitudes from 80 to 20 km due to the formation of a very dense plasma around the descent vehicle. However, formation of shock waves does not create any dense plasma. Then the researchers paid their attention to the process of burning of the heat-

shielding coating. Under these conditions, the combustion products contain molecule C_3 , which has the electron affinity energy of 2.5 eV. For this reason, the molecule leaves the surface of the heat-shielding coating in the form of a negative ion. Plasma parameters within the double electric layer correspond to those of arc discharge. At the moment of the communication session, the coolant was injected into the forward hemisphere and the communication was restored.

When space vehicles enter the dense layers of the atmosphere at the escape velocity, the heat-shielding coating should burn more intensively. The engineers faced the problem: how to save the descent vehicle. The temperature of the shock wave is quite high. Intensive convective heat exchange is realized; this fact allowed to find out the depth of the heat-shielding coating which should burn out. It turned out the depth amounted to ~ 2 m. The result was shocking. Negative ions came to the rescue. Ionization of negative ions creates an intense flow of electrons at the surface of the heat-shielding coating and together with radiant and convective heat flows makes the resultant flow so high that the skin layer explodes and heat ceases to arrive onto the surface of the spacecraft. Particular assessments showed that the heat-shielding coating should burn less at the escape velocity than at the orbital velocity. The descent vehicle of the spacecraft which circled the Moon, after having descended at the escape velocity, had the depth of burnt out heat-shielding coating of ~ 2 cm while the depth of burnt out heat-shielding coating of the vehicles descending at the orbital velocity amounted to ~ 3 cm. Combustion of the heat-shielding material at the escape velocity occurs not continuously but with separate explosive pulses.

Artificial Earth satellites (AES) flying at high altitudes are under the conditions of the free molecular flow regime. Atoms and molecules of the environment bombard the surface of the aircraft. At high altitudes in the Earth's atmosphere, oxygen atoms are present in a rather large amount. Due to high physical adhesion, oxygen atoms envelop the surface of the aircraft and create an oxygen film. Under the action of the incident flow, the atoms of the incident flow are exchanged with the oxygen atoms which leave the surface of the aircraft in the form of negative ions. As a result, the surface of the aircraft is charged positively. The induced potential on the surface of an aircraft flying at altitudes above 1000 km can reach ~ 1.5 kV. This potential, acting through a common wire, makes all electronic equipment of the satellite inoperative. This phenomenon was encountered during the first flights of artificial Earth satellites. Now it

is all in the past, but in the initial period of space exploration it was not clear why satellites at high altitudes suddenly fail.

A special situation arose around the "Gretchikhin Effect" (Gretchikhin, 2003, pp.31-33) (Gretchikhin, 1985) in 1969 based on the emission of negative oxygen ions and the formation of a double electric layer, the phenomenon of intense violet-blue glow around the front hemisphere of an AES flying at the altitudes of up to 500 km, with the maximum glowing occurring at the altitude of 110-140 km, mainly in the shadow zone of the Earth, was predicted. In 1971, during the emergency descent of the Soyuz-10 ship the cosmonauts visually observed this glow in the shadow zone of the Earth.

Based on theoretical calculations of the thickness of the double electric layer at different altitudes, the electron concentration and the energy distribution function, the nonequilibrium radiation of this layer was calculated in different spectral lines and molecular bands of nitrogen and oxygen. Figure 1 shows the results of the calculations for the ball of radius 1 m moving at a speed of 7.5 km/s. The glow of the double electrical layer at flight altitudes below 180 km is much greater than day airglow and even polar lights. At the flight altitude of ~ 120 km, the nonequilibrium glow is comparable to the magnitude of solar radiation within the range of 400-500 nm ($\sim 9.6 \text{ W/m}^2\text{sr}$). The glow varies according to the cosine law depending on the angle of attack. The maximum energy value of the nonequilibrium glow corresponds to the flight altitude of ~ 110 km both in the shadow zone of the Earth and in the illuminated zone. In the shadow zone of the Earth, the Meinel bands and the bands of the first negative system of hydrogen give a clearly pronounced maximum at the altitude of 120 ... 140 km and have maximum energy of radiation.

In accordance with the predictions of the theory, the measurements were carried out on-board of the long-term space station Salyut-4 with specially designed SFM/M photometric equipment. At the flight altitude of 350 km, there was detected a luminescence corresponding in brightness to that of the theoretical calculations in the spectral lines of oxygen, nitrogen, and in the molecular nitrogen band. A cosine distribution of the luminescence along the angle of attack was obtained, as predicted by the theory.

Similar results were obtained in the U.S.A. during STS-41 and Spacelab-1 missions (Mahon et al, 1983) ten years later. The results of these measurements are also shown in Fig. 1. The explanation of the observed frontal glow by chemiluminescence (Prince, 1985, pp.453-456) (Engebretson & Hedin, 1986, pp.109-112) or by the discharge model of

Papadopoulos (Papadopoulos, 1983, pp.227-244) does not stand up to scrutiny.

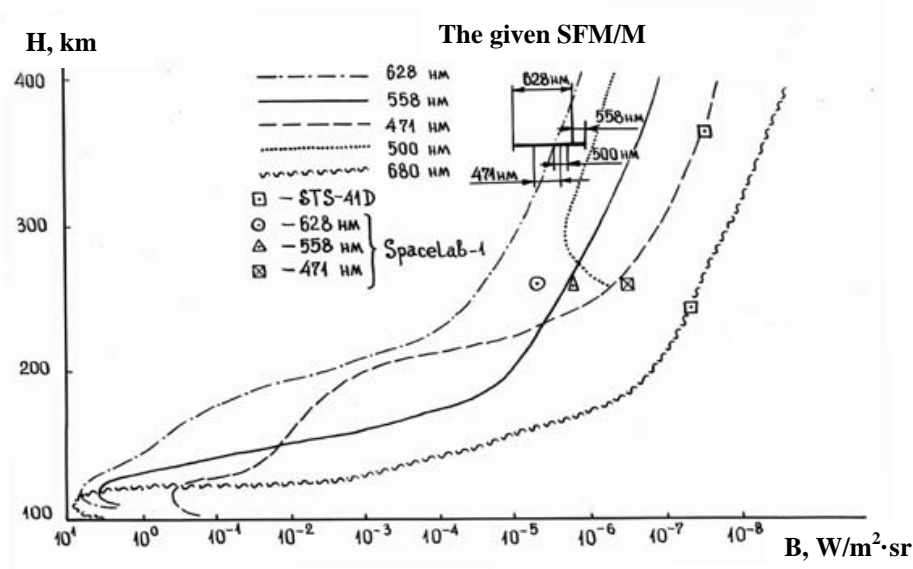


Figure 1 – Calculations of altitude curves of the non-equilibrium glow brightness in comparison to the experimental data
 Рис. 1 – Расчет высотного хода яркости неравновесного свечения по сравнению с экспериментальными данными
 Слика 1 – Израчунавање кривих јачине неравнотежног сјаја у односу на надморску висину у поређењу с експерименталним подацима

It is necessary to note one more phenomenon caused by the interaction of a solid body with the particles of near-Earth space with the participation of negative ions. Under the conditions of dynamic equilibrium, the flow of electrons in the environment is partially compensated by the flow of negative ions that escape into the surrounding space. Due to the chemical reactions of ionization of negative ions, epithermal electrons with energies in the range 0.4 ... 3.6 eV are produced. These electrons lead to the effective excitation of the energy levels of atoms and molecules, whose spontaneous emission for forbidden oxygen lines is significantly delayed. Therefore, at a certain distance from the spacecraft, there should appear a pink-red halo and the spacecraft trail must also have the same color. The pink-red halo was actually detected with the maximum at the distance of ~ 1 m from the ship (Papadopoulos, 1983, pp.227-244).

Thus, the theoretical model of the interaction of a solid body with near-earth space, in comparison to the experimental data, has been fully confirmed according to the following parameters and functions under investigation: radiation energy, spectral composition, dependences on oxygen concentrations in the environment, altitude curves of non-equilibrium glow brightness, brightness distribution around the aircraft, influence of the surface on the magnitude of radiation brightness, energy distribution of electrons, and the direct proof of the presence of negative ions near the aircraft surfaces.

Negative Ions in Nanotechnologies

Modern microelectronics engineering is developing using nanotechnologies. The negative ions play a decisive role in these technologies (Gretchikhin, 2018, pp.304-321). To form *p*- or *n*-conductivity, boron or arsenic which possess the ionization energies of 8.3 eV and 9.82 eV, accordingly, are applied onto the surface of a silicon crystal. The ionization energies of neutral boron and arsenic are located in the vicinity of the electron density distribution maximum of the first Brillouin zone of the silicon crystal. Since the atoms of boron and arsenic possess electron affinity energy, they freely capture electrons from the first Brillouin zone and are turned into negative ions with further transition to the band gap of the silicon crystal. The contact potential difference of two silicon crystals with introduced boron and arsenic is 0.5 V. The difference in the electron affinity energies corresponding to the p-n junction amounts to 0.5 V and agrees with the experimentally measured value.

When applying hardening coatings of nano-sized thicknesses, high-current arc discharges are used. When applying TiN coatings, two arc discharges with the electrodes made of titanium and copper are used to achieve more effective ionization. The electron affinity of the copper atom is 1.23 eV. The average effective temperature of electrons resulting from the ionization of negative ions of copper atoms by electron impact is 7850 K. The experimental measurements of plasma temperature by the spectroscopic method in an arc discharge between copper electrodes and under the action of laser radiation on a copper plate yielded a result of 7900 K (Gretchikhin & Minko, 1967).

For more than a century, it has been known that cathode flames in the tangential magnetic field are not deflected in accordance with Ampere's law. This phenomenon occurs as a result of negative ions ionization within the flame of the cathode spot when a reverse current, by an order greater than the charge current, is realized (Gretchikhin et al, 2016, pp.670-689). This experiment should be considered as an experimental proof of the pulse impact of the intense heat flow on the heat-shielding coating when a spacecraft re-enters the Earth's atmosphere at the escape velocity.

Negative Ions in the Human Body

The human body presents a complex electrostatic machine. Little attention is paid to this fact. In this aspect, negative ions play both a negative and a positive role. Human blood carries a positive charge formed mainly by twice ionized calcium and singly ionized potassium. The negative charge on the skin surface, amounting from 6 to 12 V, completely neutralizes the positive charge carried by blood. Blood performs a transport function, that is, delivers nutrients and takes away metabolic waste products. This is its main role. For blood to fulfill this role, it is necessary to ensure its circulation. The circulation of blood is ensured by the heart, which responds to the positive charge carried by blood, by means of pulse contractions.

Most metabolic waste products have electron affinity. As a consequence, the magnitude of the positive blood charge. As the metabolic rate in the body increases, the positive charge decreases noticeably. The spleen, together with the liver, clears blood from metabolic products, and outputs the negative charge onto the skin surface. When the complete purification of blood from metabolic products takes place, the body functions normally. The positive charge in blood is high enough to cause the contractions of the heart muscles. Otherwise, heart failure occurs which can lead to death. When intravenous laser irradiation of blood is used the negative ions are ionized. As a result, electrons are spontaneously released onto the surface, and functions of the spleen and liver are improved sharply; they now can solve their main task: to remove metabolic products from the body.

Conclusions

Based on the performed analysis of the formation and the action of negative ions under different conditions, the obtained results can be summarized as follows:

1. The electron affinity of negative ions is determined by the interaction of the electron with the built-in electric dipole moment and the induced electric dipole moment due to the polarization.

2. Under the conditions of continual flow over the frontal surface of the descent vehicles of the artificial Earth satellites at the orbital velocity, the emission of negative ions results in a double electric layer with the parameters of arc discharge plasma.

3. Under the conditions of continual flow over the frontal surface of the descent vehicles of the artificial Earth satellites at the escape velocity, the emission of negative ions and their ionization creates an explosive character of burning of the heat-shielding coating.

4. In the free molecular flow regime, intense emission of negative ions and their ionization by means of electron impact results in the formation of a double electric layer with non-equilibrium plasma which occurs under the conditions of glow discharge.

5. Nanotechnologies use arc discharges under reduced pressure with high electric currents, where plasma is determined by the ionization of negative ions, which creates back currents, exceeding the main discharge current in the cathode spots.

6. In the human body, negative ions have a beneficial effect on the blood for transporting nutrients and play a negative role when metabolic waste products produce negative ions in blood thus reducing its positive charge necessary for heart functioning.

References

Brattsev, V.F. 1966. *Tablicy atomnyh volnovyh funkcij*. Mocsow-Leningrad: Nauka (in Russian). (In the original: Братцев, В.Ф. 1966. *Таблицы атомных волновых функций*. – М.-Л.: Изд. «Наука». 1966).

Engbretson, M.J., & Hedin, A.E. 2012. DE-2 mass spectrometer observations relevant to the shuttle glow. *Geophysical Research Letters*, 13(2), pp.109-112. Available at: <https://doi.org/10.1029/gl013i002p00109>.

Gretchikhin, L.I. 1985. *Neravnovesnoe opticheskoe izluchenie vozdushnyh i kosmicheskikh letatel'nyh apparatov*. Minsk: Belarusian Polytechnic Institute. Ph.D. thesis (in Russian). (In the original: Гречихин, Л.И. 1985. *Неравновесное оптическое излучение воздушных и космических летательных аппаратов*. Минск: Белорусский политехнический институт. Докторская диссертация).

Gretchikhin, L.I. 2003. Vzaimodejstvie tverdogo tela s okruzhajushhej sredoj v rezhime svobodnomolekuljarnogo obtekanija (jeffekt Gretchikhina). In *The First Belarusian Space Congress*, Minsk, pp.31-33. October 28-30 (in Russian). (In the original: Гречихин, Л.И. 2003. Взаимодействие твердого тела с окружающей средой в режиме свободномолекулярного обтекания (эффект Гречихина). В *Первый Белорусский космический конгресс*, г. Минск, с.31-33. 28-30 октября).

Gretchikhin, L.I. 2008. *Nanochasticy i nanotehnologii*. Minsk: Pravo i ekonomika (in Russian). (In the original: Гречихин, Л.И. 2008. *Наночастицы и нанотехнологии*. Мн.: Право и экономика).

Gretchikhin, L.I. 2018. Formation of p-, n-conductivity in semiconductors. *Vojnotehnički glasnik/Military Technical Courier*, 66(2), pp.304-321. Available at: <https://doi.org/10.5937/vojtehg66-15935>.

Gretchikhin, L.I., & Kamarouskaya, V.M. 2016. Negative ions of atoms and diatomic and triatomic molecules. *Vojnotehnički glasnik/Military Technical Courier*, 64(2), pp.447-464. Available at: <https://doi.org/10.5937/vojtehg64-9685>.

Gretchikhin, L.I., Latushkina, S.D., & Kamarouskaya, V.M. 2016. Double electrical layer in the cathode spot. *Vojnotehnički glasnik/Military Technical Courier*, 64(3), pp.670-689. Available at: <https://doi.org/10.5937/vojtehg64-9851>.

Gretchikhin, L.I., & Minko, L.Y. 1967. Ob analogii fizicheskikh processov protokajushhih v impul'snom razrjade i pri vozdejstvii koncentrirovannogo lazernogo izluchenija. *Zhurnal tehnicheckoj fiziki*, 37 (in Russian). (In the original: Гречихин, Л.И., Минько, Л.Я. 1967. Об аналогии физических процессов протекающих в импульсном разряде и при воздействии концентрированного лазерного излучения. *Журнал технической физики*, 37).

Radzig, A.A., & Smirnov, B.M. 1985. *Reference Data on Atoms, Molecules, and Ions*. Berlin: Springer-Verlag.

Johnson, C.Y., & Heppner, J.P. 2012. Daytime measurement of positive and negative ion composition to 131 km by rocket-borne spectrometer. *Journal of Geophysical Research*, 61(3), pp.575-575. Available at: <https://doi.org/10.1029/jz061i003p00575>.

Mahon, W., Salter, R., Hills, R., & Delorey, D. 1983. Measured electron contribution to shuttle plasma environment, paper presented at Shuttle Environment and Operations Meeting, AIAA Paper No. AIAA-83-2598, Washington, D.C.

Massey, H. 1976. *Negative ions*. Cambridge University Press.

Papadopoulos, K. 1983. The Space Shuttle environment as evidence of critical ionization phenomena. In *Active Exp. Space. Proc. Int. Symp.*, Alpbach, Paris, pp.227-244. May 24-28.

Prince, R.H. 2012. On spacecraft-induced optical emission: A proposed second surface luminescent continuum component. *Geophysical Research Letters*, 12(7), pp.453-456. Available at: <https://doi.org/10.1029/gl012i007p00453>.

ОТРИЦАТЕЛЬНЫЕ ИОНЫ И ИХ РОЛЬ В РАЗВИТИИ НАУКИ И ТЕХНОЛОГИИ

Леонид И. Гречихин
Белорусская государственная академия связи,
г. Минск, Республика Беларусь

ОБЛАСТЬ: нанотехнологии
ВИД СТАТЬИ: оригинальная научная статья
ЯЗЫК СТАТЬИ: английский

Резюме:

Отрицательные ионы образуются при взаимодействии электрона со встроенным дипольным электрическим моментом и наведенным дипольным электрическим моментом вследствие поляризации. В континуальном режиме при первой космической скорости эмиссия отрицательных ионов с поверхности теплозащитного покрытия приводит к формированию двойного электрического слоя с очень плотной плазмой, а при второй космической скорости эта же эмиссия отрицательных ионов создает взрывной характер горения теплозащитного покрытия. При свободномолекулярном режиме обтекания эмиссия отрицательных ионов приводит к возникновению мощного фиолетово-голубого свечения, а на поверхности летательного аппарата наводятся большие положительные потенциалы. В нанотехнологиях ионизация отрицательных ионов определяет параметры вакуумного дугового разряда. Отрицательные ионы участвуют в формировании электростатической машины в человеческом организме.

Ключевые слова: отрицательные ионы, дипольный электрический момент, двойной электрический слой, поляризация, электростатическая машина.

НЕГАТИВНИ ЈОНИ И ЊИХОВА УЛОГА У РАЗВОЈУ НАУКЕ И ТЕХНОЛОГИЈЕ

Леонид И. Гречихин
Белоруска државна академија за саобраћај и везе,
Минск, Република Белорусија

ОБЛАСТ: нанотехнологије
ВРСТА ЧЛАНКА: оригинални научни чланак
ЈЕЗИК ЧЛАНКА: енглески

Сажетак:

Негативни јони се формирају у процесу интеракције између електрона с интегрисаним електричним диполним моментом и

индукованим електричним диполним моментом услед поларизације. У континуалном режиму, при орбиталној брзини, емисија негативних јона с површине топлотно-заштитног слоја доводи до формирања двоструког електричног слоја с веома густом плазмом, док при брзини ослобађања иста емисија негативних јона доводи до експлозивног сагоревања топлотно-заштитног слоја. У режиму слободног тока молекула емисија негативних јона резултира интензивним љубичастоплавим сјајем, док се на површини летелице ствара висок позитивни потенцијал. У нанотехнологијама јонизација негативних јона одређује параметре отпуштања вакуумског лука. Негативни јони учествују у формирању неке врсте електростатичке машине у људском телу.

Кључне речи: негативни јони, електрични диполни моменат, двоструки електрични слој, поларизација, електростатичка машина.

Paper received on / Дата получения работы / Датум пријема чланка: 24.04.2018.
Manuscript corrections submitted on / Дата получения исправленной версии работы / Датум достављања исправки рукописа: 02.07.2018.
Paper accepted for publishing on / Дата окончательного согласования работы / Датум коначног прихватања чланка за објављивање: 04.07.2018.

© 2018 The Author. Published by Vojnotehnički glasnik / Military Technical Courier (www.vtg.mod.gov.rs, втг.мо.упр.срб). This article is an open access article distributed under the terms and conditions of the Creative Commons Attribution license (<http://creativecommons.org/licenses/by/3.0/rs/>).

© 2018 Автор. Опубликовано в «Военно-технический вестник / Vojnotehnički glasnik / Military Technical Courier» (www.vtg.mod.gov.rs, втг.мо.упр.срб). Данная статья в открытом доступе и распространяется в соответствии с лицензией «Creative Commons» (<http://creativecommons.org/licenses/by/3.0/rs/>).

© 2018 Аутор. Објавио Војнотехнички гласник / Vojnotehnički glasnik / Military Technical Courier (www.vtg.mod.gov.rs, втг.мо.упр.срб). Ово је чланак отвореног приступа и дистрибуира се у складу са Creative Commons licencom (<http://creativecommons.org/licenses/by/3.0/rs/>).



СТРУЧНИ ЧЛАНЦИ
ПРОФЕСИОНАЛНЫЕ СТАТЬИ
PROFESSIONAL PAPERS

ANALYSIS OF RESIDUAL STRESSES IN BIOINERT INORGANIC PLASMA SPRAYED CERAMIC COATINGS

Mihailo R. Mrdak

Research and Development Center IMTEL Communications a.d.,
Belgrade, Republic of Serbia,
e-mail: miki@insimtel.com,
ORCID iD: <http://orcid.org/0000-0003-3983-1605>

DOI: 10.5937/vojtehg66-15591; <https://doi.org/10.5937/vojtehg66-15591>

FIELD: Chemical Technology
ARTICLE TYPE: Professional Paper
ARTICLE LANGUAGE: English

Summary:

One of the factors for a successful application of ceramic coatings on biomedical implants is the compatibility of the physical and mechanical properties of coatings with the metal substrates of implants. Temperature and temperature gradient in the coating during powder deposition play an important role in the final quality of the coating. The coefficients of thermal expansion and thermal conductivity of the coating and the substrate are different, which affects the growth of residual stresses in coatings. To reduce the difference between the physical characteristics of the coating and the substrate to a minimum, the coating surface temperature and the substrate surface temperature must be kept under control during the deposition of powder. It is therefore of particular importance to control residual stresses in ceramic coatings in order to secure service life of coatings and implants. The paper describes a model of plasma heat transfer and predicts the distribution of residual stresses in the deposited coatings; it also describes the radiography techniques for measuring residual stresses in ceramic coatings. The aim of this paper is to describe the effect of powder deposition rates as well as the effect of the changes in the thickness and the thermal conductivity of the ZrO_2CaO coating on the level and the sign of residual stresses.

ACKNOWLEDGEMENT: The author is thankful for the financial support from the Ministry of Education and Science of the Republic of Serbia (national project OI 174004, TR 34016).

The paper also presents the influence of the bonding coating, and the changes in the thickness of bonding and the ceramic ZrO₂MgO coating as well as the heat treatment on the level and the sign of residual stresses. It was found that the increase of the total thickness of the coating increases the proportion of residual stresses on the surface and the edges of the coating.

Keywords: substrates, stress, coatings, ceramics.

Introduction

Distribution of residual stresses in biomedical ceramic coatings based on hydroxyapatite (HA), TiO₂, Al₂O₃, ZrO₂Y₂O₃, CaO and MgO is of decisive influence on coating adhesion, cohesive strength and toughness which define coating quality and service life. The share and the distribution of residual stresses in coatings is directly related to the ratio of coefficients of thermal expansion of substrates and coatings. To minimize the influence of thermal expansion coefficients of the residual stress in the coating layer, it is necessary to reduce the temperature difference ΔT between the substrate and the layers during powder deposition. During the plasma spray process, there is a large temperature gradient between molten powder and base metal substrates. Heat shrinkage during coating curing is hindered by the base metal, so that residual stresses are formed inside the coating. Because of the low thermal conductivity of ceramics, powder particles which melt in the plasma before they hit the substrate surface cool rapidly from 10⁵°C/s to 10⁶ °C/s. During the deposition, primary cooling of layers and secondary cooling of the coating are performed to the substrate temperature to minimize the influence of thermal expansion of the coating substrate. Residual stresses in coatings can be kept under control by constant cooling of the substrate from the back side and by an additional air-cooled front on which coating layers are deposited (Limarga et al, 2011). For the substrates of implants based on Ti6Al4V superalloy, the coefficient of thermal expansion is $\alpha = 8.7-9.1 \times 10^{-6}/^{\circ}\text{C}$. For coatings used in biomedicine, the coefficients of thermal expansion are approximate values, and their values are: hydroxyapatite (HA) ($\alpha = 10.6 \times 10^{-6}/^{\circ}\text{C}$), TiO₂ ($\alpha = 8.5 \times 10^{-6}/^{\circ}\text{C}$), Al₂O₃ ($\alpha = 8.8 \times 10^{-6}/^{\circ}\text{C}$), ZrO₂ ($\alpha = 9,0 \times 10^{-6}/^{\circ}\text{C}$), ZrO₂Y₂O₃ ($\alpha = 10.0 \times 10^{-6}/^{\circ}\text{C}$), ZrO₂MgO ($\alpha = 11.0 \times 10^{-6}/^{\circ}\text{C}$), ZrO₂CaO ($\alpha = 10.5 \times 10^{-6}/^{\circ}\text{C}$) (Miyazaki et al, 2008, pp.1463-1466), (Mrdak, 2017, pp.924-936). Besides the physical properties of the substrate material and the powder to be deposited, powder deposition parameters significantly influence the stress states in coatings. The study of stresses in layers by nondestructive testing and the examination of the

coating morphology using tensile testing can show the optimum parameters of powder deposition. The residual stresses in coatings are distributed in the middle of the sample (negative compression stresses), and on the edges of the sample (positive tensile stresses). The examination of residual stresses includes their distribution and their values, as well as the way how their control can affect the life of coatings (Hobbs & Reiter, 1988, pp.33-42). Residual stresses in plasma sprayed coatings are commonly measured by the X-ray diffraction method and by the tensile testing method. High resolution of X-rays through intense long wavelengths offers a significant potential for the measurement of residual stresses in coatings. Other methods used are neutron diffraction (Kesler et al, 1998, pp.215-224), (Matejicek et al, 1999, pp.607-617), the method of measuring the curvature, the method of removing material layer by layer and by tensile testing (Teixeira et al, 1999, pp.209–216), (Greving et al, 1994, pp.379-388), (Clyne & Gill, 1996, pp.401-418), (Zhu et al, 2014, pp.127-136). These methods make it possible to establish the average stresses in coatings. However, the distribution of residual stresses through the coating thickness is rarely published (Otsubo et al, 2005, pp. 2473-2477).

The aim is to explain the residual stresses in the ceramic coatings on the basis of ZrO_2CaO and ZrO_2MgO used in biomedical applications to improve the mechanical properties of hydroxyapatite (HA). This paper presents a model of heat transfer from plasma to the coating, powder deposition rate impact, changes in the thickness and thermal conductivity of ZrO_2CaO coatings on the level and sign of residual stresses. It also shows the effect of bond coating, changes in the thickness of the bond and the ceramic ZrO_2MgO coating and heat treatment on the level and sign of residual stresses. Generally, with increasing the total thickness of the coating, the proportion of residual stresses on the coating surface and its edges also increases.

Model of plasma heat transfer and the prediction of the distribution of residual stresses in ceramic coatings

To connect residual stresses in coatings with the deposition parameters, a model of heat transfer, shown in Figure 1, was developed. Research conducted for ZrO_25CaO ceramics may be applied to another type of coating (Rickerby et al, 1988, pp.267-276). As mentioned before, the powder deposition process by plasma consists of the injection of powder particles into high-temperature plasma made of inert gases (Ar/He) with an electric arc in the nozzle cooled with water. Powder

particles injected into the plasma jet melt and then hit the surface of the substrate where they are cooled at a speed of $10^{5^{\circ}}\text{C/s}$ to $10^{6^{\circ}}\text{C/s}$. Molten powder particles arrive onto a stable surface where they collide, deposit and bind to the surface to be cooled. These sites are graded and increased while powder particles deposit on the surface. The thickness of the coating increases with speed (η). During the deposition, there was a simulation of a model of transferring heat from the coating to the substrate surface and the heat transfer by radiation from plasma to the deposition surface and by radiation of the deposition surface into the environment. When defining the heat transfer model, the basic assumption was that the plasma spray process is continuous, the thickness of the substrate is greater than the thickness of the coating, the heat loss is presented with a standard convection and radiation, and thermal and electrical properties are temperature-invariant.

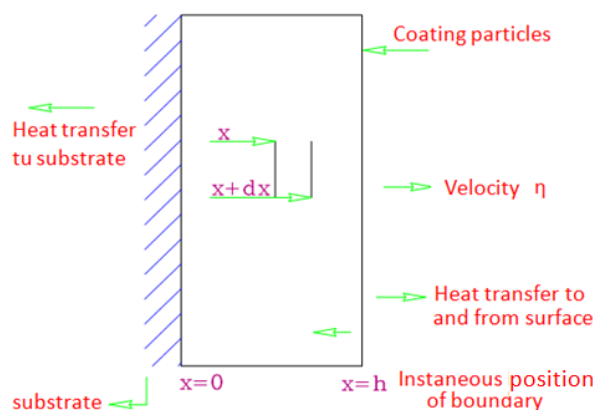


Figure 1 – The basic elements of the model of heat transfer in the process of deposition
 Рис. 1 – Основные элементы теплообмена в процессе нанесения покрытия
 Слика 1 – Основни елементи модела преноса топлоте у процесу депозиције

In order to achieve the above mentioned cooling rate ($10^{5^{\circ}}\text{C/s}$ - $10^{6^{\circ}}\text{C/s}$), methods of rapid heat removal were used together with a controlled stream of dry air (primary cooling). The main parameters used in the modeling of residual stresses in the plasma deposited coatings are shown in Table 1.

Figure 2 shows the diagram providing the variants of distribution of residual stresses in the plasma deposited $\text{ZrO}_2\text{5CaO}$ coatings as a function of the powder deposition rate (Rickerby et al, 1988, pp.267-276).

Table 1 – Parameters of the modeling of residual stresses in plasma coatings
Таблица 1 – Параметры моделирования остаточных напряжений в покрытиях плазменного напыления

Табела 1 – Параметри моделирања заосталих напона у плазма превлакама

Process parameters	Parameters of the coatings / surfaces
Deposition speed	Thermal conductivity of the coatings, specific heat and latent heat
Flame temperature	
Surface temperature	Coating density and Poisson number
Final coating thickness	Capacitance and the coefficient of the thermal expansion of the substrate
Ratio of the coating surface and the substrate surface	
Type and morphology of the substrate	

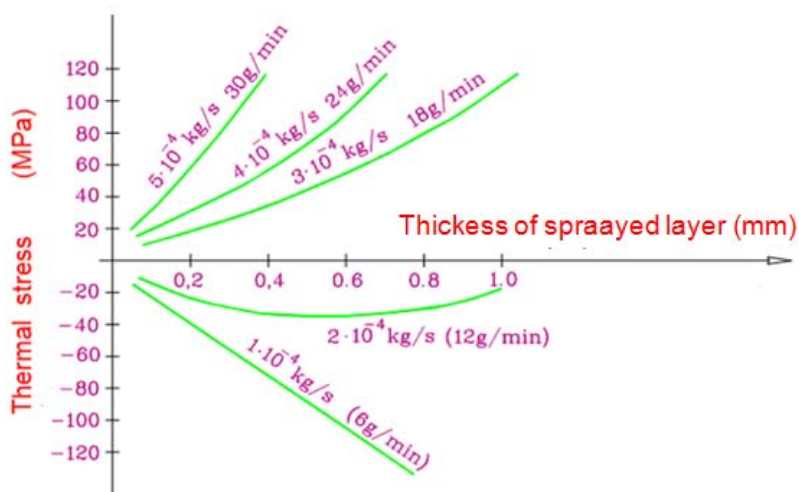


Figure 2 – Residual stresses in the $ZrO_2.5CaO$ coating as a function of deposition speed

Рис. 2 – Остаточные напряжения в покрытии $ZrO_2.5CaO$ в зависимости от скорости осаждения

Слика 2 – Заостали напони у превлаци $ZrO_2.5CaO$ у функцији брзине депозиције

The diagram shows that the increase of the deposition speed of powder in $ZrO_2.5CaO$ coating layers produce a change of state of calculated stresses. For low powder deposition speed of 6 g/min and 12 g/min, negative compression stresses are present in the layers. With the increase of the powder deposition speed to 18 g/min, stresses change

the sign from negative to positive tensile stresses (Rickerby et al, 1988, pp.267-276). Also of great importance is the effect of coating thickness on residual stresses. It is noted that a coating does not meet the requirements at a critical thickness which can be defined as the moment when the coating itself begins to separate from the substrate.

Figure 3 shows the change in the sign of residual internal stresses with the change of the total thickness of the ceramic $ZrO_2.5CaO$ coating. For coating thicknesses from 0.5 mm to 1.0 mm, residual internal stresses in the layers are negative compression stresses. By increasing the coating thickness, it is possible to create different zones of internal tensions, so that negative compression stresses remain in a part of the deposited layer on the boundary with the substrate, while in the zone close to the coating surface, positive tensile stresses can occur (Rickerby et al, 1988, pp.267-276).

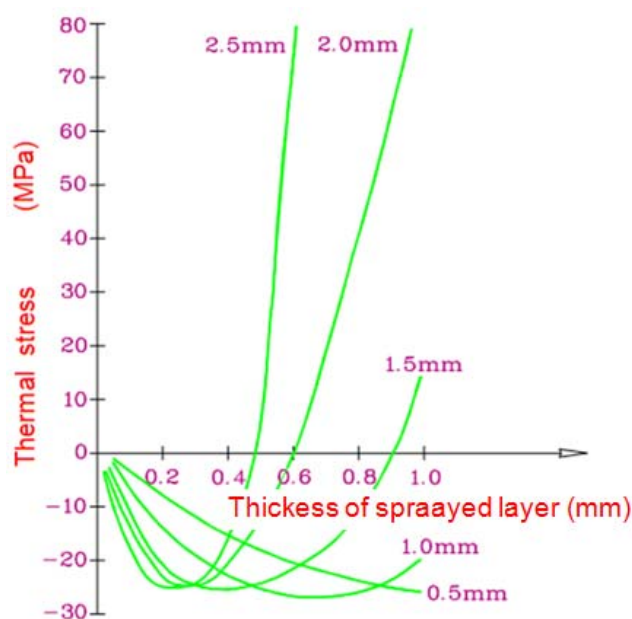


Figure 3 – The change of stresses with changing the thickness of $ZrO_2.5CaO$
 Рис. 3 – Изменение напряжения при изменении толщины слоя покрытия $ZrO_2.5CaO$

Слика 3 – Промена напона са променом дебљине слоја $ZrO_2.5CaO$

One of the important factors that influence the level of residual stresses is the thermal conductivity of the coating. Figure 4 shows how small changes in the thermal conductivity of $ZrO_2.5CaO$ coatings can

have a significant effect on the level of residual stresses. Deviation values of thermal conductivity from 1 W/mK to 0.75 W/mK can be achieved by changing the degree of porosity in the ceramic coating which affects the value and sign of residual stresses. The increase of the thermal conductivity of the coatings from 1 W/mK to 2 W/mK leads to an increase in the value of negative compression stresses. Such increase can be beneficial to the life of the coating as a counter-balance to positive tensile stresses occurring in exploitation. However, a large increase in negative compression stresses can cause cracks in the coating during the coating deposition phase. Bearing in mind different conditions regarding the temperature of the outer surface and the ceramic coating heating rate, deposition conditions must be carefully chosen since they affect internal residual stress in order to obtain an optimal state of stress in the ceramic layer upon which the coating service life depends. Therefore, recommendations for thermal conductivity as low as only 0.5 W/mK can be found in the literature (Rickerby et al, 1988, pp.267-276).

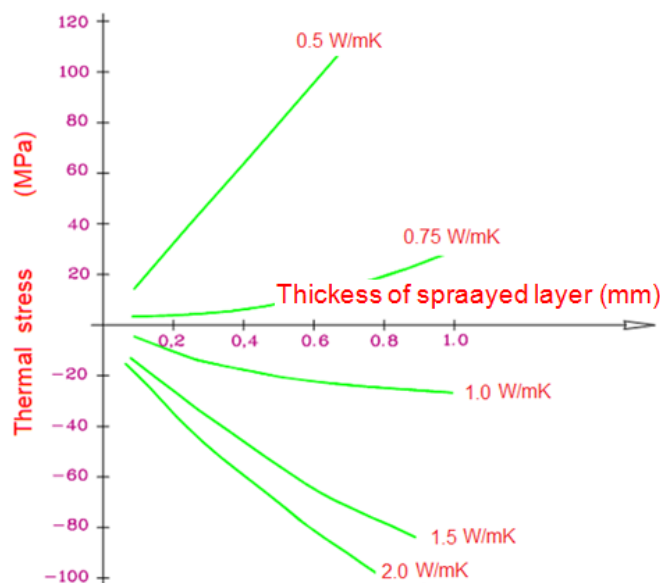


Figure 4 – Influence of thermal conductivity of residual stresses in the $ZrO_{2.5}CaO$ coating

Рис. 4 – Влияние теплопроводности на остаточные напряжения в покрытии $ZrO_{2.5}CaO$

Слика 4 – Утицај топлотне проводљивости на заостале напоне у превлаци $ZrO_{2.5}CaO$

The effect of bond coating and changes in coating thicknesses on the level of residual stresses

The level of residual stresses in deposited coatings is significantly influenced by bond coatings, changes in the thickness of bond coatings with respect to the outer ceramic coating, as well as changes in the thickness of ceramic coatings. Overall, the increase in the total coating thickness increases the proportion of residual stresses on coating surfaces and coating edges. Residual stresses in coatings can be significantly reduced by heat treatment (Zhuang & Gu, 1988, pp.277-284). D-9C is one of the instruments with which residual stresses are successfully measured with a change angle of 0.01° in coatings by the X-ray diffraction method. The theory of measuring residual stress in the coating is such that, when passing through the coating, the X-ray is reflected from a particular crystallographic plane and reduces its intensity. The measuring parameters are: operating voltage KV; operating current; CuK_α radiation and filter material (Zhuang & Gu, 1988, pp.277-284). During measurements, the angle (Ψ) between the X-ray and a vertical line on the sample surface is changed. Stress measurements are carried out in two directions $\Psi = 0^\circ$ and $\Psi = 45^\circ$, so that a corresponding dual angle of ray reflection of 2θ can be obtained. Using the theory of elasticity and the Bragg formula, the values of the residual stress along the (Ψ) direction can be calculated using the formula (1):

$$\sigma_\psi = -\frac{E}{2(1+\nu)} \cdot \frac{\pi}{180} \cdot \text{ctg}\theta_0 \frac{\partial(2\theta)}{\partial(\sin^2 \psi)} \quad (1)$$

where is: E - modulus of the coating elasticity, ν - Poisson share for the coating, $2\theta_0$ - standard Bragg angle without stresses, 2θ - double reflected angle and Ψ - X-ray angle direction.

The effect of the bonding Ni20Cr coating of a thickness of 0.2 mm with a change in the thickness of the ceramic $\text{ZrO}_2/24\text{MgO}$ coating of: 0.1; 0.2; 0.3; 0.4 and 0.5 mm on the level of residual stresses is shown in Figure 5. The residual stresses were measured in the middle of the samples by the X-ray diffraction method. Increasing the thickness of the ceramic coating increases the value of positive tensile stresses. Residual stresses are partially absorbed on the samples with the bond coating, which is a reason why two-layer coating systems have a much lower

share of residual tensile stresses compared to deposited coatings of pure $ZrO_2+24MgO$ ceramics (Zhuang & Gu, 1988, pp.277-284).

Figure 6 shows the influence of the thickness of the ceramic $ZrO_2+24MgO$ coating of 0.3; 0.4; 0.5; and 0.6 mm without the bond coating on the level of residual stresses in the middle and on the edge of the samples $\varnothing 55 \times 5$ mm. An increase in the thickness of ceramic coatings increases the values of negative compressive stresses in the middle and on the edge of the samples, which reach a maximum value for the thickest coating of 0.6 mm (Zhuang & Gu, 1988, pp.277-284). Figure 7 shows the influence of the change in the thickness of the bond layer of 0.1; 0.2; 0.3; 0.4 and 0.5 mm on the residual stresses in the two-layer system with a ceramic $ZrO_2+24MgO$ coating with a thickness of 0.2 mm.

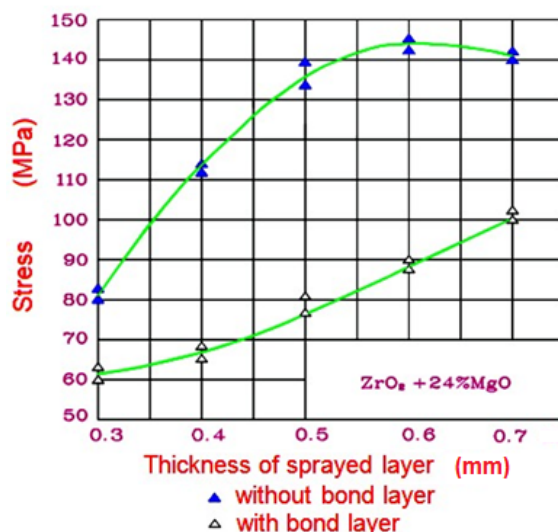


Figure 5 – Effect of the bond coating with a change in the thickness of the ceramic coating on residual stresses

Рис. 5 – Влияние связующего покрытия с измененной толщиной керамического покрытия на остаточные напряжения

Слика 5 – Утицај везне превлаке са променом дебљине керамичке превлаке на заостале напоне

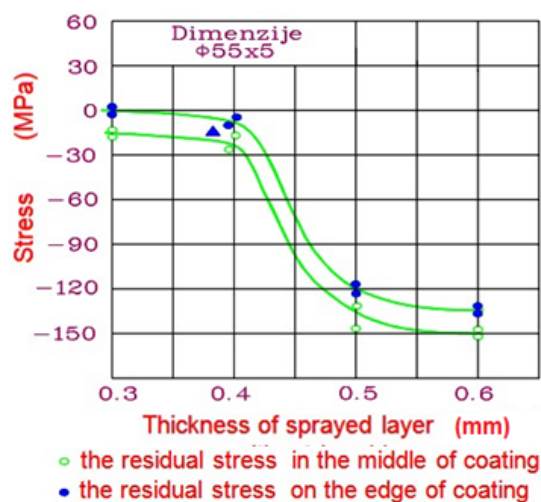


Figure 6 – Effect of the change in the thickness of the ceramic coating without the bond coating on residual stresses

Рис. 6 – Влияние изменения толщины керамического покрытия без связующего покрытия на остаточные напряжения

Слика 6 – Утицај промене дебљине керамичке превлаке без везне превлаке на заостале напоне

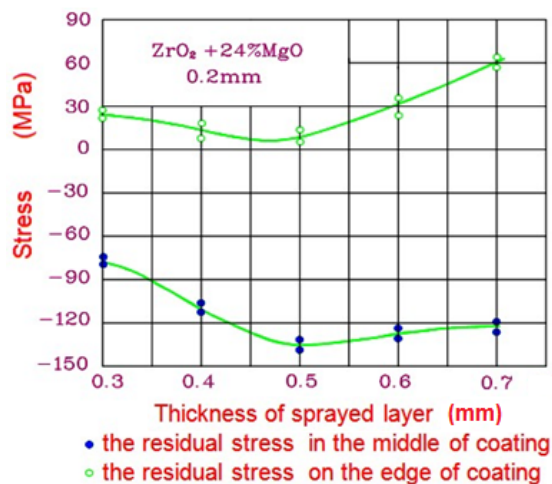


Figure 7 – The influence of the change in the bond layer thickness in the system with a ceramic coating on residual stresses

Рис. 7 – Влияние изменений толщины связующего покрытия в системе с керамическим покрытием на остаточные напряжения

Слика 7 – Утицај промене дебљине везног слоја у систему са керамичком превлаком на заостале напоне

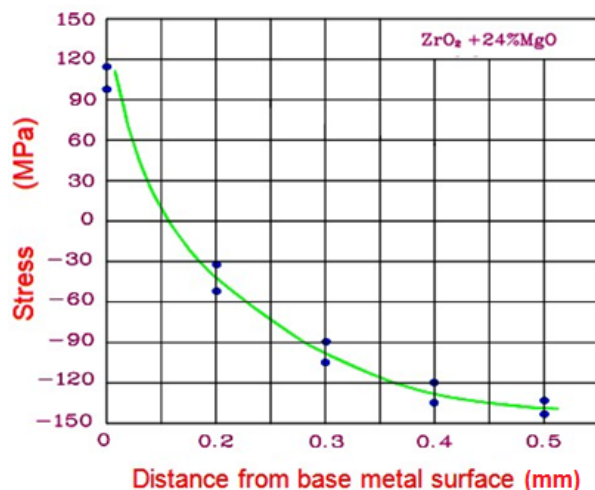


Figure – 8 Distribution of residual stresses along the depth of the ceramic coating without a bond layer

Рис. 8 – Распределение остаточных напряжений по глубине керамических покрытий без связующего слоя

Слика 8 – Распoдела заосталих напона по дубини керамичке превлаке без везног слоја

Residual stresses on the edge of the samples were positive tensile stresses, while negative compression stresses were present in the middle of the samples. The distribution of residual stresses in the direction of the growth of coating thickness or coating depth is of great importance (Rickerby et al, 1988, pp.267-276). To determine the distribution and the sign of residual stresses in the coating depth, a layer after a layer was removed by 0.1mm grinding after each measurement. Figure 8 shows the stress distribution in the depth of the ceramic $ZrO_2+24MgO$ coating of a thickness of 0.5 mm and without the bond layer, deposited on the 5 mm thick substrate. The highest values of residual stresses are found on the coating surface. Stresses on the surface and on the coating boundaries are negative compression stresses whose values decrease with the decrease of the coating thickness. When the coating thickness is reduced to 0.1 mm, the stress sign is changed, i.e. negative compression stresses change into positive tensile stresses. The highest value of positive tensile stresses is found in the coating on the interface with the substrate (Zhuang & Gu, 1988, pp.277-284). Significant reduction of residual stresses in coatings can be achieved by heat treatment. Figure 9 shows the effect of the heat treatment of the two-

layered Ni20Cr coating of a thickness of 0.2 mm and the ceramic ZrO₂24MgO coating of a thickness of 0.4 mm on residual stresses.

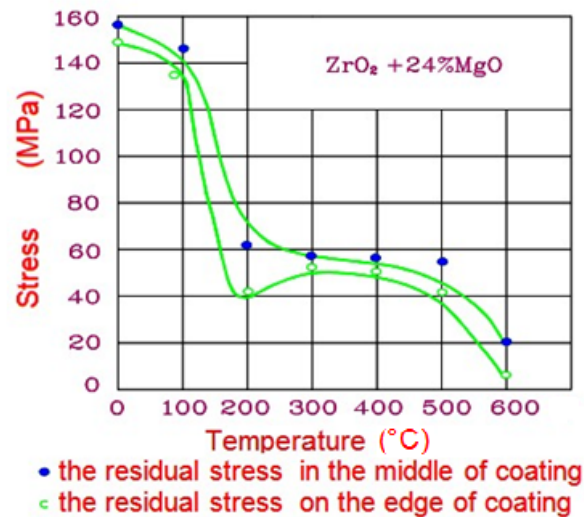


Figure 9 – Effect of coating heat treatment on residual stresses
 Рис. 9 – Влияние термической обработки покрытия на остаточные напряжения
 Слика 9 – Утицај термичке обраде превака на заостале напоне

The thermal treatment of coatings at 100°C; 200°C; 300°C; 400°C; 500°C and 600°C for a period of 2h, followed by coating cooling in the furnace to room temperature, brought about a significant reduction in residual stresses. Residual stresses in the coating decrease with the increase in the heat treatment temperature. The curves of residual stresses in the middle and at the edge of the sample are identical, indicating a more uniform stress distribution in the middle and at the edge of the coating after heat treatment.

Conclusion

The paper presents the modeling and prediction of residual stresses in the plasma sprayed ceramic ZrO₂CaO coating as well as the analysis of the stress state in the ZrO₂MgO coating. The analysis found out that the residual stresses in the ZrO₂CaO coating are significantly affected by the deposition speed. For low powder deposition speed values, negative compression stresses are present in coating layers and they change the sign into positive tensile stresses with the increase of the deposition speed. The increase of the coating thickness over 1mm results in

residual stresses changing values and the sign from compression to tensile. The increase in the coating thermal conductivity leads to an increase in the value of negative compressive stresses, which can cause cracks in the coating during coating deposition. The bond coating in a combination with the ceramic ZrO_2MgO coating partially reduces residual stresses in a two-layered coating system, which is why the coating has a lower share of residual tensile stresses compared to deposited coatings from pure ceramics. The highest stresses are on the surface of the coating. For up to 5mm-thick substrates, stresses on the surface and the edge of the coating are negative compression stresses whose value decreases with the decrease of the coating thickness. With the reduction of the coating thickness to 0.1 mm, stress changes the sign and negative compression stresses change into positive tensile stresses. The highest value of positive tensile stresses is found in the coating on the interface with the substrate. Significant reduction of residual stresses in coatings is achieved by heat treatment. The increase in the heat treatment temperature leads to the reduction of the residual stresses in the coating and their distribution is more uniform in the middle and at the edge of the sample.

References

- Clyne, T.W. & Gill, S.C. 1996. Residual Stresses in Thermal Spray Coatings and Their Effect on Interfacial Adhesion. *Journal of Thermal Spray Technology*, 5, pp.401–418. Available at: <https://doi.org/10.1007/BF02645271>.
- Greving, D.J., Rybicki, E.F. & Shadley, J.R. 1994. Through-Thickness Residual Stress Evaluations for Several Industrial Thermal Spray Coatings Using a Modified Layer-Removal Method. *Journal of Thermal Spray Technology*, 3, pp.379–388. Available at: <https://doi.org/10.1007/BF02658983>.
- Hobbs, M.K. & Reiter, H. 1988. Residual Stresses in $ZrO_2-8\%Y_2O_3$ Plasma-Sprayed Thermal Barrier Coating. *Surface and Coatings Technology*, 34(1), pp.33–42. Available at: [https://doi.org/10.1016/0257-8972\(88\)90086-2](https://doi.org/10.1016/0257-8972(88)90086-2).
- Kesler, O., Matejcek, J., Sampath, S., Suresh, S., Gnaeupel-Herold, T., Brand, P.C. & Prask, H.J. 1998. Measurement of Residual Stress in Plasma-Sprayed Metallic, Ceramic and Composite Coatings. *Materials Science and Engineering A*, 257(2), pp.215–224. Available at: [https://doi.org/10.1016/S0921-5093\(98\)00860-0](https://doi.org/10.1016/S0921-5093(98)00860-0).
- Limarga, M.A., Vaßen, R. & Clarke, R.D. 2011. Stress Distributions in Plasma-Sprayed Thermal Barrier Coatings Under Thermal Cycling in a Temperature Gradient. *Journal of Applied Mechanics*, 78(1). Available at: <https://doi.org/10.1115/1.4002209>.

Matejcek, J., Sampath, S., Brand, P.C. & Prask, H.J. 1999. Quenching, Thermal and Residual Stress in Plasma Sprayed Deposits: NiCrAlY and YSZ Coatings. *Acta Materialia*, 47(2), pp.607–617. Available at: [https://doi.org/10.1016/S1359-6454\(98\)00360-7](https://doi.org/10.1016/S1359-6454(98)00360-7).

Miyazaki, H., Ushiroda, I., Itomura, D. & Ota, T. 2008. Thermal expansion of hydroxyapatite between -100 °C and +50 °C. *Materials Science and Engineering C*, 29(4), pp.1463-1466. Available at: <https://doi.org/10.1016/j.msec.2008.12.001>.

Mrdak, M.R. 2017. Testing mechanical structural characteristics of Al₂O₃ oxide ceramics resistant to sliding friction, *Vojnotehnički glasnik / Military Technical Courier*, 65(4), pp.924-936. Available at: <https://doi.org/10.5937/vojtehg65-12000>.

Otsubo, F., Kishitake, K. & Terasaki, T. 2005. Residual Stress Distribution in Thermally Sprayed Self-Fluxing Alloy Coatings. *Materials Transactions*, 46(11), pp.2473-2477. Available at: <https://doi.org/10.2320/matertrans.46.2473>.

Rickerby, D.S., Scott, K.T., Eckold, G. & Lloyd-Thomas, D. 1988. Analysis of the Residual Stresses in Plasma Sprayed Coatings. In *1st Plasma-Technik-Symposium*, Swicerland, Lucerne, pp.267-276. May 18-20.

Teixeira, V., Andritschky, M., Fischer, W., Buchkremer, H.P. & Stöver, D. 1999. Analysis of Residual Stresses in Thermal Barrier Coatings. *Journal of Materials Processing Technology*, 92–93, pp.209–216. Available at: [https://doi.org/10.1016/S0924-0136\(99\)00157-0](https://doi.org/10.1016/S0924-0136(99)00157-0).

Zhu, J.G., Xie, H.M., Li, Y.J., Hu, Z.X., Luo, Q. & Gu, C.Z. 2014. Interfacial Residual Stress Analysis of Thermal Spray Coatings by Miniature Ring-Core Cutting Combined with DIC Method. *Experimental Mechanics*, 54(2), pp.127–136. Available at: <https://doi.org/10.1007/s11340-012-9640-2>.

Zhuang, H. & Gu, G. 1988. A Study on Residual Stress of ZrO₂+MgO Plasma Sprayed Coating. In *1st Plasma-Technik-Symposium*, Swicerland, Lucerne, pp.277-284. May 18-20.

АНАЛИЗ ОСТАТОЧНЫХ НАПРЯЖЕНИЙ В БИОИНЕРТНЫХ НЕОРГАНИЧЕСКИХ КЕРАМИЧЕСКИХ ПОКРЫТИЯХ, НАНЕСЕННЫХ ПЛАЗМЕННЫМ НАПЫЛЕНИЕМ

Михаило Р. Мрдак

Центр исследований и развития А.О. «ИМТЕЛ коммуникации», г. Белград, Республика Сербия

ОБЛАСТЬ: химические технологии

ВИД СТАТЬИ: профессиональная статья

ЯЗЫК СТАТЬИ: английский

Резюме:

Один из факторов успешного применения биомедицинской керамики в области покрытия имплантов заключается в соответствии физических и механических характеристик покрытия с металлической основой импланта. Весьма важную роль при нанесении порошка играют температура и

температурный градиент покрытий, так как от них в большей мере зависит конечное качество покрытия. Коэффициенты термического расширения и теплопроводности покрытия и основания различаются, а это влияет на увеличение остаточных напряжений в покрытиях. Для минимизирования разницы физических и механических характеристик покрытия и основания, необходимо вести постоянный контроль за температурами покрытия и основания в течение всего процесса нанесения порошка и его осаждения. В целях продления срока службы как покрытия, так и самого импланта необходимо обеспечить соответствующий контроль за остаточными напряжениями в керамических покрытиях. В данной статье представлена модель теплообмена плазмы, с предусмотренным распределением остаточных напряжений в нанесенных покрытиях, а также техника рентгенографии для измерения остаточных напряжений в керамических покрытиях. Целью данной статьи было описание эффекта скорости осаждения порошка, изменения толщины и теплопроводности ZrO_2CaO покрытий к уровню и значениям остаточных напряжений. В статье также представлено каким образом связующие покрытия, изменения толщины связующих и керамических покрытий ZrO_2MgO и термическая обработка влияют на уровень и значения остаточных напряжений. Выявлено, что при увеличении общей толщины покрытия пропорционально увеличивается доля остаточного напряжения на поверхности и краях покрытия.

Ключевые слова: основания, напряжения, покрытия, керамика.

АНАЛИЗА ЗАОСТАЛИХ НАПОНА У БИОИНЕРТНИМ НЕОРГАНСКИМ КЕРАМИЧКИМ ПЛАЗМА СПРЕЈ ПРЕВЛАКАМА

Михаило Р. Мрдак

Истраживачки и развојни центар ИМТЕЛ комуникације а.д., Београд,
Република Србија

ОБЛАСТ: хемијске технологије

ВРСТА ЧЛАНКА: стручни чланак

ЈЕЗИК ЧЛАНКА: енглески

Сажетак:

Један од фактора за успешну примену биомедицинских керамичких превлака на имплантима јесте усклађеност физичких и механичких карактеристика превлака са металним подлогама имплантата. Температуре и температурни градијент у превлакама током депозиције праха имају важну улогу на коначни квалитет превлака. Коефицијенти топлотног ширења и топлотне проводљивости превлаке и подлоге се разликују, што утиче на повећање заосталих напона у превлакама. Да би се разлика физичких карактеристика превлаке и подлоге свела на минимум,

температуре површине превлаке и подлоге морају се држати под контролом током депозиције праха. Због тога је од посебног значаја контрола заосталих напона у керамичким превлакама уколико се жели постићи корисни век превлаке и импланта. У раду је описан модел преноса топлоте плазме са предвиђањем расподеле заосталих напона у депонованим превлакама и техника рендгенографије за мерење заосталих напона у керамичким превлакама. Циљ рада јесте да се опише ефекат брзине депозиције праха, промене дебљине и топлотне проводљивости ZrO_2CaO превлаке на ниво и предзнак заосталих напона. Приказан је и утицај везне превлаке, промена дебљине везне и керамичке превлаке ZrO_2MgO и термичке обраде на ниво и предзнак заосталих напона. Установљено је да се са повећањем укупне дебљине превлака повећава удео заосталих напона на површини и ивицама превлака.

Кључне речи: подлоге, напони, превлаке, керамике.

Paper received on / Дата получения работы / Датум пријема чланка: 06.11.2017.

Manuscript corrections submitted on / Дата получения исправленной версии работы /

Датум достављања исправки рукописа: 21.04.2018.

Paper accepted for publishing on / Дата окончательного согласования работы / Датум коначног прихватања чланка за објављивање: 23.04.2018.

© 2018 The Author. Published by Vojnotehnički glasnik / Military Technical Courier (www.vtg.mod.gov.rs, втг.мо.упр.срб). This article is an open access article distributed under the terms and conditions of the Creative Commons Attribution license (<http://creativecommons.org/licenses/by/3.0/rs/>).

© 2018 Автор. Опубликовано в «Военно-технический вестник / Vojnotehnički glasnik / Military Technical Courier» (www.vtg.mod.gov.rs, втг.мо.упр.срб). Данная статья в открытом доступе и распространяется в соответствии с лицензией «Creative Commons» (<http://creativecommons.org/licenses/by/3.0/rs/>).

© 2018 Аутор. Објавио Војнотехнички гласник / Vojnotehnički glasnik / Military Technical Courier (www.vtg.mod.gov.rs, втг.мо.упр.срб). Ово је чланак отвореног приступа и дистрибуира се у складу са Creative Commons licencom (<http://creativecommons.org/licenses/by/3.0/rs/>).



FIWARE: A WEB OF THINGS DEVELOPMENT PLATFORM

Ivan A. Tot^a, Dušan Lj. Bogićević^b, Mladen B. Trikoš^c,
Komlen G. Lalović^d

^a University of Defence in Belgrade, Military Academy, Department for information systems and telecommunication engineering, Belgrade, Republic of Serbia,
e-mail: ivan.tot@va.mod.gov.rs,
ORCID iD: <http://orcid.org/0000-0002-5862-9042>

^b Serbian Armed Forces, General Staff, Department for Telecommunication and Informatics (J-6), Command Information Systems and IT Support Centre, Belgrade + University of Niš, Faculty of Electronic Engineering, Niš, Republic of Serbia,
e-mail: dusan.bogicevic@gmail.com,
ORCID iD: <http://orcid.org/0000-0002-4300-2490>

^c University of Defence in Belgrade, Military Academy, Department for information systems and telecommunication engineering, Belgrade, Republic of Serbia,
e-mail: mladen.trikos@va.mod.gov.rs,
ORCID iD: <http://orcid.org/0000-0002-5243-1326>

^d Faculty of Management, Economy and Finance, Belgrade, Republic of Serbia,
e-mail: komlen@mef.edu.rs,
ORCID iD: <http://orcid.org/0000-0002-4590-2185>

DOI: 10.5937/vojtehg66-17063; <https://doi.org/10.5937/vojtehg66-17063>

FIELD: Computer Sciences, IT
ARTICLE TYPE: Professional Paper
ARTICLE LANGUAGE: English

Abstract:

As an extension to the concept of the Internet of Things (IoT), Web of Things (WoT) represents a step towards connecting smart things to the existing web environment while considering issues such as heterogeneity, scalability, and usability. This paper is dedicated to current opportunities as well as challenges for development in the concept of WoT. The theoretical foundations of the Internet of Things concept, such as architecture, protocols, services, and things themselves, which form the basis of both concepts, are described in the paper. The paper deals with the necessary preconditions for developing the concept of Web of Things. The main contribution of the paper is a proposal of architecture based on the FIWARE platform as the basis for the development of Web of Things. The demonstration of the proposed architecture is described by a real case scenario.

Key words: *Internet of Things (IoT), Web of Things (WoT), FIWARE.*

ACKNOWLEDGMENT: The authors thank the Ministry of Defence of the Republic of Serbia through projects VA-TT/3/18-20 and VA-TT/1/17-19.

Introduction

Although the term Internet of Things (IoT) was quite accidentally conceived in 1999 as an idea that, at the time, the new technology Radio-Frequency IDentification (RFID) was presented as something new and needed, Kevin Ashton called his lecture Internet of Things, when even the Internet was also considered as new technology. The name he gave is considered to be the beginning of a new era in the Internet world. That era is characterized by communication between devices, that is machine to machine (M2M) communication (Internet of Things History).

With the development of computer networks, we have come to the era where the social network of devices is created. With the IoT concept, Things are able to use the Internet as a communication medium with services for exchanging data. When a large number of Things are connected, which will be able to be part of the World Wide Web (WWW), we come to the term Web of Things (WoT), which is the next step in the development of IoT, that is the successor to the IoT concept.

The development of IoT did not stop with M2M communication. It is still developing in different directions such as smart cities, agro-culture, animals, etc. Some of the research papers go a step further, where the big data and the web of things are connected, thus achieving the integration of humans, Things, and computers (Zhong et al, 2016).

IoT architecture

The IoT architecture is not based on one device. It is about sets of devices that collect information in different ways. When talking about IoT, the most considered topic are environments. The prefix “smart” is often found like e.g. smart homes, smart streets, smart parking lots, smart garbage cans, smart cities, etc. Smart environments can be defined as sets (federations) of sensors and actuators designed for house, building, city, transport etc. (Gubbi et al, 2013). Mark Weiser, who is considered as the founder of ubiquitous computing, has defined smart environments as a world of physical objects that are connected with sensors, actuators, displays, other environments over a network that allows interlaced connectivity (Perera et al, 2013).

From the highest level, IoT consists of three parts as shown in Figure 1 (Gubbi et al, 2013):

Part of devices: Devices or actuators with their communication components integrated with them.

Middleware part: The most complex part that implements data processing logic, stores data and provides access to data to users in

such a way that they do not care about the architecture of individual devices (actuators). This layer is made up of several parts (Object Abstraction, Service Management, Service Composition) (Botta et al, 2015).

Presentation part: This part adjusts to a specific application and performs data display, data management, etc.

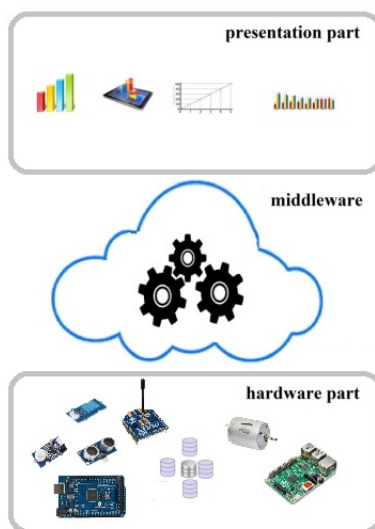


Figure 1 – IoT architecture

Рис. 1 – Архитектура интернета вещей
Слика 1 – Архитектура интернета ствари

The purpose of the device layer is to process collected mostly analogue data and to send it in the digital form over the network layer to the server layer.

The number of connected devices exceeds the number of human population. In 2010, the number of devices was almost twice the number of human population.

The architecture of the device (Things) layer should consist of three parts as shown in Figure 2 (Wortmann & Flüchter, 2015):

Middleware component, parts of software that will allow device management,

IoT component, which will collect data such as sensors (actuators), and the components through which communication with the server will occur (communication modules such as Ethernet, Wi-Fi, Bluetooth, ZigBee etc.),

Hardware part, on which the software will be executed and to which the sensors (actuators) will be connected.

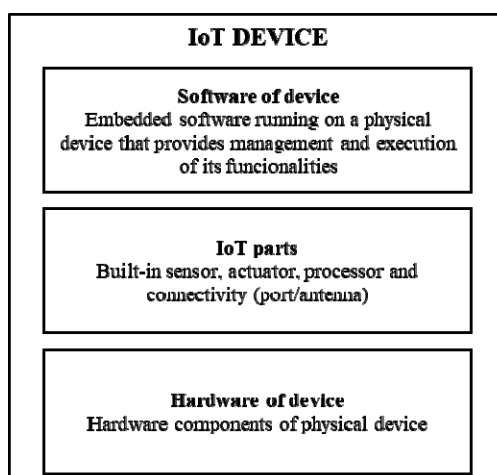


Figure 2 – Architecture of IoT device

Рис. 2 – Архитектура устройства интернета вещей

Слика 2 – Архитектура уређаја интернета ствари

As the IoT concept evolved, the protocols that were used for M2M communication were designed and improved. In addition to the Hypertext Transfer Protocol (HTTP) protocol that found application in the IoT concept, other protocols have been also designed, such as:

Extensible Messaging and Presence Protocol (XMPP):

The first version of the XMPP protocol appeared in 2000. This protocol uses a Transmission Control Protocol(TCP) protocol on the transport layer, and supports two message exchange models, both a request/response (synchronous) model and an advertiser/subscriber (asynchronous) model. The protocol is designed for short messages that are used in fast real-time applications that require small delay, or in presence-based applications. The disadvantage of this protocol is a relatively large overhead (Saint-Andre et al, 2009).

Advanced Message Queuing Protocol (AMQP Advanced Message Queuing Protocol Specification, Cisco Systems, 2018):

AMQP is an application protocol developed in 2003 by John O'Hara, for the needs of banks, and it was officially adopted in 2012 by OASIS (Organization for the Advancement of Structured Information Standards).

AMQP uses the TCP protocol on the transport layer, and has an overhead of 8 bytes. It is based on message exchange on the principle of

an advertiser/subscriber. This protocol achieves great reliability and ensures that the message is delivered even when the network breaks down. There are three mechanisms that can be used to send messages: at most once, at least once and exactly once (AMQP Advanced Message Queuing Protocol Specification, Cisco Systems, 2018).

Message Queuing Telemetry Transport (MQTT)

MQTT is an application protocol designed in 1999 by IBM and standardized in 2013, which has a relatively small overhead, thus providing a possible application on devices with limited resources (memory, processor etc.) such as IoT devices. This protocol, like the HTTP protocol, uses TCP on the transport layer, but has a smaller overhead of 2 or 4 bytes. The protocol uses the principle of advertisers and subscribers. Facebook Messenger application uses this protocol. In terms of security, this protocol uses Transport Layer Security(TLS). Brokers may require a username and a password (Stanford-Clark & Truong, 2013).

Constrained Application Protocol (CoAP)

The main goal of this protocol is to reduce the overhead to a minimum and provide a mechanism that would be used on a large number of devices that have limitations in terms of power, resources and network considerations (low-range networks such as IEEE 802.15.4, Bluetooth, Low Power Wi-Fi). The HTTP protocol was used as a model for development. It is important to note that CoAP is not a reduced HTTP, but it is a protocol optimized for M2M communication, which supports basic REpresentational State Transfer (REST) functionalities, common with the HTTP protocol. Also, CoAP in some things represents a step forward in comparison to HTTP. It supports multicast, asynchronous messaging and has a mechanism for finding resources (Sharma, 2014), (Shelby, 2014).

CoAP is an application protocol that uses two messaging models. It supports the request/response model, as well as the advertiser/subscriber model. Unlike HTTP, it relies on the User Datagram Protocol (UDP) protocol, but above UDP the DTPLS protocol can also be used to increase the security.

The most important part of the IoT architecture is the middleware part, because in that part there are services that mediate the communication with devices. In addition, the services provide the necessary data abstraction, storing and exchanging data with other services.

In order to provide the ability of communication between different platforms (hardware, computer), Web services use platform independent

data formats such as EXtensible Mark-up Language (XML) and JavaScript Object Notation (JSON).

Two basic types of services are:

SOAP (Simple Object Access Protocol) is a standard for exchanging structured information using HTTP and XML. It is platform independent, so it can be used on all computer platforms, as well as in all programming languages. The most common way to call the service method is through RPC (Remote Procedure Call) messages, where the client calls the server method and awaits its response. The SOAP protocol is based on WSDL (Web Services Description Language) and UDDI (Universal Description, Discovery, and Integration) technologies.

REST (REpresentational State Transfer) is an architectural style that was designed by Roy Thomas Fielding. Although not a protocol, it uses multiple protocols in its work, such as: HTTP, Uniform Resource Identifier(URI), JSON, and XML. The basis of this style is the HTTP protocol, which is used as a data transfer mechanism, with a limited number of commands such as: GET, POST, PUT, DELETE, etc. It is RESTfull in sense of performance, scalability, simplicity, modularity, visibility, portability and reliability.

Regarding the applicability in the IoT architecture, although both types provide similar services, in the specific constraints that are present in the IoT concept, primarily in device constraints, it is more convenient to use the RESTfull architecture (Zeng et al, 2011).

Web of Things

The foundation of Web (World Wide Web) is the Internet. The initial idea Tim Berners-Lee had for the development of the Web was to enable the interrelationships mechanism between documents in order to exploit and improve the Internet. The Web developed very rapidly and became much more than the exchange of documents. Now the Web is the largest platform that allows the development of Web applications in different domains. It has evolved from static pages, through applications, social networks to the latest stage, which is the social network of the devices, or Web of Things (Raggett, 2015).

WoT is a continuation of the IoT concept, which represents its starting point. IoT deals with access modes and communication protocols between Things and services, that is, IoT deals with the vertical structure. Unlike IoT where it is possible to send data from Things to the server and vice versa, WoT deals with the integration of Things into Web, that is, with the horizontal structure (Figure 3).

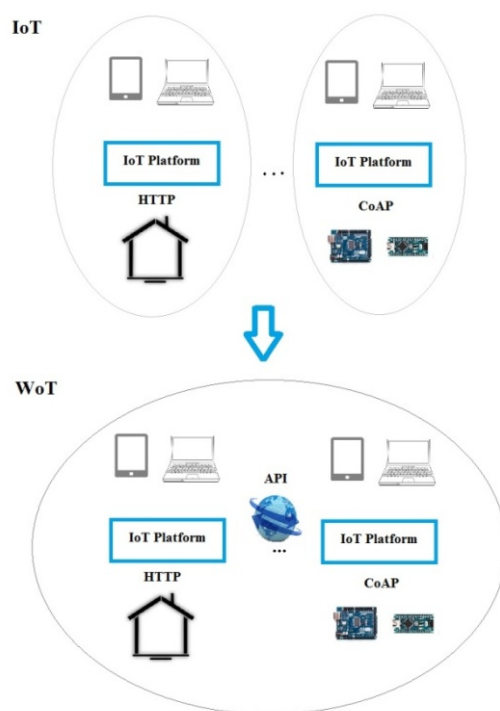


Figure 3 – Moving from IoT to WoT

Рис. 3 – Переход от интернета вещей к веб вещей

Слика 3 – Прелаз са интернета ствари на веб ствари

From Things, we now expect to be accessible through a web protocol such as HTTP, which represents a ticket for the web. The next step that needs to be done is to define a mechanism for using the IoT resources. This mechanism should be Open Source, it must take care of security and needs to be API (Application Programming Interfaces). Things will represent virtual objects that machines and people will be able to access and communicate with them.

With the development of the IoT platform, where each platform has its own mechanism, without interaction with other platforms, we will take a step backwards compared to the initial idea that Tim Berners-Lee had when designing the Web. The problem of the development of royalty-free and platform-independent standards has been discovered and there are currently working groups under the World Wide Web Consortium (W3C) that deal with the standardization and development of the WoT API since 2015 (White Paper for the Web of Things, 2016).

In terms of WoT architecture, the idea is that devices are directly linked to Cloud or through their proxies (Figure 4).

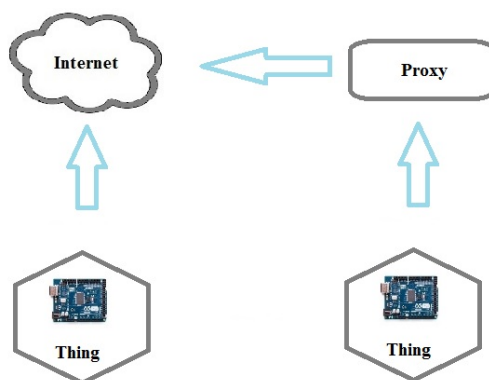


Figure 4 – Connecting Things to Web
 Рис. 4 – Связывание вещей на веб
 Слика 4 – Повезивање ствари на веб

Challenges in interconnection IoT

It is necessary to create a service architecture that will not be too much demanding for Things, so it would be possible to implement such services with the existing restrictions on Things. Such services should be able to work without an operating system, and with a limit of 8KB of memory. Such restrictions exclude the use of heavyweight Web services such as, for example, SOAP/WSDL (Guinard et al, 2011).

A protocol that meets the mentioned restrictions is the HTTP protocol, that is RESTfull architecture, which has basic access methods such as: GET, POST, PUT, DELETE. In addition to this protocol, it is also possible to use the CoAP protocol, which is similar to the HTTP protocol.

In order to make the data understandable for machine processing, they need to be in one of the languages that are understandable from the machines perspective, such as XML or JSON.

In most existing scenarios, IoT applications coincide, but are not interoperable among themselves. The goal is to harmonize the used data models as well as frameworks to minimize the human interaction in their communication. It is necessary to find an approach so that the data collected from the sensor will be reusable. It is also necessary to ensure that data can be shared (Gyrard, 2015).

In order to make Things capable of building complex systems, we need to enable certain APIs that will allow communication with each

other through HTTP or CoAP protocols or other protocols, and in this way we will create the WoT (Jara et al, 2014).

Currently in Europe, according to Google statistics, most countries have IPv6 present less than 34%, which means that it is still not possible to use all the IPv6 addressing capability (Google IPv6 Statistics). In addition, it is still not possible to expect Things to work as servers that will be able to process all the requests that come to them in terms of resources. These constraints imply the need to think about other ways to access the resources of Things (Barnaghi et al, 2013).

In terms of architecture used in the integration of Things, we encounter two types of architectures. The first is Direct Integration that for every Thing assigns an address, and has its own small embedded service. Another architecture is Indirect Integration that refers to Things that are not able to run their own services, but use other services as their proxy, often referred to as the smart gateway (Zeng et al, 2011).

Using the CoAP protocol, it is possible to reduce overhead, but the problem of finding resources using the web browser remains. This problem can be solved in several ways (Castron et al, 2016).

For Emmanuel Baccelli and Dave Raggett, there are two basic challenges to be solved in the development of the IoT concept. The first is the implementation of the IPv6 protocol at the hardware level of the IoT device. The second problem is providing end-to-end security (Baccelli & Raggett, 2015).

In summary, we can conclude that WoT's software architecture should enable:

- development of services on devices with limited resources,
- M2M communication,
- the creation of a data model that will be suitable for processing and reuse,
- an API that will allow resources to be visible from other services,
- secure communication.

In order to be able to implement these requirements independently (without using the IoT platform), we need to have a team of at least several people, who will work for several years (IoT Platforms The central backbone for the Internet of Things, 2015). This points to the need to use existing platforms, or middleware. Using middleware, which implements the mentioned requirements, we can save the time it takes to create our own applications.

There are currently a large number of IoT platforms, and most of them are commercial. Large companies such as Amazon, Google,

Microsoft, IBM etc. are present in the field of IoT platforms. One of the Open Source platforms that provides these requirements is FIWARE, which can be used in different scenarios, using open and free APIs.

Open Source FIWARE platform

FIWARE is a platform that has a layer of infrastructure, and provides the IaaS service. In addition to IaaS, the platform also provides PaaS service features. These service functionalities that the platform offers enable the development of our own IoT applications. The platform is also possible to host on your own hardware, but this feature is out of scope of this paper.

The FIWARE platform allows the creation of virtual machines in which we can create our own architecture for the IoT application. Also, the platform frees us from taking care of hardware, which makes it easier for developers to create a service for a specific application. In terms of security, it is possible to define the security policy, which will take care of security and access to the application. Security of frontend and backend parts is achieved using the OAuth2 protocol.

The basis for the functioning of the FIWARE platform is the Open API Next Generation Service Interface (NGSI). NGSI defines data model, context data interface, context availability interface. Currently, two versions of this interface have been implemented, NGSI9 and NGSI10. (FIWARE-NGSI v2 Specification).

A particularly important part for the functioning of the interface is the data model. It consists of three parts:

Context Entities: It is an entity that can represent any Thing like a sensor, an actuator, a human, an animal, a car, etc. Each entity must have its own ID. To enable later search by type, you need to assign a type attribute.

Context Attributes: These are attributes that make up an entity. These attributes, besides their name, have additional attributes that describe the entity. These attributes are value, type and metadata that further describe the attribute.

Context metadata: As mentioned before, it is an optional attribute. It consists of the basic three parts (name, type, value).

The NGSI interface allows the data to be accessed through the REST method, whereby the data can be displayed in the JSON or XML format. The developers are free of concern about the communication protocols IoT uses, thanks to the IoT Generic Enablers (GE), which

translate all data that comes from Things into the NGSI form, with which developers can then work.

The software architecture of the platform is based on Generic Enablers (GE), which are elements that build the FIWARE platform. GEs can be added depending on the needs of a specific application, and a list of all GEs is available through the FIWARE catalogue.

The FIWARE platform enables integration of more services. Data can be exchanged using the NGSI API. The service architecture is based on the REST style, where resources are accessed based on their names, using URI. In this way, the horizontal interaction with other systems is achieved, hence we come to the infrastructure that can provide the development of Web of Things. Also, the infrastructure has mechanisms for generating and using Big Data. By using additional metadata attributes, we can achieve the infrastructure for semantic web development (Start Using FIWARE Right Now, 2018).

Example of using the FIWARE platform

An example that will serve us for testing the FIWARE platform is based on reading the values from the sensor, and the actuation of the DC motor depending on the values from the sensor. The goal we want to achieve by this example is to connect the hardware of some Thing with the service, which will be used for management, and that part will represent the IoT domain. The next functionality we want to explore is the ability to access Things over the Web browser and gain value in order to check the possibility to integrate into the Web. In this way, we want to test the functionalities that the FIWARE platform provides in the WoT domain.

In the testing stage, we will use the ATmega2560 microcontroller, through which we will collect data from the sensors, as well as starting the activity to check the communication on both sides. Communication between hardware and services will be achieved over the Internet. To connect the hardware to the Internet, we will use the Wi-Fi module ESP8266 (Figure 5).

Both virtual sensor, as well as a virtual actuator, will be described using the JSON format. We will describe the sensor with the basic attributes such as ID, type, owner, hardware, location, temperature, humidity. When creating a virtual sensor, we can enter the default values. The sensor description is shown in Figure 6.

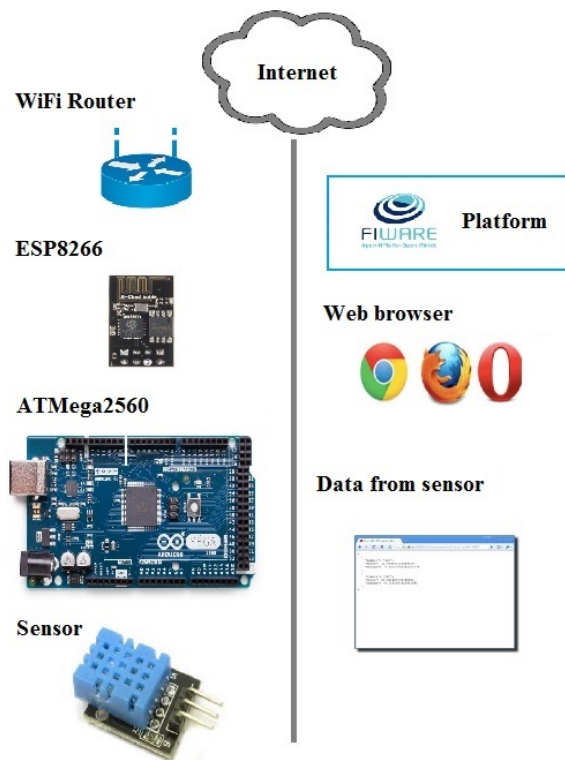


Figure 5 – Components of the example
 Рис. 5 – Компоненты примера
 Слика 5 – Компоненте примера

The state attribute refers to the status of the actuator, whether it is turned on or not, while the speed attribute represents the current motor speed. In the later physical realization, for easier display, the speed attribute will be represented by the number of LEDs that will signal the speed at which the motor is currently running.

The listed attributes will allow us to map real Things into virtual ones that will live on the Web as separate entities (Figure 7).

When the entities are created, using the NGSI API, we have to connect hardware (Things) to them, and then use the virtual sensor or actuator.

A physical sensor should send data to a virtual sensor in order to have an image of the device in real time. The virtual sensor is located at the following address: <http://130.206.xxx.xxx:1026/v2/entities/Sensor-01/>.

```
1 {
2   "id": "Sensor-01",
3   "type": "DHT11",
4   "owner": {
5     "value": "User1",
6     "type": "String"
7   },
8   "hardware": {
9     "value": "ArduinoDHT11",
10    "type": "String"
11  },
12  "location": {
13    "value": "44.7866, 20.4489",
14    "type": "geo:point"
15  },
16  "temperature_c": {
17    "value": 0,
18    "type": "Float"
19  },
20  "humidity": {
21    "value": 0,
22    "type": "Float"
23  }
24 }
```

Figure 6 – Model of a sensor
Рис. 6 – Модель датчика
Слика 6 – Модел сензора

Unlike the sensor that updates the virtual sensor, the actuator monitors the state of its virtual entity, and, depending on its condition, adjusts its state. The virtual actuator is located at the following address: <http://130.206.xxx.xxx:1026/v2/entities/Actuator-01/>.

After connecting, the data on the server represent the real state of the device, and are available through the Web browser in the JSON format. Figure 8 shows the virtual actuator data. Based on the data, we can conclude that our motor is started and running at speed 2.

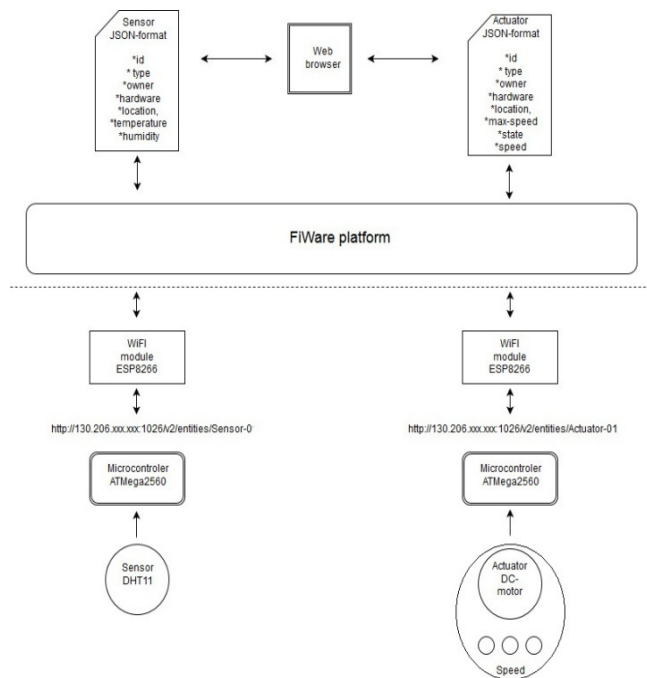


Figure 7 – Architecture of the example
 Рис. 7 – Архитектура примера
 Слика 7 – Архитектура примера

As the data is available via the Web browser, it is possible to manage actuators, or read values from the sensors using our own applications, and to connect with other sources.

In our case, the idea is that when the temperature exceeds a certain value, the actuation of a small motor at a certain speed is carried out. Another advantage of the FIWARE platform is the use of GE, such as the CEP (Complex Event Processing). We will use this GE to monitor the state of the sensor, and to start the actuator. A practical example is given in Figure 9.

```
id: "Actuator-01"  
type: "DCmotor"  
▼ hardware:  
  type: "String"  
  value: "ArduinoDCmotor"  
  metadata:  
▼ location:  
  type: "geo:point"  
  value: "44.7866, 20.4489"  
  metadata:  
▼ max-speed:  
  type: "Integer"  
  value: 3  
  metadata:  
▼ owner:  
  type: "String"  
  value: "User2"  
  metadata:  
▼ speed:  
  type: "Integer"  
  value: 2  
  metadata:  
▼ state:  
  type: "Boolean"  
  value: true  
  metadata:
```

Figure 8 – JSON model of the actuator
Рис. 8 – JSON модель актуатора
Слика 8 – JSON модел актуатора

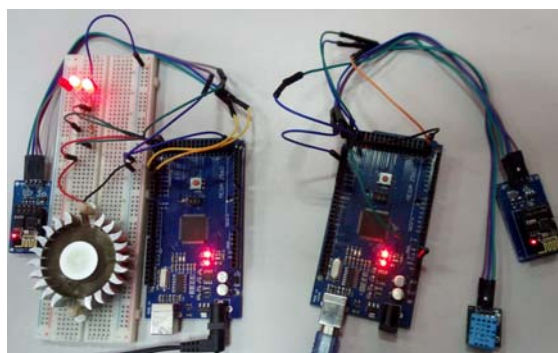


Figure 9 – Practical example
Рис. 9 – Пример из практики
Слика 9 – Практичан пример

Conclusion

Based on the presented theory and a practical example, we can conclude that the FIWARE platform allows us to create virtual devices (Things) that will reflect the state of the physical devices (Things), which have computational constraint (8KB memory). This virtual representation of the devices (Things) is displayed in a platform independent JSON format that allows later processing, and is available using the REST methods.

This system architecture allows us to manage devices (Things), that is, to use their resources by looking at them as services. The most important feature is that these resources are available using the Web protocol. The developers are free from concern about the complexity of device management (Things), using a virtual representation of the devices (Things). This functionality enables easier use in future applications.

The FIWARE platform is based on an open API, so when WoT API is created by the W3C some time in the future, it will probably be implemented on the FIWARE platform as well. Until then, the FIWARE platform provides the ability to create and test WoT applications, using the APIs that provide the necessary functionality for implementing the WoT concept.

References

- AMQP Advanced Message Queuing Protocol Specification*, Cisco Systems. 2018. [Internet]. Available at: <https://www.rabbitmq.com/resources/specs/amqp0-9-1.pdf>. Accessed: 2018 Mar 23.
- Bacelli, E., & Raggett, D. 2015. The Promise of the Internet of Things and the Web of Things. In *Special theme The Internet of Things and The Web of Thing*, ERCIM, pp.8–11. [Internet]. Available at: <https://ercim-news.ercim.eu/images/stories/EN101/EN101-web.pdf>. Accessed: 2018 Mar 28.
- Barnaghi, P., Sheth, A., & Henson, C. 2013. From Data to Actionable Knowledge: Big Data Challenges in the Web of Things [Guest Editors' Introduction]. *IEEE Intelligent Systems*, 28(6), pp.6-11. Available at: <https://doi.org/10.1109/MIS.2013.142>.
- Botta, A., Donato, W., Persico, V., & Pescapé, A. 2015. Integration of Cloud computing and Internet of Things: A survey. *Future Generation Computer Systems*, 56, pp.684-700. Available at: <https://doi.org/10.1016/j.future.2015.09.021>.

Castron, M., Jara, A., & Skarmeta, A. 2016. Enabling end-to-end CoAP-based communications for the Web of Things. *Journal of Network and Computer Applications*, 59, pp.230-236. Available at: <https://doi.org/10.1016/j.jnca.2014.09.019>.

FIWARE-NGSI v2 Specification. [Internet]. Available at: <http://docs.orioncontextbroker.apiary.io/#introduction/specification/introduction>, Accessed: 2018 Mar 12.

Google IPv6 Statistics 2018. [Internet]. Available at: <https://www.google.com/intl/en/ipv6/statistics.html#tab=per-country-ipv6-adoption&tab=per-country-ipv6-adoption>, Accessed: 2018 Mar 12.

Gubbi, J., Buyya, R., Marusic, S., & Palaniswami, M. 2013. Internet of Things (IoT): A vision, architectural elements, and future directions. *Future Generation Computer Systems*, 29(7), pp.1645-1660. Available at: <https://doi.org/10.1016/j.future.2013.01.010>.

Guinard, D., Trifa, V., Mattern, F., & Wilde, E. 2011. From the Internet of Things to the Web of Things: Resource Oriented Architecture and Best Practices. *Architecting the Internet of Things*, pp.97-129. Available at: https://doi.org/10.1007/978-3-642-19157-2_5.

Gyrard, A., Bonnet, C., Boudaoud, K., & Serrano, M. 2015. Assisting IoT Projects and Developers in Designing Interoperable Semantic Web of Things Applications. In *2015 IEEE International Conference on Data Science and Data Intensive Systems*. Institute of Electrical and Electronics Engineers (IEEE), pp.659-666. Available at: <https://doi.org/10.1109/DSDIS.2015.60>.

Internet of Things (IoT) History. [Internet]. Available at: <https://www.postscapes.com/internet-of-things-history>. Accessed: 2018 Feb 5.

IoT Platforms The central backbone for the Internet of Things. IoT Analytics GmbH. 2015. [Internet]. Available at: <http://iot-analytics.com/wp/wp-content/uploads/2016/01/White-paper-IoT-platforms-The-central-backbone-for-the-Internet-of-Things-Nov-2015-vfi5.pdf>. Accessed: 2017 Dec 23.

Jara, A.J., Olivieri, A.C., Bocchi, Y., Jung, M., Kastner, W., & Skarmeta, A.F. 2014. Semantic Web of Things: an analysis of the application semantics for the IoT moving towards the IoT convergence. *International Journal of Web and Grid Services*, 10(2/3), p.244. Available at: <https://doi.org/10.1504/IJWGS.2014.060260>.

Perera, C., Zaslavsky, A., Christen, P., & Georgakopoulos, D. 2014. Context Aware Computing for The Internet of Things: A Survey. *IEEE Communications Surveys & Tutorials*, 16(1), pp.414-454. Available at: <https://doi.org/10.1109/SURV.2013.042313.00197>.

Raggett, D. 2015. The Web of Things: Challenges and Opportunities. *Computer*, 48(5), pp.26-32. Available at: <https://doi.org/10.1109/MC.2015.149>.

Saint-Andre, P., Smith, K., & Tronçon, R. 2009. *XMPP: The Definitive Guide*. O'Reilly Media, pp.3-27.

Sharma, V. 2014. *Understanding Constrained Application Protocol*. Exilant Technologies Pvt, pp.7-18. [Internet]. Available at: www.coapsharp.com/wordpress/?wpdmdl=504, Accessed: 2017 Dec 11.

Shelby, Z. 2014. *Constrained Application Protocol (CoAP)*, Internet Engineering Task Force. Internet Engineering Task Force (IETF). [Internet]. Available at: <https://tools.ietf.org/html/rfc7252>, Accessed: 2017 Nov 10.

Stanford-Clark, A., & Truong, H.L. 2013. *MQTT for Sensor Networks (MQTT-SN) Protocol*. International Business Machines Corporation (IBM). [Internet]. Available at: http://mqtt.org/new/wp-content/uploads/2009/06/mqtt-sn_spec_v1.2.pdf. Accessed: 2016 Aug 20.

Start Using FIWARE Right Now. 2018. [Internet]. Available at: <http://fiwaretourguide.readthedocs.io/en/latest/>, Accessed: 2018 Jan 31.

White Paper for the Web of Things. 2016. [Internet], Available at: <http://w3c.github.io/wot/charters/wot-white-paper-2016.html>, Accessed: 2017 Nov 14.

Wortmann, F., & Flüchter, K. 2015. Internet of Things. *Business & Information Systems Engineering*, 57(3), pp.221-224. Available at: <https://doi.org/10.1007/s12599-015-0383-3>.

Zeng, D., Guo, S., & Cheng, Z. 2011. The Web of Things: A Survey (Invited Paper). *Journal of Communications*, 6(6). Available at: <https://doi.org/10.4304/jcm.6.6.424-438>.

Zhong, N., Yau, S.S., Ma, J., Shimojo, S., Just, M., Hu, B., Wang, G., Oiwa, K., Anzai, Y. 2016. Brain Big Data in Wisdom Web of Things. In N. Zhong, J. Ma, J. Liu, R. Huang, & X. Tao Eds., *Wisdom Web of Things*. Cham: Springer Nature., pp.339-349. Available at: https://doi.org/10.1007/978-3-319-44198-6_15.

FIWARE: РАЗВИТИЕ ПЛАТФОРМЫ ДЛЯ ИНТЕРНЕТА ВЕЩЕЙ

Иван А. Тот^а, Душан Л. Богичевич^б, Младен Б. Трикош^а, Комлен Г. Лалович^в

^а Университет обороны в г. Белград, Военная академия, Кафедра информационных систем и телекоммуникационной инженерии, г. Белград, Республика Сербия

^б Вооружённые Силы Республики Сербия, Генеральный штаб, Управление информатики и телекоммуникаций (J-6), Центр командно-информационных систем, г. Белград + Университет в г. Ниш, Факультет электроники, г. Ниш, Республика Сербия

^в Факультет прикладного менеджмента, экономики и финансов, г. Белград, Республика Сербия

ОБЛАСТЬ: компьютерные науки, информационные технологии

ВИД СТАТЬИ: профессиональная статья

ЯЗЫК СТАТЬИ: английский

Резюме:

Предметом данной статьи является Веб вещей, как продолжение развития концепта Интернета вещей. Веб вещей представляет собой шаг к связыванию умных вещей с существующим Веб

окружением, при рассмотрении актуальных проблем, таких как: гетерогенность, масштабируемость и применяемость, то есть удобство использования. Данная статья посвящена современным возможностям и вызовам для развития концепта Веб вещей. В статье представлены теоретические постулаты концепта Интернета вещей, в частности: архитектура, протоколы, услуги и собственно вещи, которые и являются основой обоих концептов. В работе описаны необходимые условия для развития концепта Веб вещей. Главным научным вкладом настоящей статьи является предложение разработанной архитектуры, основанной на платформе FIWARE, в качестве основы для развития Веб вещей. Предлагаемая архитектура основана на реальном примере.

Ключевые слова: Интернет вещей (IoT), Веб вещей (WoT), FIWARE.

FIWARE: РАЗВОЈНА ПЛАТФОРМА ЗА ВЕБ СТВАРИ

Иван А. Тот^а, Душан Љ. Богићевић^б, Младен Б. Трикош^а,
Комлен Г. Лаловић^в

^а Универзитет одбране у Београду, Војна академија,
Катедра информатичких система и телекомуникационог инжењерства,
Београд, Република Србија

^б Војска Србије, Генералштаб,
Управа за телекомуникације и информатику (Ј-6),
Центар за командно-информационе системе, Београд +
Универзитет у Нишу, Електронски факултет, Ниш, Република Србија

^в Факултет за примењени менаџмент, економију и финансије,
Београд, Република Србија

ОБЛАСТ: информатика, ИТ
ВРСТА ЧЛАНКА: стручни чланак
ЈЕЗИК ЧЛАНКА: енглески

Сажетак:

Као наставак концепта интернет ствари, веб ствари представљају корак ка повезивању интелигентних ствари са постојећим веб окружењем, уз разматрање проблема као што су хетерогеност, скалабилност и употребљивост. Овај рад је посвећен тренутним могућностима, као и изазовима за развој у концепту веб ствари. У раду су описане теоријске основе концепта интернет ствари, као што су архитектура, протоколи, услуге и саме ствари, које су основа оба концепта. Рад се бави потребним предусловима за развој концепта веб ствари. Главни допринос рада је предлог архитектуре заснован на FIWARE

платформи као основи за развој веб ствари. Демонстрација предложене архитектуре описана је реалним случајем.

Кључне речи: интернет ствари (IoT), веб ствари (WoT), FIWARE.

Paper received on / Дата получения работы / Датум пријема чланка: 04.04.2018.
Manuscript corrections submitted on / Дата получения исправленной версии работы /
Датум достављања исправки рукописа: 03.07.2018.
Paper accepted for publishing on / Дата окончательного согласования работы / Датум
коначног прихватања чланка за објављивање: 05.07.2018.

© 2018 The Authors. Published by Vojnotehnički glasnik / Military Technical Courier
(www.vtg.mod.gov.rs, втг.мо.упр.срб). This article is an open access article distributed under the
terms and conditions of the Creative Commons Attribution license
(<http://creativecommons.org/licenses/by/3.0/rs/>).

© 2018 Авторы. Опубликовано в «Военно-технический вестник / Vojnotehnički glasnik / Military
Technical Courier» (www.vtg.mod.gov.rs, втг.мо.упр.срб). Данная статья в открытом доступе и
распространяется в соответствии с лицензией «Creative Commons»
(<http://creativecommons.org/licenses/by/3.0/rs/>).

© 2018 Аутори. Објавио Војнотехнички гласник / Vojnotehnički glasnik / Military Technical Courier
(www.vtg.mod.gov.rs, втг.мо.упр.срб). Ово је чланак отвореног приступа и дистрибуира се у
складу са Creative Commons лиценцом (<http://creativecommons.org/licenses/by/3.0/rs/>).



LDPC CODES FOR PHYSICAL LAYER SECURITY

Sonja R. Kuljanski Marić

Serbian Armed Forces, General Staff,
Department for Telecommunication and Informatics (J-6),
Center for Applied Mathematics and Electronics,
Belgrade, Republic of Serbia,
e-mail: sonjakuljanski@gmail.com,
ORCID iD:  <http://orcid.org/0000-0003-4625-1035>

DOI: 10.5937/vojtehg66-14776; <https://doi.org/10.5937/vojtehg66-14776>

FIELD: Applied Mathematics
ARTICLE TYPE: Professional Paper
ARTICLE LANGUAGE: English

Summary:

Wireless communication is ubiquitous in today's society. Unfortunately, wireless transmission is by the nature of broadcasting suitable for eavesdropping. These links are usually secured by encryption protocols that rely on cryptographic algorithms whose security is based on complexity of calculation and inability to calculate in real time. The hypothesis in the field of information theory is that the eavesdropper has unlimited computer capabilities, and the use of common cryptographic protocols is uncertain. Instead, it is assumed that the legitimate recipient of the message has a better communication channel than the intrusion listening. Based on this physical advantage, it is possible to use random encoding schemes for the transmission of information at the physical level. These schemes function without the prior exchange of secret keys securely, so protection at this layer tends to significantly simplify key management in communication systems. At the end of the last and the beginning of this century, there was an idea that LDPC codes should be applied to protect data at the physical layer. In this paper, the Wyner model of the communication channel was used, and LDPC codes were constructed for the transmission of information through this channel. A comparison of the basic algorithm and its modification was made based on the following parameters: transmission of mutual information, bit-error rate and execution time. An algorithm for different sizes of LDPC codes was also performed based on the above parameters.

Key words: LDPC codes, Physical layer security, Wyner wiretap channel.

Introduction

Protection at the physical layer in the OSI model is independent of data encryption and authentication. An important feature of this protection is that secure communication can be established without the exchange of keys that have been performed in advance. In recent years, with the increasing use of mobile phones, wireless sensory networks and radio frequency identification (RFID) systems, security at the physical layer has gained significance. However, the implementation of schemes which rely on protection at the physical layer can be significantly more expensive than the implementation of security features based on cryptography. Currently, it is believed that it is best to combine cryptographic algorithms with physical layer protection. The use of security at the physical layer is recommended only for the transmission of the most sensitive information, such as key transport, key agreement or exchange of public key certificates. After the exchange of keys, the entities move to symmetric or asymmetric cryptographic algorithms.

Shannon's perfect security

In 1948, Shannon published a work (Shannon, 1948), which is considered the beginning of both the theory of information and coding theory. The diagram for transmitting information through a communication channel was described for the first time.

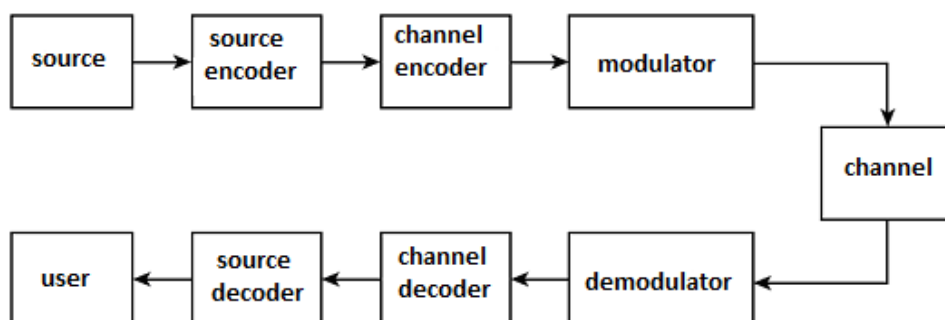


Figure 1 – Basic digital communication block by Shannon
Рис. 1 – Главная цифровая блок-диаграмма по Шеннону
Слика 1 – Основни дигитални комуникациони блок-дијаграм по Шеннону

The channel components are as follows:

1. Source as a series of bits.

2. Encoder converts the original information bit string into an alternate bit information series with a more efficient presentation of information. This operation is also called compression. Depending on the source, compression can be with loss or lossless. The source decoder returns the received alternative information to the original.

3. The channel encoder preserve a number of bits that are transmitted through a channel vulnerable to noise, signal distortion, and interference. It works by converting its input into a new sequence that has redundancy. The ratio of the number of bits that enters the channel encoder and the number of bits output from it is called code ratio and is denoted by R , $0 < R < 1$. The role of the channel decoder is the detection of a series of bits that entered the encoder of the channel.

4. The modulator converts the output string of the encoder of the channel into a form corresponding to the given channel. For example, for a wireless communication channel, a series of bits must be represented by a high-frequency signal to allow transmission with an antenna of a reasonable size. The demodulator does the opposite of the modulator, and it detects the sequence that entered the modulator.

5. Channel is the physical medium through which the modulator sends its output. The channel can add noise to the signal that passes through it, and it can interfere with other signals.

Shannon introduced the notion of perfect security in (Shannon, 1949), which means that any intercept signal does not give the attacker more information than a random signal. According to this theory, Shannon discovered that for the purpose of secure transmission, the sender and the receiver in advance need to exchange the relevant key. Moreover, this pre-shared key should be changed during each data transfer. This result represents the theoretical basis for a symmetric key cryptography.

Let the source be completely defined by the list of symbols $S(s_1, s_2, \dots, s_q)$ and the set of appropriate probabilities $P(s_i), i \in \{1, \dots, q\}$, whereby it is assumed that the symbols represent a complete set of mutually exclusive events, $\sum P(s_i) = 1$ Shannon defines entropy as the amount of uncertainty involved in the value of a random variable or the outcome of a random process

$$H(S) = \sum_{i=1}^q P(s_i) \log_2 \frac{1}{P(s_i)} = - \sum_{i=1}^q P(s_i) \log_2 P(s_i) \quad (1)$$

Perfect security is achieved if it is valid

$$H(M / X) = H(M) \quad (2)$$

otherwise if code word X is statistically independent of the message M .

In order to be able to broadcast information, the source must have at least two symbols available. Such a source is called a binary source of information. It is common to label these symbols as 0 and 1. If $P(0) = p$, then $P(1) = 1 - p$, so the entropy of the binary source is $H(S) = -p \log_2 p - (1 - p) \log_2 (1 - p)$ information bits. It is clear that entropy is maximal when the probabilities of the both symbols are equal, $p = 1 - p = 0.5$ and then entropy is 1.

Let X and Y be random variables. It is then possible to define their mutual entropy as $H(X; Y) = E[-\log_2 p_{X,Y}(X, Y)]$, where $p_{X,Y}(X, Y)$ is mutual probability of the density function X and Y then their mutual information is defined as

$$I(X, Y) = \sum_{x \in X, y \in Y} p_{X,Y}(x, y) \log_2 \frac{p_{X,Y}(x, y)}{p_X(x)p_Y(y)} \quad (3)$$

ie, mutual information for X and Y can be presented as

$$I(X, Y) = H(X) - H(X / Y) \quad (4)$$

where $H(X / Y)$ is conditional entropy which is defined as

$$H(X / Y) = \sum p_Y(y) H(X / Y = y).$$

Shannon showed that channels can be categorized according to the parameter C , called channel capacity, which measures the amount of information that can be transmitted through the given channel. Although C can be presented in several different units, in the context of the channel code rate R whose unit is bit information on the channel bit, Shannon showed that there are codes that provide arbitrary reliable communication if the code rate meets the condition $R < C$. He also showed that, for $R > C$, there is no code that provides reliable communication.

The channel capacity is defined as

$$C = \max_{P(x)} I(X, Y). \quad (5)$$

That is, the capacity is the maximum common information where the maximization is done through the distribution of the probability of the channel input $P(x)$.

The transmission system meets Shannon's definition of perfect security if the mutual information between the sent signal X (plain text) and the intercepted signal Y (encrypted text) is equal to zero, i.e. $I(X,Y) = 0$.

It is not easy to construct a security system that meets the above criteria. Shannon has proven that one-time pad systems satisfy the criterion if the key space entropy is greater than or equal to the entropy of the message space, i.e. $H(K) \geq H(X)$.

Wyner *wiretap* channel

In 1975, Wyner introduced a wiretap channel in (Wyner, 1975) and established the ability to create almost perfectly secure communications without relying on cryptographic keys. He found the difference between the two types of noise, one that got the legitimate receiver and the other that received the wiretapper and showed that it was possible to reach non-zero secret capacity. He introduced a wiretap channel notation.

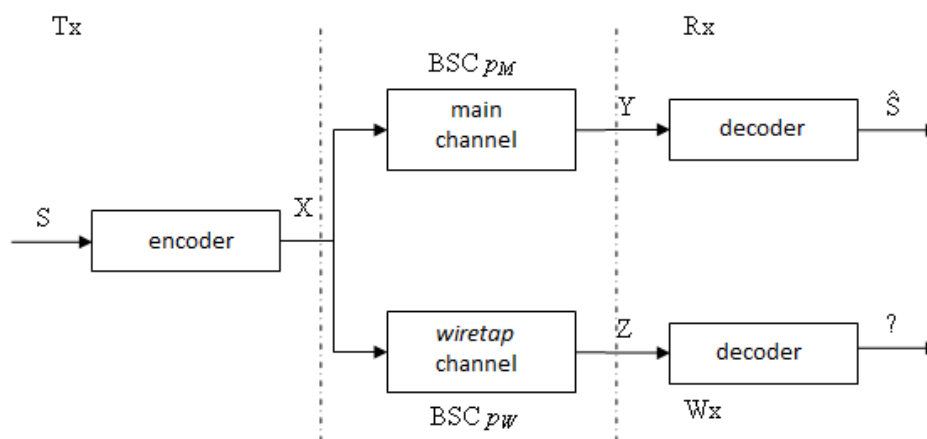


Figure 2 – Wyner's wiretap channel (Ghen & Gong, 2012)

Рис. 2 – Канал Wyner wiretap (Ghen & Gong, 2012)

Слика 2 – Wyner-ов wiretap канал (Ghen & Gong, 2012)

Secret capacity of the data transmission system is defined as

$$C = H(S/Z) - H(S/Y) \quad (6)$$

According to Shannon, perfect security requires that $I(S,Z) = 0$. Since $I(S,Z) = H(S) - H(S/Z)$, perfect security is achieved when $H(S/Z)$ is maximal, and that is exactly what Wyner's security required. The Wiretap channel does not require the exchange of keys in advance, and it is enough that the main channel has less noise than the wiretap channel so that the secrecy of the data transmission system is attainable.

The first question is how practical the implementation of this approach is. In some applicable scenarios, such as Radion Frequency Identification (RFID), a channel between an RFID reader and a valid tag is better than the channel between the tag and the illegal reader, since the illegal reader must be at a certain distance to avoid detection of the system.

The second question is how to design an encoder that is efficient, reliable and secure and how to choose a wiretap code. LDPC and Polar codes approach Shannon's channel capacity and meet the required conditions which can be mathematically defined.

LDPC codes

Wyner and Ozarow used a coset coding strategy (Ozarow & Wyner, 1984, pp.2135-2157) to show that perfect secrecy can be achieved when there are no errors in the main channel and when the input alphabet is binary.

In the 1960s, Gallager (Gallager, 1962) developed low-density parity-check codes (LDPC codes); however, they were ignored for a long time because their computer complexity was too great for technology of that time. LDPC codes have very good decoding performance. In addition, they have the ability to parallelize in decoding and simple operations to calculate. The low complexity of computability combined with parallelism and good performance to correct errors are the main reasons why LDPC codes attract so much attention.

Despite these advantages, finding good methods for constructing LDPC codes and their efficient hardware implementation is still a challenge. Approaching the capacity of the channel implies that infinitely long codes are used. Different system applications have different decoding, delay, power and costing performance. These requirements

limit the size of the code and its hardware implementation. As a result, different code lengths are recommended for different applications in order to get good performance and to meet the hardware requirements. LDPC codes can be applied in wireless, wired and optical communication systems, as well as on magnetic and compact discs. These are the reasons why it is a challenge to find ways to construct a fixed-length LDPC code and speed with good performance.

Implementation of LDPS codes in Wyner's wiretap channel

Wiretape encoding maps k message bit into the entire n -dimensional space. Therefore, there are 2^{n-k} code words for each message. One of them is randomly selected and transmitted through a wiretap channel. This coincidence is essential in securing the secrecy of the transmission through the wiretap channel.

Let there be a linear correcting code that has G as a matrix generator. The code C is a subspace of space $\{0,1\}^n$ with 2^k elements. According to the theory of error correction codes, every coset has cardinality 2^k , and there are 2^{n-k} total of them, so cosets completely divide the n -dimensional space into nonoverlapping subspaces.

Let Alice and Bob want to secretly exchange messages in Wyner's wiretap channel and let Eva want to listen to the exchange of messages. Alisa starts the communication procedure by choosing the message m length of the syndrome k . It is a secret message to be transmitted to Bob, and Eva cannot reconstruct it. Alisa finds a matrix base G for the complementary subspace C of the subspace of the code C . C and its complement C together make up the entire n -dimensional space of binary vector lengths n , i.e. $C \cup C = \{0,1\}^n$. Alice then generates a random sequence of lengths $n-k$. This is a uniformly distributed random vector, generated so that neither Bob nor Eva have any information about it. Alice then performs the following coding procedure

$$x = [mu] \begin{bmatrix} G \\ G \end{bmatrix} = mG + uG$$

the code word x is then transmitted via the wiretap channel. According to the definition, uG is the valid code word of the code C , while the message m determines one coset of the code C the cardinality of which

is 2^k . Alisa sends x through the wiretap channel. Bob receives the code word x without error. Its goal is to decode the message m , so he applies the following procedure

$$Hx^T = H(mG + uG)^T = H(mG)^T.$$

Note that Bob does not need to use information about a random vector u . He is in a favorable situation because the message is a syndrome and that each of the 2^{n-k} words in the coset serves equally well to get the message. Eve's goal is the same as Bob's, but her channel is worse than Bob's, so she gets a code word with the noise x . The randomized code schema along with a careful code design ensures that the noisy code word x reveals to Eva very little or no information about the sent message m .

The parity check matrix H is of a form $[A \ B]$, where the matrix B has to be non-singular (i.e. inverse must exist. There is an evidence that every linear code C with the generating matrix G is equivalent to a linear code C' whose generating matrix G' is derived from matrix G by bringing in reduced row echelon form - RREF), (Hofman et al, 1992).

This allows us to select a unity matrix for the matrix B without additional constraints. The generating matrix G can be constructed as

$$G = \begin{bmatrix} I_{n-k} & (B^{-1}A)^T \end{bmatrix}$$

If the code C is self-dual then $G = H$ and the matrix A must have a trait $AA^T = 0$. If the matrix A is randomly generated, then it is necessary to calculate the matrix G before starting the coding.

For simplicity, suppose that the matrix $G = [I \ P]$, then $H = [P^T \ I]$. It is necessary to calculate the matrix G . By definition,

$$x = [m \ u] \begin{bmatrix} G \\ G \end{bmatrix} = mG + uG. \text{ When decoding, we need to get}$$

$xH^T = m$, respectively

$$(mG^* + uG)H^T = mG^*H^T + \underbrace{uGH^T}_0 = mG^*H^T = m$$

follows is that $G H^T = I$. Let the matrix be $G = [G_1 \ G_2]$, then

$$G H^T = [G_1 \ G_2] H^T = [G_1 \ G_2] \cdot [P^T \ I]^T = [G_1 \ G_2] \begin{bmatrix} P \\ I \end{bmatrix} =$$

$$G_1 P + G_2 I = G_1 P + G_2 = I$$

That is, there is a mutual dependance between the matrices G_1 and G_2 . If the matrix G_1 is generated in a random way, we can calculate the matrix G_2 as $G_1 P + I$.

It has been experimentally shown that for the parity check matrix of the form $m \times 2m$ as the matrix G_1 unity matrix can be chosen without increasing mutual information, that speed up encryption since the matrix multiplication is eliminated. This significantly reduces the execution time of the algorithm in the case of a large matrix. In this case, the matrix G_2 is calculated as $IP + I = P + I$.

The construction of the self-dual code requires more time in the design of the generating and parity check matrix, but allows faster encoding. On the other hand, for non-self-dual codes, it is possible to construct the generating and verification matrix more quickly, but it takes extra time to generate a matrix G necessary for successful encryption.

The advantage of Wyner's wiretap coding in relation to other types of secret information transmission is that the attacker knows the code process as well as the legitimate participants in the communication and there is no pre-established secret key. The only condition is that legitimate participants have a better channel than an attacker.

Experimental results

For the needs of the simulation, wiretap codes are based on the use of the coset code scheme. The generating codes and the parity check matrix are constructed as follows:

$$H = [P \ I] \text{ i } G = [I \ P^T]$$

For such constructed matrices, the bit error rate, mutual information and the rate of execution of the encoding are experimentally checked. Particular cases were considered for different constructions of the matrix G . For an arbitrary size of the code $C(n, m)$, the matrix G is constructed in the following way $G = [A \ (P^T A + I)^T]$, where the matrix P is a matrix from $H = [P \ I]$, and a matrix A is randomly generated. For the

code of forms $C(2m, m)$, it is possible to construct a matrix G as $G = [I \ P + I]$.

Three cases are considered:

1. Code C has $C(n, m)$ form,
2. Code C has $C(2m, m)$ form and the matrix G has $G = \begin{bmatrix} A & (P^T A + I)^T \end{bmatrix}$ form.
3. Code C has $C(2m, m)$ form and the matrix G has $G = [I \ P + I]$ form.

Description of simulation

To modulate the messages in the simulation, QPSK (Quadrature Phase Shift Keying) modulation was selected. The selected channel is AWGN (additive White Gaussian Noise). The simulation is conceived as follows:

1. A random message of 1024 bits is generated. Then, depending on the used code, it takes the multiplication of the number of bits that is taken in the given wiretap code as information content.
2. Define the number of passes per signal-to-noise ratio in the channel in order to obtain the mean values and to obtain correct results. The number of passes is 50.
3. A simulation of the transmission of information content is initiated, with the signal-to-noise ratio going from 01 to 14 ($S/Nratio$).
 - a. A channel with the current signal-to-noise ratio is created.
 - b. Message is coded by a chosen code.
 - c. Message is modulated by QPSK modulation.
 - d. Transmission over the AWGN channel is simulated.
 - e. The demodulation of the received signal is performed.
 - f. An error is calculated at the transmission layer.
 - g. The received message is decoded.
 - h. An end-to-end error is calculated.
 - i. The mutual information between sent and received message is calculated.
 - j. The time of encoding initial message is calculated.
4. The mean error value at the transmission layer and the end-to-end error for each value $S/Nratio$ for the selected code is calculated

5. The mean value of the mutual information for each value S/N ratio for the selected code is calculated.
6. The coding time for the selected code is calculated.
7. Draw graphics.

LDPC codes of the form $C(n,m)$

Among the codes of the form $C(n,m)$ the next codes are compared $C(512,32)$, $C(512,64)$, $C(512,128)$, $C(512,256)$, $C(512,384)$, $C(512,448)$, $C(512,480)$; $C(512,496)$.

Bit error rate for the codes of the form $C(n,m)$

This feature was compared to pure BER on the channel (between the modulator and the QPSK demodulator) and the total BER on the system from the source of the message to the destination, end-to-end.

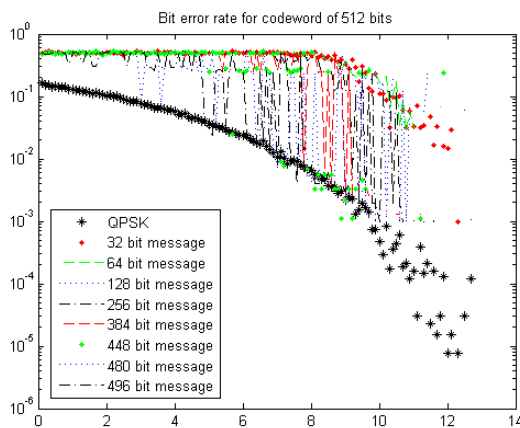


Figure 3 – BER for the code $C(512,m)$, $m < 512$ depending on the syndrom length

Рис. 3 – BER для кода формы $C(512,m)$, $m < 512$, в зависимости от продолжительности синдрома

Слика 3 – BER за код облика $C(512,m)$, $m < 512$, у зависности од дужине синдрома

As expected, the best BER has the code $C(512,32)$, while the code $C(512,496)$ has the worst BER.

Mutual information for the codes of the form $C(n,m)$

Figure 4 shows an increase in transformation as the signal-noise ratio increases. If the recipient has a signal-to-noise ratio above 12, which according to work (Baldi, 2014) is expected from the main channel, and the eavesdropper has a degraded channel, then the secrecy capacity could be calculated as the difference of these two transformations multiplied by the signaling speed that would have been used.

The biggest slope has the code $C(512,32)$, while the code $C(512,496)$ has the smallest slope.

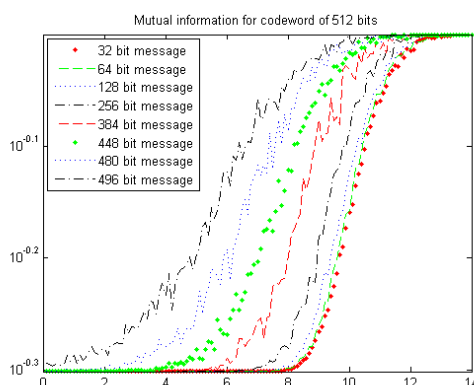


Figure 4 – Mutual information for the codes $C(512,m)$, $m < 512$ depending on the syndrom length

Рис. 4 – Совместная информация по коду формы $C(512,m)$, $m < 512$ в зависимости от продолжительности синдрома

Слика 4 – Заједничка информација за код облика $C(512,m)$, $m < 512$ у зависности од дужине синдрома

Execution speed for the codes of the form $C(n,m)$

Encoding execution time increases with increasing the length of basic information. Based on the measurement of BER and common information, it is clear that the best code is $C(512,32)$. However, this code takes the most time to encode, as shown in Figure 5.

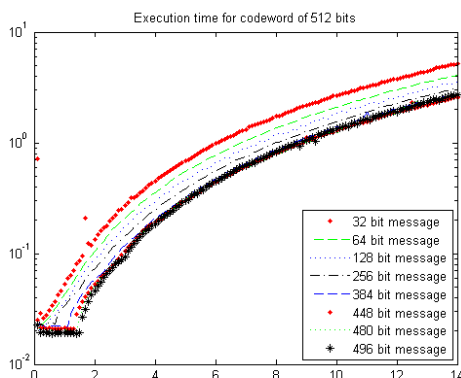


Figure 5 – Execution time for the codes $C(512, m)$, $m < 512$ depending on the syndrom length

Рис. 5 – Време выполнения по коду формы $C(512, m)$, $m < 512$ в зависимости от продолжительности синдрома

Слика 5 – Време извршавања за код облика $C(512, m)$, $m < 512$ у зависности од дужине синдрома

LDPC codes of the form $C(2m, m)$

For the codes of the form $C(2m, m)$, it is possible to make certain changes in the creation of the matrix G that lead to a significant speed up in the execution of the encoding function. Among the codes of the form $C(2m, m)$ codes $C(32, 16)$, $C(64, 32)$, $C(128, 64)$, $C(256, 128)$, $C(512, 256)$ and $C(1024, 512)$ are compared.

For each of these codes, two matrices G are created. One in a standard way, and the other in a simplified form for speeding up the encoding process.

Bit error rate for the codes of the form $C(2m, m)$

In Figures 6 and 7, it can be noticed that there is no increase in the bit error rate if the matrix G is constructed simpler for the codes of the form $C(2m, m)$.

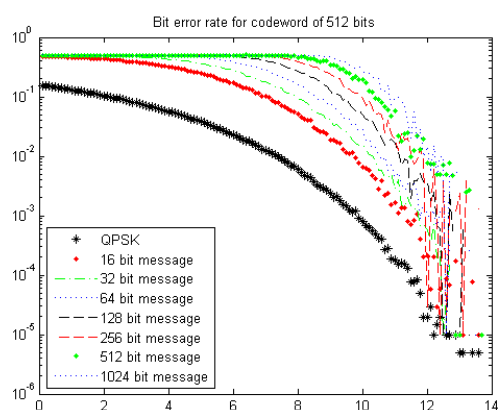


Figure 6 – BER for the code $C(2m, m)$; $m < n$ depending on the codeword length for the matrix G^* constructed in the standard way

Рис. 6 – BER для кода форми $C(2m, m)$; $m < n$ в зависимости от величины кодового слова для стандартного создания матрицы G^*
 Слика 6 – BER за код облика $C(2m, m)$; $m < n$ у зависности од дужине кодне речи за стандардан начин креирања матрице G^*

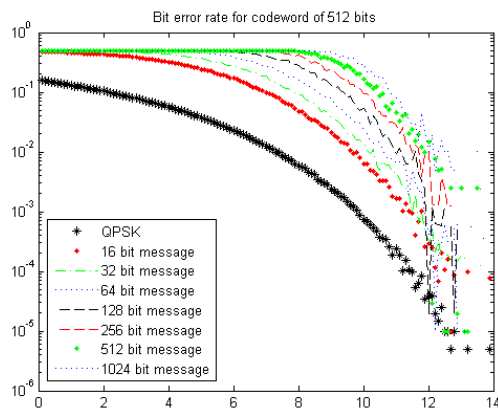


Figure 7 – BER for the codes $C(2m, m)$; $m < n$ depending on the codeword length for the matrix G^* constructed in a simplified way

Рис. 7 – BER для кода форми $C(2m, m)$; $m < n$ в зависимости от величины кодового слова для упрощенного создания матрицы G^*
 Слика 7 – BER за код облика $C(2m, m)$; $m < n$ у зависности од дужине кодне речи за поједностављен начин креирања матрице G^*

Mutual information for the codes of the form $C(2m, m)$

Also, in Figures 8 and 9, it is seen that mutual information does not increase for different constructions of the matrix G .

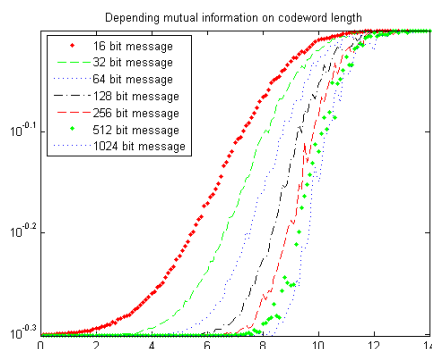


Figure 8 – Mutual information for the code $C(2m, m)$; $m < n$ depending on the codeword length for the matrix G^* constructed in the standard way

Рис. 8 – Совместная информация по коду формы $C(2m, m)$; $m < n$ в зависимости от величины кодового слова для стандартного создания матрицы G^*
Слика 8 – Заједничка информација за код облика $C(2m, m)$; $m < n$ у зависности од дужине кодне речи за стандардан начин креирања матрице G^*

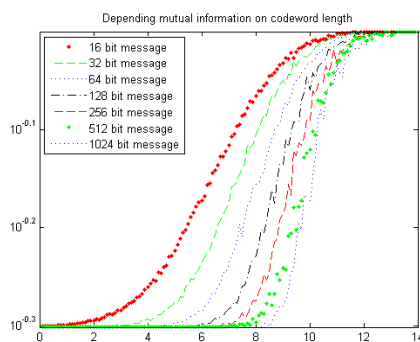


Figure 9 – Mutual information for the codes $C(2m, m)$; $m < n$ depending on the codeword length for the matrix G^* constructed in a simplified way

Рис. 9 – Совместная информация по коду формы $C(2m, m)$; $m < n$ в зависимости от величины кодового слова для упрощенного создания матрицы G^*
Слика 9 – Заједничка информација за код облика $C(2m, m)$; $m < n$ у зависности од дужине кодне речи за поједностављен начин креирања матрице G^*

Execution time for the codes of the form $C(2m,m)$

In Figures 10, 11 and 12, it can be noticed that the execution time in the standard matrix G creation is greater than the execution time if a simplified matrix G is used. This feature is more noticeable for codes for a longer codeword.

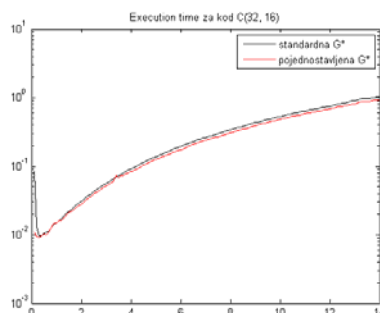


Figure 10 – Execution time for the codes $C(32,16)$ depending on the codeword length for the matrix G^* constructed in the standard way and the matrix G^* constructed in a simplified way

Рис. 10 – Време выполнения по коду $C(32,16)$ для стандартного создания матрицы G^* и упрощенного создания матрицы G^*

Слика 10 – Време извршавања за код $C(32,16)$ за стандардан начин креирања матрице G^* и поједностављен начин креирања матрице G^*

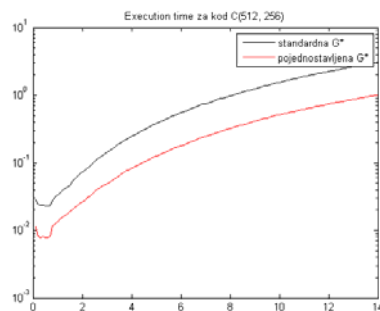


Figure 11 – Execution time for the codes $C(512,256)$ depending on the codeword length for the matrix G^* constructed in the standard way and the matrix G^* constructed in a simplified way

Рис. 11 – Време выполнения по коду $C(512,256)$ для стандартного создания матрицы G^* и упрощенного создания матрицы G^*

Слика 11 – Време извршавања за код $C(512,256)$ за стандардан начин креирања матрице G^* и поједностављен начин креирања матрице G^*

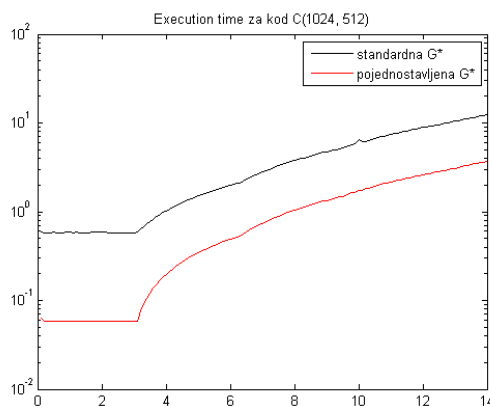


Figure 12 – Execution time for the codes $C(1024,512)$ depending on the codeword length for the matrix G^* constructed in the standard way and the matrix G^* constructed in a simplified way

Рис. 12 – Време выполнения по коду $C(1024,512)$ для стандартного создания матрицы G^* и упрощенного создания матрицы G^*

Слика 12 – Време извршавања за код $C(1024,512)$ за стандардан начин креирања матрице G^* и поједностављен начин креирања матрице G^*

Conclusion

Progress in wireless communication over the past two decades, especially at the physical layer, enables error control techniques. The aim of the paper was to present LDPC codes and their practical implementation as well as some modulations of implementation that lead to acceleration. These codes, together with Turbo codes, represent the basis of the digital and mobile revolution (3G and 4G networks) that began at the beginning of this century.

During the experimental comparison of differently constructed codes, what is measured is the error rate bit, the mutual information for the plain text and the encoded text, as well as the execution time for different lengths of the code. The expected conclusion is that the error rate bit is better when the syndrome is shorter, and the code word is longer. The same applies to mutual information. However, codes with a longer syndrome are performed faster. Accordingly, one must find the trade-off between the speed of execution on the one hand and the transmission of common information and the bit error rate on the other.

The scientific research process could be aimed at constructing and checking the properties of Gallager's, MacKay's and protograph codes as the main representatives of randomly constructed LDPC codes. The methods for the construction of codes based on Euclidean geometry and on combinatorial designs could also be studied, as the representatives of structured constrained LDPC codes.

References

- Baldi, M. 2014. *QC-LDPC Code-Based Cryptography: Chapter Low-Density Parity-Check Codes*. Springer, pp.5-23.
- Gallager, R.G. 1962. Low-density parity-check codes. *IRE Transactions on Information Theory*, January, pp.21-28.
- Ghen, L., & Gong, G. 2012. *Communication System Security: Chapter Physical-Layer Security*. CRC Press, pp.583-611.
- Ozarow, L.H., & Wyner, A.D. 1984. Wire-tap channel II. *AT&T Bell Laboratories Technical Journal*, 63(10), pp.2135-2157. Available at: <https://doi.org/10.1002/j.1538-7305.1984.tb00072.x>.
- Shannon, C.E. 1948. A mathematical theory of communication. *The Bell System Technical Journal*, 27(3), pp.379-423.
- Shannon, C.E. 1949. Communication theory of secrecy systems. *The Bell System Technical Journal*, 28(4), pp.656-715.
- Wyner, A.D. 1975. The wire-tap channel. *The Bell Systems Technical Journal*, 54(8), pp.1355-1387.

НИЗКОПЛОТНОСТНЫЕ КОДЫ ДЛЯ ЗАЩИТЫ ДАННЫХ НА ФИЗИЧЕСКОМ УРОВНЕ

Соня Р. Кулянки Мариц

Вооруженные силы Республики Сербия, Генеральный штаб,
Управление информатики и телекоммуникаций (J-6),
Центр прикладной математики и электроники,
г. Белград, Республика Сербия

ОБЛАСТЬ: прикладная математика
ВИД СТАТЬИ: профессиональная статья
ЯЗЫК СТАТЬИ: английский

Резюме:

Беспроводная коммуникация стала неотъемлемой частью современного мира. К сожалению, беспроводная передача данных имеет и свои недостатки, так например, такой вид связи очень удобен для прослушивания. Беспроводная связь обычно защищена протоколами шифрования потока данных, которые основаны на криптографических алгоритмах. Безопасность данных обеспечивается за счет сложных вычислений, которые невозможно произвести в реальном времени. В области теории

информаций существует гипотеза о том, что прослушивающее устройство имеет неограниченные вычислительные возможности, поэтому в данном случае использование обычных криптографических протоколов не совсем надежно. Вместо этого предполагается, что у законного получателя сообщения коммуникационный канал лучше, чем канал с которого ведется прослушивание. И это физическое преимущество дает возможность применения схемы случайного кодирования для передачи информации на физическом уровне. Эти схемы функционируют без предварительного обмена ключами безопасным методом, таким образом защита этого уровня стремится к значительному упрощению управления ключами в коммуникационной системе. В конце прошлого и начале этого века родилась идея о применении низкоплотностных кодов для защиты на физическом уровне. В данной статье применена модель Wyner коммуникационного канала, а для передачи информации по этому каналу были разработаны низкоплотностные коды.

Приведен сравнительный анализ главного алгоритма и его модификаций на основании следующих параметров: передача совместной информации, частота ошибок по битам (BER) и скорости выполнения. Также проведен сравнительный анализ работы алгоритма с различными величинами низкоплотностных кодов, на основании вышеприведенных параметров.

Ключевые слова: низкоплотностные коды, защита данных на физическом уровне, канал Wyner wiretap.

LDPC КОДОВИ ЗА ПОТРЕБЕ ЗАШТИТЕ ПОДАКА НА ФИЗИЧКОМ НИВОУ

Соња Р. Куљански Марић

Војска Србије, Генералштаб,
Управа за телекомуникације и информатику (Ј-6),
Центар за примењену математику и електронику,
Београд, Република Србија

ОБЛАСТ: примењена математика

ВРСТА ЧЛАНКА: стручни чланак

ЈЕЗИК ЧЛАНКА: енглески

Сажетак:

Бежична комуникација је свеprisутна у данашњем свету. Нажалост, бежични пренос података је по природи емитовања погодан за прислушкивање. Ове везе су обично осигуране протоколима за енкрипцију који се ослањају на криптографске алгоритме и чија се безбедност заснива на сложености израчунавања и немогућности израчунавања у реалном времену.

Хипотеза у области теорије информација јесте да прислушкивач има неограничене рачунарске могућности, па је коришћење уобичајених криптографских протокола несигурно. Уместо тога уводи се претпоставка да легитимни прималац поруке има бољи комуникациони канал од ентитета који прислушкује. На основу ове физичке предности могуће је користити шеме за случајно кодирање за пренос информација на физичком нивоу. Ове шеме функционишу без претходне размене тајних кључева сигурним путем, па заштита на овом нивоу тежи да значајно поједностави управљање кључевима у комуникационим системима. Крајем прошлог и почетком овог века јавила се идеја да се LDPC кодови примене приликом заштите на физичком нивоу. У раду је коришћен Вупер-ов модел комуникационог канала, а за пренос информација кроз овај канал конструисани су LDPC кодови. Вршено је поређење рада основног алгорита и његове модификације на основу следећих параметара: преноса заједничке информације, bit-error rate-а и брзине извршавања. Такође, вршено је поређење рада алгорита за различите величине LDPC кодова на основу наведених параметара.

Кључне речи: LDPC кодови, заштита података на физичком нивоу, Вајнеров wiretap канал.

Paper received on / Дата получения работы / Датум пријема чланка: 10.08.2017.
Manuscript corrections submitted on / Дата получения исправленной версии работы / Датум достављања исправки рукописа: 03.07.2018.
Paper accepted for publishing on / Дата окончательного согласования работы / Датум коначног прихватања чланка за објављивање: 05.07.2018.

© 2018 The Author. Published by Vojnotehnički glasnik / Military Technical Courier (www.vtg.mod.gov.rs, втг.мо.упр.срб). This article is an open access article distributed under the terms and conditions of the Creative Commons Attribution license (<http://creativecommons.org/licenses/by/3.0/rs/>).

© 2018 Автор. Опубликовано в «Военно-технический вестник / Vojnotehnički glasnik / Military Technical Courier» (www.vtg.mod.gov.rs, втг.мо.упр.срб). Данная статья в открытом доступе и распространяется в соответствии с лицензией «Creative Commons» (<http://creativecommons.org/licenses/by/3.0/rs/>).

© 2018 Аутор. Објавио Војнотехнички гласник / Vojnotehnički glasnik / Military Technical Courier (www.vtg.mod.gov.rs, втг.мо.упр.срб). Ово је чланак отвореног приступа и дистрибуира се у складу са Creative Commons лиценцом (<http://creativecommons.org/licenses/by/3.0/rs/>).



САВРЕМЕНО НАОРУЖАЊЕ И ВОЈНА ОПРЕМА
СОВРЕМЕННОЕ ВООРУЖЕНИЕ И ВОЕННОЕ ОБОРУДОВАНИЕ
MODERN WEAPONS AND MILITARY EQUIPMENT

Руска артиљерија изазива страх и трепет у Украјини¹

Руска војска поново унапређује конвенционалну цевну артиљерију и уводи нове, флексибилније технике гађања.

Након почетка оружаног сукоба у Украјини 2014. године, свет је коначно добио увид у руску тактику копненог рата. Нови начини употребе артиљерије потичу од 2008. године, када је и започета модернизација руске војске. Развој артиљерије у Русији довео је до драматичног повећања прецизности и ватрене моћи, али је истовремено смањен број артиљеријских јединица. Руска артиљерија уводи нове модерне приступе уз старије, мање прецизне тактике, а сви коментатори се слажу да је употреба артиљерије током лета 2014. и зиме 2015. године била врло разноврсна и инвентивна.

Приликом одбране руске националне мањине у Украјини, руска војска је употребила самоходне хаубице 152 мм МСТА-С, вучене хаубице 152 мм МСТА-В и вишецевне бацаче ракета ВМ-21 *Grad* за уништавање украјинских снага на граници између Украјине и Русије током августа 2014. године. У овим случајевима артиљеријска ватра је била концентрисана и усмерена на специфичне области, и то са разарајућим последицама по украјинску 30. механизовану бригаду. Како се кампања мењала тако се мењала и руска тактика, као и употребљена техника. Прецизност ватрених удара је повећана како су циљеви постајали покретнији. Током августа 2014. године више су коришћени системи МСТА-С и *Нона-S* који су уништавали непријатељске групе на основу података које су слале беспилотне летелице.

Примећене су беспилотне летелице типа *Orlan-10* и *Forpost*. *Orlan-10* је мала беспилотна летелица која се лансира путем катапулта, домета до 140 км од контролне станице која може остати у ваздуху до 16 сати. Летелица има максималну брзину до 150 км/час, а постиже максималну висину до 4,99 км. Може да носи терет масе до 6 кг, а обично је опремљена жироостабилизационом дневном телевизијском камером и/или инфрацрвеним сензором.

¹ JIDR June 2018



Самоходна хаубица MSTA-S



Беспилотна летелица типа Orlan-10

Са друге стране, *Forpost* је руска верзија израелске беспилотне летелице *Israel Aerospace Industries Searcher Mk II*. Максимални долет јој је до 250 км од земаљске контролне станице, а може остати у ваздушном простору до 16 сати. Њена максимална брзина је 214 км/час, а крстарећа брзина између 126 км/час и 148 км/час. Летелица достиже висину од 6,29 км и може понети користан терет тежак до 100 кг. Опремљена је дневном телевизијском камером, инфрацрвеним сензорима и ласерским даљинаром.



Беспилотна летелица типа Forpost

Поменуте летелице омогућиле су проруским артиљеријским снагама потпуно уништавање украјинске 92. механизоване бригаде током августа 2014. године.

Руске оружане снаге поседују различите комерцијалне квадрикоптере и хеликоптерске беспилотне летелице. Оне су коришћене у садејству са летелицама *Orlan-10* и *Forpost* које би лоцирале циљеве, а затим препуштале комерцијалним беспилотним летелицама одређивање координата циљева. Затим би артиљерија гађала по добијеним координатама и подешавала паљбу након првих плотуна. Један амерички посматрач је навео да би, од тренутка када би украјинска војска приметила прву беспилотну летелицу прошло између 10 и 15 минута пре него што би њихови положаји били засути гранатама и ракетама.

Електронска дејства

Током јула 2014. године амерички обавештајни извори известили су да је само једна ватрена мисија проруске артиљерије уништила два украјинска механизована батаљона за неколико минута. Ова мисија постала је позната као битка код Зеленопоља. Украјинска 79. ваздушно-десантна бригада појавила се на ватреној линији, а затим великим делом била уништена дејством вишецевних ракетних бацача *BM-21 Grad*. Необично је да је употребљен прилично стари систем који потиче још од популарних каћуша из Другог светског рата. Овај артиљеријски систем испуљује невођене ракете 122 мм са класичним високоексплозивним пуњењем на даљину до 37,5 км. Његова употреба показала је да су

проруске снаге у стању да комбинују старије артиљеријске системе за постизање жељеног ефекта. Додуше, није немогуће да су специјалне извиђачке јединице проруских снага биле присутне на том делу фронта и лоцирале украјинске снаге.

Постоје извештаји да су употребљена средства за електронско ратовање као што је *RB-301 В Borisoglebsk-2*, који је наводио артиљеријску ватру. *Borisoglebsk-2* је платформа за електронска дејства која омета радио-сигнале или пресеће комуникације мобилних телефона. Украјинске снаге су често комуницирале путем мобилних телефона ради кориговања артиљеријских напада на почетку сукоба, што је и иницирало употребу овог уређаја.



Borisoglebsk-2

Проруске снаге су почеле да употребљавају још један уређај за електронско ратовање – *Leer-3*, који је могао открити GPS координате активног мобилног телефона. Захваљујући овим уређајима проруске снаге су уништиле неколико батерија украјинских хаубица 122 мм D-30 које су припадале украјинским ваздушнодесантним снагама.

Како би се супротставиле проруским платформама за електронско ратовање, украјинске снаге су увеле у употребу дигиталне радио-станице *Harris* које им је доставило америчко министарство одбране. Радио-станице *Harris RF 7800V* раде на фреквенцијама од 30 до 108 MHz са размацима од по 25 kHz и омогућују шифровану комуникацију.

Дигиталне радио-станице су наводно обезбедиле сигурнију комуникацију, али је било случајева да су управо сигнали са тих радио-уређаја пресретнути и употребљени од проруских снага за навођење

артиљеријске ватре. Оваква пресретања омогућили су уређаји као што је *Borisoglebsk-2*.

Поред употребе наведених уређаја проруске снаге имале су снајперисте који су уз употребу борбеног система *Ratnik* омогућавали идентификацију и слање непријатељевих локација својим артиљеријским батеријама. Борбени систем *Ratnik* садржи и компјутер за откривање локација којим је могуће одмах проследити податке дежурној артиљеријској батерији.

По свему судећи проруске снаге су биле изразито ефикасне, што потврђује податак да је 90% украјинских губитака проузроковано артиљеријским и минобацачким системима.

Унапређивање артиљерије

Русија наставља са развојем нових самоходних артиљеријских система, као и нових система за управљање ватром на платформама нивоа батерије, батаљона и других састава са намером да скраћује време од откривања циљева путем сензора до отварања ватре.

Руска војска је дуго користила вучене и самоходне артиљеријске системе, али је сада тежиште на развоју нових покретних платформи и система вишецевних бацача ракета. С обзиром на величину руске војске биће потребно много година да се потпуно пређе са вучних на самоходне артиљеријске системе.

Међутим, имајући у виду дејства артиљеријских снага у Украјини, замена система не мора бити приоритет руске војске с обзиром на врло иновативно и ефикасно коришћење нових начина гађања и артиљеријских метода, као и на све већу употребу прецизне муниције.

Руске копнене снаге све више се окрећу ка мобилним артиљеријским системима, јер самоходна артиљерија тражи мањи број послужилаца, улази у дејство много брже и може извршити ватрену мисију, а затим се препозиционирати на другу позицију ради избегавања контрабатирања. Поред тога, посада је заштићена. Постоје индикације да ће циљ руских самоходних артиљеријских система бити откривање и уништавање тактичких формација ради стварања панике и расула у НАТО формацијама.

Типична руска артиљеријска оруђа су калибра 122 мм и 152 мм, али се иде на стандардизацију већег калибра 152 мм који има већи домет и испаљује ефикаснију муницију.

Русија и даље има у употреби већи број вучних хаубица 122 мм D-30 и самоходних хаубица 2S1 *Gvozdika* 122 мм који су уведени у оперативну употребу током шездесетих и седамдесетих година прошлог века. Ови системи од тада углавном нису унапређивани, па их је потребно заменити. Оба артиљеријска система користе стандардну високоексплозивну гранату са парчадним дејством 122 мм OF-462 са

максималном даљином до 15,4 км. За ова оруђа развијене су и гранате са ракетним потискивачем које повећавају даљину гађања до 21,9 км.

Руска артиљеријска оруђа могу се користити и у директном гађању циљева са високо-експлозивним гранатама ВК-6М (HEAT), али су она ограничено ефикасна против оклопних возила са модерним оклопом. Вишецевни бацачи ракета BN-21 *Grad* или самоходне хаубице MSTA-S су много ефикаснији у том погледу. Лимитирајући фактор је и кратки домет цевних артиљеријских система 122 мм.

Самоходна хаубица 2S3 *Akatsiya* 152 мм испаљује гранату OF-540 HE на даљину до 18,5 км, што може бити повећано путем употребе гранате HE RAP на 24 км, али се тада губи на прецизности.



Самоходна хаубица 2S3 *Akatsiya* 152 мм

Развијена је самоходна хаубица 2S3 са дужом цеви ради постизања већих даљина, али није јасно да ли је ушла у производњу, иако је понуђена страном тржишту.

Самоходна хаубица 2S3 допуњена је самоходном хаубицом MSTA-S 152 мм која је базирана на систему амортизације тенка Т-80 и дизел агрегату тенка Т-90. Опремљена је куполом са топом 152 мм 2А88, који је исти као и на вучној хаубици 2А65 152 мм. Максимална даљина гађања гранатом 152 мм OF-40 HE је 24,7 км, а увећава се гранатом OF-61 HE RAP до даљине 29,06 км.

У употреби је и граната 3OF64 HE *Base Bleed* са даљином гађања до 24,4 км. Новији пројектил 3OF61 HE-FRAG BB омогућава постизање даљине до 29 км. Зрна 152 мм се аутоматски пуне док се погонска

пуњења пуне ручно, а чаура се избацује са доње стране куполе након испалења.

Самоходна хаубица 2S19 је модернизована на верзије 2S19M, 2S19M1 (ASUNO FCS), 2S19M2 и MSTA-S и у њој је потпуно промењен систем за управљање ватром. Нови СУВ (систем за управљање ватром) укључује аутоматско нишањење које смањује време потребно за почетак дејства и уноси податке од радара за мерење брзине пројектила на устима цеви који се налази изнад цеви хаубице и аутоматски преноси податке након сваког испалења.

Самоходна хаубица 2S19M2 сада носи назив 2S33 (MSTA-SM 2) и већ је у оперативној употреби руске војске. Поручено је 42 возила која ће бити испоручена до краја 2019. године.

Русија је тестирала верзију самоходне хаубице 2S19 са стандардном НАТО муницијом 155 мм/52 за извозно тржиште под ознаком 2S19M1-155 која није ушла у серијску производњу.

Верзија са калибром 155 мм користи систем за управљање ватром ASUNO и погонске елементе тенка Т-90. Руски извори тврде да 2S19M1-155 има максимални домет до 30 км употребљавајући стандардни НАТО пројектил L15 HE калибра 155 мм који је развијен за хаубицу FH-70 максималног домета до 41 км, користећи гранате типа ERFB-BB (Extended Range Full Bore – Base Bleed). Самоходна хаубица носи до 45 граната са пуњењима.

Русија у свом арсеналу поседује два самоходна артиљеријска система већег калибра: 203 мм 2S7 *Pion* и минобацач 2S4 *Tyulpan*. Ова оруђа раније су била избачена из активне употребе и премештена у резерву.

Након догађаја у Украјини примећено је да је део ових оруђа ремонтован и враћен у активну оперативну употребу, али и да ова возила користе и проруске снаге и украјинска војска. Оруђа се употребљавају због свог великог домета, што им омогућује дејство ван установљених зона екслузије.

Самоходна хаубица 2S7 *Pion* испалењује дводелну муницију са максималним дометом до 37 км, док граната HE RAP има домет и до 47,5 км. Самохотка у борбеном комплету има само 4 гранате калибра 203 мм, а додатна муниција се превози специјалним возилом. Модернизована верзија 2S7M у свом борбеном комплету има осам граната, док је каденца паљбе само 2 гранате у минути. С обзиром на велики домет, самоходна хаубица 2S7M може напустити свој ватрени положај и пре него што гранате детонирају на удаљеном циљу.



Самоходна хаубица 2S7 Пион

Самоходни минобацач 2S4 240 мм испаљује конвенционалну високоексплозивну мину парчадног дејства на даљину до 9,65 км или мину типа HE-FRAG RAP на даљину до 18 км. Такође, испаљује и ласерски навођену мину *Smelchak* против мета високих вредности до даљине од 9,65 км, а по неким извештајима овакви навођени пројектили испробани су у Сирији.



Самоходни минобацач 2S4 240 мм

Вучна и самоходна оруђа точкаши

Многе државе дају предност самоходним артиљеријским оруђима точкашима над вучном артиљеријом, због ниже цене и веће стратегијске мобилности.

У овој области Русија је развила прототип самоходног артиљеријског система базираног на камиону Камаз 6560 8X8. На задњем делу камиона налази се купола наоружана топом 152 мм, док се на свакој страни куполе налазе уређаји за стабилизацију.

Са друге стране, Руска војска користи велики број вучних артиљеријских система, као што су D-30 122 мм, 2А36 152 мм и 2А65 152 мм.

Ради одржавања старих вучних система на нивоу захтева модерног бојишта, руска компанија *Russian Artillery Plant No 9* развила је и тестирала пакет за модернизацију вучног артиљеријског система D-30 под ознаком D-30А који користи топ 2А18М. Модернизација подразумева полуаутоматски систем пуњења, хромирану цев, нову колевку топа и модификовани систем трзања. Што се тиче балистичких особина ово оруђе остаје исто као и првобитни D-30 од 122 мм.

Русија је, такође, развила одређени број нових вучних артиљеријских система који још нису ушли у серијску производњу, иако су понуђени извозном тржишту. Ради се о артиљеријском систему 2А45М-155 (противтенковски топ SPRUT-В 2А45М чија је цев замењена са цеви 155 мм дужине 39 калибра).

Компанија *Russian Artillery Plant No 9* такође је пројектовала јуришни топ 122 мм М-392 који је понуђен за извоз. Главни недостатак овог система је врло кратак домет – до 8,6 км, јер користи муницију за руску хаубицу М1938 која је стара више од 80 година.

Развој система Koalitsya-SV

У току је развој самоходног артиљеријског система 152 мм под ознаком 2S35 *Koalitsya-SV* која је базирана на компонентама тенка Т-90, али се у будућности очекује да основа ове самоходне хаубице ипак буду модули система *Армата*.

Koalitsya-SV има посаду од три члана који се налазе у капсули на предњој страни возила. Купола је даљински управљана и наоружана новим топом 2А88 152 мм који има дужу цев у односу на претходне верзије, а опремљен је системом за избацивање дима и противтрзајном кочницом на цеви. Гранате се пуне преко аутоматског пуњача под било којим углом; прво се пуни пројектил, а затим пуњење. Тврди се да нова самоходна хаубица има брзину гађања чак до 16 граната у минути.

Цев је опремљена течним системом хлађења који хлади комору након сваког испаљења. Топ је опремљен микроталасним системом паљења који пали специјални микроталасни сензор на пуњењу. Овај

систем је бољи од претходног због мањег броја покретних делова, конзистентног интервала гађања и повећања брзине гранате у цеви.

Поред тога, *Koalitsya-SV* је опремљена са два радара, типа доплер, који су монтирани са сваке стране примарног наоружања. Они мере брзину граната и израчунавају предвиђено место удара, што омогућава систему за контролу ватре корекцију ватре и пре него што експлодира прва граната.



Koalitsya-SV

Koalitsya-SV има могућност удара са више граната на исти циљ када се употребљава различита елевација цеви. С обзиром на различите путање свака граната има своје време до циља.

Платформа има нови асортиман муниције са максималном даљином до 70 км. Гранате су потпомогнуте ракетним мотором за постизање максималног домета, али хаубица може испаливати и стандардну муницију 152 мм на краћим раздаљинама. Прецизност је повећана употребом пројектила са контролним крилцима на носу који употребљавају руски глобални навигациони сателитски системи.

Русија је тестирала најмање два различита упаљача који су намењени за кориговање курса. Први ради слично упаљачу SPACIDO компаније Nexter, који прима сигнал са радара система *Koalitsya* након чега користи ваздушне кочнице за мењање путање у лету. Други упаљач се наводи путем система GLONASS и сличан је комплекту за прецизно навођење *Orbital* ATK M1156, али је још у фази развоја.

Колико је тренутно познато, најновије платформе 2S35 *Koalitsya-SV* замениће вучне хаубице 2A65 MSTA-B.

Напредна муниција

Поред упаљача који омогућују промену путање, руска компанија *KBP Instrument Design Bureau* пројектовала је комплетну породицу ласерски навођених пројектила за калибре 122 мм, 152 мм и 155 мм за артиљеријска оруђа и за минобацачке мине 120 мм. То су гранате 122 мм *KM-3 Kitolov-2M*, 152 мм *2K25 Krasnopol*, 155 мм и минобацачку мину *KM-1 Krasnopol* 120 мм *KM-8 Gran*. Већина ових нових решења већ је успешно испробана у Сирији.

Гранате 155 *KM-1 Krasnopol* продате су Индији за употребу у њиховим вучним хаубицама *Bofors FH-77* које су коришћене у борбама на индијско-пакистанској граници. Француска је купила одређену количину за тестирање у својим самоходним артиљеријским системима *GCT 155* мм. Ове ласерски навођене гранате имају високоексплозивну бојеву главу парчадног дејства и полу-активни ласерски трагач и захтевају осветљавање циља до удара, што може бити компликовано, нарочито када је лоше време. За навођење оваквих граната Русија има ласерске даљиномере/означиваче типа *1D20*, *1D22* или *1D26*, два радио-уређаја и помоћне уређаје за синхронизацију. Ласерски навођени пројектили 152 мм имају максимални домет до 20 км, а домет ласерских означивача је до 7 км. Ласерски навођени пројектили 155 мм имају дужи домет и то до 25 км.

Руска компанија *KBP Instrument Design Bureau* пројектовала је преносни аутоматизовани артиљеријски систем за контролу ватре *Malakhit* који контролише лет ласерски навођених пројектила, као и конвенционалних артиљеријских граната. Ови системи укључују дневно/ноћни систем за аквизицију циљева и навигациони систем, компјутер командира и одашиљаче на топовима. Систем је пројектован за батерију од шест оруђа. Русија, такође, развија и рамџет технологију за своју артиљерију од 152 мм и 203 мм. За пројектил од 203 мм очекује се повећање домета до 70 км. Развијени су и пројектили 152 мм за напад на горњи део циља, а употребљавају се касетне гранате 122 мм и 152 мм за напад на оклопна борбена возила.

Чланице НАТО-а (осим САД) избациле су из употребе своје касетне артиљеријске гранате на основу Конвенције о касетној муницији из 2008 године.

Руска војска је развила знатан број оклопних борбених возила за употребу у артиљеријским јединицама. У питању су артиљеријска командна и извиђачка возила за употребу на нивоу батерије и батаљона.

Mashina-M је аутоматизовани систем за контролу ватре који је предвиђен за употребу на нивоу батаљона, батерије, команде батаљона и командног официра батерије. Систем прима информације од истурених посматрача, обрађује их и шаље батеријама. Очекује се да ће будуће руске копнене снаге умногоме зависити од аутоматизованих *C2* система.

Модернизовано је и артиљеријско извиђачко возило *PRP-4A* које се заснива на возилима *BMP-1/BMP-2*, али је опремљено новом куполом са

комплетном опремом за надзор и аквизицију циљева као што су комуникациона опрема, навигациони систем, радар за осматрање бојишта, ласерски даљиномер и дневно/ноћне термалне камере.



Артиљеријско извиђачко возило PRP-4A

Старији радар за лоцирање артиљеријске и минобацачке ватре SNAR-10, који се налази на возилу MT-LB, модернизован је новим радаром већег домета и веће прецизности и сада носи ознаку SNAR-10M. Руски преносни радар за лоцирање минобацача *Austenok* открива покретне циљеве на даљинама до 20 км, а много већи радар за откривање артиљеријских положаја 1L260-E има максимални домет до 65 км и користи се за корекцију артиљеријске и ракетне ватре. Русија је демонстрирала способност захватања и напада на циљеве која је импресионирала команданте НАТО-а. Руска артиљерија постаје приоритет руских копнених снага, што потврђује и скоро увођење система *Koalitsya-SV*.

Недавни извештаји америчке војске показују да је дошло до измена у доктрини руске војске, што подразумева употребу вишецевних бацача ракета у улогама директног ватреног напада, као и измене у начину напада на уочене циљеве са неприпремљених позиција. Русија поставља као приоритет аутоматизацију система С2 и система за контролу ватре. Уколико дође до успешне асимилације ових система са беспилотним летелицама за проналажење циљева доћи ће до вишеструког повећања већ сада импресивне убојне моћи руских копнених снага.

Драган М. Вучковић (*Dragan M. Vučković*),
e-mail: draganvuckovic@kbcnet.rs,
ORCID iD:  <http://orcid.org/0000-0003-1620-5601>

Тенк М-91 Vihor: југословенски тенк са америчком и руском ДНК²

Војна индустрија била је једна од најразвијенијих индустријских грана у бившој СФРЈ. За време хладног рата СФРЈ је балансирао између Истока и Запада, набављајући и развијајући домаће оружане системе засноване на технологијама обе стране. Један од најбољих производа југословенске војне индустрије, а можда и најбољи, био је тенк М-91 Vihor.

Југословенска тенковска индустрија почиње да се развија касних четрдесетих година прошлог века, након разлаза Тита и Стаљина. Како је у том периоду Совјетски Савез блокирао извоз својих тенкова Југославији, а истовремено је постојала и опасност од инвазије, на Титову иницијативу руководство фабрике „Петар Драпшин“ кренуло је у реализацију задатка. Произведено је шест тенкова који су били засновани на тенку Т-34/85 под ознаком *Тip А*.

Ипак, то није било довољно, па су југословенске власти направиле договор са Сједињеним Државама (у време добрих односа са Западом) за испоруку војне помоћи. Тада је набављен одређен број тенкова *M4A3E4 Sherman*, *M47 Patton*, *M18 Hellcat*, и *M36/M36B1 Jackson*. Након тога, у периоду отопљавања односа са СССР-ом, крајем педесетих година прошлог века СФРЈ је набавила совјетске тенкове типа Т-55, Т-54А, SU-100 и Т-34 Обг. 1960. Ови тенкови су касније замењени новијим типа Т-55А које је донирао СССР, а ради замене старијих модела истога тенка које је СФРЈ испоручила Египту током Јомкипурског рата са Израелом 1973. године.

Овакав извозни посао представљао је темељ за добре односе са СССР-ом, Тада је настојано да се дође до тенка Т-72, али то није ишло по плану. Чехословачка и Пољска добиле су лиценце за производњу овог тенка пре Југославије, што им је омогућавало десет година производње или укупан број до хиљаду комада, као и куповину одређеног броја тенкова типа Т-72М и Т-72МК.

Фабрике широм Југославије учествовале су у производњи југословенске верзије Т-72 под ознаком Т-72МЈ. Први Т-72МЈ изашао је из фабрике 1983. године и разликовао се од осталих верзија Т-72М по потпуно дигитализованом систему за управљање ватром, који се производио у Словенији, а по својим карактеристикама био је врло сличан тадашњим системима нових западних тенкова.

Југословенски инжењери увели су многа побољшања у односу на првобитну верзију Т-72М. Прецизност је била прва на листи унапређења. Метео-сензор је одмах додат, стабилизациони механизам је унапређен додатним жироскопима, а на крају је додат и потпуно дигитализовани

² The National Interest 02 July 2018

систем за управљање ватром. Ова унапређења резултирала су верзијом М-84, југословенском верзијом Т-72.

Године 1987. изашао је и унапређени модел М-84А који је имао оклоп унапређен на стандард руског тенка Т-72М1, али и нови мотор од хиљаду коњских снага V-46ТК, што је довело до знатно веће брзине и тактичке мобилности тенка. Међутим, производња тенка М-84 и М-84А, упркос новим називима, ипак је била ограничена на хиљаду примерака под оригиналном лиценцом за производњу Т-72.

Ради превазилажења овог ограничења, 1987. године тадашње руководство започиње нови пројекат под називом „Нови домаћи тенк“. Овај пројекат, који је предводио Војнотехнички институт у Београду, касније је добио ознаку М-91 *Vihor*. Било је предвиђено да прва тестирања започну током 1991. године, да се прва серија прототипова произведе до 1993. године, како би се до 1994. године почело са серијском производњом.



Тенк *Vihor*

Због распада СФРЈ, које је започето 1991. године, само су три шасије и три куполе биле комплетиране.

У суштини, *Vihor* представља наставак развоја серије тенкова М-84. Иако је заснован на истој филозофији употребе аутоматског пуњача и трочлане посаде, његова концепција је далеко одмакла од оригиналног Т-72. Срце новог тенка је модернизовани погонски агрегат. Иако је М-84А располагао са знатно јачим мотором од хиљаду коњских снага у односу на М-84, снага мотора тенка *Vihor* је још импресивнија. Ради се о турбопрехрањиваном дизел мотором ознаке V-46TK1 који је могао погонити масивни тенк брзином од око 75 километара на сат и убрзањем од седам секунди од 0 до 32 км/ч, што је било једнако или брже у односу и на тенкове са гасним турбинама из тог периода. Погонски точкови су редизајнирани, а вертикална висина на путу подигнута је са 280 мм на 350 мм, што је омогућило још бољу теренску проходност (и до 50 км/ч ван путева), а и било је много више у односу на оригинални Т-72. Погонски део тенка са прототипом шасије и куполе интензивно је тестиран са више од пређених петнаест хиљада километара.

Основно наоружање тенка представља топ 2А46М, исти онај којим је наоружан и Т-72. Пројектован је нови термални прекривач топа и нови референтни сензор на устима цеви топа (као и на западним тенковима). Предвиђена је могућност брзе замене топа. Аутоматски пуњач је унапређен у односу на пуњач AZ-72 са тенка Т-72 који је омогућавао бидирекционални покрет сличан решењу са тенка Т-64, што је повећало ефикасност и брзину пуњења (до десет граната у минути). Прецизност је повећана употребом метео-станице и комплета сензора која је мерила температуру и тачну тежину погонског експлозивног пуњења.

Хидраулично покретање куполе је замењено електричним механизмом са брзином окретања до 50 степени у секунди, што је више од два пута брже од окретања куполе оригиналног тенка Т-72. Муниција је била боље заштићена, од дубине пробоја до 554 мм на даљинама до 2500 метара, што је било сасвим довољно за заштиту од тада постојећих тенковских топова.

Развијен је заптивач на поткалибарном зрну од бакелита уместо претходног који је био састављен од бакра ради умањења растурања зрна. Совјети су касније прешли на заптивач од алуминијума.

Нишански системи били су у рангу западних нишанских справа са дигиталним зумирањем, ласерским даљиномерима, трећом генерацијом ноћних нишанских справа и термалним нишанским уређајима. Ипак, командир тенка имао је само дневно/ноћну нишанску справу без термалног уређаја, иако је имао пред собом екран којим је имао преглед термалне нишанске справе нишанције, а и могућност ротирања куполе према циљу који је пратио преко своје нишанске справе. Пријемник ласерског озрачења такође је инсталиран на куполи. Овај систем је

поседовао одређен степен одбране од надолазеће претње тако што би по детекцији ласерског озрачења окретао куполу према надолазећој претњи (противоклопној ракети) и активирао димне кутије. Овај систем је извожен и у друге земље. Коначно, *Vihor* је био опремљен шифрованим радио-уређајем са аутоматским пребацивањем фреквенција, уређајем сличним америчком систему SINCGARS. Оклоп тенка *Vihor* следио је исту филозофију која је примењивана и на совјетским тенковима. Употребљен је композитни оклоп на куполи и шасији са мешавином силицијум-карбида, алуминијума, гуме и слоја легуре испуњене кварцним песком и смолом. Нови оклоп је 3,5 тоне тежи од оклопа на тенку М-84А, што је одговарало оклопу тенка Т-72М1. Планирано је и постављање експлозивно-реактивног оклопа под ознаком М-99, али је тај програм завршен тек 1998, године. Овакав експлозивно-реактивни оклоп био је по својој ефикасности између совјетског оклопа *Kontakt-1* и *Kontakt-5* са ограниченом способношћу заштите од зрна са кинетичком енергијом.

С обзиром на распад Југославије, *Vihor* није никада ушао у серијску производњу, а имајући у виду да су многе републике, бивше чланице СФРЈ, производиле делове тенка, они су током грађанског рата коришћени за поправке и модернизације њихових тенкова М-84. Хрватска је чак успела да склопи један цели тенк *Vihor* који је додуше завршен деловима тенка М-84. По неким изворима тај тенк је учествовао у операцији заробљавања базе ЈНА у Дегману. По завршетку грађанског рата Хрватска је развила свој *Vihor* у тенк под ознаком М-95 *Degman* на који је смештен додатни композитни оклоп и нова електроника. Данас постоје два примерка М-95 *Degman* у Хрватској.

Већ 1991. године бивша СФРЈ била је на добром путу да развије тенк који би био конкурентан тадашњим западним и источним тенковима. То је могао да буде изузетно исплатив извозни посао, имајући у виду да би тај тенк био много јефтинији од тенкова сличних или лошијих карактеристика, а нарочито америчког Abramsa. С обзиром на успешан извоз тенкова М-84 Кувајту било је питање времена када би се нека следећа богата заливска земља одлучила за увоз тенка *Vihor*, што би неким западним земљама одузело огромна финансијска средства.

Осим тенка *Vihor*, Југославија је била на путу да развије и понуди врло интересантну лепезу модерног наоружања које по својим особинама није нимало заостајало за оружаним системима западног или источног порекла, али, наравно, по много приступачнијим ценама. На крају се поставља питање колико је развој југословенске одбрамбене индустрије утицао на почетак грађанског рата и распад СФРЈ...

Драган М. Вучковић (*Dragan M. Vučković*),
e-mail: draganvuckovic@kbcnet.rs,

ORCID iD:  <http://orcid.org/0000-0003-1620-5601>

Конструкцијски развој аутоматских пушака

Једна од најупечатљивијих карактеристика оружаних сукоба, посебно у модерном добу¹, свакако је изразита променљивост, у објективном и субјективном смислу. Окружење, тактика и други значајни атрибути врло су различити, а неретко се дешава и да се исти сукоб у свом трајању мења, скоро без правила. Управо искуства из оваквих ситуација у највећој мери обликују и тражњу на тржишту наменске индустрије, условљавајући произвођаче да својим производним програмима у што већој мери задовољавају очекивања купаца.



*Карабини „Colt M4 A4”, калибра 5,56 mm, прилагођени потребама блиске борбе.
Фото: Милош Јевтић*

Посебно је упадљиво да се данас неке од најреспектабилнијих армија у свету одлучују на „раскидање са традицијом”, тј. на замену основних борбених аутоматских пушчаних система, међу којима су неки деценијама били у употреби. Један од најупечатљивијих примера свакако је уговор између француске Генералне дирекције за наоружање (фра. Direction Générale de l'Armement) и компаније „Heckler & Koch”, потписан

¹ Природа оружаних сукоба се, наравно, мења у складу са технолошким и техничким развојем. Почетком двадесетог века њихова динамичност постаје очигледнија, јер је, поред осталог, убрзани развој знатно олакшао кретање људи, робе, информација, а имао и примену у наменској индустрији.

22. септембра 2016. године,² о набавци контингента система „HK 416F”, у калибру 5,56 mm, ради замене традиционалног француског „FAMAS F1”. Јасно је, дакле, да променљивост оружаних сукоба и савремених извора небезбедности (претњи и изазова) изискују и адаптације оружаних снага, поред осталог, и константним усавршавањем наоружања, опреме и средстава у употреби.

Сазнања и анализе из тренутно актуелних оружаних сукоба на Блиском истоку појачала су потребу за системима који стрелцу могу поуздано омогућити ангажовање мета на средњим дистанцама, али исто тако и ефективно дејствовање у скученом простору, посебно у урбаном окружењу (енг. close quarters battle – CQB). Јасно је да овакве потребе у највећој мери долазе од оператера снага за специјалне операције (енг. special operations forces – SOF), за које је императив да им примарни борбени систем буде способан да одговори потребама савременог борбеног окружења (енг. contemporary operating environment – COE).

Може се закључити да је врло тешко, а у овом моменту можда и немогуће, пронаћи један систем који би могао задовољити врло различите захтеве COE у одговарајућој мери. Свесни тога, произвођачи марљиво раде на увећању модуларности пушчаних система, дајући тако могућност крајњим корисницима да различитим конфигурацијама оптоелектронских и других уређаја, односно конструкцијских додатака, прилагођавају исто оружје различитим потребама на терену.

Трендови

До пре само неколико година један од главних захтева које је респектабилна јуришна пушка (енг. assault rifle) морала да задовољи на тржишту односио на што дуже бројне (најчешће по распореду 12-3-6-9) носаче „Picatinny” шина, ради прихвата различитих уређаја, па се често догађало да укупна маса монтираних уређаја буде скоро једнака маси оружја! С тим у вези, умањивање укупне масе оружја је поново добило на значају, уз увек актуелне захтеве за увећање прецизности паљбе. Наравно, шине су и даље веома важан стандард у производњи³, али изгледа да најновији трендови мењају начин на који се шине интегришу у или на сандук система.

Поред тога, за модерне SOF оператере пригушивачи пуцња постали су необично важан елемент конфигурације⁴, о чему сведочи и тренутно увећана тражња на тржишту. Рад са монтираним пригушивачем пуцња је велики изазов за конструкцију система, посебно у смислу прегревања и

² Вредност уговора износи 168 милиона евра (177 милиона USD).

³ Употреба оптоелектронских и других уређаја омогућава обученом стрелцу да оствари тактичку предност у веома измењеним условима савременог борбеног окружења.

⁴ На пример, доприносе смањењу буке при раду, умањују трзај при паљби и др.

прљања, а не треба занемарити ни увећање укупне дужине оружја, односно масе са монтираним пригушивачем.

Управо ова тенденција поставила је нове изазове пред конструкторе: који принцип рада одабрати, како умањити укупну масу оружја⁵, како сачувати компактност и како умањити могућност прегревања оружја при раду⁶. Одговор појединих произвођача био је генијалан. Тржиште је постало богатије за конструкције у виду горњег дела сандука са слободном цеви (енг. free floating handguard), што значи да сама облога не додирује цев, чиме се добија на прецизности паљбе оружја. Додатно, облоге су, по правилу, „избушене“ отворима правилног облика (примера ради, веома популарне „KeyMod“ и „M-Lok“ облоге) , чиме се истовремено штеди на маси и успорава прегревање система при дужем раду и/или у екстремним климатским условима. Такође, ти отвори омогућавају прихват оптоелектронских и других уређаја⁷, те стандардне „Picatinny“ шине нису неопходне. Шине су, по правилу, ипак задржане, али се примећује да се многи произвођачи одлучују за постављање носача само на горњу страну сандука⁸, чиме, опет, штеде на маси.



Горњи део сандука са интегрисаним пригушивачем пуцња „SIG SUR300“. Фото: Chris Heuss.

Имајући у виду актуелну увећану тражњу за пригушивачима пуцња, неколико светских произвођача одлучило се да понуди ове конструкције са специфичним, интегрисаним⁹ пригушивачима пуцња (енг. suppressed upper

⁵ Овај проблем био је врло занимљив, првенствено због тога што је употреба лаких, композитних материјала већ устаљена пракса, па се на маси морало уштедети на други начин.

⁶ До прегревања долази када је оружје изложено непрекидном или високофреквентном раду у одређеном периоду. Одговарајућом конструкцијом система овај период се може продужити.

⁷ Монтирање је брзо и једноставно; уређај са носачем монтира се помоћу „имбус“ кључа.

⁸ На захтев купца шине се, наравно, могу поставити бочно и/или на доњој страни.

⁹ Конструкције се, опционо, могу испоручити са навојима за монтирање пригушивача пуцња.

receiver group – SURG). С тим у вези, веома је значајна вест од 27. јула 2018. године, којом је потврђено да је компанија „SIG Sauer Inc” потписала петогодишњи уговор, вредан 48 милиона америчких долара, којим се обавезује на неодређену испоруку и неодређену количину („...indefinite-delivery/indefinite-quantity...”¹⁰) SURG конструкција америчкој Команди за специјалне операције (eng. USSOCOM). Ова вест је један у низу успеха које је компанија остварила у пословању са САД, а изгледа да је врло близу закључивања и посла око испоруке различитих система, међу којима је и све популарнија серија „SIG MCX”, што само потврђује увећању тржишну тражњу за компактним, лаганим, карабинским (енг. short barrel rifle – SBR) и пригушеним оружјем.

Компактност оружја дефинитивно остаје и даље важан захтев, па се од телескопских и/или преклапајућих кундака не одустаје, али се примећује популаризација изразито скелетних кундака, којима се максимално штеди на маси. Занимљиво је истаћи да је за своју серију „MCX” компанија конструисала и неколико модела алуминијумских кундака¹¹ који се монтирају на вертикално постављене „Picatinny” шине.

Закључак

Јасно је да динамичност тражње на тржишту могу да испрате само најбогатији произвођачи на свету. Чини се да најновији трендови полако али сигурно мењају конструкцију традиционалне јуришне, односно аутоматске пушке, те ће у наредним годинама бити веома занимљиво испратити овај процес до његове крајње форме, јер је питање како ће се то одразити на судбину аутомата (енг. submachine gun), који су у употреби од друге половине XX века.

Милош М. Јевтић (Miloš M. Jevtić), уредник сајта specijalne-jedinice.com,
e-mail: info@specijalne-jedinice.com,
ORCID ID: <http://orcid.org/0000-0002-1305-7618>

¹⁰ Цитат из званичног саопштења америчког Министарства одбране, број CR-144-18, 27. јула 2018.

¹¹ Примера ради, „С/Т MCX/MPX”, „Minimalist Folding MCX/MPX”.

ПОЗИВ И УПУТСТВО АУТОРИМА
ПРИГЛАШЕНИЕ И ИНСТРУКЦИИ ДЛЈА АВТОРОВ РАБОТ
CALL FOR PAPERS AND INSTRUCTIONS FOR AUTHORS

ПОЗИВ И УПУТСТВО АУТОРИМА О НАЧИНУ ПРИПРЕМЕ ЧЛАНКА

Упутство ауторима о начину припреме чланка за објављивање у *Војнотехничком гласнику* урађено је на основу Акта о уређивању научних часописа, Министарства за науку и технолошки развој Републике Србије, евиденциони број 110-00-17/2009-01, од 09. 07. 2009. године. Примена овог Акта првенствено служи унапређењу квалитета домаћих часописа и њиховог потпунијег укључивања у међународни систем размене научних информација. Засновано је на међународним стандардима ISO 4, ISO 8, ISO 18, ISO 215, ISO 214, ISO 18, ISO 690, ISO 690-2, ISO 999 и ISO 5122, односно одговарајућим домаћим стандардима.

Војнотехнички гласник / Vojnотехнички glasnik / Military Technical Courier (втг.мо.упр.срб, www.vtg.mod.gov.rs, ISSN 0042-8469 – штампано издање, е-ISSN 2217-4753 – online, UDC 623+355/359) јесте мултидисциплинарни научни часопис Министарства одбране Републике Србије, који објављује научне и стручне чланке, као и техничке информације о савременим системима наоружања и савременим војним технологијама. Часопис прати јединствену интервидовску техничку подршку Војске на принципу логистичке системске подршке, области основних, примењених и развојних истраживања, као и производњу и употребу средстава наоружања и војне опреме, те остала теоријска и практична достигнућа која доприносе усавршавању свих припадника српске, регионалне и међународне академске заједнице, а посебно припадника Министарства одбране и Војске Србије.

Министарство просвете, науке и технолошког развоја Републике Србије, сагласно одлуци из члана 27. став 1. тачка 4), а по прибављеном мишљењу из члана 25. став 1. тачка 5) Закона о научноистраживачкој делатности („Службени гласник РС”, бр. 110/05, 50/06-испр. и 18/10), утврдило је категоризацију Војнотехничког гласника, за 2017. годину:

за област технолошки развој:

– **на листи часописа за материјале и хемијске технологије:**

категирија водећи научни часопис националног значаја (**M51**),

– **на листи часописа за електронику, телекомуникације и информационе технологије:**

категирија научни часопис националног значаја (**M52**),

– **на листи часописа за машинство:**

категирија научни часопис националног значаја (**M52**),

за област основна истраживања:

– **на листи часописа за математику, рачунарске науке и механику:**

категирија научни часопис (**M53**).

Усвојене листе домаћих часописа за 2017. годину могу се видети на сајту Војнотехничког гласника, страница *Категоризација часописа* (Министарство просвете, науке и технолошког развоја Републике Србије још увек није објавило званичну категоризацију научних часописа за 2018. годину).

Детаљније информације могу се пронаћи и на сајту Министарства просвете, науке и технолошког развоја Републике Србије.

Подаци о категоризацији могу се пратити и на сајту КОБСОН-а (Конзорцијум библиотека Србије за обједињену набавку).

Категоризација часописа извршена је према Правилнику о поступку и начину вредновања и квантитативном исказивању научноистраживачких резултата истраживача, који је прописао Национални савет за научни и технолошки развој (Службени гласник РС, број 38/2008).

У складу са овим правилником и табелом о врсти и квантификацији индивидуалних научноистраживачких резултата (у саставу Правилника), објављени рад у Војнотехничком гласнику вреднује се са 2 бода (категирија М51), 1,5 бод (категирија М52) и 1 бод (категирија М53).

Часопис се прати у контексту Српског цитатног индекса – СЦИндекс (база података домаћих научних часописа) и Руског индекса научног цитирања (РИНЦ). Подвргнут је сталном вредновању (мониторингу) у зависности од утицајности (импакта) у самим базама и, посредно, у међународним (Clarivate Analytics) цитатним индексима. Детаљи о индексирању могу се видети на сајту Војнотехничког гласника, страница *Индексирање часописа*.

Војнотехнички гласник омогућава и примењује Creative Commons (CC BY) одредбе о ауторским правима. Детаљи о ауторским правима могу се видети на сајту часописа, страница *Ауторска права и политика самоархивирања*.

Радови се предају путем онлајн система за електронско уређивање АСИСТЕНТ, који је развио Центар за евалуацију у образовању и науци (ЦЕОН).

Приступ и регистрација за сервис врше се на сајту www.vtg.mod.gov.rs, преко странице АСИСТЕНТ или СЦИНДЕКС, односно директно на линку aseestant.ceon.rs/index.php/vtg.

Детаљно упутство о регистрацији и пријави за сервис налази се на сајту www.vtg.mod.gov.rs, страница *Упутство за е-Ур: Електронско уређивање – АСИСТЕНТ*.

Потребно је да се сви аутори који подносе рукопис за објављивање у Војнотехничком гласнику региструју у регистар ORCID (Open Researcher and Contributor ID), према упутству на страници сајта *Регистрација за добијање ORCID идентификационе шифре*.

Војнотехнички гласник објављује чланке на српском, руском и енглеском језику (arial, српска ћирилица или српска латиница, величина слова 11 pt, проред Single).

Поступак припреме, писања и уређивања чланка треба да буде у сагласности са *Изјавом о етичком поступању* (<http://www.vtg.mod.gov.rs/izjava-o-etickom-postupanju.html>).

Чланак треба да садржи сажетак са кључним речима, увод, разраду, закључак, литературу и резимеа са кључним речима на енглеском и руском језику (без нумерације наслова и поднаслова). Обим чланка треба да буде око једног ауторског табака (16 страница формата А4 са проредом Single), а највише 24 странице.

Чланак треба да буде написан на обрасцу за писање чланка, који се у електронској форми може преузети са сајта на страници *Образац за писање чланка*.

Наслов

Наслов треба да одражава тему чланка. У интересу је часописа и аутора да се користе речи прикладне за индексирање и претраживање. Ако таквих речи нема у наслову, пожељно је да се придода и поднаслов. Наслов треба да буде преведен и на енглески и руски језик.

Ови наслови исписују се испред сажетка на одговарајућем језику.

Текући наслов

Текући наслов се испишује са стране сваке странице чланка ради лакше идентификације, посебно копија чланака у електронском облику. Садржи презиме и иницијал имена аутора (ако аутора има више, преостали се означавају са „et al.“ или „и др.“), наслове рада и часописа и колацију (година, волумен, свеска, почетна и завршна страница). Наслови часописа и чланка могу се дати у скраћеном облику.

Име аутора

Наводи се пуно име и презиме (свих) аутора. Веома је пожељно да се наведу и средња слова аутора. Имена и презимена домаћих аутора увек се испишују у оригиналном облику (са српским дијакритичким знаковима), независно од језика на којем је написан рад.

Назив установе аутора (афилијација)

Наводи се пун (званични) назив и седиште установе у којој је аутор запослен, а евентуално и назив установе у којој је аутор обавио истраживање. У сложеним организацијама наводи се укупна хијерархија (нпр. Универзитет одбране у Београду, Војна академија, Катедра природно-математичких наука). Бар једна организација у хијерархији мора бити правно лице. Ако аутора има више, а неки потичу из исте установе, мора се, посебним ознакама или на други начин, назначити из које од наведених установа потиче сваки од наведених аутора. Афилијација се испишује непосредно након имена аутора. Функција и звање аутора се не наводе.

Контакт подаци

Адреса или е-адреса свих аутора даје се поред имена и презимена аутора.

Категорија (тип) чланка

Категоризација чланака обавеза је уредништва и од посебне је важности. Категорију чланка могу предлагати рецензенти и чланови уредништва, односно уредници рубрика, али одговорност за категоризацију сноси искључиво главни уредник.

Чланци у часописима се разврставају у следеће категорије:

Научни чланци:

1. оригиналан научни чланак (рад у којем се износе претходно необјављивани резултати сопствених истраживања научним методом);
2. прегледни чланак (рад који садржи оригиналан, детаљан и критички приказ истраживачког проблема или подручја у којем је аутор остварио одређени допринос, видљив на основу аутоцитата);
3. кратко или претходно саопштење (оригинални научни рад пуног формата, али мањег обима или прелиминарног карактера);
4. научна критика, односно полемика (расправа на одређену научну тему, заснована искључиво на научној аргументацији) и осврти.

Изузетно, у неким областима, научни рад у часопису може имати облик монографске студије, као и критичког издања научне грађе (историјско-архивске, лексикографске, библиографске, прегледа података и сл.) – дотад непознате или недовољно приступачне за научна истраживања.

Радови класификовани као научни морају имати бар две позитивне рецензије.

Ако се у часопису објављују и прилози ваннаучног карактера, научни чланци треба да буду груписани и јасно издвојени у првом делу свеске.

Стручни чланци:

1. стручни чланак (прилог у којем се нуде искуства корисна за унапређење професионалне праксе, али која нису нужно заснована на научном методу);
2. информативни прилог (уводник, коментар и сл.);
3. приказ (књиге, рачунарског програма, случаја, научног догађаја, и сл.).

Језик рада

Језик рада може бити српски, руски или енглески.

Текст мора бити језички и стилски дотеран, систематизован, без скраћеница (осим стандардних). Све физичке величине морају бити изражене у Међународном систему мерних јединица – SI. Редослед образаца (формула) означава се редним бројевима, са десне стране у округлим заградама.

Сажетак (апстракт) и резиме

Сажетак (апстракт) јесте кратак информативан приказ садржаја чланка који читаоцу омогућава да брзо и тачно оцени његову релевантност. У интересу је уредништава и аутора да сажетак садржи термине који се често користе за индексирање и претрагу чланака. Саставни делови сажетка су циљ истраживања, методи, резултати и закључак. Сажетак треба да има од 100 до 250 речи и треба да се налази између заглавља (наслов, имена аутора и др.) и кључних речи, након којих следи текст чланка. Ако је рад написан на српском или руском језику, пожељно је да се, поред сажетка на српском и руском, даје и сажетак у проширеном облику на енглеском језику – као тзв. резиме (summary). Овакав резиме треба да буде на крају чланка, након одељка Литература. Важно је да резиме буде у структурираном облику, а његова дужина може бити до 1/10 дужине чланка (опширнији је од сажетка са почетка чланка). Почетак овог резимеа може бити преведени сажетак (са почетка чланка), а затим треба да следе преведени главни наслови, поднаслови и основе закључка чланка (литература се не преводи). Потребно је да се у структурираном резимеу преведе и део текста испод наслова и подналова, водећи рачуна да он буде пропорционалан њиховој величини, а да одражава суштину. Након резимеа на енглеском језику (проширеног сажетка) додаје се његов превод на српском, да би редакција извршила проверу и лектуру.

Кључне речи

Кључне речи су термини или фразе које адекватно представљају садржај чланка за потребе индексирања и претраживања. Треба их додељивати ослањајући се на неки међународни извор (попис, речник или тезаурус) који је најшире прихваћен или унутар дате научне области. За нпр. науку уопште, то је листа кључних речи Web of Science. Број кључних речи не може бити већи од 10, а у интересу је уредништва и аутора да учесталост њихове употребе буде што већа. Кључне речи дају се на језику на којем је написан чланак (сажетак) и на енглеском језику. У чланку се пишу непосредно након сажетка, односно након резимеа.

Систем АСИСТЕНТ у ту сврху користи специјалну алатку KWASS: аутоматско екстраховање кључних речи из дисциплинарних тезауруса/речника по избору и рутине за њихов одабир, тј. прихватање односно одбацивање од стране аутора и/или уредника.

Датум прихватања чланка

Датум када је уредништво примило чланак, датум када је уредништво коначно прихватило чланак за објављивање, као и датуми када су у међувремену достављене евентуалне исправке рукописа наводе се хронолошким редоследом, на сталном месту, по правилу на крају чланка.

Захвалница

Назив и број пројекта, односно назив програма у оквиру којег је чланак настао, као и назив институције која је финансирала пројекат или програм, наводи се у посебној напомени на сталном месту, по правилу при дну прве стране чланка.

Претходне верзије рада

Ако је чланак у претходној верзији био изложен на скупу у виду усменог саопштења (под истим или сличним насловом), податак о томе треба да буде наведен у посебној напомени, по правилу при дну прве стране чланка. Рад који је већ објављен у неком часопису не може се објавити у Војнотехничком гласнику (прештампати), ни под сличним насловом и измењеном облику.

Табеларни и графички прикази

Пожељно је да наслови свих приказа, а по могућству и текстуални садржај, буду дати двојезично, на језику рада и на енглеском језику.

Табеле се пишу на исти начин као и текст, а означавају се редним бројевима са горње стране. Фотографије и цртежи треба да буду јасни, прегледни и погодни за репродукцију. Цртеже треба радити у програму word или corel. Фотографије и цртеже треба поставити на жељено место у тексту.

За слике и графиконе не сме се користити снимак са екрана рачунара програма за прикупљање података. У самом тексту чланка препоручује се употреба слика и графикона непосредно из програма за анализу података (као што су Excel, Matlab, Origin, SigmaPlot и други).

Навођење (цитирање) у тексту

Начин позивања на изворе у оквиру чланка мора бити једнообразан.

Војнотехнички гласник за референцирање (цитирање и навођење литературе) примењује Харвардски систем референци, односно Харвардски приручник за стил (Harvard Referencing System, Harvard Style Manual). У самом тексту, у обичним заградама, на месту на којем се врши позивање, односно цитирање литературе набројане на крају чланка, обавезно у обичној загради написати презиме цитираног аутора, годину издања публикације из које цитирате и, евентуално, број страница. Нпр. (Petrović, 2012, pp.10–12).

Детаљно упутство о начину цитирања, са примерима, дато је на страници сајта *Упутство за Харвардски приручник за стил*. Потребно је да се позивање на литературу у тексту уради у складу са поменутиим упутством.

Систем АСИСТЕНТ у сврху контроле навођења (цитирања) у тексту користи специјалну алатку CiteMatcher: откривање изостављених цитата у тексту рада и у попису референци.

Напомене (фусноте)

Напомене се дају при дну стране на којој се налази текст на који се односе. Могу садржати мање важне детаље, допунска објашњења, назнаке о коришћеним

изворима (на пример, научној грађи, приручницима), али не могу бити замена за цитирану литературу.

Листа референци (литература)

Цитирана литература обухвата, по правилу, библиографске изворе (чланке, монографије и сл.) и даје се искључиво у засебном одељку чланка, у виду листе референци. Референце се не преводe на језик рада и набрајају се у посебном одељку на крају чланка.

Војнотехнички гласник, као начин исписа литературе, примењује Харвардски систем референци, односно Харвардски приручник за стил (Harvard Referencing System, Harvard Style Manual).

Литература се обавезно пише на латиничном писму и набраја по абecedном редоследу, наводећи најпре презимена аутора, без нумерације.

Детаљно упутство о начину пописа референци, са примерима, дато је на страници сајта *Упутство за Харвардски приручник за стил*. Потребно је да се попис литературе на крају чланка уради у складу са поменутиm упутством.

Нестандардно, непотпуно или недоследно навођење литературе у системима вредновања часописа сматра се довољним разлогом за оспоравање научног статуса часописа.

Систем АСИСТЕНТ у сврху контроле правилног исписа листе референци користи специјалну алатку RefFormatter: контрола обликовања референци у складу са Харвардским приручником за стил.

Пропратно писмо (само за ауторе из Републике Србије и по посебном захтеву уредника)

Поред чланка доставља се пропратно писмо у којем треба истаћи о којој врсти чланка се ради, који су графички прилози (фотографије и цртежи) оригинални, а који позајмљени.

У пропратном писму наводе се и подаци аутора: име, средње слово, презиме, чин, звање, е-маил, адреса послодавца (ВП), кућна адреса, телефон на радном месту и кућни (мобилни) телефон, рачун и назив банке, СО места становања, број личне карте и ЈМБ грађана.

Сви радови подлежу стручној рецензији.

Списак рецензената Војнотехничког гласника може се видети на страници сајта *Списак рецензената*. Процес рецензирања објашњен је на страници сајта *Рецензентски поступак*.

Адреса редакције:
Војнотехнички гласник
Генерала Павла Јуришића Штурма 1
11000 Београд,
e-mail: vojnotehnicki.glasnik@mod.gov.rs.

Главни и одговорни уредник
мр *Небојша* Гаћеша, дипл. инж.
nebojsa.gacesa@mod.gov.rs,
 <http://orcid.org/0000-0003-3217-6513>,
тел.: војни 40-260 (011/3603-260),
066/8700-118

ПРИГЛАШЕНИЕ И ИНСТРУКЦИЯ ДЛЯ АВТОРОВ О ПОРЯДКЕ ПОДГОТОВКИ СТАТЬИ

Инструкция для авторов о порядке подготовки статьи к опубликованию в журнале «Военно-технический вестник» разработана в соответствии с Актом о редактировании научных журналов Министерства науки и технологического развития Республики Сербия, № 110-00-17/2009-01 от 09.07.2009 г. Применение этого Акта способствует повышению качества отечественных журналов и их более полному вовлечению в международную систему обмена научной информацией. Инструкция соответствует международным стандартам ISO 4, ISO 8, ISO 18, ISO 215, ISO 214, ISO 18, ISO 690, ISO 690-2, ISO 999, ISO 5122 и соответствующим стандартам Республики Сербия.

Военно-технический вестник (Vojnotehnički glasnik / Military Technical Courier), втг.мо.упр.срб, www.vtg.mod.gov.rs/index-ru.html, ISSN 0042-8469 – печатное издание, e-ISSN 2217-4753 – online, UDK 623+355/359, является мультидисциплинарным научным журналом Министерства обороны Республики Сербия, который публикует научные и профессиональные статьи, а также техническую информацию о современных системах вооружения и современных военных технологиях. Журнал следит за единой межвидовой технической поддержкой вооруженных сил, основанной на принципах системной логистики, за прикладными и инновационными научными исследованиями, в том числе, в области производства вооружения и военной техники, и за прочими теоретическими и практическими достижениями, которые способствуют профессиональному росту представителей сербского, регионального и международного академического сообщества, и особенно военнослужащих Министерства Обороны и Вооружённых сил Республики Сербия.

Министерство образования, науки и технологического развития Республики Сербия, согласно решению принятому в соответствии со ст. 27 абзац 1, пункт 4 и на основании толкования ст. 25 абзац 1 пункт 5 Закона о научно-исследовательской деятельности («Службени гласник РС», № 110/05, утвердило категоризацию «Военно-технического вестника» за 2017 год:

Категории в области технологического развития:

– **Область материалов и химической технологии:**

ведущий научный журнал национального значения (**M51**),

– **Область электроники, телекоммуникаций и информационных технологий:** научный журнал национального значения (**M52**),

– **Область механики:**

научный журнал национального значения (**M52**).

Категории в области основных исследований:

– **Область математика, компьютерные науки, технические науки:**

научный журнал (**M53**).

С информацией относительно категоризации за 2017 год можно ознакомиться на странице сайта «Военно-технического вестника» *Категоризация Вестника* (Министерством просвещения, науки и технологического развития Республики Сербия пока не произведено официального ранжирования научных журналов за 2018 год).

Более подробную информацию можно найти на сайте Министерства образования, науки и технологического развития Республики Сербия.

С информацией о категоризации можно ознакомиться и на сайте КОБСОН (Консорциум библиотек Республики Сербия по вопросам объединения закупок).

Категоризация Вестника проведена согласно Положению о порядке и способе категоризации научно-исследовательских результатов, утверждённого Национальным комитетом по науке и технологиям (Службени гласник РС, № 38/2008).

В соответствии с вышеуказанным Положением и таблицей с показателями классификации и категоризации индивидуальных научно-исследовательских результатов, являющейся неотъемлемой частью Положения, научная статья, опубликованная в «Военно-техническом вестнике», оценивается следующим способом: 2 балла (категория M51), 1,5 балла (категория M52) и 1,5 балл (категория M53).

Журнал соответствует стандартам Сербского индекса научного цитирования (СЦИндекс/SCIndex) – наукометрической базы данных научных журналов Республики Сербия, а также Российского индекса научного цитирования (РИНЦ). Журнал постоянно подвергается мониторингу и оценивается количественными наукометрическими показателями, отражающими его научную ценность, в т.ч. опосредованно в международных индексах цитирования (Clarivate Analytics).

С информацией об индексировании можно ознакомиться на странице сайта журнала *Индексирование Вестника*.

«Военно-технический Вестник» обеспечивает читателям возможность открытого доступа, в соответствии с положениями об авторских правах, утверждёнными Creative Commons (CC BY). С инструкцией об авторских правах можно ознакомиться на странице *Авторские права и политика самоархивирования*, перейдя по ссылке <http://www.vtg.mod.gov.rs/index-ru.html>.

Рукописи статей направляются в редакцию журнала с использованием online системы e-Ур: Электронное издательство – ASSISTANT, запущенной Центром поддержки развития образования и науки (ЦПРОН).

Регистрация в системе и оформление прав доступа выполняется по адресу <http://www.vtg.mod.gov.rs/index-ru.html>, через страницу ASSISTANT или СЦИНДЕКС (aseestant.ceon.rs/index.php/vtg).

С инструкцией по регистрации и правам доступа можно ознакомиться по адресу <http://www.vtg.mod.gov.rs/index-ru.html>, на странице *Инструкция по e-Ур: Электронное издательство ASSISTANT*.

Все авторы, предоставляющие свои рукописи для публикации в редакцию журнала «Военно-технический вестник» должны пройти предварительную регистрацию в реестре ORCID (Open Researcher and Contributor ID). Эта процедура осуществляется в соответствии с инструкцией, размещенной на странице сайта *Регистрация в реестре ORCID для присвоения идентификационного кода*.

«Военно-технический вестник» публикует статьи на сербском, русском или английском языках (Arial, шрифт 11 pt, пробел Single).

Процесс подготовки, написания и редактирования статьи должен осуществляться в соответствии с принципами *Этического кодекса* (<http://www.vtg.mod.gov.rs/eticheskiy-kodyeks.html>).

Статья должна содержать аннотацию с ключевыми словами, введение, основную часть, выводы, список использованной литературы и резюме с ключевыми словами на английском языке (без нумерации заголовков и подзаголовков). Объём статьи не должен превышать один авторский лист (16 страниц формата A4 с пробелом Single).

Статья должна быть набрана на компьютере с использованием специально подготовленного редакцией макета, который можно скачать на странице сайта *Правила и образец составления статьи*.

Заголовок

Заголовок должен отражать тему статьи. В интересах журнала и автора необходимо использовать слова и словосочетания, удобные для индексации и поиска. Если такие слова не содержатся в заголовке, то желательно их добавить в подзаголовок. Заголовок должен быть переведён на английский язык. Название заголовка (подзаголовка) пишется перед аннотацией на соответствующем языке.

Текущий заголовок

Текущий заголовок пишется в титуле каждой страницы статьи с целью упрощения процесса идентификации, в первую очередь копий статьей в электронном виде. Заголовок содержит в себе фамилию и инициал имени автора (в случае если авторов несколько, остальные обозначаются с «et al.» или «и др.»), название работы и журнала (год, том, выпуск, начальная и заключительная страница). Заголовок статьи и название журнала могут быть приведены в сокращенном виде.

ФИО автора

Приводятся полная фамилия и полное имя (всех) авторов. Желательно, чтобы были указаны инициалы отчеств авторов. Фамилия и имя авторов из Республики Сербия всегда пишутся в оригинальном виде (с сербскими диакритическими знаками), независимо от языка, на котором написана работа.

Наименование учреждения автора (аффилиация)

Приводится полное (официальное) наименование и местонахождение учреждения, в котором работает автор, а также наименование учреждения, в котором автор провёл исследование. В случае организаций со сложной структурой приводится их иерархическая соподчинённость (напр. Военная академия, кафедра военных электронных систем, г. Белград). По крайней мере, одна из организаций в иерархии должна иметь статус юридического лица. В случае если указано несколько авторов, и если некоторые из них работают в одном учреждении, нужно отдельными обозначениями или каким-либо другим способом указать в каком из приведённых учреждений работает каждый из авторов. Аффилиация пишется непосредственно после ФИО автора. Должность и специальность по диплому не указываются.

Контактные данные

Электронный адрес автора указывается рядом с его именем на первой странице статьи.

Категория (тип) статьи

Категоризация статьей является обязанностью редакции и имеет особое значение. Категорию статьи могут предлагать рецензенты и члены редакции, т.е. редакторы рубрик, но ответственность за категоризацию несет исключительно главный редактор. Статьи в журнале распределяются по следующим категориям:

Научные статьи:

1. оригинальная научная статья (работа, в которой приводятся ранее неопубликованные результаты собственных исследований, полученных научным методом);

2. обзорная статья (работа, содержащая оригинальный, детальный и критический обзор исследуемой проблемы или области, в который автор внёс определённый вклад, видимый на основе автоцитат);

3. краткое сообщение (оригинальная научная работа полного формата, но меньшего объёма или имеющая предварительный характер);

4. научная критическая статья (дискуссия-полемика на определённую научную тему, основанная исключительно на научной аргументации) и научный комментарий.

Однако, в некоторых областях знаний научная работа в журнале может иметь форму монографического исследования, а также критического обсуждения научного материала (историко-архивного, лексикографического, библиографического, обзора данных и т.п.) – до сих пор неизвестного или недостаточно доступного для научных исследований. Работы, классифицированные в качестве научных, должны иметь, по меньшей мере, две положительные рецензии.

В случае если в журнале объявляются и приложения, не имеющие научный характер, научные статьи должны быть сгруппированы и четко выделены в первой части номера.

Профессиональные статьи:

1. профессиональная работа (приложения, в которых предлагаются опыты, полезные для совершенствования профессиональной практики, но которые не должны в обязательном порядке быть обоснованы на научном методе);

2. информативное приложение (передовая статья, комментарий и т.п.);

3. обзор (книги, компьютерной программы, случая, научного события и т.п.).

Язык работы

Работа может быть написана на сербском, русском или английском языке.

Текст должен быть в лингвистическом и стилистическом смысле упорядочен, систематизирован, без сокращений (за исключением стандартных). Все физические величины должны соответствовать Международной системе единиц измерения – СИ. Очередность формул обозначается порядковыми номерами, проставляемыми с правой стороны в круглых скобках.

Аннотация (абстракт) и резюме

Аннотация (абстракт) является кратким информативным обзором содержания статьи, обеспечивающим читателю быстроту и точность оценки её релевантности. В интересах редакции и авторов, чтобы аннотация содержала термины, часто используемые для индексирования и поиска статьей. Составными частями аннотации являются цель исследования, методы и заключение. В аннотации должно быть от 100 до 250 слов, и она должна находиться между титулами (заголовок, ФИО авторов и др.) и ключевыми словами, за которыми следует текст статьи. Если работа написана на сербском или русском языке, желательно, чтобы кроме аннотации на сербском и русском, была бы предоставлена и аннотация в расширенном виде на английском языке – в качестве т.н. резюме (summary). Такое резюме должно находиться в конце статьи, после раздела Литература. Важно, чтобы резюме было в структурированном виде, и его длина может составлять до 1/10 длины статьи (оно более обширно, чем аннотация из начала статьи). Началом данного резюме может быть переведенная аннотация (из начала статьи), а затем должны следовать переведенные главные заголовки, подзаголовки и основы заключения статьи (литература не переводится). В структурированном резюме нужно перевести часть текста под заголовком и заголовком, принимая во внимание, чтобы оно было пропорционально их размеру и в то же время отражала суть.

Ключевые слова

Ключевыми словами являются термины или фразы, адекватно представляющие содержание статьи, необходимые для индексирования и поиска. Ключевые слова необходимо выбирать, опираясь при этом на какой-либо международный источник (регистр, словарь, тезаурус), наиболее используемый внутри данной научной области. Число ключевых слов не может превышать 10. В интересах редакции и авторов, чтобы частота их встречи в статье была как можно большей. Ключевые слова даются на языке, на котором написана статья (аннотация), и на английском языке. В статье они пишутся непосредственно после аннотации (в начале) и после резюме (в конце).

Программа ASSISTANT предоставляет возможность использования сервиса KWASS, автоматически фиксирующего ключевые слова из источников/словарей по выбору автора/редактора.

Дата получения статьи

Дата, когда редакция получила статью; дата, когда редакция окончательно приняла статью к публикации; а также дата, когда были предоставлены необходимые исправления рукописи, приводятся в хронологическом порядке, как правило, в конце статьи.

Выражение благодарности

Наименование и номер проекта, т.е. название программы благодаря которой статья возникла, совместно с наименованием учреждения, которое финансировало проект или программу, приводятся в отдельном примечании, как правило, внизу первой страницы статьи.

Предыдущие версии работы

В случае если статья в предыдущей версии была изложена устно (под одинаковым или похожим названием, например, в виде доклада на научной конференции), сведения об этом должны быть указаны в отдельном примечании, как правило, внизу первой страницы статьи. Работа, которая уже была опубликована в каком-либо из журналов, не может быть напечатана в «Военно-техническом вестнике» ни под похожим названием, ни в изменённом виде.

Нумерация и название таблиц и графиков

Желательно, чтобы нумерация и название таблиц и графиков были исполнены на двух языках (на языке оригинала и на английском). Таблицы подписываются таким же способом как и текст и обозначаются порядковым номером с верхней стороны. Фотографии и рисунки должны быть понятны, наглядны и удобны для репродукции. Рисунки необходимо делать в программах Word или Corel. Фотографии и рисунки надо поставить на желаемое место в тексте. Для создания изображений и графиков использование функции снимка с экрана (скриншота) не допускается. В самом тексте статьи рекомендуется применение изображений и графиков, обработанных такими компьютерными программами, как: Excel, Matlab, Origin, SigmaPlot и др.

Ссылки (цитирование) в тексте

Оформление ссылок на источники в рамках статьи должно быть однообразным. «Военно-технический вестник» для оформления ссылок, цитат и списка использованной литературы применяет Гарвардскую систему (Harvard Referencing System, Harvard Style Manual). В тексте в скобках приводится фамилия цитируемого автора (или фамилия первого автора, если авторов несколько), год

издания и по необходимости номер страницы. Например: (Petrović, 2010, pp.10-20). Рекомендации о способе цитирования размещены на странице сайта *Инструкция по использованию Гарвардского стиля*. При оформлении ссылок, цитат и списка использованной литературы необходимо придерживаться установленных норм.

Программа ASSISTANT предоставляет при цитировании возможность использования сервиса CiteMatcher, фиксирующего пропущенные цитаты в работе и в списке литературы.

Примечания (сноски)

Примечания (сноски) к тексту указываются внизу страницы, к которой они относятся. Примечания могут содержать менее важные детали, дополнительные объяснения, указания об использованных источниках (напр. научном материале, справочниках), но не могут быть заменой процедуры цитирования литературы.

Литература (референции)

Цитированной литературой охватываются, как правило, такие библиографические источники как статьи, монографии и т.п. Вся используемая литература в виде референций размещается в отдельном разделе статьи.

Названия литературных источников не переводятся на язык работы.

«Военно-технический вестник» для оформления списка использованной литературы применяет Гарвардскую систему (Harvard Style Manual). В списке литературы источники указываются в алфавитном порядке фамилий авторов или редакторов. Рекомендации о способе цитирования размещены на странице сайта *Инструкция по использованию Гарвардского стиля*. При оформлении списка использованной литературы необходимо придерживаться установленных норм.

При оформлении списка литературы программа ASSISTANT предоставляет возможность использования сервиса RefFormatter, осуществляющего контроль оформления списка литературы в соответствии со стандартами Гарвардского стиля.

Нестандартное, неполное и непоследовательное приведение литературы в системах оценки журнала считается достаточной причиной для оспаривания научного статуса журнала.

Все рукописи статей подлежат профессиональному рецензированию.

Список рецензентов журнала «Военно-технический вестник» размещён на странице сайта *Список рецензентов*. Процесс рецензирования описан в разделе *Правила рецензирования*.

Почтовый адрес редакции:

«Војнотехнички гласник»

ул. Генерала Павла Јуришича Штурма 1

11000 Белград, Република Србија

e-mail: vojnotehnicki.glasnik@mod.gov.rs.

Главный и ответственный редактор
Кандидат технических наук *Небойша* Гачеша
nebojsa.gacesa@mod.gov.rs

<http://orcid.org/0000-0003-3217-6513>

тел: +381 11 3603 260, +381 66 8700 118

CALL FOR PAPERS AND ARTICLE FORMATTING INSTRUCTIONS

The instructions to authors about the article preparation for publication in the *Military Technical Courier* are based on the Act on scientific journal editing of the Ministry of Science and Technological Development of the Republic of Serbia, No 110-00-17/2009-01 of 9th July 2009. This Act aims at improving the quality of national journals and raising the level of their compliance with the international system of scientific information exchange. It is based on international standards ISO 4, ISO 8, ISO 18, ISO 215, ISO 214, ISO 18, ISO 690, ISO 690-2, ISO 999 and ISO 5122 and their national equivalents.

The Military Technical Courier / Vojnotehnički glasnik (www.vtg.mod.gov.rs/index-e.html, втр.мо.унр.срб, ISSN 0042-8469 – print issue, e-ISSN 2217-4753 – online, UDC 623+355/359) is a multidisciplinary scientific journal of the Ministry of Defence of the Republic of Serbia. It publishes scientific and professional papers as well as technical data on modern weapon systems and military technologies. The journal covers inter-service technical support to the Army on the principle of logistic system support; fundamental, applied and development research; production and use of weapons and military equipment as well as other theoretical and practical achievements leading to professional development of all members of Serbian, regional and international academic communities, members of the Ministry of Defence and the Army of Serbia in particular.

Pursuant to the decision given in Article 27, paragraph 1, point 4, and in accordance with the acquired opinion given in Article 25, paragraph 1, point 5 of the Act on Scientific and Research Activities (Official Gazette of the Republic of Serbia, No 110/05, 50/06-cor and 18/10), the Ministry of Education, Science and Technological Development of the Republic of Serbia classified the Military Technical Courier for the year 2017

in the field technological development:

- **on the list of periodicals for materials and chemical technology**, category: leading scientific periodical of national interest (**M51**),
- **on the list of periodicals for electronics, telecommunications and IT**, category: scientific periodical of national interest (**M52**),
- **on the list of periodicals for mechanical engineering**, category: scientific periodical of national interest (**M52**),

in the field fundamental research:

- **on the list of periodicals for mathematics, computer sciences and mechanics**, category: scientific periodical (**M53**).

The approved lists of national periodicals for the year 2017 can be viewed on the website of the Military Technical Courier, page *Journal categorization* (The Ministry of Education, Science and Technological Development of the Republic of Serbia has not yet published the official evaluation of scientific journals for 2018).

More detailed information can be found on the website of the Ministry of Education, Science and Technological Development of the Republic of Serbia.

The information on the categorization can be also found on the website of KOBSON (Consortium of Libraries of Serbia for Unified Acquisition).

The periodical is categorized in compliance with the Regulations on the procedure and method of evaluation and quantitative formulation of scientific and research results of researchers, stipulated by the National Council for Scientific and Technological Development (*Official Gazette of RS*, No 38/2008). More detailed information can be found on the website of the Ministry of Education, Science and Technological Development.

In accordance with the Regulations and the table about types and quantification of individual scientific and research results (as a part of the Regulations), a paper published in the *Military Technical Courier* scores 2 (two) points (category M51), 1,5 (one and a half) point (category M52) and 1 (one) point (category M53).

The journal is in the Serbian Citation Index – SCIndex (data base of national scientific journals), in the Russian Index of Science Citation/Российский индекс научного цитирования (RINC/РИНЦ) and is constantly monitored depending on the impact within the bases themselves and indirectly in the international (e.g. Clarivate Analytics) citation indexes. More detailed information can be viewed on the website of the Military Technical Courier, page *Journal indexing*.

Military Technical Courier enables open access and applies the Creative Commons Attribution (CC BY) licence provisions on copyright. The copyright details can be found on the *Copyright notice and Self-archiving policy* page of the journal's website.

Manuscripts are submitted online, through the electronic editing system ASSISTANT, developed by the Center for Evaluation in Education and Science – CEON.

The access and the registration are through the Military Technical Courier site <http://www.vtg.mod.gov.rs/index-e.html>, on the page *ASSISTANT* or the page *SCINDEKS* or directly through the link (aseestant.ceon.rs/index.php/vtg).

The detailed instructions about the registration for the service are on the website <http://www.vtg.mod.gov.rs/index-e.html>, on the page *Instructions for e-Ur: Electronic Editing - ASSISTANT*.

All authors submitting a manuscript for publishing in the Military Technical Courier should register for an ORCID ID following the instructions on the web page *Registration for an ORCID identifier*.

The Military Technical Courier publishes articles in Serbian, Russian or English, using Arial and a font size of 11pt with Single Spacing.

The procedures of article preparation, writing and editing should be in accordance with the *Publication ethics statement* (<http://www.vtg.mod.gov.rs/publication-ethics-statement.html>).

The article should contain the abstract with keywords, introduction, body, conclusion, references and the summary in English language (without heading and subheading enumeration). The article length should not exceed 24 pages of A4 paper format.

The article should be formatted following the instructions in the Article Form which can be downloaded from website page *Article form*.

Title

The title should be informative. It is in both Journal's and author's best interest to use terms suitable for indexing and word search. If there are no such terms in the title, the author is strongly advised to add a subtitle. The title should be given in English as well.

The titles precede the abstract and the summary in an appropriate language.

Letterhead title

The letterhead title is given at a top of each page for easier identification of article copies in an electronic form in particular. It contains the author's surname and first name initial (for multiple authors add "et al"), article title, journal title and collation (year, volume, issue, first and last page). The journal and article titles can be given in a shortened form.

Author's name

Full name(s) of author(s) should be used. It is advisable to give the middle initial. Names are given in their original form (with diacritic signs if in Serbian).

Author's affiliation

The full official name and seat of the author's affiliation is given, possibly with the name of the institution where the research was carried out. For organizations with complex structures, give the whole hierarchy (for example, University of Defence in Belgrade, Military Academy, Department for Military Electronic Systems). At least one organization in the hierarchy must be a legal entity. When some of multiple authors have the same affiliation, it must be clearly stated, by special signs or in other way, which department exactly they are affiliated with. The affiliation follows the author's name. The function and title are not given.

Contact details

The postal addresses or the e-mail addresses of the authors are given in the first page.

Type of articles

Classification of articles is a duty of the editorial staff and is of special importance. Referees and the members of the editorial staff, or section editors, can propose a category, but the editor-in-chief has the sole responsibility for their classification.

Journal articles are classified as follows:

Scientific articles:

1. Original scientific paper (giving the previously unpublished results of the author's own research based on scientific methods);
2. Survey paper (giving an original, detailed and critical view of a research problem or an area to which the author has made a contribution visible through his self-citation);
3. Short or preliminary communication (original scientific paper of full format but of a smaller extent or of a preliminary character);
4. Scientific critique or forum (discussion on a particular scientific topic, based exclusively on scientific argumentation) and commentaries.

Exceptionally, in particular areas, a scientific paper in the Journal can be in a form of a monograph or a critical edition of scientific data (historical, archival, lexicographic, bibliographic, data survey, etc.) which were unknown or hardly accessible for scientific research.

Papers classified as scientific must have at least two positive reviews.

If the journal contains non-scientific contributions as well, the section with scientific papers should be clearly denoted in the first part of the Journal.

Professional articles:

1. Professional paper (contribution offering experience useful for improvement of professional practice but not necessarily based on scientific methods);
2. Informative contribution (editorial, commentary, etc.);
3. Review (of a book, software, case study, scientific event, etc.)

Language

The article can be in Serbian, Russian or English.

The grammar and style of the article should be of good quality. The systematized text should be without abbreviations (except standard ones). All measurements must be in SI units. The sequence of formulae is denoted in Arabic numerals in parentheses on the right-hand side.

Abstract and summary

An abstract is a concise informative presentation of the article content for fast and accurate evaluation of its relevance. It is both in the Editorial Office's and the author's best interest for an abstract to contain terms often used for indexing and article search. The abstract describes the purpose of the study and the methods, outlines the findings and state the conclusions. A 100- to 250- word abstract should be placed between the title and the keywords with the body text to follow. Besides an abstract in Serbian and Russian, articles in Serbian and Russian are advised to have a summary in English, at the end of the article, after the Reference list. The summary should be structured and long up to 1/10 of the article length (it is more extensive than the abstract). It can start with the translated Serbian or Russian abstract from the beginning of the article with translated main headings, subheadings and major conclusions to follow (Reference list is not translated). The structured summary should also contain the proportional informative parts of the text below the headings and subheadings.

Keywords

Keywords are terms or phrases showing adequately the article content for indexing and search purposes. They should be allocated heaving in mind widely accepted international sources (index, dictionary or thesaurus), such as the Web of Science keyword list for science in general. The higher their usage frequency is, the better. Up to 10 keywords immediately follow the abstract and the summary, in respective languages.

For this purpose, the ASSISTANT system uses a special tool KWASS for the automatic extraction of key words from disciplinary thesauruses/dictionaries by choice and the routine for their selection, i.e. acceptance or rejection by author and/or editor.

Article acceptance date

The date of the reception of the article, the dates of submitted corrections in the manuscript (optional) and the date when the Editorial Board accepted the article for publication are all given in a chronological order at the end of the article.

Acknowledgements

The name and the number of the project or programme within which the article was realised is given in a separate note at the bottom of the first page together with the name of the institution which financially supported the project or programme.

Article preliminary version

If an article preliminary version has appeared previously at a meeting in a form of an oral presentation (under the same or similar title), this should be stated in a separate note at the bottom of the first page. An article published previously cannot be published in the *Military Technical Courier* even under a similar title or in a changed form.

Tables and illustrations

All the captions should be in the original language as well as in English, together with the texts in illustrations if possible. Tables are typed in the same style as the text and are denoted by Arabic numerals at the top. Photographs and drawings, placed appropriately in the text, should be clear, precise and suitable for reproduction. Drawings should be created in Word or Corel.

For figures and graphs, proper data plot is recommended i.e. using a data analysis program such as Excel, Matlab, Origin, SigmaPlot, etc. It is not recommended to use a screen capture of a data acquisition program as a figure or a graph.

Citation in the text

Citation in the text must be uniform. The Military Technical Courier applies the Harvard Referencing System given in the Harvard Style Manual. When citing sources within your paper, i.e. for in-text references of the works listed at the end of the paper, place the year of publication of the work in parentheses and optionally the number of the page(s) after the author's name, e.g. (Petrovic, 2012, pp.10-12). A detailed guide on citing, with examples, can be found on Military Technical Courier website on the page *Instructions for Harvard Style Manual*. In-text citations should follow its guidelines.

For checking in-text citations, the ASSISTANT system uses a special tool Cite-Matcher to find out quotes left out within papers and in reference lists.

Footnotes

Footnotes are given at the bottom of the page with the text they refer to. They can contain less relevant details, additional explanations or used sources (e.g. scientific material, manuals). They cannot replace the cited literature.

Reference list (Literature)

The cited literature encompasses bibliographic sources such as articles and monographs and is given in a separate section in a form of a reference list.

References are not translated to the language of the article.

In compiling the reference list and bibliography, the Military Technical Courier applies the Harvard System – Harvard Style Manual. All bibliography items should be listed alphabetically by author's name, without numeration. A detailed guide for listing references, with examples, can be found on Military Technical Courier website on the page *Instructions for Harvard Style Manual*. Reference lists at the end of papers should follow its guidelines.

In journal evaluation systems, non-standard, insufficient or inconsequent citation is considered to be a sufficient cause for denying the scientific status to a journal.

All articles are peer reviewed.

The list of referees of the Military Technical Courier can be viewed at website page *List of referees*. The article review process is described on the *Peer Review Process* page of the website.

Address of the Editorial Office:
Vojnotehnički glasnik / Military Technical Courier
Generala Pavla Jurišića Šturma 1
11000 Belgrade, Republic of Serbia,
e-mail: vojnotehnicki.glasnik@mod.gov.rs.

Editor in chief
Nebojša Gaćeša MSc
nebojsa.gacesa@mod.gov.rs
 <http://orcid.org/0000-0003-3217-6513>
tel.: +381 11 3603 260, +381 66 8700 118

ОБАВЕШТЕЊА САРАДНИЦИМА И ЧИТАОЦИМА
СООБЩЕНИЯ ДЛЯ АВТОРОВ И ЧИТАТЕЛЕЙ
INFORMATION FOR CONTRIBUTORS AND READERS

Војнотехнички гласник постао партнер компаније *Publons*

Војнотехнички гласник је од 5. августа 2018. године постао партнер компаније *Publons*, водеће светске платформе за рецензије, која званично признаје рецензентски допринос, а која је део *Clarivate Analytics*-а.

Када рецензенти ураде рецензију чланка за *Војнотехнички гласник* биће питани да ли желе да прате, потврде и добију признање за свој рад на *Publons*-у. Рецензенти затим могу користити своју верификовану рецензију као доказ о својим доприносима научној заједници у апликацијама за промоцију, финансирање и сл.

Редакција *Војнотехничког гласника* позива садашње рецензенте, који су тренутно регистровани у систему електронског уређивања АСИСТЕНТ, као и све друге научне раднике који су заинтересовани да буду рецензенти нашег часописа, да се региструју у *Publons*-у користећи упутство на страници сајта *Позив и упутство рецензентима за регистрацију у Publons-у* (<http://www.vtg.mod.gov.rs/poziv-i-uputstvo-recenzentima-za-registraciju-u-publons.html>).

Журнал «Военно-технический вестник» стал партнером компани «Publons»

Журнал «Военно-технический вестник» 5 августа 2018 года стал партнером компани «Publons» – ведущей мировой платформой для рецензентов, которая официально оценивает рецензентский вклад в науку. Компани «Publons» входит в состав базы данных «Clarivate Analytics».

По завершении рецензии к статье, предназначенной для публикации в журнале «Военно-технический вестник» рецензенты получают вопрос, желают ли они чтобы их рецензия была оценена и признана системой Publons. Таким образом подтвержденную рецензию рецензенты смогут использовать в качестве доказательства о вкладе в науку, это может помочь им при подаче заявок на гранты, финансирование и пр.

Редакция журнала «Военно-технический вестник» приглашает всех своих рецензентов, зарегистрированных в системе электронного редактирования АССИСТЕНТ, а также других научных деятелей, которые имеют желание присоединиться к коллегии рецензентов журнала «Военно-технический вестник» зарегистрироваться на сайте Publons, с помощью инструкции, опубликованной на странице *Приглашение рецензентов и инструкция по работе с Publons* (<http://www.vtg.mod.gov.rs/priglasenie-recenzentov-i-instrukcija-po-rabote-s-publons.html>).

The Military Technical Courier became a partner with *Publons*

Since 5th August 2018, *Vojnotehnicki Glasnik/Military Technical Courier* has been a partner with *Publons*, the world's leading peer review platform, part of *Clarivate Analytics*, which officially recognizes peer review contributions.

When reviewers submit peer reviews to *The Military Technical Courier*, they are asked whether they would like to track, verify and showcase it on *Publons*. Verified peer reviews can be further used as evidence of reviewers' contributions to the scientific community for promotion, funding, grant applications, etc.

The Military Technical Courier is inviting its reviewers currently registered in the ASSISTANT electronic editing system – and all other prospective reviewers as well – to register in *Publons* using the instructions on the webpage: *Call and instructions to reviewers for the registration in Publons* (<http://www.vtg.mod.gov.rs/call-and-instructions-to-reviewers-for-the-registration-in-publons.html>).



Ликовно-графички уредник
мр *Небојша* Кујунџић
е-mail: nebojsa.kujundzic@mod.gov.rs

Техничко уређење
Небојша Гаћеша, е-mail: nebojsa.gacesa@mod.gov.rs,
<http://orcid.org/0000-0003-3217-6513>,
Марија Марић, е-mail: marija.maric@mod.gov.rs

Лектор
Добрила Милетић, професор
е-mail: dobрила.miletic@mod.gov.rs

Превод на енглески
Јасна Вишњић, професор
е-mail: jasnavisnjic@yahoo.com, <http://orcid.org/0000-0003-1728-4743>

Превод на руски
др Карина Авагјан
е-mail: karinka2576@mail.ru
Оливера Хајдуковић, професор
е-mail: oliverahajdukovic@lukoil.rs

Превод на немачки
Гордана Богдановић, професор
е-mail: gordana.bogdanovic@yahoo.com

Превод на француски
Драган Вучковић,
е-mail: draganvuckovic@kbcnet.rs, <http://orcid.org/0000-0003-1620-5601>

ЦИП – Каталогизација у публикацији:
Народна библиотека Србије, Београд

623+355 / 359
355 / 359

ВОЈНОТЕХНИЧКИ гласник : научни часопис
Министарства одбране Републике Србије =
Military Technical Courier : scientific
periodical of the Ministry of Defence of the
Republic of Serbia / одговорни уредник
Небојша Гаћеша. - Год. 1, бр. 1 (1953) -
- Београд (Браће Југовића 19) : Министарство
одбране Републике Србије, 1953- (Београд :
Војна штампарија). - 24 cm

Доступно и на: <http://www.vtg.mod.gov.rs>
Тромесечно. - Друго издање на другом медијуму:
Vojnotehnički glasnik (Online) = ISSN 2217-4753
ISSN 0042-8469 = Војнотехнички гласник
COBISS.SR-ID 4423938

Цена: 350,00 динара,
Тираж: 150 примерака

На основу мишљења Министарства за науку, технологију и развој Републике Србије,
број 413-00-1201/2001-01 од 12. 9. 2001. године,
часопис „Војнотехнички гласник“ је публикација од посебног интереса за науку.
УДК: Народна библиотека Србије, Београд

Художественный редактор
Магистр дизайна, *Небойша* Куюнджич
e-mail: nebojsa.kujundzic@mod.gov.rs

Технический редактор
Небойша Гачеша, e-mail: nebojsa.gacesa@mod.gov.rs,
<http://orcid.org/0000-0003-3217-6513>,
Мария Марич
e-mail: marija.maric@mod.gov.rs

Корректор
Добрила Милетич,
e-mail: dobrila.miletic@mod.gov.rs

Перевод на английский язык
Ясна Вишнич
e-mail: jasnavisnjic@yahoo.com, <http://orcid.org/0000-0003-1728-4743>

Перевод на русский язык
Д.филол.н. *Карина* Кареновна Авагян
e-mail: karinka2576@mail.ru
Оливера Хайдукович
e-mail: oliverahajdukovic@lukoil.rs

Перевод на немецкий язык
Гордана Богданович
e-mail: gordana.bogdanovic@yahoo.com

Перевод на французский язык
Драган Вучкович
e-mail: draganvuckovic@kbcnet.com, <http://orcid.org/0000-0003-1620-5601>

CIP – Каталогизация в публикации: Национальная библиотека Сербии, г. Белград

623+355 / 359
355 / 359

ВОЕННО-ТЕХНИЧЕСКИЙ вестник: научный журнал
Министерства обороны Республики Сербия=
Military Technical Courier : scientific
periodical of the Ministry of Defence of the
Republic of Serbia / главный редактор
Небойша Гачеша. – Первый выпуск (1953) –
г. Белград (ул. Браче Юговича, д. 19): Министерство
обороны Республики Сербия, 1953- (Белград:
Военная типография). - 24 см
Размещено на сайте:
<http://www.vtg.mod.gov.rs>
Ежеквартально - Издание в электронном виде:
Военно-технический вестник (Online) = ISSN2217-4753
ISSN 0042-8469 = Военно-технический вестник
COBISS.SR-ID 4423938

Цена: 350,00 динаров
Тираж: 150 экземпляров

На основании решения Министерства науки и технологий Республики Сербия,
№ 413-00-1201/2001-01 от 12. 9. 2001 года, журнал «Военно-технический вестник»
объявлен изданием, имеющим особое значение для науки.
УДК: Национальная библиотека Сербии, г. Белград

Graphic design editor
Nebojša Kujundžić MA
e-mail: nebojsa.kujundzic@mod.gov.rs

Copy editing
Nebojša Gaćeša, e-mail: nebojsa.gacesa@mod.gov.rs,
<http://orcid.org/0000-0003-3217-6513>,
Marija Marić
e-mail: marija.maric@mod.gov.rs

Proofreader
Dobriša Miletić BA
e-mail: dobriša.miletic@mod.gov.rs

English translation and polishing
Jasna Višnjić BA
e-mail: jasnavisnjic@yahoo.com, <http://orcid.org/0000-0003-1728-4743>

Russian translation and polishing
Karina Avagyan PhD
e-mail: karinka2576@mail.ru
Olivera Hajduković BA
e-mail: oliverahajdukovic@lukoil.rs

German translation and polishing
Gordana Bogdanović BA
e-mail: gordana.bogdanovic@yahoo.com

French translation and polishing
Dragan Vučković
e-mail: draganvuckovic@kbcnet.rs, <http://orcid.org/0000-0003-1620-5601>
CIP – Catalogisation in the publication: National Library of Serbia, Belgrade

623+355 / 359
355 / 359

ВОЈНОТЕХНИЧКИ гласник : научни часопис
Министарства одбране Републике Србије =
Military Technical Courier : scientific
periodical of the Ministry of Defence of the
Republic of Serbia / одговорни уредник
Небојша Гаћеша. - Год. 1, бр. 1 (1953) -
- Београд (Браће Југовића 19) : Министарство
одбране Републике Србије, 1953-(Београд :
Војна штампарија). - 24 cm

Доступно и на:
<http://www.vtg.mod.gov.rs>
Тромесечно. - Друго издање на другом медијуму:
Vojnotehnički glasnik (Online) = ISSN 2217-4753
ISSN 0042-8469 = Војнотехнички гласник
COBISS.SR-ID 4423938

Price: 350.00 RSD
Printed in 150 copies

According to the Opinion of the Ministry of Science and Technological Development No 413-00-1201/2001-01 of 12th September 2001, the *Military Technical Courier* is a publication of special interest for science.

UDC: National Library of Serbia, Belgrade